International Conference on

COMPUTATIONAL AND MATHEMATICAL MODELLING

2025

Conference Proceedings

Centre for Mathematical Modelling, University of Colombo
Sri Lanka

Proceedings of the International Conference on Computational and Mathematical Modelling (ICCMM) - 2025

Proceedings of the International Conference on Computational and Mathematical Modelling (ICCMM) 2025

ISBN: 978-624-5518-29-6

Proceedings edited by
Editorial Committee - ICCMM 2025

Cover designed by
Udana Wetthasinghe

Published by
Centre for Mathematical Modelling, University of Colombo

Conference Partner

Advisory Committee

- Senior Professor (Chair) HD Karunaratne, Vice Chancellor, University of Colombo, Sri Lanka
- Prof. Upul Sonnadara, Dean, Faculty of Science, University of Colombo, Sri Lanka
- Prof. Thomas Goetz, Mathematical Institute, University of Koblenz, Germany
- Dr. Toben Fattler, Department of Mathematics, TU Kaiserslautern, Germany
- Dr. Wolfgang Bock, Linnaeus University, Sweden
- Dr. Guangqu Zheng, Boston University, USA
- Prof. Andrzej Ameljanczyk, Wojskowa Akademia Techniczna, Warsaw, Poland
- Dr. Paduma Eranga, School of Arts and Sciences, Augusta Technical College, Augusta, USA
- Prof. Edy Soewono, Institute of Technology, Indonesia
- Prof. CP Lim, Swinburne University of Technology, Australia
- Prof. DB Gurung, Kathmandu University, Nepal
- Prof. Sree Hari Rao Vadrevu, Foundation for Scientific Research and Technology, India
- Prof. S Sundar, Director, NIT Mizoram, India
- Dr. Hannah E Clapham, National University of Singapore, Singapore
- Prof. Sardar Islam, Victoria University, Australia
- Prof. Joacim Rocklöv, Umea University, Sweden
- Prof. Saroj Jayasinghe, University of Colombo, Sri Lanka
- Prof. Guillaume Leduc, American University of Sharjah, UAE
- Prof. Grigore Albeanu, Spiru Haret University, Romania
- Prof. M. Mahbubur Rahman, University of North Florida, USA
- Prof. Ratnasingham Shivaji, University of North Carolina at Greensboro, USA
- Prof. Jaydev Dabas, Indian Institute of Technology Roorkee, India
- Prof. Kailash C. Patidar, University of the Western Cape, South Africa
- Prof. Weizhong Dai, Louisiana Tech University, USA
- Prof. Irina Perfilieva, University of Ostrava, Czech Republic
- Prof. Samir Bhowmik, University of Dhaka, Bangladesh
- Prof. Ping Lin, University of Dundee, Scotland
- Dr. Ravi Prakash, Universidad de Concepcio ń, Concepcio ń, Chile

- Dr. Sachin Kumar, Department of Mathematics, University of Delhi, India
- Dr. Madhav Wagley, Florida A&M University, Tallahassee, USA
- Prof. Aleksander Sandro Grm, University of Ljubljana, Slovenia
- Dr. Larry J. Pratt, Woods Hole Oceanographic Institution, USA
- Prof. Erik M Bollt, Clarkson University, USA
- Prof. Daniela Genova, University of North Florida, USA
- Prof. Pankaj Jain, Department of Mathematics, South Asian University, New Delhi, India
- Prof. Deepa Sinha, Department of Mathematics, South Asian University, New Delhi, India
- Prof. Kapil Kumar Sharma, Department of Mathematics, South Asian University, New Delhi, India
- Prof. Navnit Jha, Department of Mathematics, South Asian University, New Delhi, India
- Prof. Jagdish Chand Bansal, Department of Mathematics, South Asian University, New Delhi, India
- Prof. Danish Lohani, Department of Mathematics, South Asian University, New Delhi, India
- Prof. Saroj Kumar Sahani, Department of Mathematics, South Asian University, New Delhi, India

Organising Committee

- Conference Chair: Prof. Sanjeewa Perera
- Technical Chair: Prof. Anuradha Mahasinghe
- Conference Secretary: Dr. Hasitha Erandi
- Special Sessions Chair: Dr. Yashika Jayathunga
  Dr. Prabhath Liyanage

Proceedings of the International Conference on Computational and Mathematical Modelling

(ICCMM) - 2025

March 04 - 06, 2025
Colombo, Sri Lanka

Centre for Mathematical Modelling
University of Colombo

Scientific Committee

- Senior Professor (Chair) H.D. Karunaratne, University of Colombo, Sri Lanka
- Prof. Upul Sonnadara, University of Colombo, Sri Lanka
- Prof. Sardar M. N. Islam, Victoria University, Australia
- Prof. Crista Arangala, Elon University, USA
- Prof. Shan Suthaharan, University of North Carolina at Greensboro, USA
- Prof. Chee Peng Lim, Swinburne University of Technology, Australia
- Prof. Edy Soewono, Institut Teknologi Bandung, Indonesia
- Prof. Sree Hari Rao Vadrevu, Foundation for Scientific Research and Technological, India
- Prof. Dil Bahadur Gurung, Kathmandu University, Nepal
- Assoc. Prof. Navnit Jha, South Asian University, India
- Assoc. Prof. Rana Parshad, Iowa State University, USA

MESSAGE FROM THE VICE CHANCELLOR UNIVERSITY OF COLOMBO, SRI LANKA

As the Vice Chancellor of the University of Colombo, I am delighted to extend a warm welcome to all participants of the International Conference on Computational and Mathematical Modelling (ICCMM) 2025. The University of Colombo, recognized as the pioneer and forerunner of higher education and research in Sri Lanka, is honored to host ICCMM 2025. This esteemed conference serves as a premier platform for scholars, researchers, and practitioners from around the globe to convene and share pioneering research in the expansive fields of computational and mathematical modelling.

ICCMM 2025 is organized by the Research and Development Centre for Mathematical Modelling (CMM) within the Department of Mathematics, Faculty of Science. CMM is widely recognized for its pioneering contributions to mathematical modelling, addressing pressing challenges faced by Sri Lanka. Its research spans diverse fields, making substantial contributions to areas such as healthcare, fluid dynamics, unconventional computing and environmental sustainability, fostering innovation and progress.

In an era of rapid scientific and technological advancements, interdisciplinary dialogue and knowledge-sharing are more important than ever. This conference brings together experts from various fields, creating opportunities for insightful discussions and meaningful connections that will shape the future of research and practice.

I am confident that ICCMM 2025 will foster meaningful collaborations, stimulate innovative ideas, and contribute significantly to the advancement of computational and mathematical sciences. I encourage all participants to engage fully in the sessions, exchange knowledge, and explore the vibrant academic environment that the University of Colombo offers.

Once again, welcome to ICCMM 2025. May your experience here be both intellectually rewarding and personally enjoyable.

Senior Professor (Chair) H.D. Karunaratne
The Vice Chancellor
University of Colombo, Sri Lanka

MESSAGE FROM THE DEAN
FACULTY OF SCIENCE, UNIVERSITY OF COLOMBO

On behalf of the Faculty of Science, University of Colombo, I am honored to welcome you to the International Conference on Computational and Mathematical Modelling (ICCMM) 2025. As a faculty dedicated to academic excellence and research innovation, we take pride in supporting this event that brings together leading academics in the computational and mathematical sciences.

ICCMM 2025 offers a unique platform for researchers, industry experts and students to engage in meaningful discussions, share insights, and explore interdisciplinary approaches to solving mathematical problems. This year's conference comprises a diverse program featuring mini symposia, interdisciplinary sessions which will focus on timely topics and a distinguished line-up of invited speakers who will share their invaluable insights and expertise.

As a faculty engaged in teaching and research, we recognize the value of academic gatherings in shaping the future of scientific inquiry. We encourage all participants to take full advantage of this opportunity by presenting their findings, networking with peers, and exploring new collaborative initiatives. I extend my sincere thanks to keynote speakers, invited speakers, panelists and the organizing committee for making this event a success. Thank you for your participation and active engagement, which plays a crucial role in the success of this conference and the advancement of Computational and Mathematical Sciences.

Once again, welcome to ICCMM 2025.

Professor Upul Sonnadara
The Dean and Chair Professor of Physics
Faculty of Science, University of Colombo

MESSAGE FROM THE HEAD OF THE DEPARTMENT OF MATHEMATICS
FACULTY OF SCIENCE, UNIVERSITY OF COLOMBO

It is with great pleasure that I recognize the invaluable contributions of the Centre for Mathematical Modelling (CMM) at the Department of Mathematics, Faculty of Science, University of Colombo, in advancing research at both undergraduate and postgraduate levels. The CMM has been instrumental in fostering a vibrant research culture, and I am especially pleased with its ongoing efforts to expand collaborations beyond institutional and national boundaries through academic conferences. In this regard, the International Conference on Computational and Mathematical Modelling 2025 (ICCMM 2025), not only enhances the CMM's academic influence but also provides a valuable platform for scholars from diverse institutions and countries to engage in meaningful intellectual exchange.

Last year's conference, organized by the CMM was a resounding success, demonstrating its commitment to academic excellence. I have no doubt that this year's event will be equally, if not more, impactful. I greatly appreciate its efforts on disseminating knowledge through a well-structured conference program, including workshops that address highly relevant themes in mathematical sciences. In particular, the CMM's ability to maintain a fair balance between knowledge creation, sharing, and educating is truly commendable.

I extend my best wishes to the organizing committee and all participants for a successful conference.

Dr. Dayal Dharmasena
The Head, Department of Mathematics
University of Colombo

MESSAGE FROM THE CONFERENCE CHAIR ICCMM 2025

It is with great pleasure that I extend a warm welcome to all participants on behalf of the organizing committee and the Centre for Mathematical Modeling, Department of Mathematics, Faculty of Science, University of Colombo. We are thrilled to have you join us for the International Conference on Computational Mathematical Modeling (ICCMM-2025). As we come together for this significant event, it is a privilege to welcome scholars, researchers, and experts from around the globe to engage in a dynamic exchange of ideas, exploring the latest advancements and innovations in the field of computational mathematical modeling.

In this ever-evolving day and age, the impact of computational mathematics has never been more significant in global transformation. ICCMM-2025 serves as a unique platform for intellectual collaboration and dissemination of groundbreaking research aiming to bridge the gap between theory and application through development of practical solutions to address the complex challenges faced by diverse scientific and industrial sectors.

This year's conference lines up a distinguished group of keynote speakers, each an expert in their field, who will share their valuable insights on both the current landscape and the future trajectory of computational mathematical modeling. In addition to insightful talks, the conference will feature interactive panel discussions, workshops, and poster sessions, providing opportunities for participants to engage in meaningful discussions, exchange ideas, and build networks that will last beyond the conference itself.

I extend my heartfelt gratitude to the organizing committee, sponsors, and all volunteers whose dedication and hard work have made this conference a reality. Together, let us embark on a journey of knowledge exchange, collaboration, and innovation that will undoubtedly have a lasting impact on the future of computational mathematical modeling. I encourage each of you to actively participate, share your research, and contribute to the vibrant dialogue that will unfold over the next few days. The success of this conference depends on the collective wisdom and enthusiasm of all involved, and I am confident that our shared commitment will propel us toward new discoveries and advancements in computational mathematical modelling.

I look forward to fruitful explorations, meaningful collaborations, and the opportunity to forge lasting connections throughout ICCMM-2025.

Professor S. S. N. Perera
Chair, ICCMM 2025

Panel of Reviewers

- Prof. Sanjeewa Perera (committee member)
- Prof. Anuradha Mahasinghe (committee member)
- Prof. Crista Arangala - Elon University, USA (external)
- Prof. Angelamaria Cardone - University of Salerno, Italy (external)
- Prof. Navnit Jha - South Asian University, India (external)
- Prof. Upul Sonnadara - Dean, Faculty of Science, University of Colombo, Sri Lanka
- Prof. Sardar M. N. Islam - Victoria University, Australia
- Prof. Rana Parshad - Department of Mathematics, Iowa State University, USA
- Prof. Chee Peng Lim - Swinburne University of Technology, Australia
- Prof. Edy Soewono - Institut Teknologi Bandung, Indonesia
- Prof. Sree Hari Rao Vadrevu - Foundation for Scientific Research and Technological, India
- Prof. Dil Bahadur Gurung - Kathmandu University, Nepal
- Prof. Deepa Sinha - South Asian University, India
- Assoc. Prof. Saroj Kumar Sahani - South Asian University, India
- Prof. Pankaj Jain - South Asian University, India
- Prof. Kapil Sharma - South Asian University, India
- Assoc. Prof. Wolfgang Bock - Linnaeus University, Sweden
- Assoc. Prof. Samayan Narayanamoorthy - Bharathiar University, India
- Dr. Dipo Aldila - Universitas Indonesia, Indonesia
- Dr. Muhammad Fakhruddin - National Research and Innovation Agency (BRIN), Indonesia
- Assoc. Prof. M. Muthtamilselvan - Bharathiar University, India
- Assoc. Prof. Jagdish Chand Bansal - South Asian University, India
- Assoc. Prof. Q.M. Danish Lohani - South Asian University, India
- Assoc. Prof. Lakshmanan Shanmugam - VIT, India
- Assoc. Prof. P. Rajarajeswari - Chikkanna Government Arts College, India
- Dr. Hannah E Clapham - National University of Singapore, Singapore
- Dr. Jalina Widjaja - Institut Teknologi Bandung, Indonesia
- Dr. Yudi Soeharyadi - Institut Teknologi Bandung, Indonesia
- Dr. Tharindu Wickramaarachchi - Burnet Institute, Australia

- Dr. Miracle Amadi - Lappeenranta University of Technology, Finland
- Prof. Naleen Ganegoda - University of Sri Jayewardenepura, Sri Lanka
- Dr. Jagath Wijerathna - Department of Mathematics, University of Colombo
- Dr. Romain Jayawardene - Department of Mathematics, University of Colombo
- Dr. Thilini Piyatilake - University of Moratuwa, Sri Lanka
- Dr. Yashika Jayathunga (committee member)
- Dr. Prabhath Liyanage (committee member)
- Dr. Hasitha Erandi (committee member)
- Dr. Kushani De Silva - University of North Carolina, USA
- Dr. Nayana Wanasinghe - Department of Mathematics, University of Colombo
- Dr. Pushpi Paranamana - Saint Mary's College, IN, USA
- Dr. Kasun Fernando - Brunel University London, United Kingdom
- Dr. Sudam Surasinghe - Yale University, USA

Table of Content

Computational study of intermetallic compound

Purvee Bhardwaj[1*], **Moupiya Ghosh**[2]

[1] Department of Physical Science, Rabindranath Tagore University, Bhopal, Madhya Pradesh, 464993, India. Department of Physics, APS University, Rewa, Madhya Pradesh, 486003, India

[2] Department of Physics, Basic Science & Humanities, Institute of Engineering and Management (IEM), Kolkata, University of Engineering and Management, Newtown, Kolkata, West Bengal 700160, India.

*Corresponding author; E-mail: purveebhardwaj@gmail.com

Background

The need for these intermetallic compounds in industry and production has led to a sharp rise in their growth in recent years. Numerous intermetallic compounds with various compositions have been investigated both theoretically and empirically, and many more are now pending investigation. Material scientists have been very interested in intermetallic compounds due to their electronic, electrical, magnetic, mechanical, and thermal properties, including high tensile strength, corrosion resistance, good ductility, and thermal stability. When two or more metals are combined in specific amounts, they create intermetallics, which are solid phases that are distinctly different from their component elements. Although these materials frequently have better mechanical qualities and are more resistant to corrosion, they are typically brittle. Intermetallic compounds have garnered a lot of interest because of their varied chemical and physical characteristics, which make them promising candidates for cutting-edge technological applications. Intermetallics based on yttrium, especially YIn, are interesting because of their distinct structural, magnetic, and electrical properties. Studies using computational electronics on these materials shed light on their behaviour and aid in forecasting whether they will be suitable for real-world uses in fields like magnetism, thermoelectrics, or catalysis. With the use of computational techniques, this work aims to comprehend the electrical structure, bonding properties, and possible uses of the intermetallic compound YIn. A pressure-induced structural phase transition from the distorted tetragonal (P4/mmm) CuAu-type structure to the B2 phase is another structural phase transition is predicted for YIn [1, 2, 3, 4, 5]. The main goal of this work is to use the DFT approach to comprehend the electrical, elastic, and mechanical properties of this new class of intermetallic compounds, which include YCd, YIn, YAu, YHg, and YTl that crystallise in a CsCl-type structure. We report the ground state and electrical properties for the first time for this purpose.

Methods

YIn's electrical characteristics were examined by the application of density functional theory (DFT). The Generalised Gradient Approximation (GGA) was used to calculate the exchange-correlation functional. The Vienna Ab initio Simulation Package (VASP) was used to build the computational method, which included plane-wave basis sets and pseudopotentials. The goal of structural optimisation was to guarantee equilibrium geometries and reduce the overall energy. To gain an understanding of the electrical behaviour of the compound, the band structure, density of states (DOS), and charge density distribution were examined. Similar yttrium-based intermetallics were compared in order to find patterns and deviations.

Results and Conclusions

According to the computational analysis, YIn behaves metallically and has a sizable density of states at the Fermi level. The hybridisation of Yttrium d states and Indium p states, which leads to its distinct bonding properties, is highlighted by the band structure study. The partially ionic and covalent character of the bonding in YIn is confirmed by the charge density distribution. According to these results, YIn shows promise for use in industries that need conductive and stable materials. The obtained results confirm that this B2-type of rare-earth intermetallics has very interesting mechanical and thermal properties for structural applications. The total and partial electron density of states (DOS) were evaluated to offer a detailed explanation of the contribution of atomic orbitals in the energy bands. The ductility of the intermetallics investigated here is evaluated. We have firstly calculated lattice constants, bulk modulus, elastic constants, and mechanical properties. Furthermore, the findings lay the groundwork for additional theoretical and experimental investigation of related intermetallic compounds.

Keywords:

Intermetallic, Electronic calculations, Density Functional Theory, Band Structure Density of States

References

[1] SD Johnson, JR Young, RJ Zieve, and JC Cooley. Superconductivity in single-crystal y in3. *Solid state communications*, 152(6):513–515, 2012.

[2] Swetarekha Ram, V Kanchana, Axel Svane, SB Dugdale, and Niels Egede Christensen. Fermi surface properties of ab3 (a= y, la; b= pb, in, tl) intermetallic compounds under pressure. *Journal of Physics: Condensed Matter*, 25(15):155501, 2013.

[3] Abdessamad Sekkal, F Saidi, Abdelnour Benzair, M Sahlaoui, Claude Esling, and Jean Marc Raulot. Structural and physical properties of dycu, ndag, lacd, yin, ercu, erag, and erau rare-earth intermetallic compounds: ab initio investigations analyzed by data mining technique. *Physics of the Solid State*, 62:2305–2317, 2020.

[4] Ramesh Sharma, Gulzar Ahmed, and Yamini Sharma. Intermediate coupled superconductivity in yttrium intermetallics. *Physica C: Superconductivity and its applications*, 540:1–15, 2017.

[5] NS Stoloff, CT Liu, and SC Deevi. Emerging applications of intermetallics. *Intermetallics*, 8(9-11):1313–1320, 2000.

Mathematical models for forecasting inhibitor treatment outcomes in lung cancer

Rakesh Kumar[1], Bharti Saxena[1] Ritu Shrivastava[2] and Ramakant Bhardwaj[3*]

[1] Department of Mathematics, Rabindranath Tagore University, Bhopal, Madhya Pradesh, 464993, India.

[2] Department of Mathematics, Bahrain Polytechnic, Isa Town, 33349, Kingdom of Bahrain

[3] Department of Mathematics, Amity University, Kolkata, 700135, West Bengal, India.

*Corresponding author; E-mail: rkbharwaj100@gmail.com

Background

The increasing application of immune checkpoint inhibitors (ICIs) in treating non-small cell lung cancer (NSCLC) has underscored the urgent need for reliable predictive models to forecast individual patient responses [3]. This study presents a series of immunoediting mathematical models designed to capture the complex dynamics between tumor growth and immune response, particularly focusing on the mechanisms of resistance and treatment outcomes. We evaluate four distinct models, including a novel delayed response model, using ordinary differential equations to simulate tumor-immune interactions [1]. Our findings demonstrate that the delayed response model significantly outperforms simpler models, achieving an overall accuracy of 77% in predicting progressive disease status based solely on primary tumor measurements. By integrating biological principles of immunoediting, such as immune evasion and the emergence of resistant tumor variants, our models provide a robust framework for personalized treatment strategies [2]. This research enhances our understanding of tumor dynamics under immunotherapy and offers a clinically applicable tool for predicting treatment outcomes, aiming to improve patient management in NSCLC.

Methods

This study employed a systematic approach that integrates biological principles with mathematical formulations to develop immunoediting mathematical models capable of forecasting treatment outcomes for immune checkpoint inhibitors (ICIs) in lung cancer. The models were designed to capture the dynamics of tumor-immune interactions, focusing on the mechanisms of resistance and response to ICIs.

1. Mathematical Formulation:

We utilized ordinary differential equations (ODEs) to model the interactions between tumor cells and immune cells. The general form of the equations is as follows:

$$\frac{dT}{dt} = r_T T\left(1 - \frac{T}{K}\right) - \chi^{IT}$$

$$\frac{dI}{dt} = r_I I\left(1 - \frac{I}{K_I}\right) + \alpha T - \beta I$$

Where:

- T represents the tumor cell population.

- I represent the immune cell population.
- r_T and r_I are the growth rates of tumor and immune cells, respectively.
- K and K_I are the carrying capacities for tumor and immune cells.
- χ is the rate of immune-mediated tumor cell death.
- α and β represent immune recruitment and cell death, respectively.

Results and Conclusions

The immunoediting mathematical models presented in this study represent a significant advancement in our ability to forecast treatment outcomes for lung cancer. By bridging the gap between mathematical modeling and clinical practice, these models have the potential to support clinicians in making informed treatment decisions, ultimately improving patient outcomes in the face of this challenging disease. Continued exploration and refinement of these models will be essential for their successful integration into routine clinical care, paving the way for more personalized and effective cancer therapies.

Keywords:

Lung Cancer, Mathematical Model, Ordinary differential equation, Immunoediting, Forecasting

References

[1] Sandip Pravin Patel and Razelle Kurzrock. Pd-l1 expression as a predictive biomarker in cancer immunotherapy. *Molecular cancer therapeutics*, 14(4):847–856, 2015.

[2] SA Quezada and KS Peggs. Exploiting ctla-4, pd-1 and pd-l1 to reactivate the host immune response against cancer. *British journal of cancer*, 108(8):1560–1565, 2013.

[3] Kevin Robert Scibilia, Pirmin Schlicke, Folker Schneller, and Christina Kuttler. Predicting resistance and pseudoprogression: are minimalistic immunoediting mathematical models capable of forecasting checkpoint inhibitor treatment outcomes in lung cancer? *Mathematical Biosciences*, 376:109287, 2024.

Radial basis function-finite difference method for contaminant transport problems

W.H.D.T.Karunarathna[1,3*], **N.Kulasekera Mudiyanselage**[2] **and M.T.M.Dewasurendra**[3]
[1] Wayamba University of Sri Lanka, Kuliyapitiya, Sri Lanka
[2] Mount St Mary's University, Emmitsburg, MD, USA
[3] Postgraduate Institute of Science, University of Peradeniya, Sri Lanka
*Corresponding author; E-mail: dulashini@wyb.ac.lk

Background

The transport of contaminants in water systems can be described by the advection-dispersion equation (ADE). To solve these equations, numerical methods such as the Finite Difference Method (FDM) and the Finite Element Method (FEM) are commonly used. When employing FDM, complexities arise in implementing boundary conditions, especially those that are non-homogeneous or time-dependent. Another powerful numerical technique to tackle these problems is the Radial Basis Function-Finite Difference method (RBF-FD)[2]. The RBF-FD method is a cutting-edge approach that combines RBFs to solve differential equations in a highly accurate and efficient manner [1]. This study shows that the RBF-FD method is more effective and accurate to solve a one-dimensional ADE with constant coefficients, which describes contaminant flow for constant and oscillating boundary conditions [3]:

$$\frac{\partial}{\partial t}C(x,t) = D\frac{\partial^2}{\partial x^2}C(x,t) - u\frac{\partial}{\partial x}C(x,t) \tag{1}$$

where $C(x,t)$ is the solute concentration, D is the dispersion coefficient and u is the uniform flow velocity. The initial condition is: $C(x,0) = 0, \quad x \geq 0$. In this study, two boundary conditions are analyzed: constant and periodically fluctuating. Below equation (2) represents the constant boundary conditions (BC):

$$C(x,t) = C_0, \quad x = 0, \quad t \geq 0, \quad \text{and} \quad C(x,t) = 0, \quad x \to \infty, \quad t \geq 0. \tag{2}$$

For the second case, we considered the periodic fluctuation of concentration at the boundary $x = 0$. For these two cases, the ADE is solved numerically using the MATLAB software and the RBF-FD method.

Methods

Consider the following boundary value problem,

$$\begin{cases} \dfrac{\partial}{\partial t}C(x,t) & = DL_1C(x,t) - uL_2C(x,t), \quad x \in \Omega,\ t \in [0,T] \\ C(x,t) & = g(x,t), \qquad\qquad\qquad\quad x \in \partial\Omega,\ t \in [0,T] \\ C(x,0) & = h(x), \qquad\qquad\qquad\quad x \in \Omega. \end{cases} \tag{3}$$

where L_1 and L_2 are any linear operators. As with the interpolation problem, we assume that $C(x,t)$ is a linear combination of RBFs and polynomials. However,

notice that n is the number of neighbors, so the following process occurs locally in each cluster of nodes centered around a center node x_c.

$$C(x,t) = \sum_{i=1}^{n} \lambda_i \phi(||x - x_i||) + \sum_{j=1}^{M} \mu_i p_j(x) \tag{4}$$

The equation (4) leads to the system of equations:

$$\left(\tilde{A} = \begin{bmatrix} A & P \\ P^T & O \end{bmatrix} \right) \begin{bmatrix} \underline{\lambda} \\ \underline{\mu} \end{bmatrix} = \begin{bmatrix} \underline{u} \\ \underline{0} \end{bmatrix}. \tag{5}$$

Next, we apply the spatial operators L (L_1 and L_2) to equation (4). Therefore, since the collocation matrix $\tilde{A}$ is non-singular, we can find the λ_i and μ_i values from the equation (5), and substitute them into the system of equations produced by (4). The differentiation matrix (DM) defined as $DM = B\tilde{A}^{-1}$ is the discretized version of the operator $L(L_1, L_2)$ with B being the $1 \times (n + M)$ row vector of right hand side in equation (4). The process of constructing the DM is the RBF-FD method [2].

Results and Conclusions

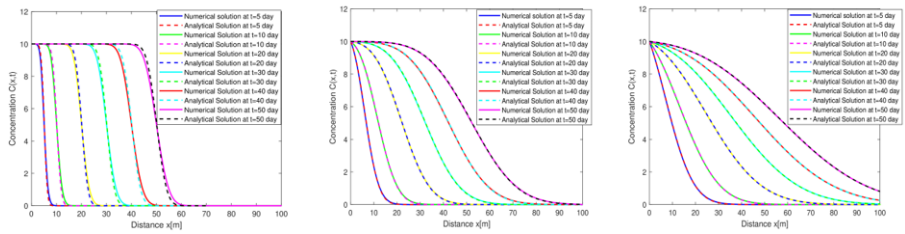

Figure 1: Comparison of numerically and analytically obtained concentration distributions with $u = 1\text{m day}^{-1}$ for different $D = 0.1\text{m}^2\text{day}^{-1}, 2.5\text{m}^2\text{day}^{-1},$ and $10\text{m}^2\text{day}^{-1}$ respectively.

To validate the numerical results against the analytical solution [3], the mean square error was calculated, yielding negligible error values on the order of 10^{-4}.

Keywords:

Inverse problems, Numerical methods, Partial differential equations, Radial basis functions.

References

[1] Fornberg B and Flyer N, A Primer on Radial Basis Functions with Applications to the Geosciences. *Society for Industrial and Applied Mathematics*, Philadelphia, PA, 2015.

[2] Larsson E, Fornberg B, A numerical study of some radial basis function-based based solution methods for elliptic PDEs. *Computers and Mathematics with Applications, 46(5),891-902*, 2003.

[3] Savovic SM, DJORDJEVICH A, Explicit finite difference solution for contaminant transport problems with constant and oscillating boundary conditions, *Thermal Science, 24(3B),2225-2231,* 2020.

Development of a geotechnical model for assessing liquefaction potential and geotechnical parameters in the greater Colombo area

I.A.N.D Idirimanna[1*], **R.M.S Bandara**[1]
[1]National Building Research Organization
*Corresponding author; E-mail: nirmanthidi@gmail.com

Background

It is a fact that the seismic events occur quite frequently in present Sri Lanka than few decades ago and also a there is a possibility of this effect increasing further. Liquefaction is a secondary effect of earthquake, where granular soil below the water table temporarily lose its strength and behave as a vicious fluid due to the sudden increase of pore water pressure. In Sri Lanka, although it is rare to find the historical data of liquefaction or related incidents, some recent studies demonstrated that there is a potential for liquefaction in some places of the island [1].

Methods

The liquefaction potential could be evaluated by using analysis of the available basic geotechnical data in the island. Here the method, originally developed by Seed and Idris (1971, 1982) with the subsequent refinement by Seed (1985)[2] has been used for the assessment of liquefaction potential in greater Colombo area. This procedure is based on the blow counts of Standard Penetration Test (SPT). Here for the analysis, more than 200 drill log data in Colombo municipal council area were gathered.

Results and Conclusions

Influence of other Geotechnical factors such as soil type variation, SPT refusal, ground water fluctuation... etc on liquefaction of Greater Colombo area was also modeled in three and two dimensional ways for the better interpretations. It is also useful to establish the regularities of properties of the sub soils for future infrastructure development. Here the RockWorks 15 software has been used for the all 3D and 2D modeling works.

Keywords:

Liquefaction, Earthquake, Vulnerability, Standard Penetration Test, Geotechnical Model

References

[1] S Premkumar and LI De Silva. Evaluation of liquefaction potential of western and eastern coastal areas in sri lanka. 2011.

[2] PK Robertson and CE Wride. Cyclic liquefaction and its evaluation based on spt and cpt: Seismic short course on evaluation and mitigation of earthquake induced liquefaction hazards. In *Proceedings of the NCEER Workshop, San Francisco, CA, USA*, volume 31, 1997.

Modeling dynamics of mutualism in prey-prey system with variable carrying capacity in the presence of predator

Randy Lee[1*], **Kening Wang**[1] **and Mahbubur Rahman**[1]
[1] University of North Florida
*Corresponding author; E-mail: n01163645@unf.edu

Background

We generalize the results of recently published work in [5] by considering the mutualism between two prey species on their variable carrying capacities in the presence of a predator species. The mutualism dynamics are represented by taking into account a fixed and a produced carrying capacities corresponding to the indirect and direct mutual interactions between symbionts. As the death rate of the predator increases, the indirect mutualism model goes through a trans-critical bifurcation, whereas, in the direct mutualism model shows a trans-critical bifurcation as well as a Hopf bifurcation.

Methods

We used XPPAUT to study the phase and bifurcation diagrams of our dynamical systems. We also used Mathematica to assist with the algebraic computations related to the steady state, Jacobian matrices, and Routh-Hurwitz criterion.

Results and Conclusions

We have examined two symbiosis models that simulate the effect of indirect and symmetrically direct symbiosis in a two prey, one predator system. These models can have the alternate interpretation of two mutualistic species withstanding the effect of predator. This is different from previously studied models about mutualism and predation [3, 2, 1]. For both models, only one species will go extinct at most. They also share a transcritical bifurcation (exchange stability) that occurs when predator death rate parameter c increases.

However, as expected, the models discerned two different functional responses will have some different behavior. The symbiosis with indirect interactions keeps the coexistence steady state stable, like the classical predator-prey model with constant carrying capacity [3, 4]. Ultimately, the coexistence steady state becomes unstable when the predator death rate gets larger. However, symbiosis with direct interaction can lead to unstable limit cycles once the predator death rate parameter increases. This unbounded growth shares similarities with other mutualism models.

Keywords:

Nonlinear differential equations, Hopf bifurcation, Limit cycles, Mathematical biology, Population dynamics.

References

[1] John F. Addicott. Stability properties of 2-species models of mutualism: Simulation studies. *Oecologia*, 49(1):42–49, 1981.

[2] M. B. Dhakne and A. B. Munde. Stability analysis of mutualistic interactions among three species with limited resources for first species and unlimited resources for second and third species. *Differential Equations and Dynamical Systems*, 20:405–414, 2012.

[3] B.S. Goh. Stability in models of mutualism. *The American Naturalist*, 113(2):261–275, 1979.

[4] Morris W. Hirsch and Stephen Smale. *Differential Equations, Dynamical Systems, and Linear Algebra*. Academic Press, 1974.

[5] E.P. Yukalova V. I. Yukalov and D. Sornette. Modeling symbiosis by interactions through species carrying capacities. *Physica*, 241(15):1270–1289, 2012.

Computational analysis of fluid dynamics in porous media: Implications in tumor therapy and industrial processes

Shazmani[1*], **Anju Saini**[1] **and Deepika Saini**[1]
[1]Graphic Era Deemed to be university
*Corresponding author; E-mail: anjusaini@geu.ac.in

Background

Fluid flow, a sub discipline of fluid mechanics, dealing with the motion of a fluid that is being subjected to unbalanced forces. Compare this with the known from clinical applications, most of drug treatments providing little or slightly more than little are not enough to eliminate malignant tumors completely, drug delivery by systemic administration is effective [3]. Thus, a more complete understanding of neoplastic process is important for the design of more therapeutic-effective molecules [1]. Modeling fluid flow in solid tumors can be done either macroscopically or microscopically [2].

The Brinkman equation has found application in many areas, such as flow in porous channel, and in biology (here, a clear example would be the flow through biological tissues). The governing equation, however, involves several parameters such as viscosity, permeability and porosity of the porous medium which need to be specified. These parameters can notably alter the velocity profile of the flowing fluid. Brinkman equation shows viscosity, permeability and porosity effects on velocity profile in porous media in which the fluid is flowing through a porous medium. Navier-Stokes equation is one of the fundamental equations in the fluid dynamics, and we have used a modified version of it, the brinkman equation, in this study.

Here we examined velocity profiles variate with different values of parameters of Brinkman equation In particular; we focus on how viscosity, permeability, and porosity influence the velocity distribution of the movie fluid in a porous media. We discuss the physical mechanisms behind fluid flow through porous media and potential industrial and biomedical applications of our results.

Methods

These docs are for a method called bvp4c which solves boundary value problems for ODEs in MATLAB. It is widely used in different fields like physics, engineering, and biology for solving boundary value problems (BVPs). It is a powerful, efficient, flexible and accurate tool for researchers and practitioners. Here, bvp4c is a collocation method to solve BVPs. Key steps are: Discretization, Collocation points, Basis functions, Residual calculation, Solution refinement etc. We solved the Brinkman equation using the bvp4c function in MATLAB. The general form of the momentum balance equation in porous media, called Brinkman model:

$$\rho\left(\frac{\partial v_i}{\partial t} + (v_i \cdot \nabla)v_i\right) = \nabla \cdot \left[-P_i + \mu(\nabla v_i + (\nabla v_i)^T) - \frac{2}{3}\mu(\nabla \cdot v_i)\right] - \left(\frac{\mu}{k} + \varphi_B - \varphi_L\right) v_i + F$$

where, $\varphi_B(r) = \frac{L_p S}{V}[P_B - P_i - \sigma_s(\pi_B - \pi_i)]$

$\varphi_L(r) = \frac{L_p S}{V}(P_i - P_L)$

At first, we converted pde into ode by similarity transformation method and then through the use of bvp4c in MATLAB further results examined.

Results and Conclusions

The Brinkman equation is then framed as a boundary value problem specified on the boundaries as velocity and pressure. We also varied the values of $[\eta]$, $[k]$, and $[p]$ across a wide range known to be observed in porous media. We calculated the velocity profile of the fluid flow for each set of parameter values. The velocity profile is largely influenced by the viscosity, permeability, and porosity values, as indicated by our results. Specifically, we found that:

- Higher fluid viscosity means lower fluid-flow velocity.
- As permeability of the porous medium is reduced, fluid flow velocity is reduced.
- Increase in porosity of the porous medium causes the fluid flow to have a higher velocity.

To our knowledge, we are the first to realize that the velocity profile has non-linear dependence on the parameter values. The velocity profile is more or less represents a flat shape which changes steeply near the edges of the porous medium and gradually upward in the interior. Using bvp4c to approximate the solution far exceeded the accuracy of the finite difference method near the boundaries. The solution also converged faster, requiring less iteration.

Molecular-level design principles: porous media with controllable hierarchical architectures employing various types of dual-porosity at a much higher specific surface area than conventional catalysts/intended catalysts for filtration, catalytic, and tissueing engineering applications. More specifically, our findings indicate the pumping profile of fluid flowing through porous medium can be adjusted by manipulating viscosity, permeability, and porosity values.

Future work can expand upon our findings by investigating the effects of other parameters (e.g., the Reynolds and Darcy numbers) on the fluid flow velocity profile in a porous medium. Moreover, numerical studies can be validated and provide physical interpretations of fluid flow through porous media by performing experimental studies.

Keywords:

viscosity, permeability, porosity, effective therapeutics, collocation.

References

[1] Judah Folkman et al. Tumor angiogenesis: therapeutic implications. *N Engl j Med*, 285(21):1182–1186, 1971.

[2] Mostafa Sefidgar, Madjid Soltani, Kaamran Raahemifar, and Hossein Bazmara. Effect of fluid friction on interstitial fluid flow coupled with blood flow through solid tumor microvascular network. *Computational and Mathematical Methods in Medicine*, 2015(1):673426, 2015.

[3] M Soltani and Pu Chen. Numerical modeling of fluid flow in solid tumors. *PloS one*, 6(6):e20344, 2011.

Sensitivity analysis and optimal control strategy for Nipah virus outbreak

Binti Mualifatul Rosydah [1,2*], **Marsudi** [1], **Wuryansari Muharini Kusumawinahyu** [1], **and Nur Shofianah** [1]

[1] Department of Mathematics, Faculty of Mathematics and Natural Sciences, University of Brawijaya, Jl. Veteran Malang 65145, Indonesia

[2] Shipbuilding Institute of Polytechnic Surabaya, Jl. Teknik Kimia Kampus ITS Sukolilo Surabaya 60111, Indonesia

*Corresponding author; E-mail: bintimualifatul@student.ub.ac.id

Background

Nipah virus (NiV) is a zoonotic virus that potentially causes outbreaks with high mortality rates, namely about 40-75%. The spread of the virus occurs through direct contact between humans and infected animals, consumption of contaminated food, or human-to-human transmission. As there is no vaccine or specific treatment for Nipah virus, a public health policy-based control is required. In this study, we developed a mathematical model to study the dynamics of Nipah virus spread. Furthermore, calculating the basic reproduction number $\mathcal{R}_0$ as an indicator of the spread of the disease, conducting sensitivity analysis of the main parameters of the model, and evaluating the effectiveness of three control strategies, namely health campaigns on exposed individuals, quarantine on infected individuals, and treatment to increase the recovery rate [3, 5]. The purpose of this study is to minimize the number of exposed and infected individuals and the control implementation cost.

Methods

The mathematical model used in this study is a compartmental model that divides the human population into five groups: susceptible (S), exposed (E), infected (I), recovered (R), and deceased (D). The transition between groups is determined by epidemiological parameters such as contact rate, infection rate, and recovery rate. The basic reproduction number $\mathcal{R}_0$ was calculated using the next-generation matrix approach, which includes the parameters of effective contact rate, transmission rate, infection rate, and recovery rate [1]. Sensitivity analysis was conducted to evaluate the effect of parameter variations such as virus transmission rate, health campaign effectiveness, quarantine compliance rate, and treatment efficiency on virus spread dynamics and control strategy effectiveness [2]. The optimal control problem was formulated to minimize a function that includes two components: the number of exposed and infected individuals, and the cost of implementing health campaigns, quarantine, and treatment. The Pontryagin Maximum Principle (PMP) is applied to solve the problem. The Forward-Backward Sweep method is used to solve optimization problem numerically [4].

Results and Conclusions

The results of the $\mathcal{R}_0$ calculation show that the effective contact rate, the duration of the incubation period, and the treatment rate are the most influence parameters in

determining the spread of the disease. Sensitivity analysis confirmed that reducing $\mathcal{R}_0$ is most effective by improving the efficiency of health campaigns and treatment.

Sensitivity analyses identified that transmission rate and quarantine compliance are the parameters that most affect the dynamics of Nipah virus spread. Enhanced quarantine compliance can reduce the number of infected individuals; reduced transmission rates through health campaigns can have a significant impact on outbreak control, and treatment is more effective when combined with strict quarantine strategies.

Health campaigns are effective in reducing infection rates in the pre-outbreak outbreak by increasing awareness and preventive behavior in the population. Quarantine had a significant impact in reducing the spread of the virus at critical stages of the outbreak by restricting interactions between infected individuals and susceptible populations. On the other hand, treatment is effective in accelerating the recovery of infected individuals and suppressing the mortality rate.

Numerical simulation results show that the optimal combination of the three control strategies significantly reduces the number of exposed and infected individuals compared to the application of one control strategy separately. With an optimally designed combination of control strategies, the implemented policy can achieve a balance between reducing virus spread and cost efficiency.

Furthermore, this study shows that total costs can be minimized by optimally allocating resources to all three control strategies. Health campaigns should be focused on the pre-outbreak stage, while quarantine and treatment are more effective in the peak and post-outbreak stages.

Keywords:

Nipah virus, mathematical model, basic reproduction number, sensitivity analysis, optimal control

References

[1] F. Brauer and C. Castillo-Chavez. *Mathematical Models in Population Biology and Epidemiology*. Springer, New York, 2012.

[2] N. Chitnis, J. M. Hyman, and J. M. Cushing. Determining important parameters in the spread of malaria through the sensitivity analysis of a mathematical model. *Bulletin of Mathematical Biology*, 70:1272–1296, 2008.

[3] N. Ilmayasinta, A. R. Soemarsono, and E. N. Rakhmawati. Model matematika penyebaran virus nipah (niv) dengan kontrol optimal menggunakan metode pontryagin maximum principle (pmp). *Jurnal Ilmiah Matematika dan Pendidikan matematika (JMP)*, 14(1), 2022.

[4] S. Lenhart and J. T. Workman. *Optimal Control Applied to Biological Models*. Chapman and Hall/CRC, New York, 2007.

[5] B. I. Omede, P. O. Ameh, A. Omame, and B. Bolaji. Modelling the transmission dynamics of nipah virus with optimal control. *arXiv preprint arXiv:2010.04111*, 2020.

Quantifying the socio-economic impacts of EV charging stations

M. Mavin De Silva[1*], **Takahiro Yabe**[2] **and Nakayama Tadachika**[3]
[1]Department of Transport Management & Logistics Engineering, Faculty of Engineering, University of Moratuwa, Katubedda, 10400, Sri Lanka and Extreme Energy-Density Research Institute, Nagaoka University of Technology, Nagaoka, Niigata, 940-2188, Japan
[2]Department of Technology Management and Innovation and the Center for Urban Science and Progress (CUSP), New York University, 370 Jay Street, Brooklyn, 11201, NY, United States
[3]Extreme Energy-Density Research Institute, Nagaoka University of Technology, Nagaoka, Niigata, 940-2188, Japan
*Corresponding author; E-mail: s225063@stn.nagaokaut.ac.jp

Background

Emerging research highlights the importance of EVCS placement in driving EV adoption and community development. Previous studies have shown that EVCSs often attract customers to nearby businesses by facilitating activities such as shopping or dining during charging times, generating demand spillovers [2]. However, these studies have limitations, including selection bias and the failure to identify comparable control groups for causal inference. Furthermore, the spatial distribution of EVCSs is closely linked to socio-demographic characteristics of neighborhoods [1], which may also influence the economic impacts of EVCSs on local businesses.

This study builds on the existing literature by employing a robust staggered difference-in-differences (DiD) methodology to estimate the causal impacts of EVCS openings on nearby businesses in NYC. By leveraging the staggered rollout of EVCS installations across the five boroughs, we aim to quantify the extent to which EVCS placement drives customer spillovers, particularly for retail and recreational establishments.

Methods

Our DiD methodology identifies treated businesses as those located within 400 meters of a new EVCS, while control businesses are selected from areas near future EVCS sites that have not yet been installed. This approach minimizes selection bias and ensures that treated and control groups are comparable in terms of neighborhood characteristics, such as socio-demographic features, business categories, and pre-existing customer volumes. The analysis incorporates visitor data collected from aggregated mobile device location records, which capture daily foot traffic to businesses. Using this data, we estimate the impact of EVCS openings on visitor volumes for treated businesses, while controlling for time-invariant business characteristics and temporal trends. Heterogeneity analyses are conducted to examine how effects vary by business type (e.g., dining, leisure, shopping) and proximity to the EVCS. Additional variables, such as EVCS type and socio-demographic features of surrounding neighborhoods, are included to assess contingent factors that influence the magnitude of spillover effects.

Results and Conclusions

The analysis reveals that EVCS installations generate significant demand spillovers for nearby businesses, with a new charging station driving a 9% average increase in daily

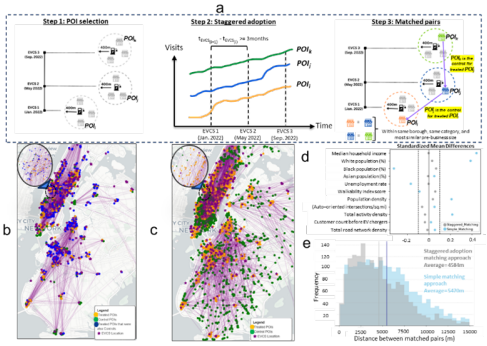

visitor volumes. This effect is particularly pronounced for businesses in recreational categories, such as dining, leisure, and shopping, where the average increase in visitor volumes exceeds 12%. Importantly, the magnitude of these spillovers diminishes with distance from the EVCS. Businesses located within 100 meters of a charging station experience the largest benefits, while those between 200 and 300 meters show more modest increases. These findings highlight the importance of proximity in capturing the economic benefits of EVCS placements. Heterogeneity analyses further reveal that EVCS type plays a critical role in influencing spillover effects. Fast-charging stations, which require shorter charging times, tend to generate smaller increases in visitor volumes compared to Level 2 chargers, which encourage longer dwell times and, consequently, higher customer engagement with nearby businesses.

This study also identifies significant socio-demographic factors that mediate the economic impacts of EVCSs. Businesses in high-income neighborhoods see disproportionately larger benefits from EVCS placements, potentially due to higher rates of EV ownership in these areas. Conversely, businesses in lower-income neighborhoods benefit to a lesser extent, suggesting that targeted subsidies or infrastructure investments may be necessary to ensure equitable economic gains. In conclusion, this study contributes to the growing body of research on EV infrastructure by providing robust evidence of the economic benefits associated with EVCS placements. By demonstrating that EVCSs can act as catalysts for local economic development, our findings offer valuable insights for policymakers, business owners, and EVCS providers seeking to balance transportation and economic objectives. Strategic investments in EV infrastructure not only promote sustainable mobility but also foster vibrant, thriving communities.

Keywords:

Electric Vehicles, Causal Impacts, Staggered EVCS, Difference-in-Difference

References

[1] Yash Babar and Gordon Burtch. Recharging retail: Estimating consumer demand spillovers from electric vehicle charging stations. *Manufacturing & Service Operations Management*, 26(3):797–813, 2024.

[2] Yunhan Zheng, David R Keith, Shenhao Wang, Mi Diao, and Jinhua Zhao. Effects of electric vehicle charging stations on the economic vitality of local businesses. *Nature Communications*, 15(1):7437, 2024.

Tracking chaotic motion: An image processing approach to analyze double pendulum systems

Sasindra R.M.N. [1], **Akalanka G.D.M.**[1] **Basnayaka D.T.**[1] **and Lakshan K.A.S.**[1*]
[1] Department of Physics, Faculty of Science, University of Ruhuna, Sri Lanka
*Corresponding author; E-mail: *kaslakshan@phy.ruh.ac.lk

Background

Chaotic motion is a motion in a dynamic system that is totally random and unpredictable, even though it is governed by deterministic laws [1]. In practical applications, there exist numerous scenarios in which chaotic motion is utilized, such as Double Pendulum, Planetary Ring Systems, Fluid Dynamics, etc. [3]. Since the unpredictability of the chaotic motion and the difficulty of simplification of the equations, there is no direct method to obtain a formula for this kind of motion. Therefore, there is a need for a simple method to develop a formula for a chaotic motion. This study primarily examines the dynamics of the double pendulum and aims to develop a straightforward and efficient method for deriving a formula through the use of image processing techniques and a numerical approach known as interpolation. The application of polynomial interpolation facilitated the derivation of an equation of motion that accurately characterizes the behaviour of the double pendulum system. In literature, there are some equations of motion for the double pendulum system, and those equations are applicable only for small oscillations [4].

$$(m_1 + m_2)l_1^2\ddot{\theta}_1 + m_2 l_1 l_2 \ddot{\theta}_2 \cos(\theta_1 - \theta_2) + m_2 l_1 l_2 \dot{\theta}_2^2 \sin(\theta_1 - \theta_2) + (m_1 + m_2) l_1 g \sin(\theta_1) = 0$$

$$m_2 l_2^2 \ddot{\theta}_2 + m_2 l_1 l_2 \ddot{\theta}_1 \cos(\theta_1 - \theta_2) - m_2 l_1 l_2 \dot{\theta}_1^2 \sin(\theta_1 - \theta_2) + m_2 l_2 g \sin(\theta_2) = 0$$

Where m_1 and m_2 are the point masses, θ_1, and θ_2 are the angles of two masses, and l_1 and l_2 are the lengths of the suspenders. Since this is only valid for small oscillations, it is not ideal for real-world large oscillations [1], [2]. Furthermore, those equations did not consider the energy loss that occurs during each oscillation. Therefore, this study focuses on deriving an equation concerning large oscillations and energy loss.

Methods

In this study, the apparatus for the double pendulum was assembled, and oscillations were conducted while the experiment was recorded using a fixed camera. Then, a digitalized image processing algorithm was created using Python programming to analyze the double pendulum system. The research worked through the PyCharm Integrated Development Environment (IDE) for coding and executing the programs. Image processing technique, video processing technique, and interpolation method played a crucial role in developing the system for this research. The video processing part mainly focuses on running through the frames in the video and uses those frames for further analysis. An image processing technique was employed to detect objects within the video frames by identifying and filtering pixels based on their RGB (Red, Green, Blue) values. Then, the x and y values of the filtered pixels are used to calculate the center coordinates of the two pendulums. After defining a reference point within the frame, it can be calculated the angle of the two bodies with respect

to the reference point. After getting the two angles, they can be plotted in two plots with respect to the frame. The interpolation method is used to initialize the smooth curves and formulas to describe the motion of the double pendulum in a known time.

Results and Conclusions

Due to energy losses, the motion of the masses beyond the observed video cannot be accurately predicted. However, the motion of the two masses within the video frames can be estimated with reasonable accuracy. The degree of the interpolation formulation cannot be precisely determined but is inferred based on the behavior of the coefficients of the time variable (X-axis). The accuracy mainly depends on the number of frames. If the number of frames is low, the accuracy of the interpolation curves and the polynomials is high. By executing the program on multiple small video clips, we can achieve results with enhanced accuracy. The main reasons for the deviations of the experimental graph from the theoretical graph are that the theoretical graph considers only small oscillations and does not consider the energy loss.

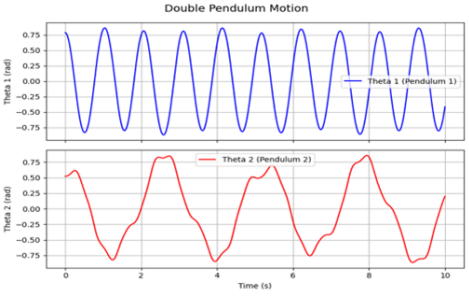

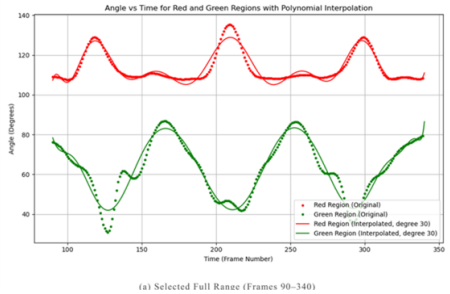

(a) Selected Full Range (Frames 90–340)

(i) Interpolation Formula for Upper Pendulum

$\theta = -(6.45210^{(}-13))t^{1}0 + (7.57410^{(}-10))t^{9} - (3.98410^{(}-7))t^{8} + (1.23710^{(}-4))t^{7} - (2.50810^{(}-2))t^{6} + (3.472)t^{5} - (332.4)t^{4} + (2.17210^{4})t^{3} - (9.27710^{5})t^{2} + (2.33810^{7})t - 2.6410^{8}$

(ii) Interpolation Formula for Lower Pendulum

$\theta = (3.76610^{(}-12))t^{1}0 - (4.22610^{(}-9))t^{9} + (2.12810^{(}-6))t^{8} - (6.33710^{(}-4))t^{7} + (0.1235)t^{6} - (16.47)t^{5} + (1521)t^{4} - (9.60910^{4})t^{3} + (3.97510^{6})t^{2} - (9.72210^{7})t + 1.06810^{9}$

Keywords:

Chaotic Motion, Double Pendulum, Image Processing, Polynomial, Interpolation, Dynamic System Modeling

References

[1] Rafał Kwiatkowski. Dynamic analysis of double pendulum with variable mass and initial velocities. *Procedia Engineering*, 136:175–180, 2016.

[2] RB Levien and SM Tan. Double pendulum: An experiment in chaos. *American Journal of Physics*, 61:1038–1038, 1993.

[3] Hollis Williams. A simple classroom double pendulum. *The Physics Teacher*, 60(9):768–770, 2022.

[4] Boran Yesilyurt. Equations of motion formulation of a pendulum containing n-point masses. *arXiv preprint arXiv:1910.12610*, 2019.

Modelling the dynamics of viral marketing based on SIR epidemiological model

K.P.C.Sewwandi [1*] **and S.D.Perera**[1]
[1] Department of Decision Sciences, University of Moratuwa, Moratuwa, Sri Lanka
*Corresponding author; E-mail: sewwandikpc.20@uom.lk

Background

In today's world, businesses have paid more attention to using modern marketing concepts like viral marketing rather than traditional marketing methods to adhere to the rapid evolution of buyers' behaviors. According to the literature, viral marketing is used to spread product or service information from one person to a few more people using the internet [3]. Identifying the dynamics of viral marketing before launching a viral marketing campaign is important for its success.

The diffusion of product information in a viral marketing context is similar to the spread of a virus in an Epidemiological context [2]. Therefore, the SIR epidemiology model, also known as the Susceptible-Infectious-Recovered model, can be used to analyse the diffusion of a product information in viral marketing context [5]. It divides individuals in the viral marketing process into three sub-classes known as Susceptible (S), Infected (I) and Recovered (R) [4]. Further, this model identifies the connection among these three classes through two parameters known as Infectivity rate (β) and Recovery rate (γ) [4]. Moreover, the practical implications of viral marketing theories can be further developed due to the absence of an accepted model to guide the research in this area [1]. Therefore, the objective of this research is to model the dynamics of viral marketing based on a quantitative analysis of the SIR Epidemiological Model.

Methods

The objective of this research is achieved by modelling how varying β and γ simultaneously affect a viral marketing campaign performance through a numerical simulation and testing the validation of the model using real-world data. It was done by first solving the differential equations in the SIR Epidemiological model using 'odeint' function from the SciPy library. A sensitivity analysis was carried out to investigate the dynamics of viral marketing with respect to parameter variability. Further, the dynamics of Infected curve (I) was plotted by varying one parameter while keeping the other constant in order to analyze how the number of days needed to reach the peak and the total number of infected people at the peak vary with β and γ separately.

Real-world data for the search terms 'BlackBerry' and 'Myspace' was downloaded from the Google Trends tool in order to assess the model's validity. The 'Minimize' function with the 'Nelder-Mead' method from the 'scipy.optimize' package was used to find the optimal values for β and γ by minimizing the sum of the squared difference between real-world data and the model's numerical solutions. The aim of the optimization is to ensure two models accurately capture the dynamics of viral marketing for two datasets.

Results and Conclusions

At the end of the simulation, the results revealed that both the β and γ had a significant simultaneous impact on the change in the number of S, I and R individuals within a viral marketing campaign. The visualizations for the variations of the total number of infected people at the peak and the number of days to reach the peak revealed the rates at which these variables change with respect to changes in β and γ. According to the results of model validation, it was evident that the model introduced in this research was able to accurately capture the real-world viral marketing process including the gradual increase, peak and gradual decline in virality by selecting appropriate initial values. Altogether, the knowledge generated in this research highlights the importance of incorporating the dynamics of the target market behavior when developing marketing plans.

However, there are some limitations to this research such as the model introduced is not applicable for accurately modelling viral marketing processes with multiple peaks. The model has to be extended by adding more parameters to model viral marketing processes with multiple peaks.

Keywords:

marketing, viral marketing, SIR epidemiological model, simulation, model validation

References

[1] Gavin L. Fox and Stephen J. Lind. A framework for viral marketing replication and mutation. *AMS Review*, 10:206–222, 2020.

[2] Ping Jiang, Xiangbin Yan, and Liyan Wang. A viral product diffusion model to forecast the market performance of products. *Hindawi-Discrete Dynamics in Nature and Society*, pages 1–10, 2017.

[3] Julia Kagan, Amilcar Chavarria, and Pete Rathburn. Viral marketing: What it is, how it works, examples, pros and cons, 2022. Accessed: 2024-06-30.

[4] Helena Sofia Rodrigues and Manuel Fonseca. Viral marketing as epidemiological model. *Cornell University-Physics and Society*, pages 946–955, 2015.

[5] J.G.S.C. Sampath, S.S.N Perera, and S.D. Perera. Susceptible-infectious-recovered model for identifying the dynamics of viral marketing. *International Conference on Multidisciplinary Approaches in Science*, pages 1–6, 2021.

Application of fuzzy logic in river water quality modelling for analysis of industrialization on Noyyal river

Mary Rose Mala. D[1*] **and S.Priyadharshini**[2]
[1] St.Joseph's College for Women,Tirupur, TamilNadu, India
[2] Kongu Vellalar Matriculation Higher Secondary School, Tirupur, Tamil Nadu, India
*Corresponding author; E-mail: dmalaamj@gmail.com

Background

Rivers are vital to human life, serving as essential sources of water for various needs and holding strategic significance worldwide. Many cities have developed along rivers due to their importance. However, increasing population and developmental activities have led to substantial waste generation, adversely impacting surface water quality through urbanization and industrialization [2].

This research focuses on assessing the effects of industrialization on the water quality of the Noyyal River using a Fuzzy Water Quality Index (WQI) model. Water quality data from four key locations along the lower Noyyal River were analyzed, incorporating various water quality parameters to develop the model.

Beyond providing fresh water, rivers play a crucial role in managing municipal and industrial wastewater. Ground water pollution prevention has emerged as a critical concern. River water quantity measures the remaining volume in natural reservoirs after extraction by treatment plants. Despite fluctuations in river water levels, these waters often contain high levels of dissolved ions, particulate matter, and living organisms. A common method for evaluating river water quality is the Water Quality Index (WQI) [1].

Numerous studies in India have analyzed the water quality of various rivers, with results evaluated for their suitability for human consumption. However, the Noyyal River has received relatively little attention regarding its water quality consistency. Water quality indices, like the drinking Water Quality Index, have been employed to determine the river's fitness for human use.

This study seeks to evaluate the effects of industrialization on surface water quality using a Fuzzy Water Quality Index model. It offers a comprehensive understanding of the factors influencing the Noyyal River's water quality. This research offers detailed insights into:

(i) Water quality modeling of the Noyyal River using a fuzzy logic approach.

(ii) The Water Quality Index (WQI) of the Noyyal River.

(iii) The effects of industrialization on the river's water quality.

(iv) Analyzing the river's self-purification capacity by assessing the strength of the Noyyal River and comparing WQI values at four specific locations.

Methods

The water quality crisp data from four locations was converted into fuzzy data using fuzzy numbers assigned to each parameter based on expert opinions. A fuzzy score for each parameter was calculated using the discharge standards set by the Central Pollution Control Board (CPCB). This fuzzy score was then multiplied by the weightage

assigned to each parameter. The overall water quality at each location was represented as a single index, calculated as the sum of the weighted fuzzy scores across all parameters.

The Noyyal River Basin was chosen for the development of the Water Quality Index. Four locations within the river basin were selected for this study. A total of 12 water quality parameters, including pH, electrical conductivity, carbon dioxide, bicarbonate, chlorine, sulfate, calcium, magnesium, sodium, potassium, and others, were analyzed based on CPCB quality criteria. The initial data for these parameters from the selected locations was transformed into fuzzy data. The subsequent steps involved defining the appropriate fuzzy numbers and determining the membership functions for each parameter to construct the fuzzy Water Quality Index model.

After defining the fuzzy numbers, the weightage for each parameter is calculated for the Water Quality Index (WQI) model. The crisp data for the water quality parameters from the selected four locations is normalized using the standard limits set by the Central Pollution Control Board (CPCB). The average fuzzy score for each parameter across all four locations is then determined. This normalized fuzzy score is multiplied by the weightage of the respective parameter. If the normalized value approaches one, it indicates that the parameter exceeds the CPCB limits. For instance, if the electrical conductivity (EC) exceeds 2,500 mg/L, its normalized value is set to 1. The individual scores for each parameter are then summed up, and the final result represents the Fuzzy Water Quality Index.

Results and Conclusions

The study highlights the application of a fuzzy mathematical model to evaluate the Water Quality Index (WQI) of the Noyyal River, with values near zero indicating poor water quality and values near one denoting good quality. The findings reveal that industrialization has adversely impacted the river's water quality, with the Kulathupudhur station showing poorer quality compared to Karumaarampalayam, which has the best WQI in the area. The study emphasizes the importance of regular monitoring by the state pollution control board to track trends, ensure compliance with pollution regulations, and implement effective pollution control measures. Correlation and principal component analyses identify industrial, domestic, sewage disposal, and agricultural runoffs as significant contributors to pollution, with a clear trend of worsening water quality over time due to industrial development.

Keywords:

Climate change, fuzzy logic, industrialization, water pollution, water quality model

References

[1] JK Bassin, MR Sharma, and AB Gupta. Water quality modelling of rivers in hilly region. *ISH Journal of Hydraulic Engineering*, 15(3):1–10, 2009.

[2] Faye L. Jackson, Robert J. Fryer, David M. Hannah, Colin P. Millar, and Iain A. Malcolm. A spatio-temporal statistical model of maximum daily river temperatures to inform the management of scotland's atlantic salmon rivers under climate change. *Science of The Total Environment*, 612:1543–1558, 2018.

Measuring black-swans of IT projects: A socio fuzzy consensus approach for benefit management

D.R.Perera[1*]
[1]Department of Management and Finance, General Sir John Kotelawala Defense University, Ratmalana, Sri Lanka
*Corresponding author; E-mail: dhinesha_drp@kdu@ac.lk

Background

Benefits are the strategic project value that flows from an organizational asset that is either cost-oriented or good-will. Benefit process consists of four phases namely benefit identification, realization planning, monitoring and measuring and benefit realization which occurs sequentially [5]. This accounts to processual benefit management and evaluation. The scope of the study is mega IT projects facilitating operational automation. Benefits of organizational projects are either targets or outcomes. Postmodern automation focus on long term outcomes and short-term targets. However, the leap in scope from outcomes to targets is challenging because the measuring techniques are not accurate nor it is systematical or unified to tech projects. Ninety percent of projects benefits are short term but non-quantifiable like customer value, investor relationship, employee satisfaction etc [1]. These intangible targets cost about seventy-eight percent project failure or mal-functioning and dying projects [4]. Benefits are fuzzy in nature and hence vague and ambiguous with difficulty to identify and measure. The project losses that are unmeasured lead to mismanagement of the project lifecycle and post governance. The study objectives were motivated by the benefit realization policy that is lacking in most organizations. Study presented a novel fuzzy framework to measure the extent to which project targets are realizable. Also, the framework incorporated fuzzy approach to analyze the stratification of benefit from target(T), through incremental enlargement(I) to target reach (TR).

Methods

The study administered a survey among nineteen IT managers and four interviews to collect and analyze through data simulation and socio fuzzy consensus. The benefit realization (BR) framework was devised using five intangible benefit factors known as project component variables (PC var). These were customer(C), cost savings(CS), stakeholder value(S), Operation Automation (OA) and HR cost(HC). Novel fuzzy inference approach was used with fuzzification, inference (FIS) and defuzzification [3]. The benefits were pairwise input to FIS that generated five variances of BR. The managers' (ITM) views were obtained to generate nine fuzzy rules for BR simulations. Socio fuzzy approached adopted opinions from four managers pertaining to the agreement and level to which benefits are realized through opinion sourcing method. Approximate reasoning and rational logic utilized in this method [2].

MATLAB and NVIVO were used for analysis. The benefit was dissected to elucidate the T. Hence, targets are intangibles PC variables which are subject to progressive target achievement levels or strata in the different project phases from initiation, growth and end. Finally, the benefit realization extents and levels were ascertained. The unit of analysis was the ITM and embedded unit of analysis was the individual project subject to BR analysis. The data was validated through a site triangulation. The trustworthiness was ensured by the cross-survey between IT and HR, finance department managers. Since automation is cross-functional IT can be correlated with the strategic fields where managers are witnesses for BR.

Results and Conclusions

(C), (S), (OA),(HC) and (CS) are intangible auxillary long-term oriented project outcomes. The classification of intangibility is based on organizational performance, measurability and quantification. The FIS results show that BR has five linguistic hedges which has quantification computational numbers .FIS generated five variances of BR namely- always, on most occasions, sometimes, seldom and never. The socio simulated sentiments revealed that benefits are achieved fully, partially or not at all as conceded by most ITM. The study established that there are intangible uncalulable benefits that are fuzzy and have a positive relationship with total BR.

Rule 1: If OA is "low" and CS is "high" then; BR is "sometimes" Rule 2: If OA is "low" and CS is "medium" then; BR is "seldom" Rule 3: If OA is "low" and CS is low then; BR is "never". Rule 4: If OA is "medium" and CS is "high" then; BR is "on most occasions". Rule 5: If OA is "medium" and CS is "medium" then; BR is "sometimes" Rule 6: If OA is "medium" and CS is "low" then; BR is "seldom" Rule 7: If OA is "high" and CS is "high" then; BR is "always". Rule 8: If OA is "high" and CS is "medium" then; BR is "on most occasions". Rule 9: If OA is "high" and CS is "low" then; BR is "sometimes".

The study implies a systematic BR framework that has utility and functional value. Extending policy implications, project owners and developers can use the benefit framework to classify and measure BR. Most of the project benefits are rather intangible. Hence, it is challenging to monitor BR unless a systematic science can be adopted. Hence BR framework is calculating and quantifying the nonprofit good of projects. The project managers can find the accountability towards investors and future stakeholders as the framework will help quantification of non profit targets and outcomes. The strategic value measured will forecast the project decisions of managers as well. The nonprofit short termed benefits of Automation has futuristic utilitarianism effect on society and stakeholders from rhetoric perspective. Future studies to explore the fuzzy benefit realization with the application of socio fuzzy consensus to ascertain clarity of vague non-calculable short term benefits. The systematic approach will increase the return on investment gained by non-monetary factors.

Keywords:

Benefits, FIS, Intangibles, IT, Socio-fuzzy consensus

References

[1] Monique Aubry, Sanaa El Boukri, and Viviane Sergi. Opening the black box of benefits management in the context of projects. *Project Management Journal*, 52(5):434–452, 2021.

[2] Richard E Bellman and Lotfi Asker Zadeh. Decision-making in a fuzzy environment. *Management science*, 17(4):B–141, 1970.

[3] Ashok Deshpande. Memories of a meeting with professor zadeh and his wife fay. *On Fuzziness: A Homage to Lotfi A. Zadeh–Volume 1*, pages 129–132, 2013.

[4] Yogesh K Dwivedi, Karthik Ravichandran, Michael D Williams, Siân Miller, Banita Lal, George V Antony, and Muktha Kartik. Is/it project failures: a review of the extant literature for deriving a taxonomy of failure factors. In *Grand Successes and Failures in IT. Public and Private Sectors: IFIP WG 8.6 International Working Conference on Transfer and Diffusion of IT, TDIT 2013, Bangalore, India, June 27-29, 2013. Proceedings*, pages 73–88. Springer, 2013.

[5] Jea Ward, Phil Taylor, and Paul Bond. Evaluation and realisation of is/it benefits: an empirical study of current practice. *European Journal of Information Systems*, 4(4):214–225, 1996.

Socio-economic determinants of out–of–pocket health related expenses among households with elders in Sri Lanka

Kodikara K.A.S.P [1*] **and Perera E.L.S.J**[2]
[1] Department of Census and Statistics, Sri Lanka
[2] Department of Demography, University of Colombo, Sri Lanka
*Corresponding author; E-mail: shyamaliekodikara@gmail.com

Background

Sri Lanka has undergone notable demographic and epidemiological transitions over the last few decades. The demographic transition has led to a rapid increase in the elderly population while the epidemiological transition has shifted morbidity patterns towards non communicable diseases which are highly associated with aging [1, 4]. This has increased the demand for caregiving. The absence of long term elderly care within public health system of the country has compelled those in needs to rely on private care facilities [2]. As a result many families with elderly members requiring long term care or treatment for chronic diseases, who are unable to afford high healthcare costs, face significant financial burdens. Further, unavailability of a social security scheme that cover the entire population increases the burden of healthcare expenses of the elderly. Despite this, evidence on the nature of health related expenditure associated with older ages remains limited. This study aims to identify socio-economic determinants of out–of–pocket healthcare expenditure among elderly households in Sri Lanka [3].

Methods

The study employed a cross-sectional design and data from the Household Income and Expenditure survey (HIES)-2016, conducted by the Department of Census and Statistics. Unit of analysis was a household, with a sample size of 9,230 households having elderly members representing 2,337,082 households. Descriptive statistics were used to identify significant predictors followed by binary logistic regression analysis using SPSS version 22[5]. Socio-economic and demographic conditions of the household and its members were taken into account with specific focus on the elderly within the household. The explanatory factors that affect household decisions in accessing health facilities were identified in three distinct groups, namely, (a) household level characteristics, (b) factors pertaining to characteristics of household members and (c) external factors. Two models were developed to assess the impact of both household level and external factors and factors related to characteristics of household members on incurring out of pocket healthcare expenses.

Results and Conclusions

The findings revealed that being in a higher income quintile, located in a rural area, living in their own houses or living in houses provided by employer or other (rent free, relief payment or compensated) and having a private healthcare facility in close vicinity are significantly associated with incurring out of pocket healthcare expenses of elderly households. Household size and indebtedness are found to be not significant. Also, having a household head that is either married or widowed/divorced/separated with secondary or tertiary level education, having chronically ill members within

the household and having children in the household were found to be significant. Total number of income earners, gender of the head of the household and whether the household head is an elderly or a non-elderly were not significantly associated with incurring out of pocket healthcare expenses. Results further revealed that as the disposable income gets curtailed due to other essential costs such as house rent, households are unlikely to incur out of pocket expenses on healthcare. It implies that there are elderly households that can afford to obtain the service of private healthcare services without facing financial hardships. But elderly households in rural areas with chronically ill members and children are faced with a higher risk of incurring out of pocket health expenses. A reduction in the demand for state healthcare services from high income households caused by widespread availability of private healthcare services will enable these low-income households to comfortably use the free healthcare services of the government. Results suggest that public private partnerships should be encouraged in the healthcare industry especially in the area of geriatric care.

Keywords:

Out–of–pocket healthcare expenditure, aging population, long term healthcare, households with elders

References

[1] WI De Silva. *Sri Lanka: Paradigm shifts in population.* National Centre for Advanced Studies in Humanities and Social Sciences, 2015.

[2] Saroj Jayasinghe. Illness and social protection: an agenda for action in sri lanka. *Sri Lanka Journal of Social Sciences*, 33(1-2), 2013.

[3] Rashidul Alam Mahumud, Abdur Razzaque Sarker, Marufa Sultana, Ziaul Islam, Jahangir Khan, and Alec Morton. Distribution and determinants of out-of-pocket healthcare expenditures in bangladesh. *Journal of Preventive Medicine and Public Health*, 50(2):91, 2017.

[4] Sunethra Perera. *Ageing population of Sri Lanka: emerging issues, needs and policy implications: thematic report based on census of population and housing 2012.* United Nations Population Fund, 2017.

[5] Saroje Kumar Sarkar and Habshah Midi. Importance of assessing the model adequacy of binary logistic regression. *Journal of Applied Sciences*, 10(6):479–486, 2010.

A model of Glucose, Insulin, β-cell, receptor, and Cortisol ($GI\beta RC$) dynamics

Mahbubur Rahman[1*], **Nicklaus Edwin Bassett**[1]
[1] University of North Florida
*Corresponding author; E-mail: mrahman@unf.edu

Background

Type-2 diabetes has been called a "global public health crisis" and its pathogenesis is desirable to study [3]. A fruitful avenue of study has been modeling insulin, glucose, and β-cell masses as quantities in a dynamical system [4]. Extensions of popular models include quantities such as insulin receptors, modeling insulin-sensitivity dynamically [2]. The HPA axis and excessive secretion of glucocorticoids are known to be related to Type-2 diabetes [1]. We study an augmentation of an existing model, including the glucocorticoid cortisol's concentration in plasma as a modeled dynamic quantity.

Methods

We present a five-dimensional dynamical model of β-cell, insulin, and glucose masses in plasma, modeling in addition the fraction of functioning insulin receptor sites, and the concentration of cortisol in plasma. We numerically analyze the ensuing system's stability and present some algebraic analysis as well. Qualitative behavior of the system is determined in full. Forcings are applied to the system numerically to measure the effect of outside interference such as food intake or external stressors, in the form of smooth impulses added to relevant system dynamics.

Results and Conclusions

We find that the produced model possesses three fixed points, with two being stable sinks and one being a saddle point. Large and quick increases in glucose, such as from some kinds of food intake, are found to be uniquely difficult for the system to regulate. The physiological fixed point corresponding to a healthy body is found to become unstable if receptor counts become too low. Applying forcings show numerical evidence of how cortisol can impair the system's ability to regulate glucose effectively. These findings replicate empirical findings regarding the metabolic system and provide support for the importance of cortisol in understanding pathological metabolic behavior.

Keywords:

Dynamical systems in biology, Mathematical modeling or simulation for problems pertaining to biology, Applications to the sciences.

References

[1] O Chan, K Inouye, M C Riddell, M Vranic, and S G Matthews. Diabetes and the hypothalamo-pituitary-adrenal (hpa) axis. *Minerva endocrinologica*, 2003.

[2] Ryan D. Hernandez, Danielle J. Lyles, Daniel B. Rubin, Thomas B. Voden, and Stephen A. Wirkus. A model of β-cell mass, insulin, glucose, and receptor dynamics with applications to diabetes. Technical report, Biometric Department, MTBI Cornell University, 2012.

[3] Frank B. Hu. Globalization of diabetes: the role of diet, lifestyle, and genes. *Diabetes Care*, 2011.

[4] Brian Topp, Keith Promislow, Gerda Devries, Robert M. Miura, and Diane T. Finegood. A model of β-cell mass, insulin, and glucose kinetics: Pathways to diabetes. *Journal of Theoretical Biology*, 2000.

Optimizing weekly-period cyclical lockdown policies: A simulation study using the A-SIR model

Benny Yong[1*] **and Arief Anbiya**[2]

[1] Center for Mathematics and Society, Department of Mathematics, Parahyangan Catholic University

[2] Independent Researcher

*Corresponding author; E-mail: benny_y@unpar.ac.id

Background

A better alternative strategy that can balance between subsiding the COVID-19 pandemic and sustain economic activity should be considered and carefully studied. One possible alternative is periodical lockdown, in which there is an alternating phase between short-term lockdown and short-term normal activity. There is a study that uses a modified SIDHARTE model to simulate an FPSP (Fast-Periodic-Switching-Policy) [1], in which their constant infection rate can alternately be maximized or damped according to the cyclical lockdown by adding a factor that changes value either 0.175 when there is lockdown or 1 when there is no lockdown. However, the simulation can be made more realistic by using infection and recovery rates that actively vary in time and conform with the real COVID-19 data.

Methods

The cyclical lockdown in this paper and in [1] is defined as the intervention of alternating states between X days of free activity and Y days of lockdown. Here we use weekly period, so that $X + Y = 7$. We use a damped Adaptive SIR (A-SIR) epidemic model with nonconstant infection and recovery rates (1). The model uses the same damping term as [1]: the infection rate is either multiplied by $\mathcal{D} = 0.175$ when there is lockdown (damping the infection), or by $\mathcal{D} = 1$ when there is no lockdown (maximizes the infection).

$$\begin{aligned} \frac{dS}{dt} &= -\mathcal{D}(t; X, Y)\beta(t)SI, \\ \frac{dI}{dt} &= \mathcal{D}(t; X, Y)\beta(t)SI - \alpha(t)I, \\ \frac{dR}{dt} &= \alpha(t)I, \end{aligned} \tag{1}$$

We include real-world COVID-19 data in the United States (www.worldometers.info), with March 1st 2020 as the initial time, to estimate the nonconstant infection and recovery rates using the Method of Variational Imbedding (MVI) and a Fixed Point Iterative technique presented in [2]. Since the United States did not implement cyclical lockdown, we estimate the rates based on system (1) with $X = 7, Y = 0$. Notice that $X = 7, Y = 0$ means $\mathcal{D} = 1$ for all time. To determine the best-fit rates $\beta(t), \alpha(t)$ for a particular country, we use the MVI that conforms with the real-world data. We set a particular date d_0 as $t = 0$, and let $\mathcal{S}_i, \mathcal{I}_i$ be the real-world data of the susceptible population and total active cases, respectively, at day $i \geq 0$. Between two consecutive

days inside $[i, i+1)$, we will estimate $\alpha(t), \beta(t)$ as constants α_i, β_i. We make the data to be more dense by approximating $\mathcal{S}_{i+0.25}, \mathcal{S}_{i+0.5}, \mathcal{S}_{i+0.75}$ and $\mathcal{I}_{i+0.25}, \mathcal{I}_{i+0.5}, \mathcal{I}_{i+0.75}$ by simple linear interpolations. Next define

$$L_S(t) = \frac{dS}{dt} + \beta(t)SI, \quad L_I(t) = \frac{dI}{dt} - \beta(t)SI + \alpha(t)I, \tag{2}$$

and define the functional

$$\mathcal{L}(S, I, \alpha, \beta) = \int_i^{i+1} \left[(L_S)^2 + (L_I)^2 + \sum_{j=0}^{4} \delta(t - t_j^*)(S(t) - \mathcal{S}_{t_j^*})^2 + \sum_{j=0}^{4} \delta(t - t_j^*)(I(t) - \mathcal{I}_{t_j^*})^2 \right] dt \tag{3}$$

where $t_j^* = i + 0.25j$ for each interval $[i, i+1)$. The functional $\mathcal{L}$ is non-negative and has minimum value 0 that is attained if and only if $L_S = L_I = 0$ and if S, I equal the real-world data points (and its interpolation) $\mathcal{S}_{t_j^*}, \mathcal{I}_{t_j^*}$ at $t = t_j^*$. Thus, the functions S, I, α, β that minimize (3), also satisfy (1) with $X = 7, Y = 0$ and conform with the real-world data. We minimize the functional in a numerical approach by first discretizing the integral and find a critical point using a fixed point iterative method.

Results and Conclusions

We found that the result of the simulation using the A-SIR model (with $X = 7, Y = 0$) approximates the real-world data accurately. We then proceed to simulate several scenarios of weekly-period cyclical lockdown using the A-SIR model with the damping function and compare our result with [1]. In our model and simulation, the $[X, Y]$ cyclical lockdown starts from the time when the total infection reaches 1% of total initial population. Using the weekly period, we found that the total infection curve will flatten without encountering another high peak for $X < 5$. For $X = 5$ the curve forms a relatively high peak before flattening, while for $X = 6$ the curve forms the highest peak (approximately 7 million) before flattening. Different from [1], our results allow more working days per week: the infection curve in their model only dissipate for the case $X = 0, 1, 2$ working days in each weekly period. .

Keywords:

epidemiology, dynamical systems, mathematical modeling, simulation of models, inverse problems.

References

[1] Michelangelo Bin. Post-lockdown abatement of covid-19 by fast periodic switching. *PLOS Computational Biology*, 17(1):1–34, 2021.

[2] Tchavdar T. Marinov. Adaptive sir model with vaccination: simultaneous identification of rates and functions illustrated with covid-19. *Scientific Reports*, 12(15688):1–13, 2022.

Dynamical analysis of lumpy skin disease model with disinfection and culling

Rizka Putri Handayani[1], **Isnani Darti**[1*], **Agus Suryanto**[1], **and Nur Shofianah**[1]
[1] Department of Mathematics, Faculty of Mathematics and Natural Sciences, University of Brawijaya, Malang, Indonesia
*Corresponding author; E-mail: isnanidarti@ub.ac.id

Background

Lumpy Skin Disease (LSD) is basically spread by the virus named lumpy skin disease virus. LSD is an acute infectious disease that affects cattle, especially buffalo and cows. The symptoms of LSD include enlarged lymph nodes, loss in appetite, and skin nodules that appear anywhere on the body [4]. Based on economic point of view, LSD has become an enormous threat for livestock-dependent countries, especially for developing countries of Africa and Asia [3]. Lumpy skin disease virus transmitted by insect vectors such as mosquitoes, flies, and ticks. In addition, contaminated grass, water, and equipment can transmit the disease [1]. LSD's virus is not zoonotic [2]. Food and Agriculture Organization [5] recommends prevention by disinfection and culling as a control to reduce the transmission of LSD. In this research, we present a new mathematical model with addition of disinfection and culling parameters to understand the dynamics of the LSD. A mathematical model is formulated with six-dimensional system of ordinary differential equations, namely three subpopulations of cow populations (susceptible, infected, and recovered), two subpopulations of mosquito populations (susceptible and infected), and virus in the environment. This model considers transmission routes including mosquito transmission, environmental transmission, and direct transmission from cow to cow.

Methods

The study begins by defining the invariant region, establishing conditions for a unique positive and bounded solution, determining an equilibrium points, calculating the basic reproduction number and the stability properties of equilibrium points, specifically focusing on the disease-free equilibrium and the endemic equilibrium. An equilibrium solution for the model system is obtained by setting the derivatives equal to zero and solving the algebraic equations. The basic reproduction number ($\mathcal{R}_0$) is calculated to assess disease transmissibility. Sensitivity analysis is performed to identify key parameters influencing $\mathcal{R}_0$.

Results and Conclusions

We show the model is well-posed through positivity and boundedness of the state variables. Two equilibrium points, i.e. disease-free (E_0) and the-endemic equilibrium point (E_1) are established. The basic reproduction number of the model was determined and the stability of disease-free equilibrium points was shown depend on $\mathcal{R}_0$. The stability of endemic equilibrium points was shown depend on Routh-Hurwitz condition. Sensitivity analysis to identify the most sensitive parameters was conducted and the disinfection and culling parameter were varied to check the effect of both disinfection and culling parameter.

Keywords:

Lumpy Skin Disease model, stability, disinfection, culling.

References

[1] W.F. Alfwzan, M.H. DarAssi, F.M. Allehiany, M.A. Khan, M.Y. Alshahrani, and E.M. Tag-eldin. A Novel Mathematical Study to Understand the Lumpy Skin Disease (LSD) using Modified Parameterized Approach. *Results in Physics*, 51:106626, 2023.

[2] World Organisation for Animal Health. *Manual of Diagnostic Tests and Vaccines for Terrestrial Animals*. OIE, Paris, 2017.

[3] A. Kononov, P. Prutnikov, I. Shumilova, S. Kononova, A. Nesterov, O. Byadovskaya, Y. Pestova, V. Diev, and Sprygin. Determination of Lumpy Skin Disease Virus in Bovine Meat and Offal Products Following Experimental Infection. *Transboundary and emerging diseases*, 66(3):1332–1340, 2019.

[4] X. Roche, A. Rozstalnyy, D. TagoPacheco, C. Pittiglio, A. Kamata, D. Beltran Alcrudo, K. Bisht, S. Karki, J. Kayamori, F. Larfaoui, E. Raizman, S. VonDobschuetz, M.S. Dhingra, and K. Sumption. Introduction and spread of lumpy skin disease in south, east and southeast asia: Qualitative risk assessment and management. *FAO animal production and health*, 183, 2020.

[5] E. Tuppurainen, T. Alexandrov, and D. Beltran-Alcrudo. *Lumpy Skin Disease: A Field Manual for Veterinarians*. Food and Agriculture Organization of the United Nations, 2017.

Proper lucky labeling for complete tripartite graph

D.A.S. Roshana[1*] and **A.A.I. Perera**[1]
[1] Department of Mathematics, Faculty of Science, University of Peradeniya
*Corresponding author; E-mail: sashiniroshana28@gmail.com

Background

Proper lucky labeling[5, 1], introduced by Rosa, is a graph labeling[3] concept where each vertex is assigned a unique natural number so that the sum of the labels of adjacent vertices is distinct for every pair of adjacent vertices. Additionally, the labels of adjacent vertices must be distinct. The proper lucky number[4] ($\eta_p(G)$) is the least natural number that labels the graph under these conditions. In this paper, we established the concept of proper lucky labeling in a complete tripartite graph ($K_{p,q,r}$), in which the vertex set is divided into three disjoint subgroups, with each vertex in one subset connected to all vertices in the other two subsets.

Methods

To apply proper lucky labeling[2] to complete tripartite graph by first dividing the vertex set U into three disjoint sets U_1, U_2, and U_3. Specifically, for any two adjacent vertices u and v where $u \in U_i$ and $v \in U_j$ with $i \neq j$, we ensure that $f(u) \neq f(v)$ and $S(u) \neq S(v)$, where f is the labeling function and S is sum of the labeling of adjacent vertices. Then we derived general formula for the proper lucky labeling based on the number of vertices in each subset.
For $p = q = r$

$$f(u_i) = \begin{cases} 1; & 0<i \leq n/3 \\ 2; & n/3<i \leq 2n/3 \\ 3; & 2n/3<i \leq n \end{cases}, \qquad S(u_i) = \begin{cases} 5n/3; & f(u_i) = 1 \\ 4n/3; & f(u_i) = 2 \\ n; & f(u_i) = 3 \end{cases}$$

For $p \neq q \neq r$

$$f(u_i, v_j, w_k) = \begin{cases} 1; & u_i \in U_1 \\ 2; & v_j \in U_2 \\ 3; & w_k \in U_3 \end{cases}, \qquad S(u_i, v_j, w_k) = \begin{cases} 2q + 3r; & f(u_i) = 1 \\ 1p + 3r; & f(u_i) = 2 \\ 1p + 2q; & f(u_i) = 3 \end{cases}$$

where n be the total number of vertices and p, q, r be number of vertices of U_1, U_2, U_3 sets respectively.

Results and Conclusions

The labeling method developed for complete tripartite graphs can be used for any finite number of vertices. We show that the proper lucky number of a complete tripartite graph is three, which is also its chromatic number[5]. This shows that the proper lucky number and the chromatic number are the same, demonstrating their relationship in graph theory.

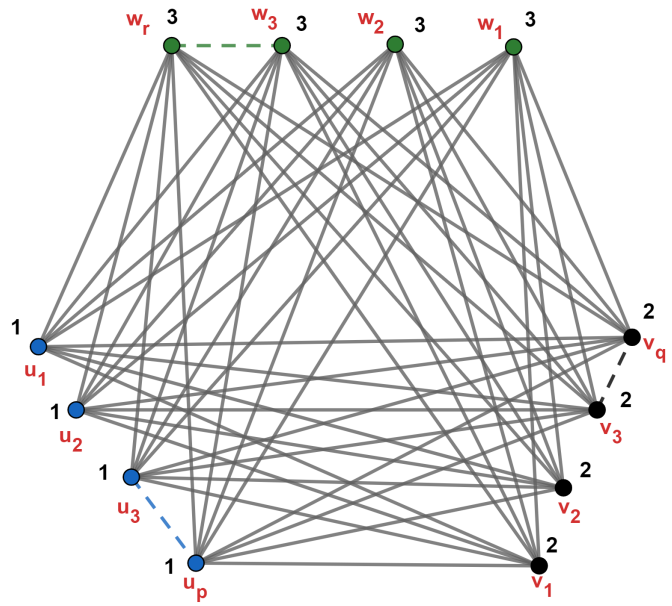

Keywords:

Proper lucky labeling, proper lucky number, complete tripartite graph, chromatic number,

References

[1] Chiranjilal Kujur, D Antony Xavier, and S Arul Amirtha Raja. Lucky labeling and proper lucky labeling for bloom graph. *IOSR Journal of Mathematics*, 13(2):52–59, 2017.

[2] TV Kumar and S Meenakshi. Triangular graphs are proper lucky and lucky. In *AIP Conference Proceedings*, volume 2451. AIP Publishing, 2022.

[3] A Nellai Murugan and R Maria Irudhaya Aspin Chitra. Lucky edge labeling of triangular graphs. *International Journal of Mathematics Trends and Technology-IJMTT*, 36, 2016.

[4] TV Sateesh Kumar and S Meenakshi. Proper lucky labeling of graph. In *Proceedings of First International Conference on Mathematical Modeling and Computational Science: ICMMCS 2020*, pages 341–351. Springer, 2021.

[5] Kins Yenoke, RC Thivyarathi, and D Anthony Xavier. Proper lucky number of mesh and it's derived architectures. *Journal of Computer and Mathematical Sciences (An International Research Journal)*, 8(5):187–195, 2017.

Dynamic behavior of Caputo fractional-order model of forest biomass, human activity, and atmospheric Carbon Dioxide concentration

Moh. Nurul Huda[1,2*], **Agus Suryanto**[1], **Isnani Darti**[1], **and Muhammad Fakhruddin**[3]

[1] Department of Mathematics, Faculty of Mathematics and Natural Sciences, University of Brawijaya, Malang, Indonesia

[2] Department of Mathematics, Faculty of Mathematics and Natural Sciences, Mulawarman University, Samarinda, Indonesia

[3] Research Center for Computing, National Research and Innovation Agency (BRIN), Bandung, Indonesia

*Corresponding author; E-mail: muh.nurulhuda@fmipa.unmul.ac.id

Background

The global environment is undergoing dramatic changes with rising temperatures triggered by greenhouse gases, particularly CO_2, which trap solar energy in the atmosphere through the greenhouse effect [3]. Human activities such as the consumption of fossil fuels and the change in land use are the main causes of the increase in CO_2 emissions, which have increased from 270 ppm (parts per million) in the preindustrial era to 421.08 ppm by 2023 [2]. Deforestation exacerbates this situation, reducing the ability of forest biomass to absorb CO_2 [4]. As a result, climate change triggers extreme weather, such as droughts and floods, crop uncertainty in agriculture, malnutrition, and infectious diseases, including infections caused by disease-carrying vectors [5]. Most mathematical models exhibit diffuse non-local effects and system memory properties, which are essential for representing biological phenomena. The extension from integers to fractional order aims to capture the impact of non-local relationships and long-term memory. The non-local characteristics of fractional-order operators offer a more accurate and realistic representation of mathematical models compared to classical-order operators [1]. The purpose of this research is to study the CO_2 concentration dynamic and its impact on human populations as well as forest biomass in a fractional order.

Methods

In this study, fractional differential equations using the Caputo derivative operator. This model consists of three compartments, namely the concentration of CO_2, human population, and forest biomass. The equilibria of the model were computed and further analyzed for local by using the Matignon condition and global asymptotic stability by using the Lyapunov function. Hopf bifurcation has been analyzed, where the derivative order parameter as bifurcation parameter. The numerical results were performed using a predictor-corrector scheme.

Results and Conclusions

The existence and uniqueness of the solution for the fractional model are shown. Non-negativity and boundedness are also proven. The fractional-order CO_2 concentration

dynamics model has four equilibria, namely human free and forest biomass free equilibrium point, equilibrium point of human population extinction, equilibrium point of forest biomass extinction, and interior equilibrium point. The human free and forest biomass free equilibrium point always exists, while the other equilibria exist under certain conditions. Based on the stability analysis, human free and forest biomass free equilibrium point is found to be unstable, while other equilibria are locally asymptotically stable under specific conditions. Interior equilibrium point is globally stable with a certain condition. Furthemore, the existence of Hopf bifurcation has been analyzed with parameter α passes the critical value $\alpha^*(= 0.9445)$. The computational results show that controlling deforestation can reduce CO_2 concentration and can be used by policy makers to make some intervention scenarios.

Keywords:

Fractional ordinary differential equations, Nonlinear ordinary differential equations and systems, Ecology, Population dynamics

References

[1] Pushpendra Kumar and Vedat Suat Erturk. A variable-order fractional mathematical model for the strategy to combat the atmospheric level of carbon dioxide. *Modeling Earth Systems and Environment*, pages 1–17, 2024.

[2] National Oceanic and Atmospheric Administration (NOAA). Climate change: Atmospheric carbon dioxide, 2024. Accessed: 2024-12-23.

[3] Eckehard Specht, Tino Redemann, and Nadine Lorenz. Simplified mathematical model for calculating global warming through anthropogenic co_2. *International Journal of Thermal Sciences*, 102:1–8, 2016.

[4] Agus Sugiarto, Sugeng Utaya, Sumarmi, Syamsul Bachri, and Rajendra P. Shrestha. Estimation of carbon stocks and co2 emissions resulting from the forest destruction in west kalimantan, indonesia. *Environmental Challenges*, 17:101010, 2024.

[5] Byomkesh Talukder, Gary W van Loon, Keith W Hipel, Sosten Chiotha, and James Orbinski. Health impacts of climate change on smallholder farmers. *One Health*, 13:100258, 2021.

Evaluating vaccination and quarantine for measles intervention strategy in Jakarta, Indonesia through mathematical modeling

Dipo Aldila[1*], Abdullah Hasan Hassan[1], Chidozie Williams Chukwu[2], Stephane Yanick Tchoumi[3,4] and Muhamad Hifzhudin Noor Aziz[5]

[1] Department of Mathematics, Faculty of Mathematics and Natural Sciences, Universitas Indonesia, Depok 16424, Indonesia

[2] Department of Mathematical Sciences, DePaul University, Chicago, IL 60614, USA

[3] Department of Mathematics and Applied Mathematics, University of Pretoria, Pretoria, South Africa

[4] Department of Mathematics and Computer Sciences ENSAI, University of Ngaoundere, Ngaoundere, Cameroon

[5] Institute of Mathematical Sciences, Faculty of Science, Universiti Malaya,50603 Kuala Lumpur, Malaysia

*Corresponding author; E-mail: aldiladipo@sci.ui.ac.id

Background

This study investigates the dynamics of measles transmission in Jakarta by introducing a seven-dimensional nonlinear differential equation model. Using weekly incidence data for parameter estimation, the research evaluates the impact of vaccination strategies. The motivation for this study lies in the pressing need to control measles outbreaks in densely populated urban settings like Jakarta, where vaccination and quarantine are critical interventions [1].

Methods

The model is analyzed to determine the existence and stability of equilibrium points and to calculate the basic reproduction number ($\mathcal{R}_0$). Dynamical analysis reveals that the disease-free equilibrium is globally asymptotically stable when $\mathcal{R}_0 < 1$, while an endemic equilibrium exists when $\mathcal{R}_0 > 1$. Global sensitivity analysis is conducted using the Partial Rank Correlation Coefficient (PRCC) method combined with Latin Hypercube Sampling (LHS) to identify influential parameters [2]. Furthermore, the model is formulated as an optimal control problem to explore effective intervention strategies. The Pontryagin's Maximum Principle is applied [4, 5], and the forward-backward sweep method [3] is used for numerical solutions.

Results and Conclusions

Sensitivity analysis indicates that the first-dose vaccination intervention significantly reduces $\mathcal{R}_0$, emphasizing its potential as a key measles control measure. Optimal control analysis reveals that a combined strategy of vaccination and quarantine is the most effective for minimizing disease transmission and associated costs. These findings underscore the importance of implementing integrated control strategies in public health policies to combat measles in urban areas.

Keywords:

measles, vaccination, quarantine, basic reproduction number, optimal control

References

[1] Muhammad Fakhruddin, Dani Suandi, Sumiati, Hilda Fahlena, Nuning Nuraini, Edy Soewono, Muhammad Fakhruddin, Dani Suandi, Sumiati, Hilda Fahlena, Nuning Nuraini, and Edy Soewono. Investigation of a measles transmission with vaccination: a case study in jakarta, indonesia. *Mathematical Biosciences and Engineering 2020 4:2998*, 17:2998–3018, 4 2020.

[2] Simeone Marino, Ian B. Hogue, Christopher J. Ray, and Denise E. Kirschner. A methodology for performing global uncertainty and sensitivity analysis in systems biology. *Journal of Theoretical Biology*, 254(1):178–196, 2008.

[3] Maia Martcheva. *An Introduction to Mathematical Epidemiology*, volume 61. Springer US, 2015.

[4] L.S. Pontryagin. Mathematical theory of optimal processes. *Mathematical Theory of Optimal Processes*, 5 2018.

[5] A Seierstad and K Sydsaeter. *Optimal control theory with economic applications*, volume 24. North-Holland Publishing, 1987.

Heat and mass transfer enhancement in magnetohydrodynamic hybrid nanofluid flow over a porous stretching sheet

Izzat Razzaq[1*] **and Xinhua Wang**[1]

[1]College of Mechanical and Energy Engineering, Beijing University of Technology, Beijing, 100124, China

*Corresponding author; E-mail: izzatrazzaq@yahoo.com

Background

Nanofluids are significant advancements in thermal management because of their enhanced thermal conductivity which improves heat transfer efficiency. This improvement is crucial in various heat transfer applications, including heat exchangers, refrigeration systems, fire suppression technologies, electronic cooling devices, building insulation, generator efficiency, and energy generation plants. Conventional fluids like engine oil, water, and ethylene glycol present limited thermal efficiency because of inherently minimal thermal conductivity. Through incorporating nanoparticles in these base fluids, nanofluids offer superior thermal properties addressing the limitations of conventional fluids. Introducing nanoparticles into these base fluids, known as nanofluids, significantly improves thermal conductivity as demonstrated by Choi[2]. Das et al. [3] explored copper-based nanofluid flow on stretching surfaces, revealing that heat transfer rates decline as nanoparticle volume fraction increases. Hayat et al. [4] numerical study of viscous nanofluid's Darcy-Forchheimer flow with Brownian motion and thermophoresis past stretching curved surfaces was conducted. Z.H. Khan et al. [5] examine magnetohydrodynamics boundary-layer flow passing on a stretching sheet through hybrid nanofluids. Babu et al. [1] explored the impacts of magnetic field and crosswise diffusion on the flow of Maxwell nanofluid over a nonlinear stretching sheet with focus on thermophoresis Brownian motion and slip conditions. This study analyzes the thermophysical properties and flow behavior of hybrid nanofluids (silver and magnesium oxide in water) on stretched surfaces using boundary layer theory and the BVP4c numerical method.

Methods

This study analyzes steady, two-dimensional MHD flow of hybrid nanofluids (magnesium oxide and silver in water) over a permeable, stretched sheet. The formulation includes Joule dissipation, viscous heating, and an external magnetic field B_0 applied perpendicular to the sheet.

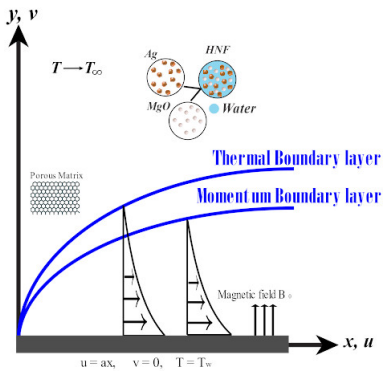

The wall velocity is $Uw(x) = ax$, with the medium modeled as isotropic and homogeneous. The governing equations follow Tiwari and Das' approach, and the ambient temperature T_∞ is greater than the wall temperature T_w as shown in Figure.

Results and Conclusions

The analysis focuses on three key profiles: velocity and temperature. The BVP4c method is applied to calculate and plot the results by using Matlab. Which shows that increasing the magnetic parameter reduces the velocity profile due to the Lorentz force opposing fluid motion, thickening the boundary layer near the surface and increase in the Darcy inverse permeability parameter (β_1) leads to a noticeable reduction in the velocity profile. At lower Ec values, viscous dissipation is negligible, leading to a thinner thermal boundary layer, whereas higher Ec values significantly enhance the temperature profile for silver and magnesium oxide nanoparticles due to intensified heat generation from kinetic energy dissipation. The porosity factor β_1 notably impacts the temperature profile, with higher β_1 values increasing temperature due to augmented heat generation caused by the reduced permeability of the porous medium. Detailed analysis of the effects of various parameters magnetic parameter (M), porosity factor (β_1), Prandtl number (Pr), and Eckert number (Ec) on the dimensionless skin friction coefficient (Cf) and Nusselt number (Nu) are calculated.

Keywords:

Hybrid nanofluids, Magnetohydrodynamics, Heat and mass transfer, bvp4c MATLAB

References

[1] B Hari Babu, BV Swarnalathamma, and M Veera Krishna. Diffusion-thermo and thermo-diffusion impacts on mhd natural convection flow of maxwell nanofluids over a stretching sheet. *Case Studies in Thermal Engineering*, 61:105016, 2024.

[2] S US Choi and Jeffrey A Eastman. Enhancing thermal conductivity of fluids with nanoparticles. Technical report, Argonne National Lab.(ANL), Argonne, IL (United States), 1995.

[3] Kalidas Das, Amit Sarkar, and Prabir Kumar Kundu. Cu-water nanofluid flow induced by a vertical stretching sheet in presence of a magnetic field with convective heat transfer. *Propulsion and Power Research*, 6(3):206–213, 2017.

[4] Tasawar Hayat, Farwa Haider, Taseer Muhammad, and Ahmed Alsaedi. Numerical study for darcy-forchheimer flow of nanofluid due to an exponentially stretching curved surface. *Results in physics*, 8:764–771, 2018.

[5] Zafar Hayat Khan, Waqar A Khan, Shaik Mohammed Ibrahim, K Swain, and Zaitang Huang. Impact of multiple slips and thermal radiation on heat and mass transfer in mhd maxwell hybrid nanofluid flow over porous stretching sheet. *Case Studies in Thermal Engineering*, 61:104906, 2024.

On BZS rings and hyperstructures

Kedukodi Babushri Srinivas[1*], Chaithra B J[1], Kuncham Syam Prasad[1], and Kavitha Koppula[1]
[1] Department of Mathematics, Manipal Institute of Technology, Manipal Academy of Higher Education, Karnataka, India.
*Corresponding author; E-mail: babushrisrinivas.k@manipal.edu

Background

Zero square rings are the rings in which every element is nilpotent of index 2 (see Stanley [5]). Anti-commutativity of such rings ensures that they are indeed locally nilpotent. Boolean rings, a well known class of commutative rings, are those in which every element is idempotent. Farag introduced the notion of boolean-zero square (BZS) rings as a generalization of boolean rings and zero square rings. In a BZS ring, we have $x^2 = x$ or $x^2 = 0$, $\forall\ x$. This property also extends Malone trivial multiplications on nearrings, a non-linear counter part of rings. Several structural properties of BZS rings are discussed in Farag and Tucci [2, 3]. Hyperstructures, are a generalization of the classical algebraic structures, with a multi-valued operation (see Davvaz and Fotea [1]). We extend the notion of BZS property to algebraic hyperstructures.

Methods

We will employ algebraic methods and develop the existing ideas further with special emphasis on standard mathematical proof techniques. To validate our findings, we construct examples having low order using GAP (Groups, Algorithms and Programming) packages [4].

Results and Conclusions

Hyperrings resembles a ring-like structure, in which the hyperoperation is distributive over the classical semigroup operation. We present structural aspects of hyperrings with respect to BZS property and provide few illustrations.

Keywords:

Boolean ring, Zero square ring, Hyperstructures

References

[1] Bijan Davvaz and Vileta Leoreanu-Fotea. *Hyperring theory and applications*. International Academic Press, Palm Harbor, USA, 2007.

[2] Mark Farag and Ralph P. Tucci. Bzs rings ii. *Journal of Algebra and Related Topics*, 9(2):29–37, 2021.

[3] Mark Farag and Ralph P. Tucci. Bzs near-rings and rings. In *Rings, Monoids and Module Theory: AUS-ICMS 2020, February 6-9*, pages 307–314, Sharjah, United Arab Emirates, 2022. Springer.

[4] The GAP Group. *GAP-Groups, Algorithms, and Programming, Version 4.14.0*, 2024.

[5] Richard P. Stanley. Zero square rings. *Pacific Journal of Mathematics*, 30(3):811–824, 1969.

Effective modeling of coupled deformation and diffusion in heterogeneous elastic media

Anju Saini[1*]
[1]Graphic Era deemed to be University, Dehradun
*Corresponding author; E-mail: anjusaini@geu.ac.in

Background

Transport processes in deformable porous media whether in the presence of reaction, are at the heart of a variety of scientific and engineering applications. For materials like lung tissue (which deforms repeatedly in a cyclic manner), these quantities can become much more complicated. In these cases, the coupling of elastic deformation and diffusive transport governs the exchange of nutrients, gases, etc., the latter of which is incredibly relevant in cases where one could have pneumonia or COVID-19 [1, 2].

Specifically, the research aims to develop a mathematical framework that models and simulates transport phenomena efficiently. Traditional numerical approaches for simulating these systems can introduce challenges tied to the balance between precision and computational efficiency, particularly at microscopic scales, given the dynamic nature of the systems involved. Here we present a multi-scale framework that connects the microscopic details to the macroscopic behavior via a formal mathematical treatment. This study treats the two-scale asymptotic expansion to derive upscaled equations that provide computationally efficient and yet accurate representations of these processes.

Methods

Microscopic Modeling

In the study, the authors begin with a rigorous microscopic model that captures the coupling of elastic deformation and diffusion. The microscopic domain is assumed to have periodic holes in orders to mimic complex geometry of the lungs tissue like materials.

- Elasticity Problem:

$$\rho\frac{\partial^2 u}{\partial t^2} - \nabla\cdot(C\varepsilon) = g_{elast} \quad \text{in } \Omega_s^E,$$

Where ρ is the density, u the displacement, C the elasticity tensor, and ε the strain tensor defined as:

$$\varepsilon = \tfrac{1}{2}(\nabla u + (\nabla u)^{'})$$

- Diffusion Problem:

Diffusion in the dynamically deforming domain is also termed in a Lagrangian-Eulerian outline:

$$\tfrac{\partial c}{\partial t} + \nabla\cdot(cv - D\nabla c) = g_{diff'}$$

where c is the concentration, v the velocity convinced by deformation, D the diffusion tensor, and g_{diff} the source term.

Numerical Implementation

Finite element methods (FEM) are employed for discretization, with the Crank-Nicholson scheme used for temporal integration. The multi-scale problem is implemented in the matlab, solving macroscopic equations and cell problems iteratively.

Results and Conclusions

Validation and Key Observations

Numerical experiments validate the upscaled models using deformation scenarios inspired by lung mechanics. A periodic boundary displacement was imposed, simulating the repetitive expansion and contraction of lung tissue. The outcomes expose:

1. Impact of Deformation on Transport:
    - Significant deformation drastically transforms the effective diffusion tensor D^* from isotropic to anisotropic depending on the strain distribution.
    - Errors due to deformation effects become relevant for the modelling of transport processes in biological tissues.
2. Effective Coefficients Reflect Microstructure:
    - J^* and D^* represent a combination of the microgeometry and deformation effects they are derived from a thorough depiction of the system's behavior.

Analysis of Multi-Scale Coupling:

The findings emphasize the merit of the two-scale approach in maintaining such microstructural fidelity while lowering the computational expense. Throughout the analysis, it was noted that unlike direct numerical simulations which account for all the scale modules, the upscaled equation of the model aggregates the micro-structural elements into "averaged" macro-equations which helps speed the calculations up without losing much detail.

Applications and Future Directions

The framework has a wide range of applications, for example, designing of deformable porous materials in engineering or examining gas exchange processes in medicine and biology. Moreover, Future research could generalize the model by considering fluid-structure interaction or more elaborate boundary conditions increasing its significance even more.

To conclude, this study addresses the problem of modeling processes of transport in deformable porous media and provides a rigorous mathematical framework for this, of particular interest is their approach that merges two-scale asymptotic expansion and numerical simulations which gives an unprecedented perspective of the relation between elastic procedures and diffusion processes. The effective models developed are a nice way to substitute for traditional direct simulations in order to enhance the potential for new applications in material science as well as biology and medicine.

Keywords:

Transport processes, elastic deformation, diffusion, porous media, finite element method

References

[1] Markus Gahn, Maria Neuss-Radu, and Iulio Sorin Pop. Homogenization of a reaction-diffusion-advection problem in an evolving micro-domain and including nonlinear boundary conditions. *Journal of Differential Equations*, 289:95–127, 2021.

[2] Georges Griso, Larysa Khilkova, Julia Orlik, and Olena Sivak. Homogenization of perforated elastic structures. *Journal of Elasticity*, 141(2):181–225, 2020.

Determining temporal variations of air pollution in Sri Lanka: An approach using wavelet transform

D.M.S.K.Maduwanthi[1*], **I.T.S.Piyatilake**[1]
[1] Department of Computational Mathematics, University of Moratuwa, Sri Lanka
*Corresponding Author; E-mail: ksachini820@gmail.com

Background

Air pollution is a global challenge that poses profound threats to human health, well-being, and environmental sustainability. Despite being often invisible, it remains a massive and growing challenge, particularly in urbanized and industrialized regions. Fine particulate matter, such as $PM_{2.5}$ and PM_{10}, can penetrate deeply into the respiratory system and bloodstream, triggering systemic inflammation and oxidative stress. Air pollution contributes to chronic health conditions, disproportionately affecting vulnerable populations. In particular, respiratory issues, developmental delays, and unfavorable pregnancy outcomes affect women, children, and the elderly. Prolonged exposure to these pollutants has also been linked to higher mortality rates, lung cancer, and other severe diseases [1].

Sri Lanka, as a rapidly developing country, faces significant air pollution challenges driven by multiple factors. Rapid urbanization has triggered increased industrial activities, construction projects, and a surge in vehicular emissions, all of which contribute substantially to the decline in air quality [2]. In addition, seasonal dry spells and varying wind speeds exacerbate the persistence and spread of harmful pollutants, compounding the problem. To effectively address air pollution-related problems in Sri Lanka, it is important to gain a better understanding of how pollutants spread throughout the country and their seasonal effects. The objective of this study is to determine whether there is a specific period during the year when particulate matter concentrations vary substantially and to examine their association with meteorological factors. This knowledge is crucial for developing and applying targeted strategies to reduce air pollution in specific areas.

Methods

This study focuses on the concentration of $PM_{2.5}$ and PM_{10} pollutants during the period from 2019 to 2020. The relevant data is gathered from the Air Resource Management & Monitoring Unit of the Central Environmental Authority. Battaramulla, a highly urbanized and densely populated area, and Kandy, located in the hill country of Sri Lanka, have been selected for the study. The relevant meteorological parameters, including temperature (°C), relative humidity (%), wind speed (m/s), and rainfall (mm), are collected from the Sri Lanka Meteorological Department [3].

The wavelet coherence analysis is employed to explore time-frequency patterns. It helps to find the specific periods with increased pollutant levels. The Morelet wavelet is used for this purpose. By analyzing the generated wavelet spectrums, the oscillation periods of the pollutants are identified [4]. Additionally, statistical techniques are used to examine the meteorological factors contributing to these oscillations. To confirm these results, the Spearman rank correlation analysis & Innovative Trend Analysis (ITA) graphs were utilized. Furthermore, the ARIMA model is applied to the time series data to forecast the concentration levels of particulate matter

for 2025 and 2026 [5]. All analyses are conducted using R statistical software which is a powerful and comprehensive environment for statistical computing and data visualization.

Results and Conclusions

The wavelet power spectrum reveals seasonal pollutant patterns in Battaramulla and Kandy. The results highlight a significant short-term fluctuation in $PM_{2.5}$ and PM_{10} levels during the first half of the year, particularly from March to May in Battaramulla and March to June in Kandy. High temperature and high wind speed are the reasons for these changes during this season. Battaramulla records the highest temperature in May ($28.89 \pm 0.85°C$) with the highest wind speed ($1.22 \pm 0.34 m/s$), while Kandy records the highest temperature ($27.11 \pm 0.99°C$) with the highest wind speed in May.

In contrast, fluctuations stabilize in the later half of the year. Specifically, the pollutant concentration is reduced from July to October in both locations. These variations are influenced by seasonal changes and meteorological factors. In Battaramulla, this period features the lowest temperature, the highest relative humidity in September ($79.76 \pm 4.79\%$), and the highest rainfall in April. In Kandy, the lowest temperatures occur in October and December, with the highest relative humidity in October ($75.43 \pm 6.45\%$) and significant rainfall in the first half of the year. It is consistent with a positive relationship between pollutant levels and air temperature as well as wind speed, with a negative relationship with relative humidity and rainfall. The Spearman rank correlation values confirm the results, while the ITA graphs reveal distinct seasonal patterns in $PM_{2.5}$ and PM_{10} concentrations during this period.

Furthermore, the ARIMA model predicts similar steady trends in $PM_{2.5}$ and PM_{10} levels for both locations. While historical data suggest steady levels consistent with fluctuations from 2025 to 2026, the estimates vary over time and remain uncertain due to changes in meteorological parameters. This highlights the urgent need for targeted interventions and enhanced air quality management.

Keywords:

Air pollution, ITA, Wavelets, Correlation, ARIMA

References

[1] Thrividya Rathnayake and Lovleen Gupta. Assessment of PM_{10} in colombo, sri lanka and its potential source regions. *E3S Web of Conferences*, 559:04044, 2024.

[2] Armin Nakhjiri and Ata Abdollahi Kakroodi. Air pollution in industrial clusters: A comprehensive analysis and prediction using multi-source data. *Ecological Informatics*, 80:102504, 2024. Under a Creative Commons license.

[3] Lakindu Mampitiya, Namal Rathnayake, Yukinobu Hoshino, and Upaka Rathnayake. Forecasting PM_{10} levels in sri lanka: A comparative analysis of machine learning models. *Journal of Hazardous Materials Advances*, 13:100395, 2024.

[4] Md. Abdul Fattah, Syed Riad Morshed, Abdulla-Al Kafy, Zullyadini A. Rahaman, and Muhammad Tauhidur Rahman. Wavelet coherence analysis of $PM_{2.5}$ variability in response to meteorological changes in south asian cities. *Atmospheric Pollution Research*, 14(5):101737, 2023.

[5] Jun Luo and Yaping Gong. Air pollutant prediction based on ARIMA-WOA-LSTM model. *Atmospheric Pollution Research*, 14(6):101761, 2023. Under a Creative Commons license.

On 3-prime graph of a semiring with respect to an ideal

Kedukodi Babushri Srinivas[1*], **Lavanya.S**[1], **Kuncham Syam Prasad** [1] **and Aishwarya.S**[1]

[1] Department of Mathematics, Manipal Institute of Technology, Manipal Academy of Higher Education, Manipal, Karnataka, India.

*Corresponding author; E-mail: babushrisrinivas.k@manipal.edu

Background

Algebra and graph theory are highly interlinked branches of mathematics. Researchers have tried to establish connections between them to further the development of both fields. Beck introduced the concept of a zero-divisor graph of a commutative ring. Semirings play a pivotal role both in abstract algebra and applied mathematics. The notion of semiring was first introduced by Vandiver in 1934. For definitions and properties of semirings and general algebra, we refer to Hebisch and Weinert [2]. The zero-divisor graphs of semirings was first introduced by Dolzan and Oblak [1]. The investigation of semiring graphs has seen significant growth in recent years, taking different directions.

Methods

The methods involve constructing graphs by representing elements of algebraic structures as vertices and defining edges based on algebraic operations. Graph-theoretic techniques are then applied to explore the structure's properties. We will employ algebraic methods and develop the existing ideas further with special emphasis on standard mathematical proof techniques such as direct proof, contraposition and contradiction. We will compute using GAP (Groups, Algorithms and Programming) packages to find semigroups and ideals.

Results and Conclusions

Let S be a semiring and I be an ideal of S. We introduce the notion of 3-prime graph of a semiring S denoted by $G_I(S)$. We examine the interplay between graph theoretic properties of $G_I(S)$ and semiring-theoretic properties of S. Moreover, we find the line graph associated with $G_I(S)$ denoted by $L(G_I(S))$ and investigate properties of this graph.

Keywords:

Semirings, Graphs and Abstract Algebra, Prime Ideal, Line Graph

References

[1] David Dolžan and Polona Oblak. The zero-divisor graphs of rings and semirings. *International Journal of Algebra and Computation*, 22(04):1250033, 2012.

[2] U. Hebisch and H. J. Weinert. *Semirings Algebraic Theory and applications in computer science*. World Scientific, 1998.

[3] B. Jagadeesha and S. Lavanya. Line graph associated with c-prime graph of a nearring. *Proceedings of the Jangjeon Mathematical Society*, 27(04):605–614, 2024.

[4] Dr Bhavanari Satyanarayana, Kuncham Syam Prasad, and Kedukodi Babushri Srinivas. Graph of a nearring with respect to an ideal. *Communications in Algebra®*, 38:1957–1967, 05 2010.

[5] Kedukodi Babushri Srinivas, B. Jagadeesha, Kuncham Syam Prasad, and Juglal Suresh. *Nearrings, Nearfields and Related Topics*, chapter Different prime graphs of a nearring with respect to an ideal, pages 185–203. World Scientific, 2017.

A numerical scheme for a two-dimensional Boussinesq equation

Arief Anbiya[1*]
[1] Independent Scholar
*Corresponding author; E-mail: ariefanbiya@gmail.com

Background

Weakly nonlinear long and shallow water waves can be modeled via a (2+1)-dimensional Boussinesq equation

$$u_{tt} = u_{xx} + u_{xxxx} + u_{yy} - 3(u^2)_{xx}, \quad x \in [-L, L], \quad y \in [-L, L], \quad t > 0 \tag{1}$$

that combines the two-way propagation of the classical Boussinesq equation with a weak dependence on the second spatial variable y [3]. In comparison with the well-known unidirectional KdV equation, (1) introduces the second order temporal derivative that allows the solution to have bidirectional waves. In this paper, we present a numerical scheme for (1) and subsequently compute the error of that scheme against the exact solutions from [2].

Using Fourier series, it can be shown that the linearized version of (1) is ill-posed and has blow-up solutions. Therefore, we cannot solve (1) by simply applying Fourier series. The method in this paper is inspired by a recent study [1] that proposes a numerical scheme for the 1D "bad" Boussinesq equation

$$u_{tt} = u_{xx} + u_{xxxx} + (u^2)_{xx}. \tag{2}$$

In [1], they rewrite (2) as a first-order system and use "trimmed" Fourier series: Fourier modes with large enough frequencies are cut-off. The cut-off is due to the fact that equation (2) was derived based on assumptions for long and shallow water waves, therefore Fourier modes with short wavelengths (large frequencies) can be omitted. The cut-off frequencies are carefully chosen to make sure that the solution of linearized (2) does not blow-up. In this paper, we also use Fourier series and trim the high-frequency modes to solve (1). However, we rewrite the equation as a system in a different way than [1] and subsequently solve it via Runge-Kutta 4 in the frequency space.

Methods

Let $v(x, y, t) = u_t(x, y, t)$ and write (1) as

$$\begin{bmatrix} u_t \\ v_t \end{bmatrix} = \begin{bmatrix} v \\ u_{xx} + u_{xxxx} + u_{yy} - 3(u^2)_{xx} \end{bmatrix} \tag{3}$$

We approximate u, v as finite 2D Fourier series

$$u(x, y, t) = \sum_{k_y \in \kappa} \sum_{k_x \in \kappa} \widehat{U(t)}_{k_x, k_y} e^{i2\pi(\omega_{k_x} x + \omega_{k_y} y)},$$

$$v(x, y, t) = \sum_{k_y \in \kappa} \sum_{k_x \in \kappa} \widehat{V(t)}_{k_x, k_y} e^{i2\pi(\omega_{k_x} x + \omega_{k_y} y)},$$

Plug this to the system (3) and we have the following sets of ODE system for $\forall k_x, k_y \in \kappa \times \kappa$

$$\begin{aligned} \widehat{U}'_{k_x,k_y} &= \widehat{V}_{k_x,k_y} \\ \widehat{V}'_{k_x,k_y} &= [-(2\pi\omega_{k_x})^2 + (2\pi\omega_{k_x})^4 - (2\pi\omega_{k_y})^2]\widehat{U}_{k_x,k_y} + 3(2\pi\omega_{k_x})^2\widehat{W}_{k_x,k_y}, \end{aligned} \tag{4}$$

Where $\widehat{W}$ is the Fourier coefficient for u^2 which can be approximated using $\widehat{U}$. To avoid the blow-up solutions as in the linearized version of (1), it can be shown that we must have $\frac{k_x^4}{k_x^2+k_y^2} \leq \frac{L^2}{\pi^2}$ for square domain. Therefore, we solve (4) only for wave numbers k_x, k_y that satisfy that bound. We use Runge-Kutta 4 and Octave software to solve (4) numerically.

Results and Conclusions

We use an exact solution from [2] of the form $u(x,y,t) = -\frac{2b_0k^4e^{kx+hy-\omega t}}{(1+b_0k^2e^{kx+hy-\omega t})^2}$, where $\omega = \sqrt{h^2+k^2+k^4}$. The error is computed as $e(t) = \max_{(x,y)\in S}|u_{approx}(x,y,t) - u(x,y,t)|$, where $S = [-L,L]\times[-L,L]$. Using $L = 100$ and $k = 0.25$, $h = 0.1$, $b_0 = 1$ for the exact solution and initial condition of a long oblique wave, the following figure shows the simulation error until time $t = 30$. The absolute maximum of initial condition is $\max(|u(x,y,0)|) = 0.031250$ and $e(30) = 1.266 \times 10^{-4}$.

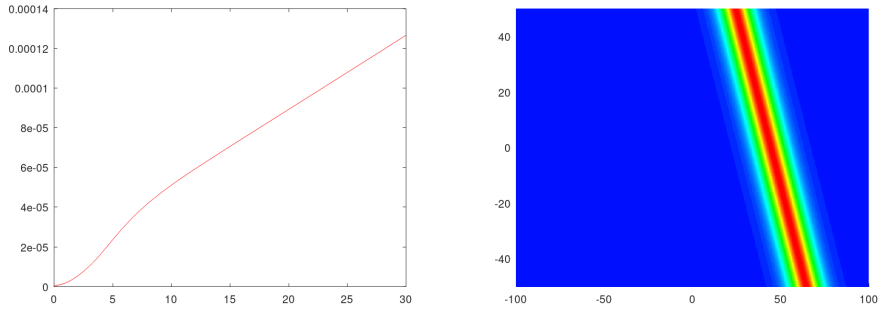

Figure 1: The error $e(t)$ (left) and cropped numerical solution at $t = 30$ (right) using $\triangle t = 0.1$, $\triangle x, \triangle y = 0.25$.

Keywords:

Nonlinear PDE, Numerical Method, Fourier Series, Mathematical Modeling, Water Waves

References

[1] Christophe Charlier et al. Numerical scheme for the solution of the "bad" boussinesq equation. *https://arxiv.org/abs/2406.02183v1*, pages 1–13, 2024.

[2] F.P. Barrera et al. Exact solutions of the two-dimensional boussinesq and dispersive water waves equations. *WIT Transactions on Engineering Sciences*, 69:293–297, 2010.

[3] R.S. Johnson. A two-dimensional boussinesq equation for water waves and some of its solutions. *Journal of Fluid Mechanics*, 323:65–78, 1996.

Algorithms for solving fuzzy linear fractional programming problem with pentagonal fuzzy number and pentagonal neutrosophic fuzzy number

P.Rajarajeswari[1*], **M.Shyamala**[2]

[1] Department of Mathematics, Chikkanna Government Arts College, Tiruppur- 641602
[2] Department of Mathematics, VLB Janakiammal College of Arts and Science, Coimbatore- 641042
*Corresponding author; E-mail: p.rajarajeswari29@gmail.com

Background:

When maximizing a ratio is essential, such as in production planning and resource allocation, linear fractional programming problem[LFPP] are frequently employed.This research paper's objective is to examine various ranking formulas and novel approaches for utilizing two types of fuzzy numbers to solve a fuzzy linear fractional programming problem[FLFPP].Because real-world problems are inherently vague, traditional linear programming techniques frequently fail to handle them effectively. In order to bridge this gap, two novel algorithms—Pentagonal Fuzzy Numbers and Pentagonal Neutrosophic Fuzzy Numbers—were created to solve FLFPP. These problems involve fuzzy numbers for all objective function coefficients and constraints, and they use fuzzy logic to model the uncertain parameters.Using the suggested three new ranking techniques, the pentagonal fuzzy number[PFN] and pentagonal neutrosophic fuzzy number [PNFN]are transformed into a crisp LPP. The best solution is then found using the simplex method.To demonstrate our findings, a few numerical examples are provided with a multiple bar chart that displays the optimal solution (OS) from the proposed and current methods.

Methods:

a) Algorithm for solving FLFPP with PFN:

Step 1: Consider FLFPP with PFN and use the complementary technique for the objective function below to convert the FLPPs to the FLPP.

$$\text{Max } S = \frac{(f_1, f_2, f_3, f_4, f_5)\, w_1 + (h_1, h_2, h_3, h_4, h_5)\, w_2}{(g_1, g_2, g_3, g_4, g_5)\, w_1 + (i_1, i_2, i_3, i_4, i_5)\, w_2}$$

$$\text{Max } S_1 = (f_1, f_2, f_3, f_4, f_5)\, \mathcal{W}_1 + (h_1, h_2, h_3, h_4, h_5)\, \mathcal{W}_2$$

$$\text{Max } S_2 = (g_1, g_2, g_3, g_4, g_5)\, \mathcal{W}_1 + (i_1, i_2, i_3, i_4, i_5)\, \mathcal{W}_2$$

$$\begin{aligned}\text{Max } S^* = {} & (f_1 - g_1, f_2 - g_2, f_3 - g_3, f_4 - g_4, f_5 - g_5)\, \mathcal{W}_1 \\ & + (h_1 - i_1, h_2 - i_2, h_3 - i_3, h_4 - i_4, h_5 - i_5)\, \mathcal{W}_2 \end{aligned} \quad (1)$$

Step 2: FLPP above was converted to a Crisp FLPP by three RFs.
RF I=[1/5](f+h+2i+j+k),RF II=[1/6](f+3h+2i+3j+k)
RF III=[1/4](3f+3h+2i+3j+3k)

Step 3: Use the simplex approach for the crisp FLPP to find the optimal solution (OS) of the FLFPP.

b) Algorithm for solving FLFPP with PNFN:

Step 1: Use the decomposition approach to split FLFPP using PNFN into two FLPPs.
Step 2: Use three RFs to convert the two FLPPs to crisp FLPPs.
RF I = [1/15](f+h+i+j+k)(2+T-I-F)
RF II = [1/6](2f+3h+2i+3j+2k)(2+T-I-F)
RF III= [1/5](f+h+2i+j+k)(2+T-I-F)
Step 3: $Z_1(x)$ and $Z_2(x)$ are the solutions obtained by applying the Simplex Method to solve the crisp FLPPs. Finally,below formula is used to derive the OS of the FLFPP.

$$\text{Max } Z(x) = \frac{Z_2(x)}{Z_1(x)}$$

Results and Conclusions:

Charnes and Cooper[1] made a major breakthrough by solving LFPP by reducing them to LPPs with extra restrictions via an analytical transformation. Optimizing ratios under fuzzy settings is the goal of fuzzy linear fractional programming problems, or FLFPPs. There are other approaches to solving FLFPPs, such as Das et al.'s[2] and others that expand the method to deal with fuzzy coefficients. In order to handle FLFPPs using pentagonal fuzzy numbers and pentagonal neutrosophic fuzzy numbers, we developed two algorithms in this study. When comparing the OS of the objective function via our proposed PFN with the base paper method[4], our PFN approach yields the most optimized value; similarly, when comparing the OS of the objective function obtained via the base paper method[3], our PNFN yields the most OS.

Keywords:

Fuzzy linear fractional programming problem , fuzzy linear programming problem , ranking functions (RF), Pentagonal Neutrosophic Fuzzy Number, and Pentagonal Fuzzy Number .

References

[1] A. Charnes and W.W. Cooper. An explicit general solution in linear fractional programming. *Naval Research Logistics*, 20(3):449–467, 1973.

[2] S.K. Das, S.A. Edalatpanah, and T. Mandal. A proposed model for solving fuzzy linear fractional programming problem: Numerical point of view. *Journal of Computational Science*, 25:367–375, 2018.

[3] A.M. Elhadidi, O.E. Emam, A.M. Abdelfadel, and M. Lotayij. Linear fractional programming based on trapezoidal neutrosophic numbers. 2023.

[4] R.J. Mitlif. A solution procedure for fully fuzzy linear fractional model with ranking functions. *Journal of College of Education*, 2016(1):93–108, 2016.

Simulation of melt spinning using the Rolie-Poly model

Sourav Banerjee[1*], **Satyananda Panda**[1] **and Renu Dhadwal**[2]
[1] Department of Mathematics, NIT Calicut, India
[2] Center for Mathematical Modelling, FLAME University, Pune, India
*Corresponding author; E-mail: sourav_p220128ma@nitc.ac.in

Background

Fibers are primarily used in the textile industries. In modern society, fiber is also leading to innovative applications in the creation of reinforced composite plastics. Melt-spinning is a fundamental technology for producing artificial fiber in which molten polymers are extruded vertically via a spinneret plate with 5000 small circular holes for the continuous production of fiber. The liquid jet undergoes stretching, cooling, and solidification due to the energy loss to the surrounding air. The solidified filament is wound up by a take-up roll at a speed higher than the mean extrusion velocity (1200-4000 m/min and greater). The thread extension tends to align the molecules along the axis, creating a stronger structure after solidification.
This work discusses a mathematical model for the non-isothermal melt spinning [2, 4] using the Rolie-Poly constitutive equations [3]. Numerical simulations illustrate the model's capability to capture the crucial effects of critical parameters such as draw ratio and convective-constraint-release (CCR) on fiber velocity, stress, and cross-sectional area. The results provide a comprehensive insight into the dynamics in stretched and unstretched fiber conditions. Significant observation leads to the existence of a solution for the unstretched RP fiber model under certain conditions. It also shows that the model can accurately fit industrial data [1] when draw ratios are higher and inertia numbers are lower. An asymptotic analysis of the relaxation parameter ratio involved in the model has been performed for the isothermal melt-spinning case, which provides a deeper understanding and validation of the model's accuracy.

Methods

The fiber model is derived using the slender filament approximation, with the governing equations for mass, momentum, and energy averaged over the fiber cross-section. The Rolie-Poly constitutive equation relates the stress tensor to the deformation. Non-dimensionalization of the equations introduces parameters like the draw ratio and Weissenberg numbers. Numerical simulations are performed using MATLAB's BVP5C solver and finite-difference methods for temperature profiles. Asymptotic analysis is performed for small relaxation time ratios to validate the model further.

Results and Conclusions

Simulation results reveal that higher draw ratios lead to increased fiber velocities and reduced cross-sectional areas. The CCR parameter influences the alignment of polymer chains, enhancing velocity in stretched models but reducing it in unstretched conditions due to elastic stress relaxation. Industrial data simulations demonstrate the model's ability to predict fiber characteristics under practical conditions. Asymptotic analysis confirms the validity of the model for small relaxation time ratios.

Future work will incorporate additional factors like air drag and gravitational effects to enhance industrial applicability.

Keywords:

Fiber dynamics, Melt-Spinning, Rolie-Poly Constitutive Model, Reptation, Non-Stretching

References

[1] Renu Dhadwal. *Fibre Spinning: Model Analysis*. Phd thesis, Technische Universität Kaiserslautern, 2005.

[2] Hans Petter Langtangen. Derivation of a mathematical model for fiber spinning. *Preprint series. Mechanics and Applied Mathematics http://urn. nb. no/URN: NBN: no-23418*, 1997.

[3] Alexei E Likhtman and Richard S Graham. Simple constitutive equation for linear polymer melts derived from molecular theory: Rolie–poly equation. *Journal of Non-Newtonian Fluid Mechanics*, 114(1):1–12, 2003.

[4] Andrzej Ziabicki and Hiromichi Kawai. *High-Speed Fiber Spinning: Science and Engineering Aspects*. Wiley, 1985.

Harmonious labeling of modified butterfly graph

Premathilaka M.H.H.D.N [1*] **and Perera A.A.I** [2]
[1] Department of Physical Sciences, Rajarata University of Sri Lanka
[2] Department of Mathematics, University of Peredeniya, Sri Lanka
*Corresponding author; E-mail: nimanthadulaj49@gmail.com

Background

Our research paper is based on a special type of graph labeling called harmonious labeling. We define a special type of which is the modified butterfly graph (shape of butterfly graph) obtained from the star graph . Also the butterfly graph with a symmetrical pattern [3].Harmonious labeling was introduced by Graham and Sloane in 1983 [2].
They also define an injective labeling $G(v, e)$, $f : v(G) \to 0, 1, 2, 3, ..., n-1$ such that the edges $[f(u) + f(v)]modn$ are distinct for all edges as $uv(edge)$ Many algorithms were developed to harmonious labeling in communication networks, code transportation, and create combinatorial designs and construct harmonious labeling for various classes of graphs [5, 4].The harmonious labeling specializes in several special types of graphs, such as stars (trees) [1]

Methods

In this section, we have generalized the butterfly graph from the star graphs. All-star graphs are harmonious. Our generalized butterfly graphs are shown below in Figure 1. When we connect degree 1, two vertices from an edge in the star graph. There are two edges that can be defined for new graph .Also we have got this new modified butterfly graph with symmetrical pattern as figure 1 The additional two edges are labeled as 0 and $n+1$, respectively, $(n+2) \mod (n+2)$ and $(n+1) \mod (n+2)$ other vertices can be labeled as remaining vertices where $N, M, m < n$ and N, M, m are label of vertices

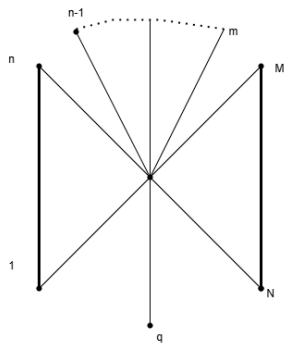

Figure 1: Modified butterfly graph

Results and Conclusions

In our research, star graphs have been harmonious, and also stars are trees. It is known the trees are harmonious. When we connect the degree one two vertices in a star graph. Also, this two edges are connected symmetrically, as figure 1 The labels of both such edges are become 0 and $n+1$ Therefore, our new graph is always harmonious, and it can be called a modified graph of the butterfly graph. In the future, we expect to modify this graph by the more than two edges to original star graph

Keywords:

Graph theory, Harmonious labeling, Star graphs, Butterfly graphs

References

[1] Christian Barrientos and Sarah Minion. Harmonious graphs from a-trees. *Electronic Journal of Graph Theory & Applications*, 9(2), 2021.

[2] Ronald L Graham and Neil James Alexander Sloane. On additive bases and harmonious graphs. *SIAM Journal on Algebraic Discrete Methods*, 1(4):382–404, 1980.

[3] J Jeba Jesintha and K Ezhilarasi Hilda. Shell-butterfly graphs are harmonious. *Advances and Applications in Discrete Mathematics*, 14(1):39–50, 2014.

[4] M Subbiah. A study on some variations of graph labeling and its applications in various fields. 2011.

[5] Roberto Tamassia. *Handbook of graph drawing and visualization*. CRC press, 2013.

Prime labeling of the snake-like graph and its generalization

Jayasundara J.H.M.R.M [1*] **and Perera A.A.I** [2]
[1] Department of Physical Sciences, Rajarata University of Sri Lanka
[2] Department of Mathematics, University of Peradeniya, Sri Lanka
*Corresponding author; E-mail: rasikajayasundara36@gmail.com

Background

Graph labeling is one of the most important areas in graph theory, as it explores ways to assign labels to graph elements under specific conditions. Among the various labeling methods, prime labeling is particularly significant due to its unique connection to number theory and its applications in coding, cryptography, and network design.[4, 3] Roger Entringer introduced the concept of prime labeling in the 1980s. A graph is said to have prime labeling if its vertices can be labeled with distinct integers 1, 2, ..., n such that for every edge uv, the greatest common divisor (gcd) of the labels of vertices u and v is 1, meaning the labels of vertices connected by an edge must be relatively prime.[1]

Our work focuses on prime labeling for a snake-like graph and its generalization formed by connecting a special type of graph iteratively in a linear sequence.

Methods

In this section, we prove that our snake-like graph admits prime labeling by assigning natural numbers. This special type of graph is defined by using K_2, C_3 and C_4. We connect n times of special type graph in a linear sequence, forming a structure with $6n$+1 vertices.

In our labeling, the initial vertex of each special type of graph is labeled as $6n$-5, while the remaining vertices are labeled according to the pattern shown in Figure 1 [5]

$gcd[6n\text{-}5\ ,\ 6n\text{-}4]=1$
$gcd[6n\text{-}4\ ,\ 6n\text{-}3]=1$
$gcd[6n\text{-}2\ ,\ 6n\text{-}1]=1$
$gcd[6n\text{-}1\ ,\ 6n]\ =1$
$gcd[6n\ ,\ 6n{+}1]\ =1$
$gcd[6n\text{-}2\ ,\ 6n{+}1]=1$
$gcd[6n\text{-}3\ ,\ 6n\text{-}1]=1$
$gcd[6n\text{-}4\ ,\ 6n\text{-}1]=1$

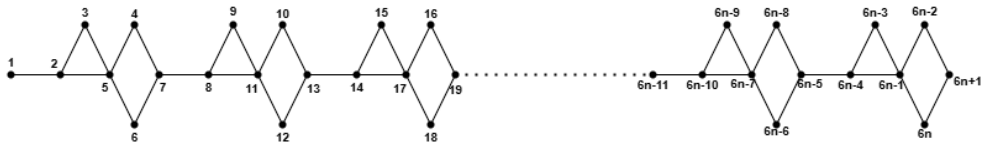

Figure 1: prime labeling of snake-like graph with n number of units with $6n$+1 vertices

We have generalized our snake-like graph according to the prime labeling condition. By connecting the initial vertex and the terminal vertex, it is evident that the

greatest common divisor (gcd) of 1 and $6n+1$ is 1, satisfying the condition for prime labeling. Consequently, the circular graph formed by this connection also admits prime labeling.

Results and Conclusions

Prime labeling is a significant area of graph theory due to its theoretical depth and practical applications. In this research paper we discussed the prime labeling of snake-like graphs using natural numbers. Then we defined the algorithm for labeling the above graph. In this paper, we discuss a new pattern for a circular graph as a belt by connecting an initial vertex and a terminal vertex.

In our future work, we plan to generalize this result by including larger cycles of polygons and exploring potential applications of this prime labeling in various fields.

Keywords:

Prime labeling, Graph theory, Snake graphs, Cycle graphs, Natural numbers

References

[1] Minusha Indunil and A.A.I Perera. Prime labelling of skeleton of a spider graph. 10 2021.

[2] Michael Lesk and Brian Kernighan. Computer typesetting of technical journals on UNIX. In *Proceedings of American Federation of Information Processing Societies: 1977 National Computer Conference*, pages 879–888, Dallas, Texas, 1977.

[3] Ajaz Ahmad Pir and A Parthiban. Prime distance graphs and applications of graph labeling: A modelling approach. 2022.

[4] N Ramya, K Rangarajan, and R Sattanathan. On prime labeling of some classes of graphs. *International Journal of Computer Applications*, 44(4):975–8887, 2012.

[5] Amanda Ross. A brief look at arithmetic and geometric sequences. In *Pedagogy and Content in Middle and High School Mathematics*, pages 77–80. Brill, 2017.

An alternative approach for antimagic labeling of generalized wheel graph

Malinda M.P.I [1*] **and Perera A.A.I**[2]
[1] Department of Physical Science, Rajarata University of Sri Lanka
[2] Department of Mathematics, University of Peradeniya
*Corresponding author; E-mail: imeshmalinda592@gmail.com

Background

An antimagic labeling of a graph *G=(V,E)* is a graph labeling in which the edges of the graph are labeled with different positive integers 1, 2, 3,.., m such that the sum of the labels of the incident edges at each vertex is distinct and unique for all vertices[4, 2]. Presenting a proof for K_2, an antimagic labeling concept was introduced by Hartsfield and Ringel[1]. In this paper, we discuss the antimagicity of the wheel graph and generalization for W_6. We proved a general equation for generalized wheel graph to anti-magic labeling[3].

Methods

Consider W_6, $n = 6$. Then, the number of outer cycles(O_c) is N and the number of outer vertex(O_v) is (n-1).

Edge labeling

Edge labeling can be written as an arithmetic sequence[5].

For outer cycles	For Spokes
1, 11, 21, 31,....., (1+2k-O_v), (1+2k)	6, 16, 26, 36,....., (6+2k-O_v), (6+2k)
2, 12, 22, 32,....., (2+2k-O_v), (2+2k)	7, 17, 27, 37,....., (7+2k-O_v), (7+2k)
3, 13, 23, 33,....., (3+2k-O_v), (3+2k)	8, 18, 28, 38,....., (8+2k-O_v), (8+2k)
4, 14, 24, 34,....., (4+2k-O_v), (4+2k)	9, 19, 29, 39,....., (9+2k-O_v), (9+2k)
5, 15, 25, 35,....., (5+2k-O_v), (5+2k)	10, 20, 30, 40,....., (10+2k-O_v), (10+2k)

Table 1: Edge labeling for W_6 with n^{th} number of outer cycles

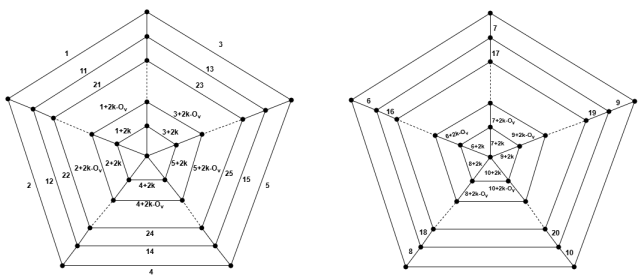

Figure 1: Edge labeling for outer cycles and spokes of W_6^N

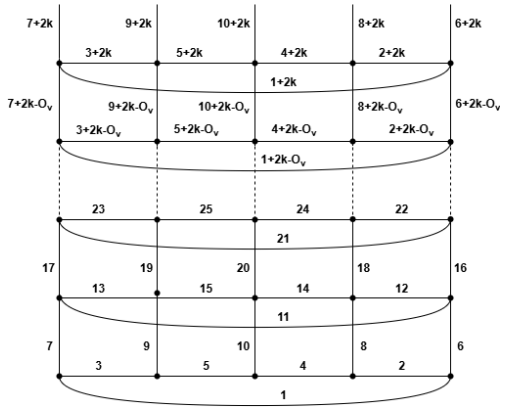

Figure 2: Edge labeling for outer cycles and spokes of expanding W_6^N

Results and Conclusions

The wheel graph can be labeled according to the anti-magic labeling concept[3]. In this paper, we have given an anti-magic label for the generalized wheel graph *(W_6^N; $n = 6$, $N \geq 1$, $N,n \in Z^+$)* and have proven that our generalized wheel graph (W_6^N) is also anti-magic. In our future work, we plan to label the generalized wheel graph when $n \geq 4$, $n \in Z^+$.

Keywords:

Anti-magic labeling, Arithmetic sequence, Edge labeling, Wheel graph

References

[1] N Hartsfield and G Ringel. Pearls in graph theory academic press. *United Kingdom*, 1994.

[2] Ancy Kandathil Joseph and Joseph Varghese Kureethara. The cartesian product of wheel graph and path graph is antimagic. *Communications in Combinatorics and Optimization*, 8(4):639–647, 2023.

[3] KMPGSC Kapuhennayake and AAI Perera. An alternative approach for the anti-magic labelling of a wheel graph and a pendant graph. *J. Sci*, 12:47–60, 2021.

[4] Vinothkumar Latchoumanane and Murugan Varadhan. Antimagic labeling for product of regular graphs. *Symmetry*, 14(6):1235, 2022.

[5] Amanda Ross. A brief look at arithmetic and geometric sequences. In *Pedagogy and Content in Middle and High School Mathematics*, pages 77–80. Brill, 2017.

Risk-adjusted performance comparison across different financial indices

Guillaume Leduc[1*]
[1] American University of Sharjah, Sharjah, UAE.
*Corresponding author; E-mail: gleduc@aus.edu

Background

A crucial factor in any investment is the balance between risk and reward. Higher-risk investments should offer greater returns compared to conservative ones. Which level of risk is better? Asset performance is commonly assessed using metrics like the Sharpe ratio, Jensen's alpha, and Treynor ratio, which simplify risk using measures such as standard deviation and beta. While variance-based methods suit normal distributions, they may overlook key risks features. Alternatives like the Calmar and Sortino ratios consider downside risk but remain simplistic. Value-at-Risk (VaR), Conditional Value-at-Risk (CVaR), Tail Value-at-Risk (TVaR), and modified Value-at-Risk (mVaR) provides a more sophisticated assessment of risk compared to standard deviation or drawdown.

Risk-adjusted performance metrics have been developed to incorporate risk measures, represented as the ratio of excess return to risk, expressed as

$$\frac{\text{expected return on investment - risk free rate}}{\text{measure of risk at a level of confidence } \alpha}.$$

In [1], the economic implications of applying such risk-adjusted performance metrics are analyzed. A particularly interesting risk-adjusted performance metrics is introduced in [2]. It has several interesting properties and coincides with the well-known Sharpe ratio under the assumption of normally distributed returns. It is defined as

$$RtV_S(\alpha) = \frac{\partial \bar{R}_\Lambda}{\partial VaR_\Lambda(\alpha)},$$

where $\bar{R}_\Lambda$ is the expected return of portfolio Λ, and $VaR_\Lambda(\alpha)$ is its value at risk at a level of confidence $0 \leq \alpha \leq 1$.

It turns out to be true—albeit not immediately obvious—that a greater marginal reward $\partial \bar{R}_\Lambda / \partial VaR_\Lambda(\alpha)$ leads to a higher expected reward $\bar{R}_\Lambda$ at a given confidence level α. However, since derivatives represent local properties, it is certainly not the case that a significantly greater marginal reward results in a significantly greater expected reward. This becomes particularly relevant when the highest-performing asset only slightly outperforms, or does not statistically significantly outperform, another asset that offers superior complementary attributes, such as enhanced diversification, improved tax efficiency, or better alignment with ethical or environmental objectives.

Methods

To tackle this issue, we propose the concept of Reward-VaR curves, $RV_S(\alpha)$. Assume that the risk-adjusted performance of L assets, $S_1, ..., S_L$ is to be assessed. First we define the minimum level of confidence, α_0, such that all assets have a positive

VaR at levels $\alpha \geq \alpha_0$. For each asset S_i and each level of confidence α, a portfolio, Λ_i, containing the risk free asset and the asset itself is constituted. The portfolios $\Lambda_1, ..., \Lambda_L$ are designed in such a way that they all have the same value at risk, ν. Then we define the maximum amount at risk achievable by all of these portfolios, $\nu(\alpha)$, under the constraints that the risk free asset cannot be shorted. This allows us to define the *Reward-VaR curves*, $RV_{S_i}(\alpha)$, as

$$RV_{S_i}(\alpha) = r_f + (r_f + v_0(\alpha)) RtV_{S_i}(\alpha).$$

It is clear that the ranking of risk-adjusted performance by the Reward-VaR curve and the Reward-to-VaR ratio coincide. However, when measuring the historical performance of those asset over a given period of time, bootstrapping can be used to determine if the most performant asset is significantly more performant or only marginally more performant than the other assets. For instance, asset S_1 can be considered more performant than asset S_2 if the difference $RV_{S_1} - RV_{S_2}$ exceeds one standard deviation of the bootstrapped sample distribution.

We use the Reward-VaR curve risk-adjusted performance metric to analyze and compare the performance of various stock indices across different market conditions—bull, bear, and overall periods—spanning from January 2, 1997, to July 1, 2024. Our analysis covers nine global markets, where we compute the Reward-to-VaR ratio at various confidence levels and horizons. The market cycles are segmented using the Dow Jones Industrial Average, defining distinct bull and bear periods. Performance comparisons are conducted through bootstrapped Reward-VaR distributions, with the average and standard deviation of the Reward-VaR difference used to assess statistical significance. This approach allows us to determine risk levels for which one index significantly outperforms the other.

Results and Conclusions

A phase diagram pattern is often observed: one index performs better at high confidence levels, the other index performs better at low confidence levels, and both become statistically equivalent at mid-range confidence levels. Furthermore, the pattern observed in bull markets often mirrors that of bear markets, with the index that performs better at high confidence levels becoming the better performer at low confidence levels. When a statistically significant difference is observed, our risk-adjusted performance metric can assist investors in selecting optimal assets based on their risk preferences: risk-averse investors may prefer stocks that perform best at high confidence levels, while those seeking higher returns with greater risk may opt for stocks offering the highest rewards at lower confidence levels.

Keywords:

Portfolio theory, Statistical methods; risk measures, Applications of statistics to actuarial sciences and financial mathematics, Asset pricing,Corporate finance

References

[1] Gordon J Alexander and Alexandre M Baptista. Economic implications of using a mean-var model for portfolio selection: A comparison with mean-variance analysis. *Journal of Economic Dynamics and Control*, 26(7-8):1159–1193, 2002.

[2] Gordon J Alexander and Alexandre M Baptista. Portfolio performance evaluation using value at risk. *The Journal of Portfolio Management*, 29(4):93–102, 2003.

Modeling Dengue emergence risk with temperature-dependent extrinsic incubation period

Piyumi Chathurangika[1,2*], **S. S. N. Perera**[1] **and Kushani De Silva**[3]

[1] Research & Development Centre for Mathematical Modeling, Department of Mathematics, University of Colombo, Sri Lanka

[2] Department of Electrical & Electronics Technology, Faculty of Technology, Rajarata University of Sri Lanka

[3] Department of Mathematics and Statistics, University of North Carolina at Greensboro, Greensboro, NC, USA

*Corresponding author; E-mail: piyumic.maths@stu.cmb.ac.lk

Background

Dengue, a vector-borne disease, accounts for over 390 million cases annually, posing a significant global health burden. Mathematical modeling has been identified to be a useful tool in devising effective prevention strategies in advance, in order to mitigate the dengue emergence risk (DER). Vectorial capacity (V_s), a key metric in assessing DER quantifies the number of secondary infections caused by a single infected individual in a susceptible population. It takes into account factors such as vector density, biting rate, mortality rate, vector competence, and the extrinsic incubation period (EIP) [1].

Temperature critically influences DER by affecting vector survival and metabolism, particularly the EIP, which represents the latency between a vector taking a viremic blood meal and becoming infected [2, 3]. This study introduces a temperature-dependent DER model incorporating the relationship between temperature and EIP using the V_s equation. Applying the model to temperature data from Sri Lanka's Colombo district, the region with the highest dengue incidence, it is aimed to identify seasonal patterns of DER with respect to temperature.

Methods

The relationship between temperature and EIP is established by drawing an analogy between particle activity and vector metabolism in response to temperature, using the Maxwell-Boltzmann distribution in Eq. (1),

$$f(EIP) = 4\pi EIP^2 \left(\frac{m}{2\pi kT}\right)^{3/2} e^{-\frac{mEIP^2}{2kT}}, \tag{1}$$

where m is the vector life span and T is temperature. Parameter k needed to be estimated relative to the context of dengue emergence. For that, experimental results on the temperature-EIP relationship were gathered from literature. A non-linear data fitting approach was first applied to the gathered information to eliminate inconsistencies in the data. Maxwell-Boltzmann distributions were generated for several temperature values, with each distribution constructed such that its peak corresponded to the EIP value for the respective temperature. To achieve this, the parameter k was adjusted through a trial-and-error method. The adjusted k values obtained at different temperatures were used to calculate a scaling factor relative to the minimum k. An exponential curve was then fitted to describe the relationship between temperature and the scaling factor of k, resulting in the equation for parameter k: $k = 2.2841 \times 10^{38} e^{-0.3143T}$. DER was then estimated for different temperature values via the V_s equation,

$$V_s(t) = zb^2 v_c \left(\frac{e^{-\mu_v EIP}}{\mu_v} \right), \tag{2}$$

where, z is the per-capita vector density, v_c is the vector competence, μ_v is the vector mortality rate and EIP is the extrinsic incubation period. Per-capita vector density was taken with respect to mean seasonal rainfall. Four seasons were defined (based on annual dengue emergence pattern) and in each season, minimum and maximum temperatures were recorded using weather data. For these temperature values, V_s was calculated using Eq. (1) and (2). These values, derived from the minimum and maximum temperatures, defined a maximum V_s ($V_s(\max)$) and a minimum V_s ($V_s(\max)$), from which we obtained a V_s range ($V_s(\max) - V_s(\min)$) for each season, capturing the effects of temperature fluctuations.

Results and Conclusions

Table 1: V_s (min), V_s (max) and V_s range and mean seasonal rainfall in the 4 season.

Season	1	2	3	4
V_s (min)	245.81	256.44	234.39	227.43
V_s (max)	295.98	292.38	290.92	295.69
V_s range	50.17	35.94	56.54	68.26
Seasonal rainfall	35.83	52.12	36.21	30.98

While $V_s(\max)$ show minor seasonal differences, $V_s(\min)$ varies significantly, with Season 2 being the highest and Season 4 the lowest. Seasons 1 and 3 have moderate $V_s(\min)$ values. Season 4, with the lowest $V_s(\min)$, largest V_s range and the lowest mean rainfall, shows the most fluctuation, while Season 2, with the highest $V_s(\min)$, smallest V_s range, and highest mean rainfall, shows the highest DER. Seasons 1 and 3 exhibit moderate fluctuations in DER.

In conclusion, the finding of this study reveals that the highest DER in Colombo district occurs in season 2 (August - October) corresponding to highest rainfall and minimum temperature fluctuations. DER in seasons 1, 3, and 4 exhibit greater fluctuations corresponding to temperature fluctuations and moderate rainfall. Consequently, this study highlights the time periods to which attention should be given in controlling DER in the Colombo district of Sri Lanka further showcasing the importance of utilizing environmental factors in assessing DER.

Keywords:

Mathematical modeling, Probability distributions, Climate science and climate modeling

References

[1] C Garrett-Jones, Joaquim Alves Ferreira Neto, World Health Organization, et al. The prognosis for interruption of malaria transmission through assessment of the mosquito's vectorial capacity. Technical report, World Health Organization, 1964.

[2] A Rohani, YC Wong, I Zamre, HL Lee, MN Zurainee, et al. The effect of extrinsic incubation temperature on development of dengue serotype 2 and 4 viruses in aedes aegypti (l.). *Southeast Asian Journal of Tropical Medicine and Public Health*, 40(5):942, 2009.

[3] Fang-Zhen Xiao, Yi Zhang, Yan-Qin Deng, Si He, Han-Guo Xie, Xiao-Nong Zhou, and Yan-Sheng Yan. The effect of temperature on the extrinsic incubation period and infection rate of dengue virus serotype 2 infection in aedes albopictus. *Archives of virology*, 159:3053–3057, 2014.

Assessing the economic benefits towards value added tourism plans in Sri Lanka

N.A.T.P. Nishshanka[1*], **K.K.W.H. Erandi**[1] , **H.O.W. Peiris**[2] **and S.S.N. Perera**[1]
[1] Centre for Mathematical Modelling, University of Colombo, Sri Lanka
[2] Department of Mathematics and Computer Science, Open University, Sri Lanka
*Corresponding author; E-mail: tharukaprabashwari99@gmail.com

Background

Tourism is considered as an important economic activity around the world due to its direct economic impact as well as its significant indirect and induced impacts. The tourism sector is the third largest source of export revenue in Sri Lanka and is essential for economic growth. The worldwide epidemic and the Easter attack had an adverse impact on Sri Lanka's tourist sector. This has prevented the sector from reaching its full potential since 2019 [1].

This study looks at value-adding techniques that other nations have used to survive the difficult times caused by pandemics, and assesses the applicability of these approaches to Sri Lanka for the purpose of optimizing economic gains.

Methods

The primary challenge in accomplishing the goals of this research is the insufficiency of statistical data necessary to complete the project. This is because the research essentially estimates the overall levels of economic benefit that will be generated with the implementation of the suggested value-added strategies. A fuzzy approach was used to accomplish the ultimate goal of this research [2].

The model used in this study deals with three variables, Arrival Impact, Job Creation, and Revenue Generation. Setting the weights is the first step towards obtaining the final output from the model. Pairwise comparisons based on expert insight were conducted as part of this approach. The linguistic levels for each variable in each value addition technique are obtained. once the model weights have been determined. The final output is obtained by a series of consecutive processes after the weights and linguistic levels for each value addition method under each variable are obtained.

The fuzzy numbers of the weights and linguistic levels are multiplied for each value addition method, giving single fuzzy numbers for each variable. The centroid method is then used to defuzzify in order to provide a single defuzzified value for every variable in each value addition method. Lastly, the three membership values that were obtained for each value addition method are aggregated again using the LOWA method [3].

Results and Conclusions

According to the results, promoting authentic local dishes and handicrafts represents best practices across various tourism sectors, contributing to cultural preservation and economic growth. Cleanliness emerges as a critical factor in the Beach and Adventure sectors, capable of amplifying positive economic impacts. Strategies such as effective branding, leveraging social media platforms, and collaborating with travel

influencers are recommended for fostering interconnectedness across all tourism sectors. However, excessive infrastructural development should be avoided as it may have a negative impact on the scenic beauty and rich biodiversity of the wildlife and adventure sectors. Additionally, the influx of backpackers plays a significant role in economic diversification and fostering sustainable growth.

Keywords:

Fuzzy set, Fuzzy logic, Decision making, Tourism

References

[1] Sri Lanka Tourism Development Authority. 2019 statistical annual report. Published report, Sri Lanka Tourism Development Authority, Research and International Relations Division, 2019. Available at: `https://www.sltda.gov.lk/en/annual-statistical-report` (Accessed: 9 January 2024).

[2] L.A. Zadeh. Fuzzy sets. *Information and Control*, 8(3):338–353, 1965.

[3] HOW Peiris, SSN Perera, S Chakraverty, and SMW Ranwala. Development of a mathematical model to evaluate the rate of aggregate risk of invasive alien plant species: Fuzzy risk assessment approach. *International Journal of Biomathematics*, 11(04):1850049, 2018.

Quantitative evaluation model for customer satisfaction in the private banking sector in Sri Lanka

S.Y. Munasinghe[1*], K.K.W.H. Erandi[1], H.O.W. Peris[2] and S.S.N. Perera[1]
[1] Centre for Mathematical Modeling, Department of Mathematics, University of Colombo,Sri Lanka;
[2] Department of Mathematics,Open University of Sri Lanka,Sri Lanka
*Corresponding author; E-mail: sammaniemunasinghe@gmail.com

Background

Customer satisfaction is a concept that is characterized by vagueness due to the uncertainty inherent in human judgments and various factors that affect them. In the competitive landscape of banking, understanding, evaluating, and enhancing customer satisfaction stands as an essential requirement. Hence, this study aims to develop a mathematical model that could capture this uncertainty to evaluate customer satisfaction in the banking sector as a case study for Sri Lanka. In this work, we construct two models with linguistic inputs to evaluate customer satisfaction [1].

Methods

The methodology has started with identifying the factors that affect customer satisfaction. In this work, two customer satisfaction models have been developed particularly for the banks with the majority of Private and Government employees and banks with the majority of self-employees. As the next step, the weights of each co-factor to the main factor and the weights of each main factor to the overall customer satisfaction were obtained using a pairwise comparison among experts in the banking industry and results were aggregated using the Linguistic Ordered Weighted Average (LOWA) method [2]. Then considering the weights of co-factors and the customer satisfaction levels given by the customers, the customer satisfaction level for a main factor has been obtained again using the LOWA method [3]. Finally, those two models are capable of aggregate satisfaction levels across various co-factors and provide an overall measure of customer satisfaction for each customer.

Results and Conclusions

After the development of the model, we validated the model with data from a survey and produced significant satisfaction levels. This linguistic approach is highly beneficial since the performance values cannot be expressed using numerical values, and this approach gives a more flexible way to deal with evaluating customer satisfaction using qualitative information.

The study identifies key factors influencing customer satisfaction in private banks in Sri Lanka, highlighting "Products and Services" and "Cost and Pricing" as the most significant across all employee categories. For private and government employees, additional factors such as "Confidentiality" and "Service Quality" play a crucial role due to their stable incomes, time constraints, and security concerns. Self-employed individuals, on the other hand, prioritize business-supportive financial services, competitive pricing, and digital banking solutions. Strengths identified include confidentiality, transparency, and friendly staff, while weaknesses such as long

wait times, inadequate parking, inefficient customer service, and high charges require improvement.

The study also notes that customer satisfaction with e-banking varies by age, with younger customers favoring digital platforms while older customers prefer traditional banking. Future research aims to extend the model to include unemployed individuals and refine customer satisfaction analysis by incorporating the age factor.

Keywords:

Fuzzy logic, Fuzzy operator theory, Logic of vagueness

References

[1] Lotfi Asker Zadeh. The concept of a linguistic variable and its application to approximate reasoning—i. *Information sciences*, 8(3):199–249, 1975.

[2] Tarifa S Almulhim, Ludmil Mikhailov, and Dong-Ling Xu. Deriving weights from group fuzzy pairwise comparison judgement matrices. In *Advances in Information Systems and Technologies*, pages 545–555. Springer, 2013.

[3] H.C. Huang and C.C. Ho. Applying the fuzzy analytic hierarchy process to consumer decision-making regarding home stays. *International Journal of Advancements in Computing Technology*, pages 981–990, 2013.

Enhancing YouTube content safety: Muting harmful voice and validating information using NLP

Lalithya Nawanjana Heiyanthuduwa[1*] **and Chandula Rajapaksha**[1]
[1] National Institute of Business Management (NIBM), Sri Lanka
*Corresponding author; E-mail: lalithyanawanjana@gmail.com

Background

YouTube has become the leading platform for online video sharing among social media platforms. According to Statista, YouTube is estimated to have 2.7 billion users worldwide by 2024 [1]. YouTube offers diverse content and monetization but faces criticism for spreading harmful content, misinformation, and cyberbullying, leading to negative user experiences.

This research addresses the lack of existing solutions for detecting harmful voices and false information on YouTube by exploring innovative techniques for identifying such content in entertainment videos.

Methods

The goal is to conduct feasibility studies, collect data, and apply NLP techniques and ML models. A survey was also conducted to gather user feedback on harmful voices and false information on YouTube.

The research framework uses ML and NLP techniques to detect harmful voices and validate information on YouTube. Data is collected from videos and comments, preprocessed to clean and analyze text, and categorized as true, false, or neutral. ML models are then developed for accurate detection, with a user-friendly interface and a backend system using REST APIs for communication with the YouTube platform.

Separate research has been conducted to investigate harmful voice and false information detection on YouTube.

Alshamrani et al. used machine learning to analyze toxic behavior in YouTube news videos, identifying vulgar and hate speech, especially in topics like religion and crime [2]. MacLachlan examined hateful music videos promoting anti-Muslim sentiment in Myanmar, criticizing YouTube's role in spreading toxic speech [3]. Obadimu et al. applied epidemiological models to study toxicity spread in comments, highlighting control mechanisms [4]. Rahman and Sahayu studied YouTube gaming content's impact on children, finding inappropriate speech that could influence young audiences [5].

Results and Conclusions

YouTube struggles with detecting harmful content due to language limitations, content information, and algorithmic biases. Current research focuses mainly on English, highlighting the need for broader linguistic coverage. Ongoing efforts are crucial to improve accuracy and address these challenges across diverse languages.

The developed system achieved an accuracy of 87.43%, demonstrating its effectiveness in detecting harmful voices and validating false information. While the

results are promising, there remains room for improvement, particularly in enhancing precision and recall to better handle nuanced and multilingual content.

The research addressed ethical and social concerns by using advanced NLP, ML models, and user-friendly interfaces to reduce false information. This system improves content detection, creating a safer, more trustworthy YouTube experience and offering a practical solution to mitigate the impact of false information.

This research highlights harmful voices and misinformation in YouTube content, affecting users of all ages. It calls for improved moderation and neutrality measures, with trust in AI detection systems. Future recommendations include expanding system capabilities, automating processes, and enhancing multilingual support for better detection.

This research has contributed to creating a safer and more user-friendly online environment for users of the YouTube platform.

Keywords:

Detection, Harmful Voice , False Information , Natural Language Processing (NLP), Machine Learning (ML)

References

[1] J. Degenhard. Global: Youtube users 2020–2029. Technical report, Statista, 2024.

[2] A. Alshamrani, Q. Li, L. Hu, and Z. Li. Comprehensive analysis of toxic behavior in youtube comments on news videos using deep learning. *Journal of Artificial Intelligence Research*, 67:45–67, 2019.

[3] H. MacLachlan. The role of hateful music videos on youtube in promoting anti-muslim sentiment and violence in myanmar. *Human Rights and Digital Media Journal*, 15:134–152, 2019.

[4] A. Obadimu, M. Elsherief, H. M. Nguyen, and X. Liu. Modeling toxicity in youtube comments using epidemiological models. *Social Network Analysis and Mining*, 9:22–35, 2020.

[5] T. Rahman and S. M. Sahayu. The impact of youtube game content on children's development: Evidence of inappropriate speech acts in gaming streams. *Journal of Media and Child Development*, 11:211–223, 2023.

Pricing loan protection insurance product: Fuzzy logic approach

W. Dilmi Imesha Karunarathne[1*], **S.S.N. Perera**[1],**G.N. Karunathunge**[1] **and H.O.W. Peiris**[2]

[1] Centre for Mathematical Modeling, Department of Mathematics, University of Colombo,Sri Lanka;

[2] Department of Mathematics,Open University of Sri Lanka,Sri Lanka

*Corresponding author; E-mail: dilmi.karunarathne123@gmail.com

Introduction

Loan protection insurance is designed to help policyholders by providing financial support in times of need. Whether the need is due to death, disability or unemployment, this insurance can help cover monthly loan payments and protect the insured from default. This particular insurance product guarantees to pay the remaining balance of a loan as a benefit in the events of pre-agreed circumstances: death, disability and unemployment. It can offer either level payments or lump-sum payments [2].

As the benefit of this insurance product is offered when the policyholder defaults on the loan, the premium of the insurance product was assessed based on the policyholder's default risk. Default risk arises from default events such as the policyholder's death, disability, and unemployment, which are influenced by the policyholder's health conditions and job security.

Insurance pricing accuracy is fundamental to any insurance policy as it involves determining the appropriate premium to charge for a particular risk (pre-defined risks). Inaccurate pricing can lead to significant losses for both the financial institution and customers purchasing the insurance policy, as they may end up paying more than the actual value of the insurance product. Insurance institutes need to use accurate and relevant data for pricing insurance products. That data should included with personal data that is relevant to the future inflows and outflows associated with the insurance policy [1].

Methods

This study engages in analyzing premiums of loan protection insurance/decreasing term insurance policies by evaluating the risk of death or disability due to health factors, including existing and non-existent health conditions, and by assessing the risk of unemployment during the loan period.

Firstly, we selected default risk factors and sub-risk factors that affect default events such as death, disability, and unemployment. The sub-risk factors were defined as factors that affect the default risk factors. Then, we developed 0-10 index scales for each default sub-risk factor. Using fuzzy membership functions, we mapped these index scales into fuzzy membership functions. The continuous variables are converted using the sigmoid fuzzy membership function and discrete variables are converted to fuzzy sets using the singleton fuzzy membership function.

Subsequently, the fuzzy membership function values were aggregated using the Hamacher aggregation operator. This aggregation is performed pairwise. We determined the respective default risk levels for both existing health conditions and job security by utilizing linguistic fuzzy membership functions. The likelihood of the total

default risk value was determined by aggregating the likelihood of default values due to existing, and non-existing health conditions, and job security.

Finally, we developed a model for the premium of insurance products using the equivalence principle in actuarial mathematics.

Results and Conclusions

In this study, We defined the default risk levels for both existing health conditions and job security using the linguistic fuzzy membership function. Each default risk factor: existing health conditions and job security, contained seven default risk levels. Then there were a total of 49 categories of default risk. We calculated the premium of this particular insurance product for each of these 49 default-risk categories assuming a policyholder's information. This constituted another innovative feature of our study.

When discussing the results of this study, the validated dilution/concentration factors for each risk level showed significant differences. The "Unlikely" and "Very low" risk levels were determined as concentration factors because these risk levels were negatively impacted by default risk. This means that as these risk levels represented low risk, the total default risk was reduced compared to the general default risk. Conversely, the "Medium", "High" and "Very High" risk levels were determined as dilution factors because they were positively impacted by default risk. This indicates that as these risk levels represented high risk, the total default risk was increased compared to the general default risk. The "Extremely High" level was determined as a very high dilution factor, signifying that the total default risk significantly increased.

According to the calculated premiums for all risk categories, the premium of the insurance product increased with the rise in risk levels. This implies that when either the job security risk level or health risk level increased, the premium of the insurance also increased accordingly. From this observation, we concluded that risk level had a strong positive relationship with the premium of the insurance product. Additionally, policies that exhibited an "Extremely High" risk level for either job security or health were deemed ineligible to be offered.

According to the sensitivity analysis, it was found that the loan amount, age of the policyholder and loan term had a significant positive relationship with the premium of the insurance product while interest rate (fixed) had a negative relationship with the premium.

Keywords:

Fuzzy logic, Risk models (general), Actuarial mathematics, Derivative securities

References

[1] FasterCapital. Guideline Premium: The Benchmark for Insurance Pricing Accuracy - FasterCapital — fastercapital.com, 2024.

[2] ANA GONZALEZ RIBEIRO. Is Loan Protection Insurance Right for You? — investopedia.com. https://www.investopedia.com/articles/pf/08/loan-protection-insurance.asp, 2021. [Accessed 23-03-2024].

Impact of agrochemical ban reversal on rice retail prices in Sri Lanka

Yifei Zhu[1*], **Hasitha Erandi**[2], **and Sanjeewa Perera**[2]
[1] Graduate School of Humanities and Social Sciences, Hiroshima University, Japan
[2] Centre for Mathematical Modelling, University of Colombo, Sri Lanka
*Corresponding author; E-mail: d221575@hiroshima-u.ac.jp

Background

In order to fully organically grow within a decade, the Sri Lankan government banned the import of traditional agrochemicals (fertilisers and pesticides) on 6 May 2021 [1]. The ban led to reduced crop yields and increased food prices, exacerbating economic challenges during the COVID-19 pandemic and subsequent economic crisis. To address these issues, the government reversed its policy on 31 May 2022, allowing the use of chemical fertilisers. This study examines the effect of these policy changes on rice retail prices, addressing a gap in macro-level analyses of such interventions.

Methods

Weekly rice retail prices from 2021 and 2022 were obtained from the Department of Census and Statistics. Seven domestic rice types were analysed in 2021, while nine types, including imported varieties, were analysed in 2022. The missing data were linearly interpolated. The regression discontinuity design (RDD) was applied to assess causal effects, adopting a fuzzy design where treatment probabilities varied. Statistical analyses were performed using STATA 16.

Results and Conclusions

The data did not conform to a normal distribution, even after transformations; hence, non-parametric methods were employed. Analysis from 2021 revealed no significant discontinuities in rice prices when the agrochemical ban was implemented. However, the policy reversal in 2022 resulted in an 8.5% increase in rice retail prices, at 5% significant level.

To verify these findings, robustness checks were conducted by combining data from 2021, 2022, and 2023. Structural break tests were performed to identify significant changes in price trends [2]. When the structural break date was assumed to align with the ban reversal in 2022, the results supported the earlier findings, confirming a significant price change. When no specific date was assumed, the analysis identified an additional structural break in December 2023, suggesting that rice prices might decrease after this period.

The results highlight unexpected outcomes. In 2021, the government provided a preparatory period between announcing and implementing the ban, allowing stakeholders to adjust. Furthermore, sufficient reserves of agricultural inputs mitigated immediate price changes. In contrast, the restriction was lifted in 2022 during an economic crisis, with restricted access to agricultural supplies and price limitations imposed by a few domestic providers. These factors, together with trade imbalances, caused a significant increase in production costs and retail rice prices.

This study highlights how rapid policy changes, such as the reversal of the agrochemical ban, can inadvertently harm stakeholders. Policymakers should carefully evaluate the timing of such decisions and account for the diverse needs of affected parties to minimize adverse impacts.

Keywords:

Agrochemical ban, Regression discontinuity design, Panel data models, Structural breaks

References

[1] Mariano J Beillard and Ayodya Galappattige. Sri lanka restricts and bans the import of fertilizers and agrochemicals. 2021.

[2] Yiannis Karavias and Elias Tzavalis. Testing for unit roots in short panels allowing for a structural break. *Computational Statistics & Data Analysis*, 76:391–407, 2014.

Impact of probability distribution choices on standard precipitation index (SPI)

Sachini Karunarathne[1*], **Sanjeewa Perera**[1] **and Kushani De Silva**[2]
[1] Centre for Mathematical Modeling, Department of Mathematics, University of Colombo.
[2] Department of Mathematics and Statistics, University of North Carolina at Greensboro, Greensboro, North Carolina
*Corresponding author; E-mail: sachinik.maths@stu.cmb.ac.lk

Background

Drought is a natural phenomenon that occurs due to prolonged periods of deficient precipitation, resulting significant impacts to livelihood, agriculture, ecosystems, and water resources. Therefore, assessing and monitoring drought conditions are essential in mitigating the consequences of drought events. The Standard Precipitation Index (SPI) is a widely used tool in monitoring drought incidents. The SPI is constructed by fitting a Gamma distribution to long-term precipitation data, then estimating the cumulative probability, and finally transforming into a standard normal distribution. The negative SPI values indicate dry conditions while positive SPI values indicate wet conditions. The choice of probability distributions play a pivotal role in SPI calculations [1, 4] as it directly affects the process of constructing SPI values. Different probability distributions may lead to variations in drought re-occurrence periods, affecting the reliability of predictions of future droughts. Therefore, this study aims to investigate the uncertainty in drought re-occurrence periods arising from the use of different probability distributions to enhance SPI - based drought monitoring and improve decision-making processes, particularly in agricultural planning, in Sri Lanka.

Methods

This study analyzes the monthly rainfall data (mm) from 1981 to 2021, obtained from the Meteorological Department of Sri Lanka, with a focus on the North Central Province. Using these rainfall data, the Standardized Precipitation Index (SPI) was constructed considering the Gamma, Lognormal, and Weibull probability distributions, which are widely utilized in hydrological studies [1, 4, 2]. Drought events were identified based on the SPI threshold of -1 [3], and two key drought characteristics: drought severity (S) and duration (D) were then calculated. Drought severity is determined by taking the absolute value of the integral area under the SPI threshold value (-1). The drought duration is determined by counting the consecutive months or time units during which the indicator remains below the threshold value (-1). After identifying these drought characteristics, the interrelationship between these drought characteristics were captured using an appropriate copula with the use of Cramér-von Mises statistic. Finally, drought re-occurrence periods were estimated by constructing drought frequency curves.

Results and Conclusions

The Gamma, Lognormal, and Weibull probability distributions were fitted into monthly rainfall data of the North Central province. The SPIs were then constructed using each of these probability distributions. Thereafter the drought characteristics were identified based on the SPI threshold -1, revealing variations in the D and S depending on the chosen probability distribution. To model S and D, gamma and

exponential distributions were fitted respectively. The obtained Kendall's τ between D and S were 0.399, -0.019, and 0.431 for Gamma, Lognormal, and Weibull probability distributions respectively. Based on these dependency measures, the best-fitted copulas were then identified as Clayton for Gamma and Weibull distributions, and Frank for Lognormal distribution. Finally, using these selected best copulas, drought frequency curves were constructed which represent the relationship between drought re-occurrence periods and combinations of drought duration and severity (see Fig. 1). The obtained frequency curves emphasize the significant impact of the chosen probability distribution on drought analysis. Fig. 1 indicates that while all three probability distributions were used to model drought events, the Lognormal and Weibull distributions were more effective in detecting drought events with shorter drought duration and severity, compared to the Gamma distribution. Generally, the Lognormal distribution is known for its heavier tail, and the Weibull distribution, with a shape parameter ($k = 0.73$), also demonstrated the ability to capture heavier tails, supporting its suitability for modeling drought events with shorter drought duration and less severity [2]. Therefore, these findings confirm that the Lognormal and Weibull distributions are better suited for modeling drought events. Identifying less severe but more frequent drought events is crucial for agricultural planning as the droughts can severely affect on the crop yields. The Lognormal and Weibull distributions prove to be more beneficial in drought monitoring in North Central province, a region heavily reliant on agriculture in Sri Lanka. Moreover, these results underscore the importance of the choice of the appropriate probability distribution in drought monitoring as it directly affects the drought characteristics and the drought re-occurrence periods.

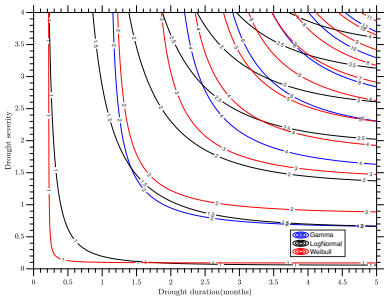

Figure 1: Drought re-occurrence periods obtained from Gamma, Lognormal and Weibull probability distributions.

Keywords:

Drought, drought duration, drought severity, copula, frequency curve

References

[1] Benedetta Moccia, Claudio Mineo, Elena Ridolfi, Fabio Russo, and Francesco Napolitano. Spi-based drought classification in italy: influence of different probability distribution functions. *Water*, 14(22):3668, 2022.

[2] SM Papalexiou, D Koutsoyiannis, and C Makropoulos. How extreme is extreme? an assessment of daily rainfall distribution tails. *Hydrology & Earth System Sciences Discussions*, 9(5), 2012.

[3] JT Shiau. Fitting drought duration and severity with two-dimensional copulas. *Water Resources Management*, 20:795–815, 2006.

[4] James H Stagge, Lena M Tallaksen, Lukas Gudmundsson, Anne F Van Loon, and Kerstin Stahl. Candidate distributions for climatological drought indices (spi and spei). *International Journal of Climatology*, 35(13):4027–4040, 2015.

New generalized algorithm for incidence coloring of square grid graph

S.S. Nuwanthi[1*], **A.A.I. Perera**[2],**M.A.M. Mohommad**[1]
[1] Department of Physical Science, Faculty of Applied Sciences, Rajarata University of Sri Lanka
[2] Department of Mathematics, Faculty of Science, University of Peradeniya, Sri Lanka
*Corresponding author; E-mail: nuwanthishyamika@gmail.com

Background

Graph theory is a fundamental area of discrete mathematics with wide-ranging applications in computer science, urban planning, transportation systems, and network optimization. This research focuses on incidence coloring, a variation of graph coloring, where colors are assigned to incidences so that adjacent incidences receive different colors. This concept was first introduced by Brualdi and Quinn Massey in 1993, involves determining the incidence chromatic number, which is the minimum number of colors required to satisfy incidence coloring conditions [1]. An incidence in a graph G is a pair (v,e), where v is a vertex incident to an edge e. Two incidences (v,e) and (w,f) are adjacent if one of the following conditions holds: (i) $v=w$, (ii) $e=f$, (iii) $vw=e$ or $vw=f$. These conditions ensure that adjacent incidences are assigned different colors, while non-adjacent incidences can share the same color. The study aims to develop algorithms for incidence coloring of the square grid graph and the step ladder graph.

Incidence coloring concept has been studied for various graph types, including trees, cubic graphs, planar graphs, and mesh structures, with research focusing on determining the incidence chromatic numbers for different graph classes [2],[3],[4]. However, no generalized algorithm has been developed for incidence coloring of square grid graphs. In this research, we develop a novel algorithm for the coloring of the incidence of square grid graphs, a type of graph, where the vertices are arranged in a two-dimensional grid and connected horizontally or vertically, forming a grid of squares. Practical applications of incidence coloring of square grid graphs include optimizing wireless network grids, Optimizing resource allocation in grid based scheduling systems and Cryptographic designs.

Methods

First, we must identify the structures of these square grid graphs by examining their vertices, edges, and how these vertices are interconnected. Square grid graphs are represented as the Cartesian product of the path graphs $Pm \times Pn$. Here, Pm and Pn are path graphs with m and n vertices, respectively. Assign distinct numerical values to each incidence, representing unique colors, while satisfying the conditions of incidence coloring. Systematically label vertices in the Square grid graph (e.g.,U_1 ,U_2,. . . ,U_n), and label incidences of each vertex (e.g. For the first vertex, label the incidences as $U_{1,1}$, $U_{1,2}$, ..., and continue similarly for the other vertices.) in a clockwise or anticlockwise manner. Using these labels and their corresponding values, identify patterns in the coloring process. Generalize these patterns into mathematical equations to develop a new algorithm for incidence coloring of Square grid graphs.

Results and Conclusions

The developed algorithm efficiently performs incidence coloring of square grid graphs with any finite number of vertices, ensuring the use of the minimum number of colors required for the process. This approach optimizes the coloring solution while adhering to the conditions of incidence coloring.

Keywords:

Graph Coloring, Incidence Coloring, Square Grid Graph

References

[1] Richard A Brualdi and Jennifer J Quinn Massey. Incidence and strong edge colorings of graphs. *Discrete Mathematics*, 122(1-3):51–58, 1993.

[2] Cheng-I Huang, Yue-Li Wang, and Sheng-Shiung Chung. The incidence coloring numbers of meshes. *Computers & Mathematics with Applications*, 48(10-11):1643–1649, 2004.

[3] Deming Li and Mingju Liu. Incidence coloring of the squares of some graphs. *Discrete mathematics*, 308(24):6569–6574, 2008.

[4] Shu-Dong Wang, Dong-Ling Chen, and Shan-Chen Pang. The incidence coloring number of halin graphs and outerplanar graphs. *Discrete Mathematics*, 256(1-2):397–405, 2002.

Hidden drivers of criminal violent behaviour of male convicts in Sri Lanka: A PLS-SEM approach

Chanika Jayasinghe[1*], Minasha Abeykoon[1], Seneviratne Somaratne[2], Ruwan Illeperuma[1], Isuru Thomas[1] and Thelma Abeysinghe[3]
[1]Department of Zoology, Faculty of Natural Sciences, The Open University of Sri Lanka, Nawala, Nugegoda
[2]Department of Botany, Faculty of Natural Sciences, The Open University of Sri Lanka, Nawala, Nugegoda
[3]Department of Chemistry, Faculty of Natural Sciences, The Open University of Sri Lanka, Nawala, Nugegoda
*Corresponding author; E-mail: cdjay@ou.ac.lk

Background

Criminal violence remains as one of the most pressing societal issues with enduring impacts on public safety, social stability, and individual well-being. The present study explores the causal relationships between genetic (Monoamine Oxidase A and Dopamine Transporter-1 genetic variants), childhood maltreatment, and impulsivity-driven tendencies in the manifestation of criminal violence of male convicts in Sri Lanka. Partial Lease Square Structural Equation Modelling (PLS-SEM) was used to assess and determine mediatory effects among these selected latent variables. PLS-SEM is an evolution of traditional linear modelling methods such as multiple regression and analysis of variance (ANOVA). Thus, PLS-SEM can be described as a process that combines factor analysis and multiple regression analysis simultaneously [1]. PLS-SEM is often used in predictions and exploratory research. In particular, PLS-SEM solves the difficulties of differentiating confirmatory and predictive methods because PLS-SEM has higher predictive accuracy while grounded in well-framed causal explanations [3]. Therefore, PLS-SEM was chosen for the analysis of data considering the following aspects [2]; a) Inadequacy of sample size, b) Scarcity of available theories, c) Requirement of higher predictive accuracy and d) Unawareness of the specification of the correct model.

Methods

The causal relationships and the mediatory effects of the genetic variants and questionnaire items were evaluated by developing a model using PLS-SEM SmartPLS 4 analysis. Indicators with zero standard deviation, a correlation of 1.00, and a collinearity of more than 5 were eliminated from the dataset prior to the construction of the model. Then, confirmatory composite factor analysis was conducted and the refinement procedure involved eliminating indicators based on their outer loading ($\leq$ 0.70) and higher cross-loadings ($>$ 0.50) from the initial model, resulting in a final path model. The significance of the path coefficients was evaluated by bootstrapping using 5000 iterations. The assessment of model validity followed a two-step process. Assessing the measurement model involved both discriminant and convergent validity tests. Convergent validity was confirmed using measures like Cronbach's Alpha, rho_A Composite Reliability, and Average Variance Extracted (AVE). Discriminant validity was assessed using cross-loadings and the Fornell-Larcker criterion, demonstrating the validity and reliability of the measurement model was valid and reliable. After

validating the measurement model, the inner model was assessed through predictive relevance and the relationships between constructs were analyzed using metrics like the coefficient of determination (R^2), the path coefficient (β value), T-statistics, effect size (f^2), and Goodness-of-Fit (GOF). These indicators collectively confirmed the robustness of the inner structural model. The model fit summary showed that the SRMR value was 0.055 for both measurement and structural models and the d_ULS ($<$ bootstrapped HI 95% of d_ULS) along with d_G ($<$ bootstrapped HI 95% of d_G), indicating that the models fit the data well.

Results and Conclusions

A conceptual framework was developed based on the literature and tested with PLS-SEM. The initial PLS-SEM model was constructed priory with 74 indicators (4 genetic variants from each gene, 28 Childhood Trauma Questionnaire items, 30 Barratt Impulsivity Scale-11 items and 8 crime types) and 64 indicators were purged out from the dataset based on the factor loadings (≥ 0.70), cross-loadings and VIF to construct the final model. The statistically significant path coefficients of direct effects and the total effects were used to conclude the determinants of criminal violence. The results extracted from the final model highlighted that *MAOA-L**3R and *DAT-1**9R/10R genetic variants, childhood maltreatment triggered by both emotional and physical negligence, and high impulsiveness triggered by lack of self-control are key determinants in committing violent crimes, particularly manslaughter. From a practical perspective, these findings underscore the critical importance of a child's mental well-being as a pivotal factor in shaping favorable behavioral patterns. This suggests that early childhood interventions may play a significant role in mitigating long-term behavioral changes and emotional consequences that could contribute to criminal tendencies.

Keywords:

PLS-SEM, Monoamine Oxidase A (MAOA), Dopamine Transporter-1 (DAT-1), Childhood Maltreatment, and Impulsivity

References

[1] Joe F Hair Jr, Lucy M Matthews, Ryan L Matthews, and Marko Sarstedt. Pls-sem or cb-sem: updated guidelines on which method to use. *International Journal of Multivariate Data Analysis*, 1(2):107–123, 2017.

[2] Heungsun Hwang, Naresh K Malhotra, Youngchan Kim, Marc A Tomiuk, and Sungjin Hong. A comparative study on parameter recovery of three approaches to structural equation modeling. *Journal of Marketing research*, 47(4):699–712, 2010.

[3] Marko Sarstedt, Joseph F Hair, Mandy Pick, Benjamin D Liengaard, Lăcrămioara Radomir, and Christian M Ringle. Progress in partial least squares structural equation modeling use in marketing research in the last decade. *Psychology & Marketing*, 39(5):1035–1064, 2022.

Relationship between perceived and actual dietary habits and glycemic control on patients attending the diabetic clinic of district general hospital Negombo

D.N.A.W.Samarakoon1[1*], U.P.Liyanage[2] , T. Samarasekara[3], H.K.Diwyanjalee [1] and R.S.M.P.Jayasooriya[1]

[1]Department of Biomedical science, Faculty of Health Sciences, KIU
[2]Deparment of Mathematics, Faculty of Science, University of Colombo
[3]Consultant endocrinology Unit, District General Hospital, Negambo
*Corresponding author; E-mail: Nirmani@kiu.ac.lk

Background

Diabetes mellitus has become a global health concern [2] with a prevalence of 14.2% for men, 13.5% for women in Sri Lanka [3]. The risk is increasing daily, bad dietary habits has been one of the major reasons behind improper glycemic control leading to diabetes-related complications [1].

This study aimed to identify the relationship between dietary habits and glycemic control among patients attending the diabetes clinic of District General Hospital Negombo.

Methods

The study was conducted with ethical approval from the KIU ethics review committee (KIU/ERC/24/027). An interviewer-administered questionnaire was given to a random sample of 350 patients to assess their dietary patterns, and glycemic control was evaluated through the questionnaire and clinical reports. Data analysis involved the use of chi-square tests and correlation assessments to identify significant patterns and relationships.

Results and Conclusions

According to the results obtained the mean age of the patient group is 54.54 ± 11.6, most of the patients were females (258(73.5%)). All the patients confirmed that they were taking the prescribed diet plan but none of the patients had any idea about the carbohydrate or calorie counts in the diet. The majority believed they have good glycemic control (99.7%), but according to the clinical reports 50(14.2%) have had blood glucose levels higher than 300mg/dL, and 11(3.1%) of the patients have had less than 60mg/dL blood glucose levels in the previous report. There was a significant difference between diabetes control perception and the actual blood glucose level ($p = 0.001$) among the patients. A total of 61(17.3%) of patients have misconceptions about their glycemic control.

In conclusion, the study reveals a significant gap between the perceived and actual glycemic control among type 2 diabetes mellitus patients ($p = 0.001$). Additionally, despite adherence to prescribed diet plans, there was a lack of understanding regarding carbohydrate and calorie content, which may contribute to poor glucose management.

Further there is a significant association between the perceived dietary control and carbohydrate counting of the patients ($P = 0.047$) as even though all patients perceive a good dietary control of diabetes, 342/351 do not count carbohydrate counts in their daily diet.

Keywords:

Diabetes Mellitus, glycemic control, dietary management, calories

References

[1] Yeo Jin Choi, Sang-Min Jeon, and Sooyoung Shin. Impact of a ketogenic diet on metabolic parameters in patients with obesity or overweight and with or without type 2 diabetes: a meta-analysis of randomized controlled trials. *Nutrients*, 12(7):2005, 2020.

[2] Nita Gandhi Forouhi and Nicholas J Wareham. Epidemiology of diabetes. *Medicine*, 38(11):602–606, 2010.

[3] Prasad Katulanda, Priyanga Ranasinghe, R Jayawardena, Rezvi Sheriff, and DR Matthews. The influence of family history of diabetes on disease prevalence and associated metabolic risk factors among sri lankan adults. *Diabetic Medicine*, 32(3):314–323, 2015.

Edge metric dimension of bicyclic graphs

K.G.E.H. Gayathrika[1*], and K.K.K.R. Perera[1]
[1] Department of Mathematics, University of Kelaniya
*Corresponding author; E-mail: erandakiringoda@gmail.com

Background

Slater introduced the 'metric dimension'(MD) concept in 1975 [4] to provide a framework for uniquely identifying the location of vertices in a connected graph using distances to a specific subset of vertices. In the last decade, this concept has drawn considerable interest from researchers, due to the wide range of applications in computer science, social networks, chemistry, biology, and many others. In 1976, Harary and Melter [5] further investigated the concept and introduced the term 'resolving set'. The Resolving set is a subset of vertices such that every vertex on the graph can be uniquely identified by its distances to the vertices in this subset, and the MD is the size of the smallest resolving set of that graph.

MD has several variants, and 'edge metric dimension'(EMD) introduced by Kelenc *et al.* focuses on identifying edges using a minimal resolving set [1]. Notably, this parameter can also be interpreted as the MD of the line graph, where the vertices represent the edges of the original graph and two vertices are connected if they are adjacent in the original graph. EMD is used to design resilient networks and optimize resources in systems. Recently, the EMD of certain families of graphs such as cycles, trees, complete bipartite graphs, trees and circulant graphs has been studied [3]. This study focuses on finding EMD in three types of bicyclic graphs that have not previously been studied. Bicyclic graphs play a vital role in chemical compound analysis, biological networks, and network design etc. Despite significant research on MD, its variant, EMD remained largely unexplored in the context of bicyclic graphs, and the objective here is to fill this research gap.

Methods

In this paper, graph is represented by G and it's line graph as $L(G)$. Vertex set $v_1, v_2, ..., v_n$ and edge set $e_1, e_2, ..., e_n$ of G is represented by $V(G)$ and $E(G)$ respectively. For simplicity, edge metric dimension of graph G is represented by $(\dim_E(G))$. Three types of bicyclic graphs defined in [2] are used in this research. We denote the number of vertices in two cycles by n and m and the length of the path as r.
Type I: $C_{n,m}(n, m \geq 3)$: Two disjoint cycles sharing a vertex.
Type II: $C_{n,r,m}(n, m \geq 3, r \geq 1)$: Two disjoint cycles connected by a path
Type III: $(\theta_{n,n,n}(n \geq 1))$: Three pairs of internally disjoint paths, each of length n, were constructed to connect two vertices.

Starting from the proper labeling of three types of bicyclic graphs(G) and the corresponding line graphs were constructed (Figures 1 to 4). The EMD is determined analytically and using Python simulations by varying the number of vertices in cycles and paths (n, m, r). Resolving sets (W) were identified, and vertex sets were partitioned based on their distances to W. A case study demonstrated that all vertices have distinct representations with respect to W, establishing $|W|$ as an upper bound for EMD. Using mathematical proofs, the lower bound was also shown to be equal to $|W|$, concluding that $\dim_E(G) = |W|$ for the analyzed graphs.

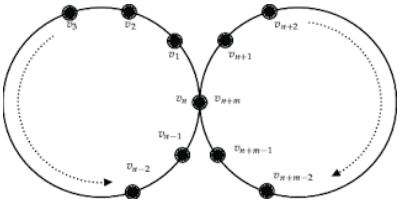

Figure 1: Type I bicyclic graph

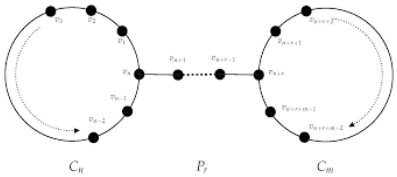

Figure 2: Type II bicyclic graph

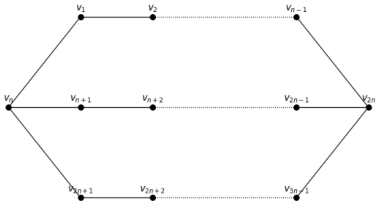

Figure 3: Type III bicyclic graph

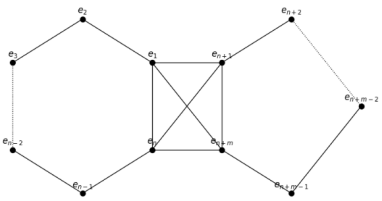

Figure 4: Line graph of type I

Results and Conclusions

The results revealed that all bicyclic graphs have a constant EMD and depend on structural properties, specifically the number of vertices in their cycles and paths. The edge metric dimensions of the type I, II, and III bicyclic graphs are $\dim_E(C_{n,m}) = 3$, $\dim_E(C_{n,r,m}) = 2$, $\dim_E(\theta_{n,n,n}) = 2$, respectively. For a Type I bicyclic graph, the edge metric basis is $W = \{e_1, e_n, e_{n+m}\}$, for a Type II, $W = \{e_1, e_{n+r+m}\}$, and for a specific case of Type III θ-graphs, $W = \{e_1, e_{n+1}\}$.
Having constant EMDs for all bicyclic graphs highlights their efficiency in applications such as resilient network design and molecular modeling. The study contributes to graph theory by addressing a theoretical gap and providing a foundation for exploring metric dimensions in more complex graphs.

Keywords:

Edge metric dimension, metric dimension, bicyclic graph, graph distance, resolving sets

References

[1] Aleksander Kelenc, Niko Tratnik, and Ismael G Yero. Uniquely identifying the edges of a graph: the edge metric dimension. *Discrete Applied Mathematics*, 251:204–220, 2018.

[2] Asad Khan, Ghulam Haidar, Naeem Abbas, Murad Ul Islam Khan, Azmat Ullah Khan Niazi, and Asad Ul Islam Khan. Metric dimensions of bicyclic graphs. *Mathematics*, 11(4):869, 2023.

[3] Lv X. & Nasir R. Lv, J. he edge version of metric dimension for the family of circulant graphs c (1, 2). *IEEE Access*, 9:78165–78173, 2021.

[4] Slater P.J. Leaves of trees. In *Proceedings of the 6th Southeastern Conference on Combinatorics, Graph Theory, and Computing*, pages 549–559, 1975.

[5] Harary F. & Melter R.A. On the metric dimension of a graph. *Ars Combinatoria*, 2:191–195, 1976.

Optimal placement of Bezier curve control points for efficient road design

M.P.D.S. Gunawardana[1*], **N. Yapage**[1]
[1] Department of Mathematics, Faculty of Science, University of Ruhuna, Matara, Sri Lanka
*Corresponding author; E-mail: gunawardana10771@usci.ruh.ac.lk

Background

Modern road design requires innovative methods that integrate safety, efficiency, environmental sustainability, and aesthetics. Bezier curves have emerged as a powerful tool in designing road geometries, enabling precision and flexibility in optimization. This research focuses on optimizing the placement of Bezier curve control points to achieve smooth transitions, minimal environmental impact, and compliance with safety standards like Stopping Sight Distance (SSD). The study aims to develop a robust framework to address the multidimensional challenges of modern transportation engineering [1, 2].

Methods

The study utilizes Bezier curves, defined through Bernstein polynomials, as the basic tool for optimizing road geometry. Computational methods, including Casteljau's Algorithm and the Simplex Search Method, were employed to refine curve configurations. A new algorithm was developed to enhance computational efficiency and precision. Empirical data were gathered from road surveys conducted by the Colombo Municipal Council and the Road Development Authority in Sri Lanka. Simulations were carried out using MATLAB, with additional visualization frameworks built with HTML (Hypertext Markup Language) and CSS (Cascading Style Sheet). The developed platform is capable of constructing various curve types, such as horizontal and vertical curves, including simple, compound, inverse, deviation, sag, and crest curves. The general mathematical equation for the Bezier curve of degree n is defined by $n+1$ control points $P_0, P_1, P_2, ..., P_n$ and given by [2, 3]

$$B(t) = \sum_{i=0}^{n} P_i b_{i,n}(t) \ ; 0 \leq t \leq 1,$$

where t is a real parameter and the Bernstein polynomial of degree n is defined by

$$b_{i,n}(t) = \binom{n}{i}(1-t)^{n-i}(t)^i \ ; 0 \leq t \leq 1.$$

Curve length $S(t)$ for a regular curve $\underline{r} = \underline{r}(t)$ over the interval $I = [t_0, t]$ is given by

$$S(t) = \int_{t_0}^{t} \left| \frac{d\underline{r}(t)}{dt} \right| dt.$$

Also, the relation between curve length and Bezier curve is given by

$$B'(t) = n \sum_{i=0}^{n-1} (P_{i+1} - P_i) b_{i,n-1}(t),$$

$$S(t) = \int_0^1 |B'(t)|\, dt = \int_0^1 \left| n \sum_{i=0}^{n-1} (P_{i+1} - P_i) b_{i,n-1}(t) \right| dt.$$

Results and Conclusions

- **A New Algorithm for Finding Suitable Curve Types:**
  To further optimize road design, a new algorithm introduced to find the most appropriate curve for a given road segment. This algorithm uses a multi-criteria optimization approach, considering factors such as road safety, environmental conditions, and vehicle dynamics. The algorithm evaluates various road parameters such as curvature, slope, and terrain type, selecting the most suitable Bezier curve that minimizes abrupt changes in direction, ensures ample SSD, and aligns with the natural terrain. This new algorithm employs an iterative search process, dynamically adjusting control points and analyzing the resulting curve using both geometric and physical criteria. The optimization process ensures that the final curve design maximizes safety while minimizing resource usage, contributing to both the environmental and economic sustainability of the road construction.
- **Development of a New Bezier Curve-Based Road Design Platform:**
  An innovative road design platform developed in MATLAB using the computer languages HTML and CSS, integrating the above algorithms for automated curve design and optimization. Key features of the platform include real-time control point adjustment for curve refinement and visualization of road geometry in 2D and 3D environments. This methodology demonstrates the potential of Bezier curves to innovate road designing process by improving safety, reducing environmental impact, and optimizing resources.

This study demonstrates the effectiveness of Bezier curves in optimizing road design by enhancing efficiency, safety, and sustainability. Their adaptability and precision improve road geometry, ensuring smoother transitions and minimal environmental impact. By integrating mathematical modeling with practical application, this approach redefines industry standards, offering engineers and designers a transformative tool for infrastructure development [4, 5].

Keywords:

Bernstein polynomial, Bezier curve, Casteljau's algorithm, Simplex search method, Stopping Sight Distance

References

[1] Ekinhan Eriskin, Sebnem Karahancer, Serdal Terzi, and Mehmet Saltan. Highway geometric design using bezier curve approximation. *Journal of Innovative Transportation*, 1(1):1104, 2020.

[2] Gerald Farin. *Curves and surfaces for CAGD: a practical guide*. Elsevier, 2001.

[3] Xi-An Han, YiChen Ma, and XiLi Huang. The cubic trigonometric bezier curve with two shape parameters. *Applied Mathematics Letters*, 22(2):226–231, 2009.

[4] Samuel Labi. *Introduction to civil engineering systems: A systems perspective to the development of civil engineering facilities*. John Wiley & Sons, 2014.

[5] Fred L Mannering and Scott S Washburn. *Principles of highway engineering and traffic analysis*. John Wiley & Sons, 2020.

Modeling and controlling learner retention and dropout dynamics in peer-assisted distance learning

W.A.L. Niwanthi[1*]
[1] Department of Mathematics & Philosophy of Engineering, The Open University of Sri Lanka, Nawala, Nugegoda
*Corresponding author; E-mail: waniw@ou.ac.lk

Background

Dropout is common in Distance Learning(DL) institutions due to various factors, including professional, academic, health, family, financial, and personal reasons. The impact of these factors varies based on the institution, program, subject selection, workload, peer support, and available learner assistance.

Many of studies on dropout rates of learners in DL system has carried out using statistical methods to analyse retain and drop out rates of distance learners using some selected courses. As a mathematical approach, Wickramaarachchi in [2] has defined a mathematical model using a system of non-linear differential equations to investigate the retention and dropout dynamic of students in an Open Distance Learning(ODL) environment.

Here by following the system introduced in [2], we define a model which describe the dynamics of learner retention and dropout in a peer assisted open distance learning environment to apply an intervention with a switching prevention strategy which was proposed in a epidemiological model in [1], to control the dropout rate in a distance learning environment due to the peer interactions. A dropout of a student from the system is not only because of the peer interaction among students but also due to the personal issues and university involvements. But here we do not count those situations and we analysis the system with student interactions and then figure out when the university need to be take a part to retain students in the system.

Methods

By following the mathematical model in [2], we divide the total student intake for a particular program into two compartments, namely, potential retained students S i.e., who are likely to continue and finish the studies, and potential dropped out students I i.e., who are intent to drop out from the study program. Let

$$\begin{pmatrix} \dot{I} \\ \dot{S} \end{pmatrix} = \begin{pmatrix} \beta IS - \gamma I \\ \lambda - \beta IS - \mu S \end{pmatrix} \tag{1}$$

where λ, μ, γ represents students rates of enrollment, graduation, and the potential drop out becomes actual dropped out from the system respectively and β indicate the effective rate of peer interaction among students.

Re scaling both I and S in (1) by $\frac{\mu}{\lambda}$ and in time, we get the equivalent system

$$\begin{pmatrix} \dot{I} \\ \dot{S} \end{pmatrix} = \begin{pmatrix} R_0 IS - I \\ -R_0 IS - \alpha S + \alpha \end{pmatrix} \tag{2}$$

where $R_0 = \frac{\lambda\beta}{\gamma\mu}$ and $\alpha = \frac{\mu}{\gamma}$. We will use the so-called non-ideal relay operator as the switching strategy similar to Chladná et al [1] as below:

$$R_0(t) = \begin{cases} R_0^{nat} & \text{if either } I(\tau) < I_{int} \text{ for all } \tau \in [0,\ t] \text{ or there is } t_1 \in [0,\ t] \\ & \text{ such that } I(t_1) \leq I_{nat} \text{ and } I(\tau) < I_{int} \text{ for all } \tau \in (t_1, t] \\ R_0^{int} & \text{if there is } t_1 \in [0, t] \text{ such that } I(t_1) \geq I_{int} \text{ and} \\ & I(\tau) > I_{nat} \text{ for all } \tau \in (t_1, t] \end{cases} \tag{3}$$

Due to the switching prevention strategy, the intervening is occur only when the number of dropouts exceeds a critical level and stops whenever this number drops below a different (lower) threshold. The equilibria of (2) are found as $E^* = (I_{E^*},\ S_{E^*}) = (0,\ 1)$ and $E = (I_E,\ S_E) = \left(\alpha\left(1 - \frac{1}{R_0}\right),\ \frac{1}{R_0}\right)$ and E^* is a stable equilibrium of (2) if $R_0 < 1$. So, if $R_0 < 1$ then the dropouts are getting vanish in the long run. And E will be a focus equilibrium for the system (2) if $\alpha^2 R_0^2 - 4\alpha R_0 + 4\alpha < 0$ i.e., if $\alpha R_0^2 < 4(R_0 - 1)$. The switched system (2)-(3) is considered in the positive quadrant $I, S \geq 0$ and we assume that $R_0^{int} < 1 < R_0^{nat}$ so that the system (2) with the fixed $R_0 = R_0^{int}$ has only a globally stable dropout free equilibrium at E^*, and the same system with $R_0 = R_0^{nat}$ has unstable dropout free equilibrium E^* and the endemic, positive. stable equilibrium E.

We will assume that the switching thresholds satisfying $I_{nat} < I_E < I_{int} < I_H$. Then the system (2)-(3) satisfies Theorem 1 and Proposition 1 of Chladná et al [1] and it conclude the result in next section.

Results and Conclusions

If an intervention is not applied, the number of dropouts can grow very large before it settles at the equilibrium E. So, combination of the switching strategy with the model prevent outbreaks of epidemic which can potentially lead to much higher number of dropouts before the system settles at the endemic equilibrium E.
In the way of intervention introduced, when the number of dropouts falls below I_{nat} the intervention stops and only system (2) would count with $R_0 = R_{nat} > 1$. So, the switching strategy built in to the model keeps the maximal number of dropouts at a relatively low level (less than I_{int}) at all the time without requiring permanent intervention measures. Furthermore, Theorem 1 and Remark 5 in Chladná et al [1] follows that the choice of the value for I_{nat} should not be too small and Proposition 1 in Chladná et al [1] follows that I_{nat} should not be too closed to I_{int} as we do not need infinitely many switches for the system (2)-(3).

Keywords:

Drop out rates, Mathematical Model, Ordinary Differential Equatoins, Switched transmissions, Dynamics

References

[1] Zuzana Chladná, Jana Kopfová, Dmitrii Rachinskii, and Samiha C Rouf. Global dynamics of sir model with switched transmission rate. *Journal of Mathematical Biology*, 80(4):1209–1233, 2020.

[2] W.P.T.M. Wickramaarachchi. The dynamics of learner retention and dropout in a peer-assisted open distance learning environment: A mathematical model. In *Proceedings of The Open University Research Sessions: 2019*, pages 45–47, OUSL, Sri Lanka, 2019.

Symmetry analysis and Painlevé test for the SIR epidemic model

Tharuka Supun Anthony[1*], **Dilruk Gallage**[1]
[1] Department of Mathematics, University of Colombo
*Corresponding author; E-mail: tharukasupunanthony@gmail.com

Background

Compartmental models are widely used in the mathematical modeling of infectious diseases. One of the most fundamental models is the SIR model, introduced by Kermack and McKendrick in 1927 [4]. The SIR model divides the population into three distinct compartments based on their status: susceptible, infected, or recovered. Individuals may move between these compartments and the flow between compartments is modeled using a system of nonlinear ordinary differential equations (NODEs). The rates of change between compartments (e.g., disease transmission rate, recovery rate) may vary based on different epidemiological scenarios and initial conditions.

Numerical techniques, including Runge-Kutta methods (RK4, RK5, etc.), finite difference methods, implicit methods (backward Euler, Crank-Nicholson), and multistep methods (Adams-Bashforth, Adams-Moulton), are typically used to solve this system of NODEs. However, numerical approaches do not provide closed-form expressions, which are necessary to understand the dynamics of the system under extreme circumstances, and some degree of error is inherent in any numerical approximations.

This study aims to derive an analytical solution for the SIR model. However, finding such a solution for a system of NODEs, like the SIR model in particular, is challenging due to its nonlinear nature. Since standard solving methods are ineffective in this case, we first employ the Painlevé analysis to leverage the Lie symmetry method for deriving solutions systematically.

In this study, we have slightly modified the classical SIR model[4] as follows.

$$\dot{S} = -\beta SI - \mu_1 S, \tag{1}$$

$$\dot{I} = \beta SI - \mu_2 I - \gamma I, \tag{2}$$

$$\dot{R} = \gamma I - \mu_3 R. \tag{3}$$

Here,

- $S(t)$ - Number of susceptible individuals at time t
- $I(t)$ - Number of infected individuals at time t
- $R(t)$ - Number of recovered individuals at time t
- β - Disease transmission rate
- γ - Recovery rate
- μ_1 - Death rate for susceptible individuals
- μ_2 - Death rate for infected individuals
- μ_3 - Death rate for recovered individuals

Methods

First, the system (1)-(3) is reduced to

$$\dot{I} = \frac{\dot{I}^2}{I} - \beta I\dot{I} - \mu_1\dot{I} - (\gamma + \mu_2)\beta I^2 - \mu_1(\gamma + \mu_2)I \tag{4}$$

. Then, we apply the Painlevé test to equation (4). The Painlevé test checks whether equation (4) possesses the Painlevé property. An ODE is said to possess the Painlevé property if all its solutions are free from movable essential singularities. (i.e., singularities that depend on the initial conditions). When an ODE does not possess the Painlevé property, it may exhibit complex, chaotic behavior and is often non-integrable.[5, 3, 1]

After that, we apply the Lie symmetry techniques [2] to equation (4). The Lie symmetry method for differential equations relies on the invariance of differential equations under transformations of independent and dependent variables. In simple terms, this method seeks a transformation that simplifies a given complex ODE to be easily solvable.

Results and Conclusions

One of the key findings of our study is that equation (4) passes the Painlevé test if $\gamma = \mu_1 - \mu_2$. This indicates that equation (4) does not exhibit chaotic behavior under this condition and is, therefore, integrable. Consequently, we derive the analytical solution for this scenario using the Lie Symmetry method.

However, in most situations, it is not always feasible to directly assume that $\gamma = \mu_1 - \mu_2$. Still, the Lie Symmetry method provides a powerful systematic approach for finding the analytical solution as long as this condition holds.

Keywords:

SIR Model, Painlevé Test, Lie Symmetry Analysis, Analytical Solution

References

[1] Anatoliy Aristov, Anna Kholomeeva, and Evgeniy Moiseev. Application of the painleve test to a nonlinear partial differential equation. *Lobachevskii Journal of Mathematics*, 43(7):1791–1794, 2022.

[2] Peter Ellsworth Hydon. *Symmetry methods for differential equations: a beginner's guide*. Number 22. Cambridge University Press, 2000.

[3] Edward L Ince. *Ordinary differential equations*. Courier Corporation, 1956.

[4] William Ogilvy Kermack and Anderson G McKendrick. A contribution to the mathematical theory of epidemics. *Proceedings of the royal society of london. Series A, Containing papers of a mathematical and physical character*, 115(772):700–721, 1927.

[5] V Tsegel'nik. The painlevé test for nonlinear system of differential equations with complex chaotic behavior. In *Journal of Physics: Conference Series*, volume 788, page 012035. IOP Publishing, 2017.

On $p-(\alpha-\beta)$ - quasi class (Q) operators

Sathyavathi.N[1*], **Radharamani.A**[1]
[1] Department of Mathematics, Chikkanna Government Arts College, Tiruppur, Tamil Nadu, India.
*Corresponding author; E-mail: sathyavathiphd@gmail.com

Background

Let H be a complex Hilbert space. If $TT^* = T^*T$, then operator T is normal; if $TT^* = T^*T = I$, then operator T is unitary. Assuming $T^*T = I$ then T is isometric. We will examine several characteristics of (α,β) – quasi class (Q) operators. As discussed in [4], this has been accomplished by relaxing some conditions of normality and creating classes such as (α,β) - quasi normal. Wanjala Victor and Nyongesa A M [5] studied some properties of (α,β) - class (Q) operators on Hilbert space. According to that, Brown A [2] studied on a class of operators in 1953. Halmos P R [3] discussed a Hilbert space problem book in 1967. Throughout this work, $B(H)$ is the Banach algebra of all bounded linear algebras on an infinite dimensional separable Hilbert space H, and H is the typical Hilbert space over the complex field. Also, the extension of (α,β) – quasi class (Q) to $p-(\alpha,\beta)$ – quasi class (Q) on Hilbert space H. Within this chapter, we introduced the definitions of (α,β) – quasi class (Q) and $p-(\alpha,\beta)$ – quasi class (Q) operators and essential theorems that are established on Hilbert space over the complex field. Additionally, few numerical illustrations of operators on Hilbert space are provided.

Methods

It is referred to as an operator $T \in B(H)$ is said to be class (Q) if $T^{*2}T^2 = \left(T^*T\right)^2$.
It is referred to as an operator $T \in B(H)$ is said to be (α,β) - class (Q) if

$$[\alpha^2 T^* T^2] \leq (T^* T)^2 \leq [\beta^2 T^* T^2]$$

Results and Conclusions

Consider the operator T = (1 1 0 0 0 1 0 0 0 1 0 0 0 0 0 0) acting on acting on the $\mathbb{R}^4$. Direct computations shows that T satisfies the following condition

$$T\left[\alpha\left\|T^4w\right\|\right] \leq \left[\left\|T^*T^3w\right\|\right]T \leq T\left[\beta\left\|T^4w\right\|\right],$$

but not satisfies

$$T\left[\alpha\left\|T^3w\right\|\right] \leq \left[\left\|T^*T^2w\right\|\right]T \leq T\left[\beta\left\|T^3w\right\|\right],$$

Clearly T is a $2-(\alpha,\beta)$ - quasi class (Q) operator but not a $1-(\alpha,\beta)$ - quasi class (Q) operator.

In this work, we given the idea on (α,β) - quasi class (Q) and $p-(\alpha,\beta)$ - quasi class (Q) operators are relatively new. We have attempted to prove some of

the properties of (α, β) - quasi class (Q) and $p-(\alpha, \beta)$ - quasi class (Q) operators in complex Hilbert space. Our analysis has led to summarize key results such as new theorems, generalizations to other operator classes.

Keywords

Normal, Class (Q), Quasi-Class Q, (α, β) -Quasi Normal and (α, β) Quasi-Class (Q) operators.

References

[1] Ariyadasa Aluthge. On p-hyponormal operators for 0¡ p¡ 1. *Integral Equations and Operator Theory*, 13:307–315, 1990.

[2] Arlen Brown. On a class of operators. *Proceedings of the American Mathematical Society*, 4(5):723–728, 1953.

[3] Paul Richard Halmos. *A Hilbert space problem book*, volume 19. Springer Science & Business Media, 2012.

[4] D Senthilkumar, P Maheswari Naik, and D Kiruthika. Quasi class q* composition operators. *International J. of Math. Sci. and Engg. Appls.(IJMSEA)*, 4:1–9, 2011.

[5] Wanjala Victor and AM Nyongesa. On (α, β)-class (q) operators. *International Journal of Mathematics and its Applications*, 9(2):111–113, 2021.

Classification of road signs for autonomous vehicles using quantum support vector machines

K. D. Jansz[1*], **N. Yapage**[1]
[1] Department of Mathematics, Faculty of Science, University of Ruhuna, Matara, Sri Lanka
*Corresponding author; E-mail: 1999janszkd1028@gmail.com

Background

Road sign classification is a critical component of autonomous vehicle systems, ensuring accurate recognition for safe navigation. Traditional machine learning models, such as classical Support Vector Machines (SVM) and deep neural networks, have succeeded but face challenges in efficiently handling high-dimensional data. Recent advancements in quantum computing offer promising alternatives, leveraging quantum parallelism and kernel-based methods to enhance classification performance. The Quantum Fourier Transform (QFT) further enhances feature representation, making Quantum Support Vector Machines (QSVM) a viable approach for real-time road sign classification[1]. QSVMs utilize quantum kernels to map input data into higher-dimensional spaces, potentially improving class separability[2]. While quantum machine learning remains in its early stages, its potential to outperform classical methods in complex pattern recognition tasks has driven research into its practical applications, including autonomous vehicle technology.

Methods

The present study focuses on QSVM's ability to handle high-dimensional classification. Let X be the input space of road sign images, and $Y = \{y_1, y_2, \ldots, y_n\}$ the set of road sign categories. While classical SVMs use linear hyperplanes for decision boundaries, QSVMs map X to a higher-dimensional Hilbert space H via a unitary transformation U, allowing non-linear boundaries.
We used the German Traffic Sign Recognition Benchmark (GTSRB) dataset, (https://www.kaggle.com/datasets/meowmeowmeowmeowmeow/gtsrb-german-traffic-sign) consisting of over 50,000 labeled images across 43 classes. The preprocessing steps included grayscale conversion to reduce computational complexity while preserving important features, downscaling the images to 32×32 pixels for quantum encoding, and normalizing pixel values to the range [0,1] for efficient quantum state transformation[3].
The preprocessed images are encoded into quantum states via amplitude encoding, where pixel intensities are coefficients in a quantum state $|\phi(x)\rangle = \sum_i c_i |i\rangle$. The QFT extracts frequency domain features using the following formula

$$\mathrm{QFT}|\psi(x)\rangle = \sum_i \alpha_i |i\rangle,$$

Then the quantum kernel K given below is computed using quantum states and it shows how much overlap goes between considered quantum states

$$K(x, x') = |\langle\psi(x)|\psi(x')\rangle|^2,$$

This kernel enables similarity computation between images in the transformed Hilbert space.

The QSVM training process minimizes a convex optimization problem to maximize the margin between classes. Given training samples $\{(x_i, y_i)\}$, where x_i are feature vectors of road sign images and $y_i \in \{-1, 1\}$ are class labels, the objective is to find

$$\min_{w,b,\epsilon_i} \left(\frac{1}{2}\|w\|^2 + C \sum_i \epsilon_i \right), \quad \text{subject to} \quad y_i(\langle w, x_i \rangle + b) \geq 1 - \epsilon_i,$$

where w is the weight vector and $|| \cdot ||$ denotes Euclidean norm, b is the bias term, ϵ_i are slack variables allowing misclassification, and C is the regularization parameter that balances margin maximization and classification errors.
When it comes to programming, Google Cirq was used for QSVM implementation, encoding images into quantum states, computing quantum kernels, and training and testing the QSVM for effective road sign classification.

Results and Conclusions

QSVM performs competitively with traditional methods, demonstrating quantum algorithms' potential for image classification. The model performs well on distinct categories like regulatory and prohibition signs but struggles with similar ones, such as speed limits and warnings. Quantum Kernal Heatmaps show improved class separability with larger datasets. Tuning the parameter C via grid search and 3-fold cross-validation resulted in higher test accuracy with more training data: 76.51% (50 images), 82.67% (100 images), 90.99% (200 images), and 95.15% (400 images). These results confirm QSVM's competitiveness with classical models in real-time classification.
The present work highlights QSVM's potential in high-dimensional classification tasks like road sign recognition for autonomous vehicles. Using quantum techniques like amplitude encoding, QFT, and quantum kernels, QSVM achieves competitive accuracy and captures complex patterns. It generalizes well to unseen data and meets real-time requirements for autonomous systems. Challenges include reliance on quantum simulations (Google Cirq) and scalability issues with larger datasets and high-resolution images, necessitating advancements in quantum hardware. QSVM's growing potential extends beyond road sign classification to applications in facial recognition, medical imaging, and financial modeling, offering significant benefits for autonomous vehicle navigation and safety. Future work should focus on optimization, scalability, hybrid models, and broader QSVM applications.

Keywords:

Autonomous vehicles, Quantum computing , Quantum Fourier Transform , Quantum Support Vector Machine , Road sign classification

References

[1] Riley T. Perry. *The Temple of Quantum Computing.* Riley T. Perry, 2004.

[2] P. Rebentrost et al. Quantum support vector machines. *Quantum Information and Computation*, 2014.

[3] J. Zhang, Q. Wu, and Y. Yang. Deep learning for traffic sign recognition: A review. *International Journal of Automation and Computing*, 2018.

Multi criteria decision making using the cubic spherical neutrosophic Frank aggregation operator

A. Kavitha[1*], K. Vishalakshi[2], K.Kavithamani[3] and S. Gomathi[2]
[1] Department of Mathematics, Karpagam College of Engineering, Tamilnadu, India- 641 032.
[2] Department of Mathematics, Dr. Mahalingam College of Engineering and Technology, Tamilnadu, India- 642003.
[3] Department of Mathematics, Hindusthan College of Engineering and Technology Tamilnadu, India- 643021.
*Corresponding author; E-mail: kavitha.a@kce.ac.in

Background

In 1997, Klement et al. [3] pioneered the introduction of the triangular norm and triangular co-norm, illuminating the foundational forms and attributes of these math ematical constructs, thereby establishing a robust platform for subsequent research in the field. Frank triangular norms and triangular conorms [1], as distinguished by Jin dong Qin and Xinwang Liu [4], extend beyond conventional norms by incorporating additional parameters to modulate the exponentiation of argument values. Frank's comprehensive study [1] delves into the intricacies of these norms, while Ulrich Florian Simo and Henri Gw´et contribute significantly to the domain with their exploration of fuzzy triangular aggregation operators, enriching both practical applications and theoretical frameworks in fuzzy logic and aggregation functions.

S. Gomathi [2] introduces cubic spherical neutrosophic sets, offering a geomet ric representation and aggregate operator that finds utility in multicriteria decision making scenarios. These contributions collectively advance the understanding and application of norm and conorm operators across various mathematical frameworks and practical domains.

The motivation behind exploring the incorporation of the Frank aggregation opera tor in cubic spherical neutrosophic sets lies in the need to enhance decision-making methodologies, particularly in managing uncertainty. Traditional decision-making approaches often struggle to adequately address the complexities and ambiguities in herent in real-world decision scenarios. By leveraging the Frank aggregation operator within the framework of cubic spherical neutrosophic sets, decision-makers gain access to a more robust and flexible tool for handling uncertainty and making informed deci sions. The motivation is further fueled by the potential of this approach to bridge the gap between theoretical advancements and practical applications in decision science.

The incorporation of the Frank aggregation operator in cubic spherical neutrosophic sets marks a significant advancement in decision-making methodologies. A cubic spherical neutrosophic set, representing collections of neutrosophic sets encapsulated within spheres, enables decision makers' preferences to be converted into spherical representations by determining the center and radius. This paper explores the theo retical and practical implications of utilizing the Frank aggregation operator within this framework. Through mathematical analysis and case studies, the study showcases its efficacy in handling complex decision scenarios. By bridging theoretical underpin nings with practical applications, it contributes to the evolution of decision science, particularly in managing uncertainty in contemporary decision-making paradigms.

Methods

Advancing Decision Science: Ultimately, the exploration of the Frank aggregation operator within cubic spherical neutrosophic sets contributes to the advancement of decision science. It equips decision-makers with innovative tools and methodologies for navigating uncertainty, fostering more informed and robust decision-making pro cesses across various domains.

Results and Conclusions

The utilization of the Frank aggregation operator within cubic spherical neutrosophic sets emerges as a promising avenue for enhancing decision-making processes in com plex and uncertain contexts. The numerical illustration provided at the paper's con clusion, alongside comparative analyses with existing methodologies, underscores the heightened accuracy and efficacy offered by the current Frank operator. Future en deavors could explore the scalability and adaptability of this methodology across diverse domains, including finance, engineering, and risk management. Additionally, further research might delve into refining the mathematical foundations and explor ing extensions to accommodate even more intricate decision scenarios. By embracing these avenues, future work can continue to advance decision science and refine our approaches to managing uncertainty in decision-making processes.

Keywords:

cubic spherical neutrosophic set, extension of cubic spherical neutrosophic set, cubic spherical neutrosophic Frank aggregation operator.

References

[1] Maurice J Frank. On the simultaneous associativity of f (x, y) and x+ y- f (x, y). *Aequationes mathematicae*, 19:194–226, 1979.

[2] S Gomathi, S Krishnaprakash, M Karpagadevi, and Said Broumi. Cubic spherical neutrosophic sets. *International Journal of Neutrosophic Science*, 21(4):172–72, 2023.

[3] Mirko Navara. Nearly frank t-norms and the characterization of t-measures. In *Proceedings of the 19th Linz Seminar on Fuzzy Set Theory*, pages 9–16. Citeseer, 1998.

[4] Jindong Qin and Xinwang Liu. Frank aggregation operators for triangular interval type-2 fuzzy set and its application in multiple attribute group decision making. *Journal of Applied Mathematics*, 2014(1):923213, 2014.

Mathematical optimization for nutritional equity: A decision-making and transportation model for implementing SDG-10

Amali Theresa.S[1,2*] **and Sahaya Sudha** [1]
[1] Nirmala College for Women, Coimbatore
[2] Nehru Institute of Technology, Coimbatore
*Corresponding author; E-mail: amalitheresa2018@gmail.com

Background

The Sustainable Development Goal 10 (SDG-10) aims to reduce inequalities within and among countries, including disparities in healthcare and nutrition. This study focuses on developing a mathematical model to assist in selecting the most nutritious food based on key health criteria—calcium, vitamins, carbohydrates, and proteins. By employing multi-criteria decision-making (MCDM) techniques, the optimal food choice is determined to enhance health equity. Furthermore, the transportation problem is used to minimize the cost of distributing this nutritional knowledge and resources to a larger population. The integration of these mathematical approaches ensures that nutritious food choices are both effective and accessible, contributing to a reduction in health-related inequalities.

Methods

Problem Definition

- Emphasizes the role of SDG-10 in reducing health inequalities.
- Highlights the need for optimal food selection based on essential nutrients.

Selection of Alternatives and Criteria

- **Alternatives:** Different types of foods.
- **Criteria:** Calcium, Vitamins, Carbohydrates, Proteins.

Mathematical Model for Optimal Food Selection

- Uses **Advanced Best Alternative Optimal Solution (MCDM)** methods.
- **Digital Survey Method:** Assigning weightage to criteria to select the best nutrient-dense food with minimum investment.

Optimization Using the Transportation Model

- Develops a transportation model for cost-effective distribution.
- Focuses on spreading nutritional knowledge to a wider population.

Implementation and Analysis

- Validates the model with real-world data.
- Assesses effectiveness in reducing health inequalities.

Results and Conclusions

The proposed mathematical model effectively identifies the most nutritious food option based on key criteria—calcium, vitamins, carbohydrates, and proteins—using Multi-Criteria Decision-Making (MCDM) techniques such as the Advanced Best Alternative Optimal Solution method. The results indicate that food items with a balanced nutritional profile rank higher in the selection process. This structured approach ensures that dietary decisions prioritize nutrition while minimizing costs.

In the second phase, the transportation model optimizes the cost/time-effective distribution of nutritional awareness and food supply using minimal resources. By reducing transportation expenses and maximizing outreach to underprivileged populations, the model contributes to reducing health inequalities in alignment with SDG-10.

The findings emphasize the significance of mathematical optimization techniques in addressing health equity. The integration of MCDM for food selection and the transportation model for efficient dissemination offers a robust approach to minimizing nutritional disparities and promoting accessible, cost-effective nutrition solutions.

This study demonstrates the effectiveness of mathematical modeling in promoting health equality through optimal food selection and cost-efficient distribution. By integrating MCDM techniques with the transportation model, we provide a framework for making informed decisions about nutrition while ensuring widespread accessibility at a minimal cost.

The findings support the broader goal of SDG-10 by addressing disparities in health and nutrition. Future research can extend this model by incorporating additional factors such as affordability, availability, and regional dietary preferences. The implementation of such models in public health policies can significantly contribute to reducing inequalities and improving overall well-being.

Keywords:

Sustainable Development Goal 10 (SDG-10), Health Inequality, Multi-Criteria Decision-Making (MCDM), Nutrition Optimization, Transportation.

References

[1] Mollah Mesbahuddin Ahmed, Md Amirul Islam, Momotaz Katun, Sabiha Yesmin, and Md Sharif Uddin. New procedure of finding an initial basic feasible solution of the time minimizing transportation problems. *Open Journal of Applied Sciences*, 5(10):634–640, 2015.

[2] Aykan Akincilar and Metin Dagdeviren. A hybrid multi-criteria decision making model to evaluate hotel websites. *International Journal of Hospitality Management*, 36:263–271, 2014.

[3] Hamed Taherdoost and Mitra Madanchian. Multi-criteria decision making (mcdm) methods and concepts. *Encyclopedia*, 3(1):77–87, 2023.

Enhanced image fusion through picture fuzzy sets

Rajarajeswari. P[1] **and Reshma. R**[1*]
[1]Department of Mathematics, Chikkanna Govt Arts College, Tiruppur, Tamil Nadu, India.
*Corresponding author; E-mail: reshmaranganathan1608@gmail.com

Background

Zadeh [3] introduced fuzzy set theory in 1965, and it has since evolved into numerous advanced variations. In 2014, P. Balasubramaniam and V.P. Ananthi [1] discussed a novel approach for image fusion using intuitionistic fuzzy sets. Maruturi and Velmathi [4] introduced an enhanced multimodal medical image fusion based on Pythagorean fuzzy sets. Cuong [2] established picture fuzzy sets in 2014, which have membership degree, neutral degree, and non-membership degree, whose sum is less than or equal to one. Picture Fuzzy Sets (PFS) and Intuitionistic Fuzzy Sets (IFS) are extensions of traditional fuzzy sets, designed to handle uncertainty and vagueness in data. However, PFS introduces an additional dimension neutral membership which allows for a more nuanced representation of uncertainty compared to IFS.Image fusion combines images from different environments into a single, more useful image for further processing. This paper introduces a novel approach using Picture Fuzzy Sets (PFS) with maximum and minimum operations. PFS effectively handles uncertainties and ambiguities in digital images through membership, non-membership, and neutral membership degrees. The proposed method transforms images into Picture Fuzzy Images (PFIs), employs entropy for optimal parameter determination, and fuses image blocks based on blackness and whiteness counts. Compared to existing techniques like AVG, PCA, DWT, SWT, DTCWT, MSVD, NSCT, IFS, SIFS, GFF, CSE and LEG. our experimental results show superior luminance, contrast, and overall image quality, making PFS ideal for image fusion tasks, especially with complex uncertainties and ambiguities.

Methodos for Picture Fuzzy Sets (PFS)

Let the two input images be denoted by I_1 and I_2, respectively(Step 1).Fuzzify the input images using an appropriate equation $\frac{\mathfrak{g}-\mathfrak{g}_{min}}{\mathfrak{g}_{max}-\mathfrak{g}_{min}}$.Calculate the optimal value of λ using an entropy measure equation for both input images separately(Step 2).Then calculate the degrees of membership (μ), non-membership (ν), neutrality (η), and hesitation (π) using appropriate equations for both input images. with their optimal λ value. The resulting images are denoted by PF1 and PF2 (Step 3).

$\mu_{PFS}\left(P\left(i,j\right),k\right) = 1-\left(1-\mu_P\left(P\left(i,j\right)\right)\right)^k,\ k \geq 0, \quad \eta_{PFS}\left(P\left(i,j\right),k\right) = \left(1-\mu_P\left(P\left(i,j\right)\right)\right)^k-\left(1-\mu_P\left(P\left(i,j\right)\right)\right)^{k(k+1)},\ k\geq 0,\ \nu_{PFS}\left(P\left(i,j\right),k\right) = \left(1-\mu_P\left(P\left(i,j\right)\right)\right)^{k(k+1)}-\left(1-\mu_P\left(P\left(i,j\right)\right)\right)^{k(k+2)},\ k \geq 0$ and $r_{PFS}\left(P\left(i,j\right),k\right) = \left(1-\mu_P\left(P\left(i,j\right)\right)\right)^{k(k+2)}$

Decompose the two images obtained from step 3 into $p \times q$ blocks. Denote the k^{th} image block of the two decomposed images by PF_{1k} and PF_{2k}, respectively (Step 4). Next compute the Total Count of Blackness, Whiteness, and Neutrality of two corresponding blocks.(Step 5) Reconstruct the k^{th} Block of the Blended Image as follows(Step 6):

If count(blackness) > count(whiteness) and count(blackness) > count(neutrality), then $PF_{jk}\left(i,j\right) = min\left(PF_{1k}\left(i,j\right),PF_{2k}\left(i,j\right)\right)$

If count(whiteness) > count(blackness) and count(whiteness) > count(neutrality), then $PF_{jk}\left(i,j\right) = max\left(PF_{1k}\left(i,j\right),PF_{2k}\left(i,j\right)\right)$

If count(neutrality) > count(blackness) and count(neutrality) > count(whiteness), then $PF_{jk}(i,j) = average(PF_{1k}(i,j), PF_{2k}(i,j))$

After that,reconstruct the image from the blocks obtained from step 6 to get a fused Picture Fuzzy Image(PFI)(Step 7).Lastly,defuzzify the PFI obtained from step 7 to get a crisp image using a defuzzification function for PFS by extending the defuzzification formula provided for IFS (Step 8). $I(i,j) = (g_{max} - g_{min}) \times \mu_{PS}(P(i,j)) + g_{min}$

Results and Conclusions

The study presents a new image fusion approach using Picture Fuzzy Sets (PFS), comparing it against multiple established methods: Simple Averaging (AVG), Principal Component Analysis (PCA), Discrete Wavelet Transform (DWT), Stationary Wavelet Transform (SWT), Dual Tree Complex Wavelet Transform (DTCWT), Multi-Resolution Singular Value Decomposition (MSVD), Non-Subsampled Contourlet Transform (NSCT), Intuitionistic Fuzzy Sets (IFS), Sugeno Intuitionistic Fuzzy Sets (SIFS), Guided Filter Fusion (GFF), Contrast and Structure Extraction (CSE), and Local Energy and Gradient (LEG). Testing encompassed medical, infrared-visible, and multi-focused images. For medical images, PFS fusion exhibited enhanced luminance and contrast, with superior MEAN, SF, and STD values, leveraging its capability to manage uncertainties and vagueness in poorly illuminated images with inherent defects. While IFS demonstrates strong performance in both quantitative metrics (RMSE, PFE, MAE, CORR, SNR, PSNR, MI, QI, SSIM) and qualitative assessments, PFS consistently outperforms it across all evaluations, offering enhanced flexibility and robustness through its three-dimensional representation.

The paper concludes that the proposed image fusion using picture fuzzy sets is highly effective in combining images from various sources, such as medical, infrared-visible, and multi-focused images. PFS's inclusion of neutral membership allows for a more nuanced representation of uncertainty, making it particularly effective in handling complex and uncertain image data. This leads to superior fusion results compared to traditional methods and even Intuitionistic Fuzzy Sets.The experimental results demonstrate that the PFS method outperforms existing fusion techniques, including IFS, in terms of both qualitative (visual inspection) and quantitative evaluations. The fused images produced by PFS exhibit higher luminance, contrast, and overall quality, making them more useful for further image processing tasks.

In the future work, we suggest integrating PFS with advanced machine learning techniques, such as neural networks, to further improve fusion results. Additionally, exploring PFS in other domains, such as video fusion and 3D image fusion, could be a promising direction.

Keywords:

Picture Fuzzy Sets, Picture fuzzy Image entropy and Image fusion

References

[1] Pagavathigounder Balasubramaniam and VP Ananthi. Image fusion using intuitionistic fuzzy sets. *Information fusion*, 20:21–30, 2014.

[2] Bui Cong Cuong and Vladik Kreinovich. Picture fuzzy sets-a new concept for computational intelligence problems. In *2013 third world congress on information and communication technologies (WICT 2013)*, pages 1–6. IEEE, 2013.

[3] Joseph A Goguen. La zadeh. fuzzy sets. information and control, vol. 8 (1965), pp. 338–353.-la zadeh. similarity relations and fuzzy orderings. information sciences, vol. 3 (1971), pp. 177–200. *The Journal of Symbolic Logic*, 38(4):656–657, 1973.

[4] Maruturi Haribabu and Velmathi Guruviah. Enhanced multimodal medical image fusion based on pythagorean fuzzy set: an innovative approach. *Scientific Reports*, 13(1):16726, 2023.

An innovative method for determining IBFS of a transportation problem with interval-valued picture fuzzy numbers

P. Rajarajeswari[1] **and K. Vanithamani**[1*]
[1]Department of Mathematics, Chikkanna Government Arts College, Tirupur
*Corresponding author; E-mail: vanitha200985@gmail.com

Background

Transportation problems have long been studied in optimization and logistics, with a primary focus on minimizing transportation cost. However, in many real-world applications, data is not always precise, and uncertainty plays a significant role in transportation problem. Traditional transportation models, such as the classical Transportation Problem (TP), assume deterministic values for supply, demand, and transportation costs, not handle uncertainty roll. To address this limitations, In 1965, Lotfi A. Zadeh [4] introduced Fuzzy Sets(FS) as a means of expressing ambiguity and uncertainty. A fuzzy set's degree of membership, which ranges from 0 to 1, indicates how much an element belongs to the set. Another proposal from Zadeh was Interval Valued Fuzzy Set, which is a generalization of FSs [4]. Atanassov [1] presented the concept of Intuitionistic Fuzzy Sets (IFS), which have two functions that are the membership function and the nonmembership function. Intuitionistic fuzzy sets with interval values Interval Valued Intuitionistic Fuzzy Sets (IVIFS) were introduced by Gargov and Atanassov [1]. Coung [2] expanded on the idea of Picture Fuzzy Sets (PFS) by declaring that the sum of the three PFS components neutral, non-membership, and membership function must fall within the closed unit interval, which allows for a richer and more comprehensive representation of uncertainty. Coung [2] given the hard work to the IVFS and PFS concepts are combined in IVPFS. Fuzzy Transportation Problems (FTP) include the concept of fuzzy into the transportation problems, allowing the representation of supply, demand, and cost under uncertain environment. The integration of Interval-Valued Fuzzy Sets into the transportation domain has added another layer of flexibility, as it accommodates the use of interval data rather than single-point values, reflecting more realistic ranges for costs, supplies, or demands. In the transportation cost problem, Sathya Geetha and Selva Nayaki employed picture fuzzy numbers and determine their IBFS.The Interval-Valued Picture Fuzzy Transportation Problem (IVPFTP) [3] extends this framework, assimilating the advantages of Interval-Valued Fuzzy Sets and Picture Fuzzy Sets to deal with more complex and uncertain transportation scenarios. In this article we introduced a new defuzzification method to convert the Interval valued picture fuzzy numbers into a single crisp value in the IVPFTP. After converting the crisp value, we used a VAM method for finding Initial Basic Feasible Solution of IVPFTP. A numerical example is illustrated to show the efficiency of the proposed technique and the results are compared with some of the already existing methods.

Methods

In the context of the IVPFTP, the goal is to handle uncertainty in the transportation problem, where the costs, supply and demand are represented by Interval-Valued Picture Fuzzy Numbers. In this work, we propose a new defuzzification method using

a specific formula that takes into account multiple degrees of uncertainty associated with each parameter in the IVPFTP model. The formula provided is:

1. For each element in the transportation table (representing either supply, demand, or transportation cost), determine the six parameters: $[a, b], [c, d], [e, f]$. These values are derived from the interval-valued picture fuzzy numbers that represents the degree of membership, non-membership, and neutrality.
2. For interval valued picture fuzzy numbers of transportation table, the defuzzified value is computed using the formula:

   Defuzzified Value= $[3 * (a + b) * (c + d) * (e + f)]/[2 * ((a + b) * (c + d) + (c + d) * (e + f) + (e + f) * (a + b))]$ where:

   $[a, b]$ represents the interval-valued parameters to the membership degree.

   $[c, d]$ represents the interval-valued parameters to the neutral degree.

   $[e, f]$ represents the interval-valued parameter to non-membership degree.

   The formula is structured to combine the membership and non-membership values with the neutrality values in a way that balances the different types of uncertainty.
3. After applying the formula for all the relevant transportation table elements, each interval valued picture fuzzy value is converted into a crisp value. These crisp values represent a deterministic approximation of the uncertain transportation parameters (e.g., supply, demand, and cost), which can then be used in the subsequent optimization steps.
4. The resulting defuzzified values are now ready to be used in solving the **IVPFTP** by VAM method.

Results and Conclusions

The proposed defuzzification approach using the formula provides a robust mechanism for converting interval-valued picture fuzzy data into crisp values that can be used for optimization. By considering multiple degrees of uncertainty, this methodology offers an advanced solution to handling real-world transportation problems where data is imprecise and vague.

Keywords:

Picture Fuzzy Set, Interval Valued Picture Fuzzy Set, Transportation Problem

References

[1] K Atanassov and G Gargov. Interval valued intuitionistic fuzzy sets. *Fuzzy Sets and Systems*, 31(3):343–349, 1989.

[2] B.C. Cuong. Picture fuzzy sets. *Journal of Computer Science and Cybernetics*, 30(4):409, Dec. 2014.

[3] P. Rajarajeswari and K. Vanithamani. A new approach for finding ibfs to interval valued picture fuzzy transportation problem. *0972-0766*, 96(12), 2023.

[4] L.A. Zadeh. Fuzzy sets. *Information and Control*, 8(3):338–353, 1965.

Some new distance measures for solving MADM problems using interval valued picture fuzzy numbers in CRADIS method

P. Rajarajeswari[1] **and D. Nandhini**[2*]
[1] Department of Mathematics, Chikkanna Government Arts College, Tirupur, Tamil Nadu, India.
*Corresponding author; E-mail: nandhinidurairaj27@gmail.com

Background

In real life, numerous phenomena involving ambiguity or uncertainty that traditional mathematical methods cannot effectively explain. To address these challenges, Zadeh introduced fuzzy theory in 1965, which has since been extensively applied in Multi-Attribute Decision Making (MADM) to manage problems involving fuzzy uncertainty. Later, Atanassov [1] advanced this theory by proposing intuitionistic fuzzy sets (IFS). Cuong [2] expanded the concept of intuitionistic fuzzy sets by introducing picture fuzzy sets (PFS) and analysing their fundamental algorithms and characteristics. Picture fuzzy sets are particularly suited for scenarios requiring multiple response types, such as approval, neutrality, opposition, and abstention, allowing for a broader range of decisions compared to intuitionistic fuzzy sets which highlights the practicality and advantages of picture fuzzy set theory. Dutta [3] introduced distance measures for Picture Fuzzy Sets (PFSs) based on established metrics such as Euclidean and Hamming distances, with initial applications in medical diagnosis. Singh proposed several Picture Fuzzy distance measures grounded in the geometric distance model, which were utilized to assess flood disaster risk in southern India. Khan [4] defined a novel two-parameter distance measure for PFSs, applying it to fields like pattern recognition and medical diagnosis. Picture fuzzy set theory offers a robust approach to representing complex real-world scenarios and effectively capturing the uncertainty and vagueness of subjective judgments. Its unique features make it particularly well-suited for addressing imprecise, uncertain, and inconsistent information in Multi-Attribute Decision Making (MADM) problems. Consequently, analysing MADM problems using picture fuzzy sets holds significant importance. combining the advantages of MARCOS, ARAS, and TOPSIS methods. This approach leverages the strengths of these three techniques to provide a simpler and more comprehensive solution to Multi-Attribute Decision Making (MADM) problems. An interval-valued picture fuzzy set (IVPFS) is an extension of the traditional picture fuzzy set (PFS), which incorporates a range of values for each membership grade instead of a single fixed value. In an IVPFS, each element is represented by a membership function that assigns a range of values to the degrees of membership, non-membership, and hesitancy. This structure provides more flexibility in capturing uncertainty and ambiguity, as it allows the representation of information with varying degrees of truth, falsehood, and uncertainty, rather than relying on a precise, fixed value. However, a thorough literature review indicates that the CRADIS method has not been applied in the context of a interval valued picture fuzzy environment In this paper Compromise Ranking of Alternatives from Distance to Ideal Solution (CRADIS) method with interval-valued picture fuzzy sets. By incorporating interval-valued picture fuzzy sets, this approach captures a broader range of possible responses (such as approval, neutrality, opposition, and abstention) and provides a more flexible framework for decision-making. This enhances the accuracy and robustness of the decision-making process, especially in complex

and ambiguous Multi-Attribute Decision Making (MADM) problems, while offering a more comprehensive and realistic evaluation of alternatives.

Methods

A new picture fuzzy CRADIS decision-making system is designed by integrating the newly developed interval-valued picture fuzzy distance measure with the CRADIS approach.

Results and Conclusions

In this study, we introduced a novel IVPF distance measure based on Jensen–Shannon divergence. The proposed IVPF distance measure adheres to the properties of metric space and effectively addresses counterintuitive cases, as demonstrated through proofs and examples. To address issues related to pattern recognition we applied both the proposed and existing IVPF distance measures, with experimental results highlighting the advantages of our approach. Additionally, we utilized the proposed IVPF distance measure in conjunction with the maximum deviation method to determine attribute weights within an interval-valued picture fuzzy environment. Furthermore, we extended the CRADIS method to the interval-valued picture fuzzy context, employing our IVPF distance measure to compute the deviation degree, thereby enhancing its effectiveness and practicality in MADM problems.

Keywords:

Picture Fuzzy set, Picture Fuzzy distance measure, Interval valued picture Fuzzy set.

References

[1] Krassimir T Atanassov. Intuitionistic fuzzy sets. *Fuzzy Sets and Systems*, 20(1):87–96, 1986.

[2] Bùi Công Cng. Picture fuzzy sets. *Journal of Computer Science and Cybernetics*, 30(4):409, Dec. 2014.

[3] Palash Dutta. Medical diagnosis based on distance measures between picture fuzzy sets. *International Journal of Fuzzy System Applications (IJFSA)*, 7(4):15–36, 2018.

[4] Muhammad Jabir Khan, Poom Kumam, Wejdan Deebani, Wiyada Kumam, and Zahir Shah. Bi-parametric distance and similarity measures of picture fuzzy sets and their applications in medical diagnosis. *Egyptian Informatics Journal*, 22(2):201–212, 2021.

Bayesian Nash equilibrium in triopoly games with triangular intuitionistic fuzzy payoffs and its application in market share

S.A.Sahathana Thasneem[1*] **and A.Radharamani**[1]
[1] Department of Mathematics, Chikkanna Government Arts College-641602, Tirupur(TN),India
*Corresponding author; E-mail: sahathana.latheef@gmail.com

Background

A Bayesian game is a strategic decision-making model in game theory that makes the assumption that players don't have all the knowledge they need. The payoffs are not widely known since players may possess confidential information related to the game. According to [2] the incomplete information in the decision making situation is categorized into three main types

i The players might not be aware of how each strategy affects the game's physical outcome function.

ii It's possible that the players are unaware of the payoff functions that defines the payoffs for themselves or another player.

iii The players can be unaware of their own strategy spaces or those of other players.

This paper presents a novel approach for analysing a triopoly game under conditions of incomplete information. In this scenario, players possess private information about payoffs, which is not commonly shared. To address this, we propose a method to determine the Bayesian Nash equilibrium in triopoly game with Triangular Intuitionistic fuzzy payoffs, focusing on the distribution of market share among competing food companies [1]. This technique offers a robust framework for understanding strategic interactions in markets with asymmetric information.

Methods

A Bayesian Nash Equilibrium (BNE) is a strategy profile that maximizes each player's expected return based on their beliefs and the strategies used by other players. A strategy profile s is a Bayesian Nash equilibrium if and only if, while all other players' strategies remain constant, strategy $s_i \in S_i$ maximizes player i's anticipated payoff.

For a Bayesian game $\widehat{G} = (N, (\Phi_i), (S_i), (p_i), (u_i))$ a profile of type agent strategies

$$s^* = \left((s^*{}_{\theta_1})_{\theta_1 \in \phi_1}, (s^*{}_{\theta_2})_{\theta_2 \in \phi_2}, \cdots, (s^*{}_{\theta_n})_{\theta_n \in \phi_n} \right)$$

Is said to be a Bayesian Nash Equilibrium of $\widehat{G}$ if for all $i \in N, \forall \theta_i \in \phi_i$,

$u_{\theta_i}(s^*{}_{\theta_i}, s^*{}_{-\theta_i}) \geq u_{\theta_i}(s_i, s^*{}_{-\theta_i}), \forall s_i \in S_i, \forall \theta_{-i} \in \Phi_{-i}.$

Results and Conclusions

In this paper, the concept of Triopoly games with incomplete information is introduced. The Bayesian probabilities are used to model the market share problem of companies, and their payoffs are represented by Triangular Intuitionistic fuzzy numbers. To investigate the Bayesian Nash equilibrium of the market share problem, the aggregation and ranking of TIFN's are used, ensuring the existence of an equilibrium.

Keywords:

Intuitionistic Fuzzy set, Triangular Intuitionistic Fuzzy Number, Bayesian Game, Nash Equilibrium, Triopoly Game.

References

[1] Richard M Cyert and Morris H DeGroot. Bayesian analysis and duopoly theory. *Journal of Political Economy*, 78(5):1168–1184, 1970.

[2] John C Harsanyi. Games with incomplete information played by "bayesian" players, i–iii part i. the basic model. *Management science*, 14(3):159–182, 1967.

[3] Kwang-Ho Lee and Ross Baldick. Solving three-player games by the matrix approach with application to an electric power market. *IEEE Transactions on Power Systems*, 18(4):1573–1580, 2003.

[4] Junhai Ma, Lijian Sun, and Xueli Zhan. Study on triopoly dynamic game model based on different demand forecast methods in the market. *Complexity*, 2017(1):5434680, 2017.

[5] Mijanur Rahaman Seikh, Prasun Kumar Nayak, and Madhumangal Pal. Generalized triangular fuzzy numbers in intuitionistic fuzzy environment. *International journal of engineering research and development*, 5(1):08–13, 2012.

Solving interval-valued intuitionistic fuzzy game problems in decision-making using (α,β)-cut & its applications

R.Umamaheswari[1*] **and A.Radharamani**[1]
[1] Chikkanna Govt. Arts college, Tirupur,Tamilnadu, India
*Corresponding author; E-mail:mahiramasamyuma@gmail.com

Background

Game theory is the study of the way in which strategies interactions among rational players produce outcomes with respect to the preference of those players, none of which might have intended by any of them. A two person game where two players are defined as decision makers is a simplest case of game theory. In real game situation, usually players are not able to evaluate exactly the of the game due to lack of information. Therefore, Fuzzy game theory is studied by various researchers now a days.

In this paper, a two person zero sum games with fuzzy payoffs are considered. The Payoff elements are taken to be Pentagonal intuitionistic fuzzy numbers. The aim of this paper is to develop a method to solve such games. Each Pentagonal intuitionistic fuzzy numbers using (α,β) – cuts. P. Grezewski's theorem has been used to transform the obtained intervals to Grezewski's intervals. The intervals are then compared using acceptability index to get the saddle point.

Methods

It follows from the definition that $\overline{A}_\beta$ is a closed interval, denoted by,

$$\overline{A}_\beta = [a_L(\beta), a_R(\beta)]$$

Where,

$$a_L(\beta) = (a - 2l) + \frac{(1-\beta)l}{1-u_a}$$
$$a_R(\beta) = (a + 2r) - \frac{(1-\beta)r}{1-u_a}$$

It can be easily proven that for $\overline{A} = \langle 2l, l, a, r, 2r; w_a, u_a \rangle$ belonging to the pentagonal intuitionistic fuzzy number $\mathbb{R}$. And for any $\alpha \in [0, w_a]$ and $\beta \in [u_a, 1]$, where $0 \leq \alpha + \beta \leq 1$.

Results and Conclusions

matrix game with payoff as pentagonal intuitionistic fuzzy numbers is considered. A new Approach to solve such a problem proposed. The proposed method finds the saddle point of the game matrix by converting the pentagonal intuitionistic fuzzy number to interval by taking (α,β)- cuts, which are then used to convert the given problem to two different problem with entries as crisp intervals. Saddle point of the two problem is obtained by finding the row minimum and column maximum by acceptability index

approach. The two obtained saddle point corresponds to same pentagonal intuitionistic fuzzy number.it is also noted that different values of α and β will corresponds to the same saddle point.

The proposed method can be applied extensively in the field of game theory as much of the information in the real world is rarely precisely known.

Keywords:

Two person zero-sum game, fuzzy payoff, Pentagonal Intuitionistic fuzzy number, (α,β) – cuts, Acceptability index, Saddle point

References

[1] Krassimir T Atanassov. Intuitionistic fuzzy sets. *Fuzzy Sets and Systems*, 20(1):87–96, 1986.

[2] Sibasis Bandyopadhyay and Prasun Kumar Nayak. Matrix games with trapezoidal fuzzy payoff. *International Journal of Engineering Research and Development*, 5(7):21–29, 2013.

[3] CR Bector, Suresh Chandra, and V Vidyottama. Matrix games with fuzzy goals and fuzzy linear programming duality. *Fuzzy Optimization and Decision Making*, 3:255–269, 2004.

[4] CR Bector, Suresh Chandra, and Vidyottama Vijay. Duality in linear programming with fuzzy parameters and matrix games with fuzzy pay-offs. *Fuzzy sets and systems*, 146(2):253–269, 2004.

[5] Lourdes Campos. Fuzzy linear programming models to solve fuzzy matrix games. *Fuzzy sets and systems*, 32(3):275–289, 1989.

Improved fermatean m-polar fuzzy composition relation and its applications

A.Radharamani[1], **S.Rajeswari**[1*]
[1]Department of Mathematics,Chikkanna Govt.Arts College,Tiruppur
*Corresponding author; E-mail: s.rajeswariphd2023@gmail.com

Background

In this paper, we explore the fermatean m-polar fuzzy max-min-max composition relation and propose an improved approach for better results. The validity of the enhanced fermatean m-polar fuzzy composition relation is tested through numerical experiments, comparing it to the traditional fermatean m-polar fuzzy max-min-max composition relation. The results demonstrate that the improved fermatean m-polar fuzzy composition relation provides superior output.

Methods

The composition method in mathematics usually refers to function composition, which is a way of combining two functions to create a new function. It is denoted as: $(f \circ g)(x) = f(g(x))$.

Results and Conclusions

In conclusion, the improved Fermatean m-polar fuzzy relation provides a powerful and flexible approach for handling uncertainty in real-life decision-making problems. By incorporating higher degrees of membership, non-membership, and hesitation, this method enhances accuracy and reliability in complex scenarios such as medical diagnosis, risk assessment, and multi-criteria decision-making. Its ability to process vague and imprecise information makes it a valuable tool for decision-makers, ensuring more informed and rational choices across various fields.

Keywords:

Fuzzy set ,Fermatean m-Polar Fuzzy Set, Fermatean m-Polar Fuzzy relation, real-life decision-making problems

References

[1] Juanjuan Chen, Shenggang Li, Shengquan Ma, and Xueping Wang. m-polar fuzzy sets: an extension of bipolar fuzzy sets. *The scientific world journal*, 2014(1):416530, 2014.

[2] PA Ejegwa and BO Onasanya. Improved intuitionistic fuzzy composite relation and its application to medical diagnostic process. *Note IFS*, 25(1):43–58, 2019.

[3] Tapan Senapati and Ronald R Yager. Some new operations over fermatean fuzzy numbers and application of fermatean fuzzy wpm in multiple criteria decision making. *Informatica*, 30(2):391–412, 2019.

[4] Atiqa Siraj, Tehreem Fatima, Deeba Afzal, Khalid Naeem, and Faruk Karaaslan. Pythagorean m-polar fuzzy neutrosophic topology with applications. *Neutrosophic Sets Syst*, 48:251–290, 2022.

[5] Lotfi A Zadeh. Fuzzy sets. *Information and Control*, 1965.

Optimal impulsive chemotherapy strategies for cancer

Prabodya H.A.S[1*], **Somathilake L.W**[1]
[1] Department of Mathematics, Faculty of Science, University of Ruhuna
*Corresponding author; E-mail: prabodyaharankahaarachchigesas@gmail.com

Background

Immunotherapy, chemotherapy, and radiotherapy are the main treatment types for cancer. Chemotherapy is a type of anticancer drug treatment. It works by killing cancer cells. The main aim of this research is to investigate the optimal impulsive chemotherapy strategies based on a mathematical model for the dynamics of chemotherapy and cancer. In this research, optimization by the amount of the drug and release time are considered. By applying a time rescaling technique and Pontryagin's maximum principle, the optimal treatment strategies are obtained by minimizing predefined cost functional using the fminsearch function in MATLAB. The key finding shows that optimization by release time is more important than optimization by amount of the drug in the cancer control process.

Methods

Consider the following mathematical model for impulsive chemotherapy for cancer growth reported in [1].

$$\begin{aligned} \frac{dy}{dt} &= ry(1-by) - \alpha_2(1-e^{-z})y, t \neq k\tau \\ \frac{dz}{dt} &= -d_2 z, t \neq k\tau \\ y(t^+) &= y(t), t = k\tau \\ z(t^+) &= z(t) + \mu, t = k\tau, k = 1, 2, ..., N, \end{aligned} \tag{1}$$

with initial conditions $y(0) = y^0$, $z(0) = z^0$.

Here y is the number of tumor cells, z is the blood drug concentration, μ is the increment of blood drug concentration due to chemotherapy, b is the tumor cells carrying capacity, α_2 is the fraction of tumor cells killed by chemotherapy, d_2 is the rate of chemotherapy drug decay, and r is the tumor cells growth rate. $\tau > 0$ is the release period, $(N-1)$ is the number of treatments, $N\tau = T$.

Therapeutic periods π are defined by $(\tau_1, \tau_2, ..., \tau_N)$ and the time transformation $t = \sum_{j=1}^{k-1} \tau_j + \tau_k s, s \in (0, 1]$ is used for computational convenience. Assume that μ and each τ_k for $k = 1, 2, ..., N$ are bounded. We optimize transformed cost functionals using the fminsearch function in MATLAB.

Optimization by amount of the drug (amount control): find the releasing parameter μ such that the number of tumor cells at the terminal time T and the total cost of the chemotherapy dose are minimized. The corresponding cost functional is $J(\mu) = y(T) + c_0(N-1)\mu$, where c_0 is the cost per unit dose of increment of blood drug concentration.

Optimization by release time (time control): find the releasing parameter π such that the number of tumor cells at the terminal time T and the total cost of

the chemotherapy dose are minimized. The corresponding cost functional is $J(\pi) = y(T) + c_0(N-1)\mu$, where c_0 is the cost per unit dose of increment of blood drug concentration.

Results and Conclusions

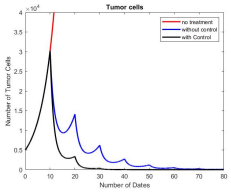

Figure 1: Amount control (case: 1)

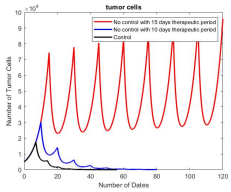

Figure 2: Time control (case: 1)

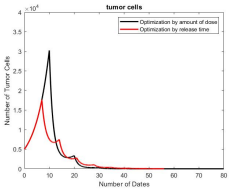

Figure 3: Compare amount and time control (case: 1)

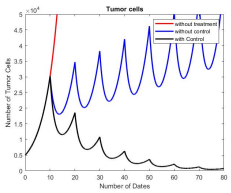

Figure 4: Amount control (case: 2)

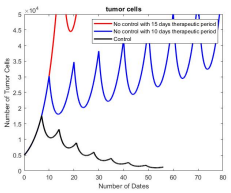

Figure 5: Time control (case: 2)

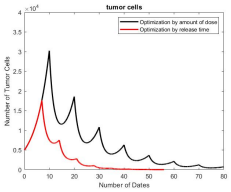

Figure 6: Compare amount and time control (case: 2)

Figure 7: Number of tumor cell variations relevant to seven doses

The initial conditions are $y(0) = 5 \times 10^3$ *tumor cells*, $z(0) = 0$. Under case: 1 initial increment of blood drug concentration and therapeutic periods are $1.4mg/l$, $[10, 10, 10, 10, 10, 10, 10, 10]$ in days, respectively. The optimal treatment strategies (case: 1) obtained for the control of the amount and time are $2.8mg/l$, $[7, 7, 7, 7, 7, 7, 7, 7]$ in days, respectively. Under case: 2 initial increment of blood drug concentration and therapeutic periods are $0.8mg/l$, $[10, 10, 10, 10, 10, 10, 10, 10]$ in days, respectively. The optimal treatment strategies (case: 2) obtained for the control of the amount and time are $1.2mg/l$, $[7, 7, 7, 7, 7, 7, 7, 7]$ in days, respectively. According to Fig. (3), (6) optimization by release time can control the cancer better than optimization by amount of the drug. According to Fig. (4) optimizing the drug amount can still reduce the disease even in cases where conventional treatments fail.

Keywords:

Nonlinear equations and systems, Differential equations with impulses, Impulsive optimal control problems

References

[1] Liuyong Pang, Lin Shen, Zhong Zhao, et al. Mathematical modelling and analysis of the tumor treatment regimens with pulsed immunotherapy and chemotherapy. *Computational and Mathematical Methods in Medicine*, 2016(1), 2016.

A novel method for solving multi-opinion picture fuzzy Bi-matrix games

P.Rajarajeswari[1] and A.Maryshanthi[1*]

[1]Department of Mathematics, Chikkanna Govt. Arts College , Tirupur-02
*Corresponding author; E-mail: maryshanthi83@gmail.com

Background

One of the best tools for examining conflicts of interest between several players is game theory which was originated by Neumann and Morgenstern [5]. According to game theory, everyone wants to maximize profits by selecting the optimal option from a finite set of possible strategies. Decisions made by two or more players always have an impact on each other's output. By selecting pure or mixed strategies, each player in the bi-matrix game theory aims to achieve the largest payoffs possible. The environment's unpredictability makes it difficult to access clear payoffs in real-life scenarios. In order to effectively describe the uncertain information of payoffs in bi-matrix games, we can apply the concept of Fuzzy which was introduced by Zadeh [3]. To deal uncertainty in most effective way, Atanassov [1]developed the concept of intuitionistic fuzzy sets (IFS) which is the extension of Fuzzy. Researchers have recently focused a lot of attention on solving bi-matrix games with intuitionistic fuzzy payoffs. The concept of Picture Fuzzy Sets(PFS) were introduced by Cuong [2], which is considered as the advancement of fuzzy sets and IFSs because it contains neutrality degree along with membership and non-membership degrees. A new approach to solving bi-matrix game problems with intuitionistic fuzzy payoffs where the payoff values are determined by the opinions of various experts was recently developed by Singla et al.[4]. In this paper, we contribute the following (i)solution procedure is designed to solve the fuzzy bi-matrix game problem with the collective payoff matrices from group of experts with pay off values as picture fuzzy numbers.(ii) An aggregation operator-based technique is developed to fuse the opinion of a group of experts. (iii) Comparison and analyzation of the proposed techniques with the some of the available existing methods and illustrated the results by using a numerical example.

Methods

The algorithm for solving fuzzy bi-matrix games with picture fuzzy payoffs by multi experts is as follows:

Step 1: Let A_1 and A_2 be two players. Let $T = \{\sigma_1, \sigma_2, \ldots, \sigma_m\}$ and $U = \{\tau_1, \tau_2, \ldots, \tau_n\}$ be the set of pure strategies of players A_1 and A_2, respectively. Let $\{E_1, E_2, \ldots, E_l\}$ be the set of experts who gave their opinions about the strategies of the players. Thus, the payoffs of player A_1, given by different experts with $m \times n$ strategies, can be expressed in the form of picture fuzzy index matrices as follows:

$$\hat{R}(E_l) = \left(T, U, \langle (E_l)^{A_1}_{\alpha_i j}, (E_l)^{A_1}_{\beta_i j}, (E_l)^{A_1}_{\gamma_i j} \rangle\right) =$$

$$\begin{array}{c} \\ \sigma_1 \\ \sigma_2 \\ \vdots \\ \sigma_n \end{array} \begin{array}{c} \begin{array}{cccc} \tau_1 & \tau_2 & \cdots & \tau_n \end{array} \\ \begin{bmatrix} \langle (E_l)^{A_1}_{\alpha_{11}}, (E_l)^{A_1}_{\beta_{11}}, (E_l)^{A_1}_{\gamma_{11}} \rangle & \langle (E_l)^{A_1}_{\alpha_{12}}, (E_l)^{A_1}_{\beta_{12}}, (E_l)^{A_1}_{\gamma_{12}} \rangle & \cdots & \langle (E_l)^{A_1}_{\alpha_{1n}}, (E_l)^{A_1}_{\beta_{1n}}, (E_l)^{A_1}_{\gamma_{1n}} \rangle \\ \langle (E_l)^{A_1}_{\alpha_{21}}, (E_l)^{A_1}_{\beta_{21}}, (E_l)^{A_1}_{\gamma_{21}} \rangle & \langle (E_l)^{A_1}_{\alpha_{22}}, (E_l)^{A_1}_{\beta_{22}}, (E_l)^{A_1}_{\gamma_{22}} \rangle & \cdots & \langle (E_l)^{A_1}_{\alpha_{2n}}, (E_l)^{A_1}_{\beta_{2n}}, (E_l)^{A_1}_{\gamma_{2n}} \rangle \\ \vdots & \vdots & \ddots & \vdots \\ \langle (E_l)^{A_1}_{\alpha_{m1}}, (E_l)^{A_1}_{\beta_{m1}}, (E_l)^{A_1}_{\gamma_{m1}} \rangle & \langle (E_l)^{A_1}_{\alpha_{m2}}, (E_l)^{A_1}_{\beta_{m2}}, (E_l)^{A_1}_{\gamma_{m2}} \rangle & \cdots & \langle (E_l)^{A_1}_{\alpha_{mn}}, (E_l)^{A_1}_{\beta_{mn}}, (E_l)^{A_1}_{\gamma_{mn}} \rangle \end{bmatrix} \end{array}$$

Where l = 1, 2 , 3 , . . . , k

Similarly, the payoffs of player A_2, given by different experts with $m \times n$ strategies, can be expressed in the form of intuitionistic fuzzy index matrices as follows:

$$\hat{S}(E_l) = \left(T, U, \langle (E_l)^{A_2}_{\alpha_i j}, (E_l)^{A_2}_{\beta_i j}, (E_l)^{A_2}_{\gamma_i j} \rangle\right) =$$

$$\begin{array}{c} \\ \sigma_1 \\ \sigma_2 \\ \vdots \\ \sigma_i \end{array} \begin{array}{c} \begin{array}{cccc} \tau_1 & \tau_2 & \cdots & \tau_n \end{array} \\ \begin{bmatrix} \langle (E_l)^{A_2}_{\alpha_{11}}, (E_l)^{A_2}_{\beta_{11}}, (E_l)^{A_2}_{\gamma_{11}} \rangle & \langle (E_l)^{A_2}_{\alpha_{12}}, (E_l)^{A_2}_{\beta_{12}}, (E_l)^{A_2}_{\gamma_{12}} \rangle & \cdots & \langle (E_l)^{A_2}_{\alpha_{1n}}, (E_l)^{A_2}_{\beta_{1n}}, (E_l)^{A_2}_{\gamma_{1n}} \rangle \\ \langle (E_l)^{A_2}_{\alpha_{21}}, (E_l)^{A_2}_{\beta_{21}}, (E_l)^{A_2}_{\gamma_{21}} \rangle & \langle (E_l)^{A_2}_{\alpha_{22}}, (E_l)^{A_2}_{\beta_{22}}, (E_l)^{A_2}_{\gamma_{22}} \rangle & \cdots & \langle (E_l)^{A_2}_{\alpha_{2n}}, (E_l)^{A_2}_{\beta_{2n}}, (E_l)^{A_2}_{\gamma_{2n}} \rangle \\ \vdots & \vdots & \ddots & \vdots \\ \langle (E_l)^{A_2}_{\alpha_{m1}}, (E_l)^{A_2}_{\beta_{m1}}, (E_l)^{A_2}_{\gamma_{m1}} \rangle & \langle (E_l)^{A_2}_{\alpha_{m2}}, (E_l)^{A_2}_{\beta_{m2}}, (E_l)^{A_2}_{\gamma_{m2}} \rangle & \cdots & \langle (E_l)^{A_2}_{\alpha_{mn}}, (E_l)^{A_2}_{\beta_{mn}}, (E_l)^{A_2}_{\gamma_{mn}} \rangle \end{bmatrix} \end{array}$$

Where l = 1, 2 , 3 , . . . , k

Step 2: By using the aggregation operators which is an essential tool provided in this article, to aggregate the different opinions of a set of experts.
Step 3: Convert into bilinear programming model and solving using GUROBI software and obtain the value of the bi matrix game and optimum strategies of both the players.

Results and Conclusions

In this paper, we have proposed a method to solve the fuzzy bi-matrix game problem with payoffs from more than one expert in which the pay off values are represented by picture fuzzy numbers. Also we have proposed a new aggregation techniques for Picture fuzzy values, to fuse multi experts picture fuzzy pay off values into a single one . Since in the proposed method, the Pay off values are represented as picture fuzzy values which are advanced than intuitionistic fuzzy, our proposed method will improve the accuracy in decision making and provides better results. Our advanced method overcomes the shortcomings of some of existing methods like Li's[3] method. A numerical example has been illustrated to show the applicability and superiority of the proposed method. Also the results are analyzed and compared with some of the existing techniques.

Keywords:

Game theory, bi-matrix game, picture fuzzy number, picture fuzzy bi-matrix game.

References

[1] Krassimir T. Atanassov. Intuitionistic fuzzy sets. *Fuzzy Sets and Systems*, 20(1):87–96, 1986.

[2] Bui Cong Cuong. Pythagorean picture fuzzy sets (ppfs), part 2-some main picture logic operators on ppfs and some picture inference processes in ppf systems. *Journal of Computer Science and Cybernetics*, 38(1):1–14, 2022.

[3] Joseph A Goguen. La zadeh. fuzzy sets. information and control, vol. 8 (1965), pp. 338–353.-la zadeh. similarity relations and fuzzy orderings. information sciences, vol. 3 (1971), pp. 177–200. *The Journal of Symbolic Logic*, 38(4):656–657, 1973.

[4] Parmpreet Kaur, Umesh Chandra Gupta, et al. A new method to solve intuitionistic fuzzy matrix game based on the evaluation of different experts. *Journal of Intelligent & Fuzzy Systems*, 41(2):2665–2674, 2021.

[5] John Von Neumann and Oskar Morgenstern. Theory of games and economic behaviour. *Toward a History of Game Theory*, 24:77, 1992.

Novel image fusion approach using Fermatean fuzzy sets

Rajarajeswari. P[1] **and Vengatesh. S**[1*]

[1] Department of Mathematics, Chikkanna Govt Arts College, Tiruppur, Tamil Nadu, India.
*Corresponding author; E-mail: vengateshmaths@gmail.com

Background

Fuzzy set theory was first presented by Zadeh [4] in 1965 and it has since developed into many refined variations. Using intuitionistic fuzzy sets, P. Balasubramaniam and V.P. Ananthi [1] presented a novel method for image fusion in 2014. Maruturi and Velmathi [5] introduced an enhanced multimodal medical image fusion based on Pythagorean fuzzy sets. Picture fuzzy sets with Membership, non-membership and indeterminacy degrees whose sum is less than or equal to one were created by Cuong [3] in 2014. Gülçin Büyüközkan, Deniz Uztürk and Öykü Ilıcak [2] in Fermatean fuzzy sets and its extensions: a systematic literature review. Traditional fuzzy sets have been extended to handle ambiguity and uncertainty in data with Fermatean Fuzzy Sets (FFS) and Intuitionistic Fuzzy Sets (IFS).Images from various settings are combined through image fusion to create a single, more useful image for additional processing. A new method utilizing Fermatean Fuzzy Sets *(FFS)* with maximum and minimum operations is presented in this paper. Membership, non-membership, and indeterminacy degrees are three ways that *FFS* efficiently manages ambiguities and uncertainties in digital images. The suggested technique converts images into Fermatean Fuzzy Images *(FFIs)*, fuses image blocks according to blackness and whiteness counts, and uses entropy to determine the ideal parameters. In contrast to commonly used methods such as AVG, PCA, DWT, SWT, DTCWT, MSVD, NSCT, IFS, SIFS, GFF, CSE, and LEG. According to our test results, *FFS* is perfect for image fusion tasks, particularly when dealing with intricate uncertainties and ambiguities, because it exhibits superior luminance, contrast, and overall image quality.

Methods for Fermatean Fuzzy Sets (FFS)

Assign I_1 and I_2 to the two input images, respectively(Step 1). Fuzzify the input images using an appropriate equation $S - S_{min}/S_{max} - S_{min}$ and calculate the optimal value of (λ) using an entropy measure equation for both input images separately(Step 2).Then,calculate the degrees of membership (α), non-membership (β), and hesitation (γ) using appropriate equations for both input images (Step 3).

$$\alpha_{FFS}\left(P\left(\widetilde{x},\widetilde{y}\right),\widetilde{z}\right)=1-\left(1-\alpha_F\left(P\left(\widetilde{x},\widetilde{y}\right)\right)\right)^{\widetilde{z}},\widetilde{z}\geq 0,\beta_{FFS}\left(P\left(\widetilde{x},\widetilde{y}\right),\widetilde{z}\right)=$$
$$\left(1-\alpha_F\left(P\left(\widetilde{x},\widetilde{y}\right)\right)\right)^{\widetilde{Z}(\widetilde{z}+1)}-\left(1-\alpha_F\left(P\left(\widetilde{x},\widetilde{y}\right)\right)\right)^{\widetilde{Z}(\widetilde{z}+2)},\widetilde{z}\geq 0$$

and $\gamma_{FFS}\left(P\left(\widetilde{x},\widetilde{y}\right),\widetilde{z}\right)=\left(1-\alpha_F\left(P\left(\widetilde{x},\widetilde{y}\right)\right)\right)^{\widetilde{Z}(\widetilde{z}+2)},\widetilde{z}\geq 0$ with their optimal λ value. The resulting images are denoted by FF_1 and FF_2.

Decompose the two images obtained from step 3 into $p \times q$ blocks. Denote the $\widetilde{z}^{th}$ image block of the two decomposed images by $FF_{1\widetilde{z}}$ and $FF_{2\widetilde{z}}$ respectively (Step 4). Next,compute the Total Count of Blackness, Whiteness and Neutrality of two corresponding blocks(Step 5) Reconstruct the $\widetilde{z}^{th}$ **Block of the Blended Image** as follows (Step 6): If count(blackness) > count(whiteness) and count(blackness) > count(neutrality), then $FF_{\widetilde{y}\widetilde{z}}\left(\widetilde{x},\widetilde{y}\right)=min\left(FF_{1\widetilde{z}}\left(\widetilde{x},\widetilde{y}\right),FF_{2\widetilde{z}}\left(\widetilde{x},\widetilde{y}\right)\right)$

If count(whiteness) > count(blackness) and count(whiteness) > count(neutrality), then $FF_{\widetilde{y}\widetilde{z}}(\widetilde{x},\widetilde{y}) = max\left(FF_{1\widetilde{z}}(\widetilde{x},\widetilde{y}), FF_{2\widetilde{z}}(\widetilde{x},\widetilde{y})\right)$
If count(neutrality) > count(blackness) and count(neutrality) > count(whiteness), then $FF_{\widetilde{y}\widetilde{z}}(\widetilde{x},\widetilde{y}) = average\left(FF_{1\widetilde{z}}(\widetilde{x},\widetilde{y}), FF_{2\widetilde{z}}(\widetilde{x},\widetilde{y})\right)$

Reconstruct the image from the blocks obtained from step 6 to get a fused Fermatean Fuzzy Image *(FFI)*(Step 7). Defuzzify the *FFI* obtained from step 7 to get a crisp image using a defuzzification function for *FFS* by extending the defuzzification formula provided for *IFS*(Step 8). $I(\widetilde{x},\widetilde{y}) = (S_{max} - S_{min}) \times \alpha_{FFS}(P(\widetilde{x},\widetilde{y})) + S_{min}$

Results and Conclusions

Comparing a novel image fusion technique with Fermatean Fuzzy Sets *(FFS)* to several well-known approaches : Simple Averaging (AVG), Principal Component Analysis (PCA), Dual Tree Complex Wavelet Transform (DTCWT), Stationary Wavelet Transform (SWT), Discrete Wavelet Transform (DWT), Intuitionistic Fuzzy Sets *(IFS)*, Sugeno Intuitionistic Fuzzy Sets *(SIFS)*, Guided Filter Fusion (GFF), Contrast and Structure Extraction (CSE), Multi-Resolution Singular Value Decomposition (MSVD), Non-Subsampled Contourlet Transform (NSCT) and Local Energy and Gradient (LEG). Multi-focused, medical, and infrared-visible images were all tested. *FFS* fusion demonstrated improved luminance and contrast for medical images, with superior MEAN, SF, and STD values. This was due to its ability to control for ambiguity and uncertainty in poorly lit images that have imperfections. *FFS* continuously beats *IFS* in every evaluation, providing more flexibility, even though IFS performs well in both quantitative metrics (RMSE, PFE, MAE, CORR, SNR, PSNR, MI, QI, SSIM) and qualitative assessments.

This paper introduces a new method for combining images with a Fermatean fuzzy set to improve clinical diagnosis. The four stages primarily outline the fundamental idea of our suggested approach. Using two-scale decomposition, the source images were first broken down into base and detail layer images. After that, a Fermatean fuzzy set was used to fuse the base layers of two source images in order to extract additional structural information. The SF was then used to fuse the intricate layers. An improved fused image was ultimately created by combining the base and detailed fused images. We used five medical databases for the fusion process in this paper, and experimental results show that it is superior to other methods in both visual and quantitative ways.

Keywords:

Picture Fuzzy Sets, Picture fuzzy Image entropy and Image fusion

References

[1] Pagavathigounder Balasubramaniam and VP Ananthi. Image fusion using intuitionistic fuzzy sets. *Information fusion*, 20:21–30, 2014.

[2] Gülçin Büyüközkan, Deniz Uztürk, and Öykü Ilıcak. Fermatean fuzzy sets and its extensions: a systematic literature review. *Artificial Intelligence Review*, 57(6):138, 2024.

[3] Bui Cong Cuong and Vladik Kreinovich. Picture fuzzy sets-a new concept for computational intelligence problems. In *2013 third world congress on information and communication technologies (WICT 2013)*, pages 1–6. IEEE, 2013.

[4] Joseph A Goguen. La zadeh. fuzzy sets. information and control, vol. 8 (1965), pp. 338–353.-la zadeh. similarity relations and fuzzy orderings. information sciences, vol. 3 (1971), pp. 177–200. *The Journal of Symbolic Logic*, 38(4):656–657, 1973.

[5] Maruturi Haribabu and Velmathi Guruviah. Enhanced multimodal medical image fusion based on pythagorean fuzzy set: an innovative approach. *Scientific Reports*, 13(1):16726, 2023.

Integrating multi-criteria decision-making framework with Java programming to enhance AI role in multimedia applications

S.Iswariya [1*] **and A.Sahaya Sudha**[1]

[1] PG & Research Department of Mathematics, Nirmala College for Women, Coimbatore
*Corresponding author; E-mail: iswariya25041999@gmail.com

Background

In modern education, Artificial Intelligence (AI) assumes a significant role in refining educational strategies, assisting educators in navigating the diverse array of multimedia choices at their disposal. This research paper investigates the function of AI tools in the learning methodologies of Multimedia in Education using a proposed multi-criteria decision-making (MCDM) framework under a Hesitant fuzzy scenario. The suggested MCDM framework facilitates thorough evaluation and selection process, considering the interconnectedness of AI technologies and uncertainties inherent in decision-making. JAVA is also utilized to evaluate the process in detail, providing a robust programming environment that supports the implementation of complex algorithms necessary for handling the multi-faceted criteria and the hesitation aspects within the fuzzy logic. This integration ensures that the framework is both efficient and scalable, allowing for comprehensive analysis and accurate decision-making in educational contexts. Additionally, a comparison between the suggested MCDM framework and Java coding is explained, highlighting the strengths and limitations of each approach in the context of multimedia in education.

Methods

In this section, we have developed a new decision-making scheme to deal with the MCDM problems on HFS domain.

1. Conduct a literature review on multimedia in education, MCDM frameworks, hesitant fuzzy logic, and AI tools.
2. Identify challenges in multimedia selection and define evaluation criteria.
3. Develop an MCDM framework using hesitant fuzzy logic to handle uncertainties.
4. Implement the MCDM framework in Java with modular and scalable algorithms.
5. Simulate decision-making scenarios using test cases for multimedia alternatives.
6. Compare the performance of the MCDM framework with direct Java implementation.
7. Validate the framework through real-world case studies and collect feedback.
8. Analyze results, discuss implications, and provide practical recommendations.
9. Summarize findings, contributions, and suggest future research directions.

Results and Conclusions

The proposed MCDM framework effectively addressed the challenges of multimedia selection in education by integrating hesitant fuzzy logic to handle uncertainties and hesitation in decision-making. The Java implementation validated its scalability and computational efficiency, demonstrating its ability to process complex criteria and multiple alternatives seamlessly. Comparative analysis showed that the MCDM framework was more adaptable to uncertain scenarios and user-friendly, while the direct Java implementation excelled in deterministic cases with slightly faster performance. Validation through case studies confirmed the framework's practical utility, providing educators with objective and reliable recommendations. Feedback highlighted its ease of integration into existing workflows and its effectiveness in optimizing multimedia learning strategies. The framework strikes a balance between accuracy, adaptability, and usability, offering a valuable tool for educators. Future research could incorporate advanced AI techniques or extend the framework to other educational domains, emphasizing its transformative potential in modern education.

Keywords:

Hesitant fuzzy Set (HFS), Artificial Intelligence, Multimedia, JAVA, Multi Criteria Decision Making (MCDM).

References

[1] Ibrahim Badi and Dragan Pamucar. Supplier selection for steelmaking company by using combined grey-marcos methods. *Decision Making: Applications in Management and Engineering*, 3(2):37–48, 2020.

[2] Abeer Hadi and Mahmood Zaki Abdullah. Web and iot-based hospital location determination with criteria weight analysis. *Bulletin of Electrical Engineering and Informatics*, 11(1):386–395, 2022.

[3] Mahyar Kamali Saraji, Abbas Mardani, Mario Köppen, Arunodaya Raj Mishra, and Pratibha Rani. An extended hesitant fuzzy set using swara-multimoora approach to adapt online education for the control of the pandemic spread of covid-19 in higher education institutions. *Artif. Intell. Rev.*, 55(1):181–206, January 2022.

[4] Lotfi Asker Zadeh. Fuzzy sets. *Information and control*, 8(3):338–353, 1965.

Mathematical modelling of flank and bottom edges cutting effects of the end-milling force analysis

P.Y.Y.P. Yapa[1*], **Achala Pallegedara**[2]
Department of Manufacturing and Industrial Engineering, University of Peradeniya, Sri Lanka
*Corresponding author; E-mail: pyyehan@gmail.com

Background

End milling is a widely used machining technique in manufacturing, particularly in the aerospace, automotive, and die-mold industries, where high precision and complex shapes are essential. A crucial aspect of this process is cutting force analysis, which plays a key role in optimizing operations by influencing surface quality, tool wear, and machining stability. Accurate modeling of cutting forces enables effective milling process planning and real-time adaptive control, helping manufacturers enhance productivity while ensuring dimensional accuracy and tool reliability.

A major challenge in end milling is the cutting forces at the flank and bottom edges, which affect machining efficiency, surface finish, tool life, and chatter risk. High cutting forces can lead to tool wear, vibrations, and poor surface quality, making accurate force prediction essential for process optimization.

Consequently, this research introduces a new mechanistic cutting force model specifically for flat-end milling. A key feature of this model is that it accounts for the overall cutting forces generated by both the flank edge and the bottom edge cuttings simultaneously.

Methods

In the formulation of the model, to account for the size effect during flank cutting, the coefficients for the flank cutting force are treated as an exponential function of the instantaneous uncut chip thickness, and are determined using the nonlinear least-squares algorithm. Utilizing the identified flank cutting force coefficients, the bottom cutting force coefficients are calibrated in real-time by deducting the flank force component from the total measured force. It has been found that the bottom cutting force coefficients can be considered constant. The effectiveness of the suggested cutting force model is validated through experiments conducted under a broad spectrum of cutting conditions. It appears that the cutting at the bottom edge significantly influences the total cutting forces when the axial depth of cut is comparatively small. Typically, total cutting forces are computed through numerical integration, which aggregates a specified number of elementary cutting forces generated by the individual cutter edges. A review of literature indicates that two types of cutting force models are present, based on the method of obtaining cutting force coefficients, namely, the transformation method from orthogonal to oblique cutting and the direct calibration method. In this context, we employ the direct calibration method.

In the direct calibration method, cutting force coefficients are obtained directly from milling experiments involving a specific cutter and workpiece combination. This method was initially introduced by Kline et al. [3] to establish a mechanistic cutting force model for peripheral end milling. The cutting forces were considered to have a

direct relationship with the uncut chip thickness, suggesting that the cutting force coefficients were constant. Despite the significant contributions made in flat-end milling, it is often presumed that the flank edge is the primary contributor to the total cutting forces, and there has been limited research on the impact of the bottom edge [1]. In real-world applications, the bottom edge is continuously engaged during the milling process. Utilizing the direct calibration technique for cutting force coefficients and building upon the previous research by Wan et al. [4, 5], this paper presents a new cutting force model that incorporates the effects of the bottom edge and proposes an innovative procedure for calibrating cutting force coefficients for this model.

To calibrate cutter runout parameters, flank cutting force coefficients, and bottom cutting force coefficients we have to get some experimental data sets. To do that a cutting parameter set in Dang et al. [2] used with an HSS 3-flute cutting tool with a diameter of 12.7 mm with a block of aluminum 6063 as the workpiece with dimensions of 75mm x 75mm x 15mm in a pinnacle lv85 vertical machining center.

Results and Conclusions

Parameters for cutter runout, including offset and position angle, were initially calibrated using experimental data. The coefficients for flank cutting forces were obtained through two tests that maintained consistent spindle speeds, radial depths of cut, and feed per tooth, yet varied in their axial depths of cut. By subtracting the cutting forces recorded at the smaller axial depth from those at the larger depth, the forces produced by a single flank edge segment were isolated.

The correlation between instantaneous cutting force coefficients on the flank and uncut chip thickness was determined utilizing the linear least-squares method and the Levenberg–Marquardt method. The cutting forces of the bottom edge were derived by deducting the cutting forces of the flank from the total experimental forces, after which the relevant coefficients for the tangential, radial, and axial components were calibrated. These coefficients were subsequently applied to predict cutting forces in further tests.

Keywords:

End-Milling, Flank edge cutting, Bottom edge cutting, the linear least-square method, Levenberg–Marquardt Method.

References

[1] E.J.A. Armarego and N.P. Deshpande. Computerized predictive cutting models for forces in end-milling including eccentricity effects. *Annals of the CIRP*, 38:45–49, 1992.

[2] J.W. Dang, W.H. Zhang, Y. Yang, and M. Wan. Cutting force modeling for flat end milling including bottom edge cutting effect. *International Journal of Machine Tools and Manufacture*, 50(11):986–997, 2010.

[3] W.A. Kline, R.E. DeVor, and J.R. Lindberg. The prediction of cutting forces in end milling with application of cornering cuts. *International Journal of Machine Tool Design and Research*, 22(1):7–22, 1982.

[4] M. Wan, W.H. Zhang, J.W. Dang, and Y. Yang. A novel cutting force modeling method for cylindrical end milling. *Applied Mathematical Modelling*, 34:823–836, 2010.

[5] M. Wan, W.H. Zhang, G. Tan, and G.H. Qin. New algorithm for calibration of instantaneous cutting-force coefficients and radial run-out parameters in flat end milling. *Proceedings of the Institution of the Mechanical Engineers, Part B: Journal of Engineering Manufacture*, 221:1007–1019, 2007.

Multi-objective optimization for integrating battery storage with solar power generation using PSO

R.M.T. Lakmali[1*]
[1] Uva Wellassa University of Sri Lanka
*Corresponding author; E-mail: rmtlakma@gmail.com

Background

The increasing global demand for energy requires a transition to renewable energy sources. Solar photovoltaic (PV) systems have gained prominence as a sustainable energy solution. Fluctuations in solar irradiance cause intermittency issues in PV systems, which can be mitigated by integrating Battery Energy Storage Systems (BESS)[2, 4]. BESS helps stabilize the power supply, enhance peak shaving, and reduce dependence on conventional power grids.

A major challenge in integrating BESS with solar PV systems is determining the optimal battery size. This requires balancing multiple factors, including cost, battery lifespan, and energy efficiency. Each of these factors influences the system's performance and economic feasibility, making optimization a complex task. This study focuses on optimizing energy generation and storage by considering these factors. By comparing different optimization techniques, Particle Swarm Optimization (PSO) is selected to develop the mathematical model for this research [2]. Inspired by the collective movement of bird flocks, PSO is a population-based metaheuristic algorithm that efficiently solves complex multi-objective problems [2, 3]. In this study, PSO is applied to determine the optimal battery size and operational strategy for a solar PV-BESS system by selecting the most suitable weighting factors according to local constraints.

The proposed approach enhances power system reliability, reduces energy and battery costs, and improves energy management. Furthermore, by incorporating PSO-based optimization, this research contributes to the development of efficient peak shaving and load balancing strategies for PV-BESS systems. The findings provide valuable insights into configuring battery storage for renewable energy applications, supporting economic and operational sustainability in modern power systems[1].

Methods

The methodology involves a structured computational approach that integrates PSO with solar PV-battery storage optimization. The first stage involves data collection, where power generation and demand data from a solar power plant are gathered, and the feasibility of battery system integration is analyzed. The most influential factors for battery storage selection are gathered and analyzed through a literature survey and practical constraints[3].

Subsequently, a multi-objective optimization framework is formulated, with objective functions defined to achieve an optimal trade-off between cost, battery lifespan, and peak shaving performance. The primary objectives include minimizing total system cost (investment, operational, and maintenance costs), maximizing peak shaving efficiency, and extending battery lifespan by reducing excessive deep discharge cycles. These objectives are subject to constraints related to power balance, battery depth of discharge (DOD), and grid interaction limits [4, 3]. Selecting the most suitable weighting factors for multi-objective optimization is a key aspect of this study. Sensitivity

Analysis, Analytic Hierarchy Process (AHP), Entropy Weighting, and Multi-Criteria Decision Analysis (TOPSIS) are applied and their results analyzed results to identify relevant weighting factors for battery storage sizing [3].

PSO algorithm is then implemented by initializing a swarm of candidate battery sizes, each assigned to a fitness value based on the objective function. The particles iteratively adjust their positions based on both their individual best performance and the global best solution found by the swarm. The optimization process continues until convergence is achieved, ensuring that the selected battery capacity meets the optimal balance among the defined objectives [2].

Finally, the optimized solution is validated using MATLAB, where the proposed PSO-based solution is simulated under different operational conditions to evaluate the improvement in system performance, efficiency, and economic feasibility [4].

Results and Conclusions

The study identified cost, battery lifespan, and peak shaving performance as the most significant factors influencing battery capacity selection for solar PV-battery integrated systems. The results indicate that the multi-objective optimization process effectively balances economic feasibility, peak shaving efficiency, and battery longevity [3]. A key aspect of this optimization is the identification of appropriate weighting factors for the multi-objective function, which determines the balance between cost reduction, peak demand management, and battery degradation minimization [3, 1].

To determine the optimal weighting factors, a combined approach incorporating Sensitivity Analysis, Analytic Hierarchy Process (AHP), Entropy Weighting, and Multi-Criteria Decision Analysis (TOPSIS) was applied. The study found that a weighting distribution of 0.35 for cost, 0.21 for peak shaving, and 0.44 for battery degradation produced optimal results, ensuring both economic viability and technical efficiency.

This research is ongoing, with further improvements in progress. At the end of the study, an Energy Management System (EMS) for solar PV-battery storage will be developed, incorporating an optimized battery capacity for practical implementation.

In conclusion, Particle Swarm Optimization (PSO) provides a reliable and efficient approach for optimizing solar PV-battery integration, ensuring a cost-effective, technically feasible, and sustainable energy storage solution.

Keywords:

Multi-objective Optimization, Particle Swarm Optimization (PSO), Battery Energy Storage Systems (BESS), Solar PV Integration

References

[1] Fadi Agha Kassab, Rusber Rodriguez, Berk Celik, Fabrice Locment, and Manuela Sechilariu. A comprehensive review of sizing and energy management strategies for optimal planning of microgrids with pv and other renewable integration. *Applied Sciences*, 14(22):10479, 2024.

[2] Singiresu S Rao. *Engineering optimization: theory and practice*. John Wiley & Sons, 2019.

[3] Mehmet Şahin. A comprehensive analysis of weighting and multicriteria methods in the context of sustainable energy. *International Journal of Environmental Science and Technology*, 18(6):1591–1616, 2021.

[4] Meiqi Yao and Xu Cai. Energy storage sizing optimization for large-scale pv power plant. *IEEE Access*, 9:75599–75607, 2021.

Enhancing grid stability and reliability through integrated solar forecasting and demand prediction in Sri Lanka

S.J.U. Senerath[1*], **T.R.V. Muthukumari**[1],**W.B.S. Nanayakkara**[1],
P. Weerasekara[1],**Samadhi Rathnayake**[1],**Mahil Fernando**[2],**Pipuni Wijesiri**[1]
[1] Sri Lanka Institute of Information Technology,Sri Lanka
[2] Windforce PLC
*Corresponding author; E-mail: jsenarathhh@gmail.com

Background

Sri Lanka is making strides toward a renewable energy future, but the integration of solar power into the national grid presents challenges due to the intermittency of solar energy. Although the country's tropical climate offers substantial solar potential, fluctuations in irradiance can disrupt grid stability and reliability. This study seeks to address these challenges by leveraging advanced machine learning forecasts of solar irradiance and electricity demand to improve grid management.

Methods

Data collection encompassed historical meteorological records for solar forecasting and long-term electricity consumption data for demand prediction. In the data preprocessing phase, missing values were rectified, and datasets were normalized for consistency. Exploratory data analysis (EDA) was used to identify influential features for both forecasting tasks. Long Short-Term Memory (LSTM) and Seasonal Autoregressive Integrated Moving Average with Exogenous variables (SARIMAX) models were evaluated.

Results and Conclusions

The LSTM model proved to be the most accurate for solar irradiance forecasting, while SARIMAX outperformed other models in predicting electricity demand. The integration of these models into a grid stability analysis framework demonstrated significant improvements in frequency and voltage stability, particularly during late-afternoon load surges when solar generation naturally decreases.

The study demonstrates that accurate solar forecasting and demand prediction are critical for managing the challenges of renewable energy integration. The synergy of LSTM for solar forecasting and SARIMAX for demand prediction offers a robust framework for improving grid stability and supporting Sri Lanka's renewable energy transition.

Keywords:

Grid Stability, Renewable Energy Integration, Machine Learning, LSTM, SARIMAX

References

[1] A.M. Alam, I.A. Razee, and M. Zunaed. Solar pv power forecasting using traditional methods and machine learning techniques. In *IEEE Kansas Power and Energy Conference (KPEC)*, pages 1–5, 2021.

[2] M. Elsaraiti and A. Merabet. Solar power forecasting using deep learning techniques. *IEEE Access*, 10:31692–31698, 2022.

[3] P.D. Huy, V.K. Ramachandaramurthy, and H.M. Pesaran. Optimal selection of location, sizing and power factor for solar pv plants using differential evolution. In *2015 IEEE Innovative Smart Grid Technologies-Asia (ISGT ASIA)*, pages 1–6, 2015.

[4] M. Karunanithi, A.A.S. Braitea, A.A. Rizvi, and T.A. Khan. Forecasting solar irradiance using machine learning methods. In *2023 IEEE 64th International Scientific Conference on Information Technology and Management Science of Riga Technical University (ITMS)*, pages 1–4, 2023.

[5] A. Tuohy, J. Zack, S.E. Haupt, J. Sharp, M. Ahlstrom, S. Dise, E. Grimit, C. Mohrlen, M. Lange, M.G. Casado, and J. Black. Solar forecasting: methods, challenges, and performance. *IEEE Power and Energy Magazine*, 13(6):50–59, 2015.

Competition dynamic model as evolutionary game theory

Dwi Purliantoro[1,3*], **Agus Yodi Gunawan**[2] **and Dewi Handayani**[2]
[1] Doctoral Program of Mathematics, Faculty of Mathematics and Natural Sciences, Institut Teknologi Bandung, Bandung 43123, Indonesia;
[2] Faculty of Mathematics and Natural Sciences, Institut Teknologi Bandung, Bandung 43123, Indonesia;
[3] Faculty of Mathematics and Natural Sciences, Universitas Muhammadiyah Bandung, Bandung 40614, Indonesia.
*Corresponding author; E-mail: dwi.purliantoro@umbandung.ac.id

Background

Evolutionary game theory based on dynamical systems is a powerful mathematical tool for studying the evolution of strategies within a population, particularly through nonlinear dynamical system models [1]. This study aims to investigate the linear stability of competition dynamic model as evolutionary game theory. The governing equations in term of dimensionless form are given as follows:

$$\begin{cases} \dfrac{dp}{d\theta} = \beta_1 p - \beta_2(1 - w_1 x)pq, \\ \dfrac{dq}{d\theta} = q(1-q) - \beta_3(1 - w_2 x)pq, \\ \dfrac{dx}{d\theta} = x(x-1)(D_g x + D_r(1-x)), \end{cases} \tag{1}$$

The first two equations describe the population dynamics under competition, while the third equation indicates the presence of replicator equation evolution within the system. The variables p and q represent two competing populations over time θ, while $x \in [0, 1]$ represents the share of the population cooperating. The model has seven positve parameters. Parameter β_1 represents the growth rate, β_2 and β_3 represent interaction rates between two populations. Furthermore, parameter $w_1 \in [0, 1]$ represents the weight that describes the influence of cooperative behavior on the competition rate effect of population q on population p, while $w_2 \in [0, 1]$ represents the weight that describes the influence of cooperative behavior on the competition rate effect of population p on population q. The parameters D_g and D_r respectively determine the type of game in the presence of the gamble-intending dilemma (GID) or the risk-averting dilemma (RAD) [2]. In the present study we will explore the Stag Hunt Game as RAD-type and the Chicken Game as GID-type. The invariant set of system (1) is given by

$$\mathcal{A} = \{[p, q, x] \in \mathbb{R}^3_+ : p \geq 0, q \geq 0, 0 \leq x \leq 1\}$$

which ensures the system remains within the specified non-negative domain. By analyzing this system, we aim to explore how cooperation influences competitive interactions and how evolutionary game dynamics shape population outcomes. This approach provides new insights into competition models by incorporating both strategic decision-making and ecological interactions.

Methods

In order to investigate the competition dynamic model, we employ stability analysis, numerical simulation, and interpretations based on evolutionary game theory. Stability analysis is conducted by calculating the equilibrium points of system (1) then examining their stability through the Jacobian matrix and eigenvalue analysis. Linear stability diagrams are generated to identify stability transitions and critical thresholds where cooperation behavior significantly alters the dynamics, we denote $\overline{\beta} = \beta_1$ and $\underline{\beta} = \dfrac{\beta_1}{1 - w_1}$ as critical threshold. Numerical simulations are performed using the fourth-order Runge-Kutta method to solve the system (1). Various parameter values are explored to study the impact of cooperative behavior on competitive interactions. The system is further interpreted through the lens of evolutionary game theory by examining how cooperative strategies evolve within a competitive framework. Additionally, we generate a Basin of attraction diagrams that illustrates how the determination of initial conditions influences the system's final outcome as it moves toward its attractor

Results and Conclusions

Through analysis of equilibrium, it is found that the presence of the replicator equation results in nine equilibrium points under the parameter conditions $\beta_2 > \overline{\beta}$ and $\beta_2 > \underline{\beta}$, compared to the initial model, which only has three equilibrium points. To obtain numerical solution of the system, we set parameters as follow: $\beta_1 = 3$, $\beta_2 = 10$, $\beta_3 = 5$, $w_1 = 0.6$, $w_2 = 0.6$, and initial condition $p_0 = 0.5, q_0 = 1.1, x_0 = 0.6$.

(a) *Chicken Game* (b) *Stag Hunt Game*

Figure 1: Dynamic Plot (a) *Chicken Game* (b) *Stag Hunt Game*

Figure 1 shows (a) Dynamic plot over time in the case of *Chicken Game*, where $D_g > 0$ and $D_r < 0$, showing the tendency of population x to become polymorphic. Meanwhile (b) in the case of *Stag Hunt Game*, where $D_g < 0$ and $D_r > 0$, the entire population x tends to cooperate.

Keywords:

competition dynamic model, evolutionary game theory, replicator equation, basin of attraction

References

[1] D. Madeo and C. Mocenni. Evolutionary game theoretic insights on the sirs model of the covid-19 pandemic. *IFAC-PapersOnLine*, 54(17):1–6, 2021. 6th IFAC Conference on Analysis and Control of Chaotic Systems CHAOS 2021.

[2] Jun Tanimoto. *Fundamentals of Evolutionary Game Theory and its Applications*. Springer Japan, Japan, oct 2015.

Efficacy of genetic algorithm in stock market analysis

C. Karen Felicita [1*] **and A. Sahaya Sudha**[1]
[1] Department of Mathematics, Nirmala College for Women, Coimbatore, Tamil Nadu, India
*Corresponding author; E-mail: karenfelicita.research@gmail.com

Background

The stock market is a highly dynamic and complex system influenced by numerous factors, making accurate predictions challenging. Traditional analytical models often struggle to capture its nonlinear nature, necessitating the use of advanced computational techniques. This study explores the efficacy of Genetic Algorithms (GA) in optimizing machine learning models for stock market analysis. Genetic Algorithms, inspired by natural selection, enable efficient feature selection, hyper parameter tuning, and model optimization, leading to improved predictive performance. By integrating GA with machine learning techniques such as Support Vector Machines (SVM), Random Forest, and Neural Networks, we evaluate its impact on prediction accuracy, feature selection efficiency, and computational cost. Experimental results demonstrate that GA-enhanced models outperform baseline models in forecasting stock price trends, reducing overfitting, and enhancing generalizability.

Methods

Data Collection

- Stock market data is obtained from reliable financial sources (Yahoo Finance, Bloomberg, or NSE/BSE datasets).
- Data includes historical stock prices, trading volume, technical indicators (e.g., Moving Averages, RSI, MACD), and macroeconomic factors.

Pre processing Feature Engineering

- Data cleaning: Handling missing values, outlier removal, and normalization.
- Feature extraction: Computing technical indicators and transforming raw data into meaningful features.
- Splitting into training and testing sets (80-20 ratio).

Machine Learning Models

- Selection of baseline models: Support Vector Machine (SVM), Random Forest, and Neural Networks.
- Training initial models without GA optimization for benchmark comparison.

Genetic Algorithm Optimization

- **Encoding:** Representing model hyperparameters and selected features as chromosomes.
- **Initialization:** Creating a population of possible solutions.

- **Fitness Function:** Evaluating models based on prediction accuracy and error metrics (e.g., RMSE, MAPE).
- **Selection:** Choosing the best-performing individuals for reproduction.
- **Crossover Mutation:** Generating new candidate solutions through crossover and mutation operators.
- **Iteration:** Running multiple generations to optimize model performance.

Performance Evaluation

- Comparing GA-optimized models with non-optimized models using accuracy, precision, recall, and computational efficiency.
- Conducting statistical tests (e.g., paired t-tests) to validate improvements.

Conclusion Future Work

- Summarizing key findings on GA's efficacy in stock market prediction.
- Identifying limitations and suggesting enhancements for future research, such as hybrid algorithms and deep learning integration.

Results and Conclusions

This research highlights the potential of GA as a powerful optimization tool in financial market analysis, paving the way for more robust and adaptive predictive models.

Keywords:

Genetic Algorithm (GA), Stock Market Prediction, Machine Learning, Feature Selection, Hyperparameter Optimization, Support Vector Machine (SVM)

References

[1] Ying-Hua Chang and Chen-Wei Huang. Utilizing genetic algorithms in conjunction with ann-based stock valuation models to enhance the optimization of stock investment decisions. *AI*, 5(3):1011–1029, 2024.

[2] Norberto Ritzmann Junior and Julio Cesar Nievola. A generalized financial time series forecasting model based on automatic feature engineering using genetic algorithms and support vector machine. *arXiv e-prints*, pages arXiv–1809, 2018.

[3] Xinye Sha. Time series stock price forecasting based on genetic algorithm (ga)-long short-term memory network (lstm) optimization. *arXiv preprint arXiv:2405.03151*, 2024.

[4] P Shanmukh Kali Prasad, Vadlamani Madhav, Ramanuj Lal, and Vadlamani Ravi. Optimal technical indicator-based trading strategies using nsga-ii. *arXiv e-prints*, pages arXiv–2111, 2021.

[5] Zhengxin Joseph Ye and Bjorn W Schuller. Capturing dynamics of post-earnings-announcement drift using genetic algorithm-optimised supervised learning. *arXiv preprint arXiv:2009.03094*, 2020.

Investigating the impact of magnetic fields on viscous fingering instabilities in enhanced oil recovery

C. W. Sahabandu[1*] **and A. E. K. P. Weerasinghe** [1]

[1] Department of Mathematics, The Open University of Sri Lanka, Nawala, Nugegoda, 10250, Sri Lanka

*Corresponding author; E-mail: cwsah@ou.ac.lk

Background

Viscous fingering is a critical instability that affects the displacement efficiency in enhanced oil recovery (EOR). One of the major challenges in EOR is the development of viscous fingering instabilities, which occur when a less viscous fluid displaces a more viscous one, leading to inefficient oil recovery. Traditional approaches focus on optimizing fluid viscosity and injection rates, but recent studies suggest that external forces, such as magnetic fields, can influence fluid dynamics. Several researchers have studied fingering instability in EOR in different perspectives. Sahabandu et al. investigated CFD simulations of miscible and immiscible fingering instability in enhanced oil recovery using COMSOL Multiphysics [2]. Kumar et al. introduced a new numerical model in COMSOL Multiphysics by coupling two different physics modules to simulate miscible viscous fingering in two-dimensional homogeneous porous media with both small and large porosities [1]. Several studies have been done by Sahabandu et al. exploring semi-analytical solutions for miscible and miscible fingering instability [4, 3].

Methods

In this study, we investigate how the implementation of an external magnetic field affects behavior of the viscous fingering in a homogeneous porous medium during carbonated water injection. Using COMSOL Multiphysics 6.2, we simulate the displacement process and analyze the effect of magnetic field on the stabilization of the interface between fluids. In this investigation, we examined homogeneous, isotropic porous matrix with constant permeability and porosity ϵ_p.

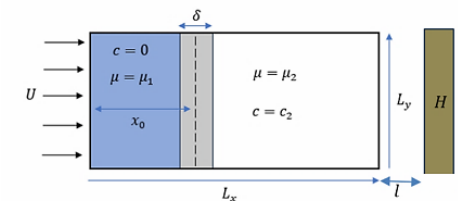

Figure 1: Domian of miscible fluid movement in two-dimensional homogenous porous media with magnetic field effect H.

Figure 1 illustrates the geometry, which consists of a horizontal rectangular domain with a length of $L_x = 1.0\ m$ and a width of $L_y = 0.3\ m$.
Another rectangular domain representing the magnet H, with a length of $0.3m$ and a width of $0.1\ m$. The distance between the outlet and the magnet is $l = 0.1\ m$. Assume both fluids have the same density, . Without loss of generality, for an injective fluid with a viscosity of $_1$,$c = 0\ molm^{-3}$, and for a native fluid (oil) with a viscosity of μ_2, $c = c_2\ molm^{-3}$ and here, c stands for the concentration of a solute in the solvent. Since this results in an instanta-

neous thin transition zone (at the interface) between the fluids, we begin our simulations by assuming that the fluids are miscible, and we assume the thickness of that as (see Figure 1). At x_0, the initial interface concentration is $c = c_2/2\ molm^{-3}$. Mainly using the continuity equation (mass conservation), the Darcy law, the convection-diffusion equation for transfer of solute concentration [2] and the magnetic field for x-direction $H = 0.1\ x$ underlining the magnetic field effect using COMSOL Multiphysics 6.2 we have obtained following results.

Results and Conclusions

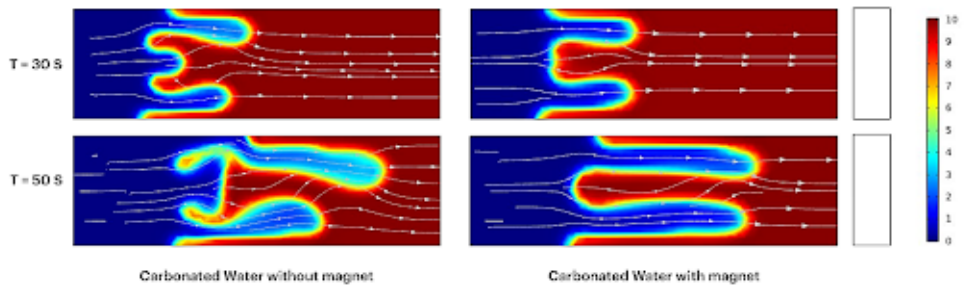

Figure 2: spatio-temporal evaluation of fingering instability of carbonated water injection at T=30 s and T=50 s.

Comparing the results with and without a magnetic field at certain times, we observe significant differences in the development of viscous fingers (see Figure 2). Without the magnetic field, the displacement process exhibits highly irregular and branched fingering patterns, leading to poor oil recovery occurring trapped oil. However, by incorporating a magnetic field, the fingering patterns become more stabilized, and the displacement front remains more uniform. This confirms that the magnetic field mitigates interfacial instabilities by modifying the velocity profile and controlling fingering growth. We can conclude that magnetic interactions can alter the flow mobility, reducing the instability of fingers and promoting a more uniform displacement process.

Keywords:

Carbonated water, COMSOL Multiphysics 6.2, Enhanced oil recovery, Magnetic field

References

[1] Anoop Kumar, Satyajit Pramanik, and Manoranjan Mishra. Comsol multiphysics® modeling in darcian and non-darcian porous media. In *Proceedings of the 2016 COMSOL Conference, Bangalore, India*, pages 20–21, 2016.

[2] CW Sahabandu and M Dewasurendra. Cfd simulation for miscible and immiscible viscous fingering formation for distinct injective fluids. 2024.

[3] CW Sahabandu and MTM Dewasurendra. Modelling and semi-analytical solutions for fingering instability during zero-dimensional nano floodings. *Ceylon Journal of Science*, 53(4), 2024.

[4] CW Sahabandu, ZAMS Juman, K Vajravelu, B Spangler, and M Dewasurendra. Modeling and semi-analytical solution for immiscible and miscible fingers formation during enhanced oil recovery. *International Journal of Modelling and Simulation*, pages 1–12, 2023.

Multi-objective non-linear programming problems in picture fuzzy numbers

C.Saranya[1,2*] **and A.Sahaya Sudha**[1]

[1] Department of Mathematics, Nirmala College for Women, (Affiliated to Bharathiar University)

[2] Assistant Professor, Department of Mathematics, SNS College of Technology, (Affiliated to Anna University)

*Corresponding author; E-mail: saranya.c.math@snsct.org

Background

Multi-objective Optimization is a key research area in operations research and decision-making with applications to engineering economics, management and economics. Real-world problems often involve conflicting objectives and uncertainty making traditional optimization techniques inadequate. Fuzzy set theory provides a mathematical framework to deal with imprecision but standard fuzzy sets lack the ability of depicting membership, non-membership and hesitation simultaneously. To address this the intuitionistic fuzzy sets and picture fuzzy sets have been introduced. Picture fuzzy sets proposed by Cuong and Kreinovich extend intuitionistic fuzzy set extensions by integrating neutral membership. This makes them well-suited for problems with ambiguity, in addition to the Applying picture fuzzy sets to multi-objective non-linear programming (MONLP) presents new challenges due mainly to non-linearity of the functions and additional uncertainty. This study proposes a modified NSGA-basic approach that is tailored for picture fuzzy MONLP tailoring optimality and stability. A numerical example demonstrates the method's effectiveness in handling complex, uncertain conditions.

Methods

The study addresses multi-objective nonlinear programming problems by integrating picture fuzzy calculations with a modified non-dominated sorting genetic algorithm (NSGA). Real-world optimization problems often involve conflicting objectives and uncertainty that make conventional optimization methods inadequate. By incorporating picture fuzzy numbers (PFNs), which account for membership, non-membership and hesitation values the proposed approach well models imprecise parameters along with enhancement of decision-making under uncertainty. In the proposed methodology genetic operators are tailored to keep the integrity of the fuzzy set in the fuzzy picture. The Specifically picture fuzzy crossover and mutation operators are designed to introduce diversity without disrupting the overall structure of the fuzzy data. This ensures that the search space is efficiently explored while preserving the essential qualities of PFNs. The ranking mechanism evaluates candidate solutions based on picture fuzzy numbers, providing a structured approach to handling uncertainty in the decision-making process. The algorithm iteratively balances conflicting objectives by identifying and refining Pareto-optimal solutions. This is accomplished by applying the algorithm as a By leveraging the flexibility of PFNs the proposed NSGA-based framework enhance both optimality and stability of solutions adding to its appeal as a powerful tool for solving complex MONLP problems. A numerical example illustrates the practical applicability and effectiveness of the methodology, demonstrating

its robustness in handling uncertainty and its superiority over traditional optimization techniques.

Results

proposed approach effectively solved multi-objective non linear programming problems (MONLP) in a picture fuzzy set framework. By incorporating picture fuzzy numbers (PFNs), the method demonstrated improved uncertainty modeling by incorporating picture fuzzy values (PFNs); this enhanced representation of imprecisite information ensure The modified NSGA efficiently generated well-distributed Pareto fronts and produced better optimality and stability than traditional methods. Comparative analysis highlights the superiority of the proposed technique showing improved solution quality while maintaining computational efficiency. Sensitivity analysis confirmed the robustness of the approach under varying picture fuzzy conditions reinforcing its reliability in handling uncertainty.

Conclusions

The study established an advanced optimization framework for MONLP problems using picture fuzzy numbers and modified NSGA. The results demonstrated that the approach effectively manages uncertainty and ambiguity making it suitable for real-world applications where precise information is incomplete. The ability to generate high-quality Pareto-optimal solutions suggests its practical applicability in diverse decision -making scenarios. Future research could explore the dynamic extensions of decision making, integrating hybrid optimization techniques and adaptive strategies to enhance computational efficiency and solution robustness.

Keywords:

Multi-objective non linear programming, Fuzzy logic and fuzzy set theory , Picture fuzzy numbers.

References

[1] Bùi Công Cng. Picture fuzzy sets. *Journal of Computer Science and Cybernetics*, 30(4):409, Dec. 2014.

[2] Nguyen Van Dinh, N Xuan Thao, and N Xuan. Some measures of picture fuzzy sets and their application in multi-attribute decision making. *Int. J. Math. Sci. Comput.(IJMSC)*, 4(3):23–41, 2018.

[3] R Bellman. Decision-makking in a fuzzy environment. *Management science*, 17:8141–8164, 1970.

[4] Amalendu Si, Sujit Das, and Samarjit Kar. An approach to rank picture fuzzy numbers for decision making problems. *Decision Making: Applications in Management and Engineering*, 2(2):54–64, 2019.

Stochastic pharmacokinetic - pharmacodynamic modeling of metformin for the treatment of type II diabetes mellitus

A.K.K.K. Athukorala[1*]
[1] Faculty of Graduate Studies, University of Colombo
*Corresponding author; E-mail: kalpanakumudukumari@gmail.com

Background

Diabetes Mellitus, commonly referred as diabetes is a chronic disease that affects millions of people worldwide. This situation is same for Sri Lankan context as well. According to the World Health Organization (WHO), the diabetic population in Sri Lanka is approximately 24%. Therefore one person in every four persons is a victim of diabetes. The diabetic population can be classified into three parts such as pre-diabetic, diabetic and diabetic with complications. Diabetes is a metabolic disorder which leads to several complications such as renal failures, cardiovascular diseases, skin problems, blind vision etc. Therefore, Diabetes mellitus can be considered as a silent killer nowadays. Diabetes is caused mainly due to two reasons. The first reason is insufficient insulin production in pancreas and it is the common version of diabetes. The other reason is the tissue resistance against secreted insulin. Both biological reasons in the human body lead to high concentration of excessive glucose and it is harmful for many organs in the human body [2]. According to these two reasons, diabetes can be mainly classified into two types such as type I diabetes (T1DM) and type II diabetes (T2DM). Type 1 diabetes mellitus, previously known as insulin-dependent diabetes mellitus (IDDM) is an autoimmune disorder where the immune system attacks and destroys the pancreatic -cells responsible for producing insulin. This leads to a complete insulin deficiency and the presence of anti-insulin or anti-islet cell antibodies in the blood [1]. Type 2 diabetes mellitus is characterized by the body's insensitivity to insulin, leading to decreased insulin production, resistance to insulin, and eventual decline in the function of pancreatic -cells. This results in decreased transport of glucose into the liver, muscle, and fat cells. The peripheral insulin resistance, which is linked to -cell depletion, prevents low blood sugar levels even if blood insulin levels are high, due to modifications to the insulin receptors responsible for insulin activity [1]. Type II diabetes is the common type and this study is mainly focused type II diabetes mellitus treatments.

Metformin is first line oral treatment which is used worldwide as an anti-hyperglycemic agent [1]. In this study, the Metformin concentration of four compartments in human digestive system is modeled with time. The four compartments are gastrointestinal (GI) lumen, gastrointestinal (GI) wall, liver (central compartment) and periphery [2]. The four compartments pharmacokinetic model with ordinary differential equations shows the oral and intravenous drug administration, drug transferring among different compartments and drug elimination via fecal route and urination.

Methods

The four compartment deterministic pharmacokinetic model in [2] was modified by using Geometric Brownian Motion. The deterministic model and modified stochastic model is simulated by using MATLAB. There are four stochastic differential equations

(SDE) for each compartment such as GI lumen, GI wall, liver and periphery. The initial dose was considered as 500mg and each model equation was simulated for 24 hours by using Euler method. The root mean square difference (RMSD) was calculated for each compartment by comparing deterministic and stochastic models.

Results and Conclusions

The amounts of metformin of each compartment were represented graphically. The amount of drug in GI lumen was exponentially decaying over time. The amount of drug in GI wall is exponentially increasing and converging to 250 mg over time. The amount of drug in liver is exponentially increasing and converging to 150 mg over time. The amount of drug in periphery lasts approximately constant value around 25mg. The root mean square differences (RSMD) of GI lumen, GI wall, liver and periphery are 54.6, 62.1, 30.7 and 5.8 respectively.

Since there were high RMSD values for GI lumen and GI wall, it doesn't provide a reasonable approximation for stochastic dynamics. A lower RMSD value for the liver (central) compartment comparing to the GI lumen and GI wall, demonstrates that the deterministic model aligns more closely with the stochastic model in the liver, where drug metabolism dominates. The lowest RMSD value of periphery indicates significant deviation due to higher noice levels. The alignment between the deterministic model and stochastic model can be improved by adapting parameters, reducing the time steps and introducing hybrid modeling approaches.

Keywords:

Diabetes Mellitus, Pharmacokinetic, Phamacodynamic, Metformin, Insulin, Geometric Brownian Motion

References

[1] Suein Choi, Sangil Jeon, and Seunghoon Han. Population pharmacokinetic analysis of metformin administered as fixed-dose combination in korean healthy adults. *Translational and clinical pharmacology*, 26(1):25, 2018.

[2] Lin Sun, Ezra Kwok, Bhushan Gopaluni, and Omid Vahidi. Pharmacokinetic-pharmacodynamic modeling of metformin for the treatment of type ii diabetes mellitus. *The open biomedical engineering journal*, 5:1, 2011.

Mathematical and AI-driven framework for identifying sudden stops, loss of control, and lane changes

Dissanayake D. J. R [1*], **H. D. S. R. Sualakkana**[1], **Rizmaan M. F. M**[1], **Kuhaananth C.** [1], **Samadhi R.** [1] **and Nelum A.** [1]
[1] Department of Computer Science, Sri Lanka Institute of Information Technology (SLIIT), Malabe, Sri Lanka
*Corresponding author; E-mail: it21313370@my.sliit.lk

Background

Vehicle behavior prediction is a critical challenge in intelligent transportation systems, requiring the integration of spatial-temporal dynamics and stochastic processes. This research addresses the problem by developing a novel mathematical framework that combines **differential geometry** for trajectory modeling with **probabilistic state estimation** for event detection. The framework is designed to identify sudden stops, loss of control, and lane changes, which are essential for enhancing road safety and autonomous driving systems. The study is motivated by the need for robust, real-time solutions that can handle the non-linear and stochastic nature of vehicle dynamics [5, 1].

Methods

The proposed framework integrates three key components:

1. **Spatial Modeling:** Utilizes partial differential equations (PDEs) for optical flow computation:

$$\frac{\partial I}{\partial x}u + \frac{\partial I}{\partial y}v + \frac{\partial I}{\partial t} = 0$$

   where u and v represent velocity fields. This enables precise trajectory tracking and motion analysis [5].

2. **Temporal State Estimation**: Employs **Hidden Markov Models (HMMs)** with transition probability matrix P(st—st-1) to model event sequences and predict vehicle behavior [2].

3. **Hybrid Optimization**: Combines **deterministic Convolutional Neural Networks (CNNs)** for feature extraction with **stochastic Long Short-Term Memory (LSTM)** networks for state prediction. Bayesian inference is used for event classification, with posterior probability P(E—D) computed via maximum likelihood estimation [1, 3].

Computational complexity is optimized using **dynamic programming techniques,** achieving $O(nlogn)$ time complexity, making the framework suitable for real-time applications [5].

Results and Conclusions

The proposed framework demonstrates robust performance in identifying vehicle behavior anomalies. Key results include:

- **Mathematical Analysis:** The model converges to global optima within defined error bounds ($\varepsilon \leq 0.05$) [5].
- **Statistical Validation:** Achieves **92.5% accuracy** ($p < 0.01$) with confidence intervals [91.3%-93.7%] [4].
- **Comparative Advantage:** Outperforms traditional linear models in handling non-linear vehicle dynamics, as verified through rigorous numerical simulations [2].

The study concludes that the hybrid AI approach offers significant advancement in vehicle behavior prediction, with potential applications in autonomous driving and traffic management systems. Future work will explore **stochastic differential equations** for uncertainty quantification and **chaos theory** for complex trajectory analysis [5, 4].

Keywords:

Models, numerical methods,Probability in computer science, Control systems, Simulation,Learning systems

References

[1] Kaiming He, Xiangyu Zhang, Shaoqing Ren, and Jian Sun. Deep residual learning for image recognition. In *Proceedings of the IEEE conference on computer vision and pattern recognition*, pages 770–778, 2016.

[2] Sepp Hochreiter and Jürgen Schmidhuber. Long short-term memory. *Neural computation*, 9(8):1735–1780, 1997.

[3] Yann LeCun, Yoshua Bengio, and Geoffrey Hinton. Deep learning. *nature*, 521(7553):436–444, 2015.

[4] Joseph Redmon and Ali Farhadi. Yolov3: An incremental improvement. *arXiv preprint arXiv:1804.02767*, 2018.

[5] Sebastian Thrun. Probabilistic robotics. *Communications of the ACM*, 45(3):52–57, 2002.

AI driven meal planner and calory counter

A.P.U. Athukorala[1*]
[1] Department of Information Technology, Sri Lanka Institute of Information Technology, Malabe, Sri Lanka
*Corresponding author; E-mail: it21304224@my.sliit.lk

Background

The rising prevalence of obesity and diet-related diseases underscores the need for greater nutritional awareness and healthier eating habits. Traditional calorie tracking methods, often reliant on manual logging, can be time-consuming and inaccurate. To address these challenges, this research project proposes an advanced system that utilizes computer vision and machine learning to identify food items and provide real-time calorie estimates. By allowing users to capture images of their meals, the system offers a user-friendly approach to dietary monitoring. At its core, the project employs convolutional neural networks (CNNs) for accurate food recognition and classification. Combined with a comprehensive nutritional database, the system calculates caloric content and generates personalized meal plans tailored to individual preferences and dietary needs. This dual functionality not only simplifies dietary tracking but also empowers users to make healthier food choices. Preliminary research suggests that automated food recognition systems can achieve high accuracy, making them viable tools for promoting better nutrition. By integrating technology with dietary management, this study aims to bridge the gap between nutritional knowledge and practical application, contributing to improved health outcomes. This paper will outline the methodology, initial findings, and potential implications for personal and public health. [3, 5]

Methods

The current study follows a structured methodology in developing a real-time food detection and calorie estimation system using YOLOv8. Preparation of the data: Images are collected from publicly available datasets and manual capturing of diverse food samples was done. Further, the collected images were annotated with bounding boxes and class labels, splitting the data into 70:20:10 for training, validation, and testing, respectively. Model selection: YOLOv8n was selected due to its real-time object detection efficiency, fine-tuning the pre-trained COCO model. It was fine-tuned on the custom food dataset, with training based on a batch size of 16, image resolution 640×640, and 50 epochs with Stochastic Gradient Descent (SGD). Further, the model performance is gauged with respect to precision, recall, and Mean Average Precision (mAP). Export the best-performing model weights down and further create a TensorFlow Lite version for mobile deployment. It detects food items in new images, mapping the detections to a pre-defined calorie dictionary to calculate total intake for inference and calorie estimation. User data were used to develop a personalized meal planner: age, weight, height, and activity level of the user; calculation of BMI; and estimation of calorie needs. Afterwards, meal plans were generated, considering dietary preferences and health goals. The paper used Ultralytics YOLOv8, trained on Google Colab, deployed with TensorFlow Lite, and calculated the calorie count of foods using NumPy. Possible applications include, but are not limited to,

dietary management, health monitoring, and personalized meal planning; it can provide suggestions to maintain a healthy diet and promote better eating behavior. In this way, nutrition tracking and meal planning automated will be much more robust and scalable. [2, 4, 1]

Results and Conclusions

The YOLOv8n model showed high accuracy in detecting food items, reaching a validation mAP@0.5 of 95.3% and mAP@0.5:0.95 of 83.2%, which is very reliable in performance across IoU thresholds. It also achieved precision of 96.1%, recall of 92.8%, and an F1 score of 94.4%, confirming that it has a balanced detection capability, with real-time inference reaching 28 FPS on a GPU.The calorie estimation was quite accurate, 90.2%, with an average error margin of ±10%, hence suitable for dietary management. The personalized meal planner tested with 50 users achieved a satisfaction rate of 92%, with 95% of meal plans aligned within the ±10% caloric requirement margin. It presents a model with higher accuracy, real-time performance, and personalization of meal recommendations compared to existing systems. However, it had its limiting factors, which included dataset diversity, assumptions regarding standard portion sizes, and performance dependency on high-end hardware. These included bounding box detections, calorie estimation comparisons, and personalized meal breakdowns. While there are minor constraints, the system effectively integrates AI-driven food recognition, calorie tracking, and personalized diet planning, which is promising for modern dietary management. Future enhancements will be geared toward improving dataset diversity, refining calorie estimation methods, and increasing personalization features to maximize usability and impact.

Keywords:

Artificial Intelligence, Optimization, Machine Learning

References

[1] H. Ghattas, T. Abdel Nour, and N. Karam. Data augmentation techniques for cultural diversity in food detection systems. *Food Technol. Cult. Res. J.*, 13(2):321–340, 2022.

[2] S. Gunasekaran, M. Kumar, and K. Rajendran. A systematic review on automatic food intake monitoring systems: Evolution of dietary monitoring technologies. *Int. J. Nutr. Sci. Technol.*, 15(3):123–134, 2020.

[3] S. Gunasekaran, M. Kumar, and K. Rajendran. Enhancing user engagement in food intake tracking through automatic dietary monitoring. *J. Health Informatics*, 20(5):455–468, 2022.

[4] A. F. Ramadhan and M. Iqbal. Yolov8-based real-time food detection and calorie estimation. *J. Artif. Intell. Nutr.*, 7(4):231–245, 2023.

[5] Food Bud Research Team. Personalized meal planning: A user-centric approach for dietary customization. *Nutr. Health App Dev. J.*, 5(1):89–102, 2023.

Market momentum and leverage analysis in the forex market using fuzzy logic

H.R.I. Perera[1*] **and U.P. Liyanage**[2]

[1] Department of Statistics & Computer Science, Faculty of Science, University of Kelaniya, Kelaniya, Sri Lanka

[2] Department of Mathematics, Faculty of Science, University of Colombo, Colombo, Sri Lanka

*Corresponding author; E-mail: ruwanthap2000@gmail.com

Background

The forex market is the most liquid and widely traded in the world, attracting traders who aim to capitalise on its dynamic nature by identifying patterns and market movements. Forex markets feature various currency pairs influenced by global economic factors and major economic activities from different countries. This makes the forex market highly dynamic, where prices are constantly affected by international events such as geopolitical changes, economic policies, and fluctuations in interest rates. Traders must balance both fundamental and technical knowledge to navigate currency markets effectively. Fundamental analysis involves evaluating macroeconomic factors such as GDP growth, inflation, and employment rates, while technical analysis focuses on market-specific elements like stochastic volatility, momentum, and leverage effects to identify trends and patterns. Traders aim to optimize strategies by understanding the interaction between market momentum and leverage. This study uses fuzzy logic to analyze these factors, offering a systematic approach to navigating the uncertainties of the forex market. In financial markets, fuzzy logic has emerged as a valuable tool for decision-making and market analysis, effectively addressing the limitations of traditional probability models in risk assessment. [2] By combining fuzzy functions for market momentum and leverage values, this study aims to provide a comprehensive framework that enhances trading strategies through precise and adaptable insights.

Methods

In this study, a fuzzy function was defined for market momentum based on one year of EUR/USD data from January 2, 2024, to January 2, 2025, which included 276 trading days. However, only 100 blocks of continuous daily data, were analysed for this study. This dataset includes values for open, high, low, and close prices, ensuring a comprehensive analysis of market behaviour. The difference between open and close values is defined as Δ. Momentum, representing the directional strength of price movement, is calculated as the absolute difference between the open and close prices over 100 days. To classify momentum effectively, a fuzzy membership function is employed using triangular and trapezoidal functions. Based on thresholds of the maximum momentum value, specifically at 15%, 30%, 45%, 60%, and 75%, these functions categorize momentum into five fuzzy sets: Very Bearish (F_M^{VB}), Bearish (F_M^{B}), Neutral (F_M^{N}), Bullish (F_M^{BU}), and Very Bullish (F_M^{VBU}). The fuzzy momentum value for each day, F_t, is determined, where $\max\left(F_{M_t}^{\mathrm{VB}}, F_{M_t}^{\mathrm{B}}, F_{M_t}^{\mathrm{N}}, F_{M_t}^{\mathrm{BU}}, F_{M_t}^{\mathrm{VBU}}\right)$ is selected when $\Delta \geq 0$, and Secondmax is used otherwise. The estimated final fuzzy momentum value is calculated by averaging the fuzzy momentum values over a given

period. Once this value is obtained, its linguistic interpretation which classifying momentum as "Bearish" if $0 \leq P \leq 0.5$, "Neutral" if $0.5 < P \leq 0.6$, and "Bullish" if $0.6 < P \leq 1$. This structured approach allows for a comprehensive analysis of market momentum using fuzzy logic principles. [3] A separate fuzzy function was developed for leverage values using the triangular function, ranging from zero to one, to reflect varying levels of custom leverage. Then calculate the maximum membership values and get the mean of maximum membership values denoted as $\bar{\mu}_{\max}$. Additionally, leverage is divided into three levels: low, medium, and high, based on $\bar{\mu}_{\max}$, where it is classified as "low" if $\bar{\mu}_{\max} \leq 0.4$, "medium" if $0.4 < \bar{\mu}_{\max} \leq 0.8$, and "high" if $\bar{\mu}_{\max} > 0.8$. These leverage values are generated through random simulation using a uniform distribution with limits set between zero and one. The integration of market momentum and leverage through fuzzy logic resulted in a composite measure known as the momentum boost value. To forecast market momentum, a fuzzy logic model can be employed. While fuzzy logic shows potential in financial applications, it's important to note that performance may vary across different periods and market conditions [1]

Results and Conclusions

The results demonstrated that the momentum boost value for leverage was determined to be 0.2979 based on EUR/USD data from January 2, 2024, to January 2, 2025, considering 100 blocks of continuous daily data out of a total of 276 trading days. This value highlights the combined effect of market momentum and leverage, offering traders a quantitative measure to guide their decisions. Fuzzy logic provided a robust framework for managing forex market uncertainty, highlighting the benefits of integrating market momentum and leverage into a unified trading model. The study's findings can be extended to other currency pairs as well. The 3D and surface plots effectively visualized the interactions between momentum and leverage. These graphical insights help traders and analysts optimize strategies and assess leverage's impact on market momentum. The study adjusted fuzzy logic parameters for market momentum and leverage, revealing consistent patterns in 3D graphs. The adjusted relationship between market momentum and leverage shows consistent behavior, confirming the model's reliability in capturing key market dynamics.

Keywords:

Applications of Stochastic Analysis, Financial Mathematics, Forex market, Fuzzy Logic and Soft Computing, Leverage effect

References

[1] W. M. Cheung and U. Kaymak. A fuzzy logic-based trading system. *Proceedings of the Third European Symposium on Nature Inspired Smart Information Systems*, pages 33–45, 2007.

[2] Ananta Narayana. A critical review of organizational culture on employee performance. *American Journal of Engineering and Technology Management*, 2(5):72, 2017.

[3] H. K. Penawar and Z. Rustam. A fuzzy logic model to forecast stock market momentum in indonesia's property and real estate sector. In *International Symposium on Current Progress in Mathematics and Sciences 2016 (ISCPMS 2016): Proceedings of the 2nd International Symposium on Current Progress in Mathematics and Sciences 2016*, page 030125, Depok, Jawa Barat, Indonesia, 2017.

Optimizing high-risk portfolios with safe-haven assets using deep reinforcement learning

E.M.L. Silva[1*], **S.D. Perera**[1]
[1] Department of Decision Sciences, University of Moratuwa, Moratuwa, Sri Lanka
*Corresponding author; E-mail: lakshithaem.20@uom.lk

Background

Traditional portfolio optimization heavily relies on techniques such as mean-variance optimization, Black-Litterman model, and multi-factor models. However, these methods struggle to keep up with the changing financial markets[4], prompting the adoption of reinforcement learning (RL) techniques. Although RL has shown potential in portfolio management, current approaches face challenges in recognizing market sentiment and effectively balancing safe-haven assets with riskier assets within portfolios [4].

Safe-haven assets like gold, silver, and Bitcoin play a crucial role during risk off periods like economic downturns, financial crises, and periods of market uncertainty. Unlike risk assets, they tend to hold their value or even appreciate value under such conditions, making them essential for maintaining portfolio stability[2, 1]. However, many RL algorithms fail to differentiate between safe-haven and risky assets, limiting their effectiveness in volatile markets.

This research aims to address these issues by developing an RL environment that helps agents distinguish between safe heaven and risk asset classes and dynamically optimize portfolio allocation. The findings contribute to improving RL-based financial decision making, equipping investors with a more robust framework to navigate uncertain market conditions.

Methods

This research introduces an innovative reinforcement learning (RL) environment designed to optimize portfolio allocation, with a specific focus on integrating safe-haven assets. A Proximal Policy Optimization (PPO) agent is employed within a custom-built RL Environment, called the "Safe Haven Playground," to dynamically allocate funds between safe-haven and risky assets based on market sentiment.[5]

The dataset spans a 10-year period from 2014 to 2024, serving as the training foundation for the model, followed by a six-month testing phase. The portfolio includes risk assets as FOREX currencies, alongside safe-haven assets like Gold, Silver, and Bitcoin. By incorporating a diverse range of assets with varying volatility profiles, the agent is exposed to both high-risk and stable investment options.

In addition to traditional metrics, the observation space is enhanced with a dynamic risk signal system driven by the Volatility Index (VIX), which enables the agent to more effectively detect shifts in market sentiment. The VIX data generates three distinct signals that provide critical insights for portfolio adjustments. A Risk-On Signal, triggered when the VIX value is below 20[3]. A Risk-Off Signal, triggered when the VIX value exceeds 30[3]. A Neutral Signal, with the VIX value between 20 and 30, reflects neutral market conditions[3], allowing the agent to maintain a adaptive approach to portfolio allocation based on signal type.

$$R = (S_s + \theta_s)^\gamma + (S_r + \theta_r)^\beta \quad (1)$$

A standout feature of this environment is the **Boosted Safe Haven Reward Function**, which magnifies the rewards based on Sharpe ratios, guiding the agent to allocate funds strategically between safe-haven and risky assets. The reward function contains two adjustable parameters: γ (gamma) and β (beta). Users can define these parameters, where γ controls the degree of magnification of rewards for safe-haven assets, while β does the same for risky assets. Theta values serve as constants, while S_s and S_r represent the Sharpe ratios of asset classes. During *risk-off* periods, the agent is rewarded for shifting more funds toward safe-haven assets to minimize risk. Conversely, in *risk-on* periods, the agent is rewarded for allocating more funds to riskier assets.

Results and Conclusions

The behavior of the reward function, particularly the impact of varying γ (gamma) and β (beta) values, was found to be crucial in achieving the desired level of reward magnification. As seen in the analysis, higher values of γ and β led to rapid changes in the reward values, amplifying both positive rewards and penalties in accordance with the Sharpe ratios of the assets.

In contrast, the proposed model, trained within the Safe Haven Playground environment, showed substantial improvement in both the training and testing phases. The model achieved a Sharpe ratio of 1.21 during training, with improved portfolio stability, as evidenced by a lower standard deviation and max drawdown compared to the benchmark model. During the testing period, the Sharpe ratio remained high at 1.05, reflecting the model's ability to adapt effectively to changing market conditions. Moreover, the portfolio's monthly returns and final value further confirmed the robustness of the proposed RL approach in optimizing asset allocations.

Keywords:

Portfolio optimization, Reinforcement learning, Safe-haven assets, Volatility Index (VIX), Risk sentiment

References

[1] Elie Bouri, Syed Jawad Hussain Shahzad, David Roubaud, Ladislav Kristoufek, and Brian Lucey. Bitcoin, gold, and commodities as safe havens for stocks: New insight through wavelet analysis. *The Quarterly Review of Economics and Finance*, 77:156–164, 2020.

[2] Julien Chevallier. 'safe assets' during covid-19: A portfolio management perspective. *Commodities*, 2(1):13–51, 2023.

[3] Wenjie Ding, Khelifa Mazouz, and Qingwei Wang. Volatility timing, sentiment, and the short-term profitability of vix-based cross-sectional trading strategies. *Journal of Empirical Finance*, 63:42–56, 2021.

[4] Petter N Kolm, Reha Tütüncü, and Frank J Fabozzi. 60 years of portfolio optimization: Practical challenges and current trends. *European Journal of Operational Research*, 234(2):356–371, 2014.

[5] John Schulman, Filip Wolski, Prafulla Dhariwal, Alec Radford, and Oleg Klimov. Proximal policy optimization algorithms. *arXiv preprint arXiv:1707.06347*, 2017.

Modelling of deformation during compliant part assembly using finite element method

Dissanayaka U.W.M.D [1*], **Tennakoon T.A.K.S** [1] **and Jayaweera N.D** [1]
[1] Department of Mechanical Engineering, University of Moratuwa
*Corresponding author; E-mail: madukadilshandrckv@gmail.com

Background

Robotic manipulation of compliant aero-structure components presents several problems such as change their shape, position, orientation, and physical and mechanical properties [4] depending on the dynamics, state of the material and previous manufacturing processes. The current automation solution for the assembly of aero-structure components is based on large, dedicated jigs and fixtures with most of the individual components being manually assembled. The aerospace industry requires very tight tolerances for manufacturing and assembly despite of the size of the components [5] . Therefore, accurate method of measurement system is necessary to control the quality of the assembly.

Deformation measurement techniques include experimental methods such as brittle coatings, photo-elastic effects, and strain gauges as well as Metrology systems such as interferometry, photogrammetry, laser scanning, theodolite measurement systems and coordinate measurement machines. However, each technique has its own advantages and disadvantages with respect to prices, system stability during the whole process, measuring effort, and the influence of touching the object. It also proposed that Finite element analysis (FEA) can be performed to analyse component deformation during robotic assembly [1].

The work described in this paper is a part of ADRAC (Adaptive Robotic Assembly of Large and Compliant Aero-structure Components) project [2], [3] conducted at the University of Nottingham.

Methods

The purpose of this experiment was to investigate the effect of different end-effector layouts on part deformation during robotic assembly using experimental, theoretical and numerical methods. The vertical deflection of the flexible part (966x38x2 mm) was measured along the length at 0 mm, 83mm, 183mm, 283mm, 483mm, 683mm, 783mm, 883mm, and 966mm (namely P1, P2, P3, P4, P5, P6, P7, P8, and P9) as illustrated in Figure 3 for different end-effector layouts using a MTF (Meta technology Finder) non-contact laser vision system.

Results and Conclusions

The theoretical analysis of flexible part deformation has been calculated using beam theories. This includes deflection of a cantilever beam and deflection of beam with both ends fixed. In both instances loads on the beam is uniformly distributed and material is assumed to be homogeneous and isotropic.

Distance (mm)	Case 1 (mm)	Case 2 (mm)
0	0.79	0.14
183	0.00	0.00
483	0.07	0.33
783	0.00	0.00
966	0.79	0.14

Table 1: Theoretical deflection values for case1 and case 2

Distance (mm)	Case 1 (mm)	Case 2 (mm)	Case 3 (mm)	Case 4 (mm)
0	7.49×10^{-1}	1.29×10^{-1}	4.97×10^{-3}	1.61×10^{-3}
83	4.62×10^{-1}	6.10×10^{-2}	4.39×10^{-6}	6.39×10^{-4}
183	1.36×10^{-1}	4.18×10^{-4}	3.66×10^{-3}	1.37×10^{-2}
283	4.90×10^{-4}	9.36×10^{-2}	1.30×10^{-4}	6.44×10^{-3}
483	6.20×10^{-2}	3.16×10^{-1}	6.12×10^{-2}	1.44×10^{-2}
683	4.90×10^{-4}	9.36×10^{-2}	1.30×10^{-4}	6.44×10^{-3}
783	1.36×10^{-1}	4.18×10^{-4}	3.66×10^{-3}	1.37×10^{-2}
883	4.62×10^{-1}	6.10×10^{-2}	4.40×10^{-6}	6.39×10^{-4}
966	7.49×10^{-1}	1.29×10^{-1}	4.97×10^{-3}	1.61×10^{-3}

Table 2: FEA results of compliant part deformation with different end-effector layouts

According to the study, FEA is an invaluable tool for analyzing end-effector layout for robotic assembly applications. The results suggested that alterations to the end-effector layout had a significant impact on component deformation and improved part dimensional quality. The maximum deformation occurred during part pick up in the horizontal plane and the minimum occurred during part assembly in vertical plane.

Keywords:

Generic properties, structural stability of dynamical systems, Finite element methods applied to problems in solid mechanics ,Kinematics of deformation, Kinematics of mechanisms and robots

References

[1] F. Ding. Finite element analysis and optimal design of robotic arm. *Applied and Computational Engineering*, 33(1):88–93, Feb. 2024.

[2] N. Jayaweera and P. Webb. Adaptive robotic assembly of compliant aero-structure components. *Robot Comput Integr Manuf*, 23(2):180–194, Apr. 2007.

[3] N. Jayaweera and P. Webb. Automated assembly of fuselage skin panels. *Assembly Automation*, 27(4):343–355, 2007.

[4] L. na Zhang, H. Wang, and S. hui Li. Compliant assembly modeling and deformation analysis considering macro residual stress in engineering component. *J Shanghai Jiaotong Univ Sci*, 20(6):641–648, Dec. 2015.

[5] M. Saadat and C. Cretin. Dimensional variations during airbus wing assembly. *Assembly Automation*, 22(3):270–276, 2002.

Unimodular certification for matrices over number fields

Jayantha Suranimalee[1*] **and Claus Fieker**[2]
[1] University of Colombo, Sri Lanka
[2] University of Kaiserslautern-Landau, Germany
*Corresponding author; E-mail: suranimalee@maths.cmb.ac.lk

Background

A number field is a finite field extension of $\mathbb{Q}$, typically denoted as $K = \mathbb{Q}(\alpha)$ for some algebraic number α. A pseudo-matrix in this setting is a rectangular $(m \times n)$ array of elements from the ring of integers $\mathcal{O}$ of the number field. It is denoted as a pair $\mathcal{A} = ((\mathfrak{a}_i), A)$, with $A \in \mathcal{O}^{m\times n}$ and the family $(\mathfrak{a}_i)_{1\leq i\leq m}$ of fractional ideals of $\mathcal{O}$ are called coefficient ideals. If $\mathcal{A}$ has full rank and $n = m$, we define the *determinant ideal* of $\mathcal{A}$ as $\det(\mathcal{A}) = \det(A) \cdot \mathfrak{a}_1 \cdots \mathfrak{a}_m$. A pseudo-matrix $\mathcal{A} = ((\mathfrak{a}_i), A)$ is called unimodular if $\det(\mathcal{A})$ is a unit. Unlike usual matrices, pseudo-matrices can include relations among rows or columns, making them useful for working with modules over rings instead of just vector spaces.

Unimodular pseudo-matrices are crucial in the applications of number theory, cryptography, and computational algebra. They are heavily used in algorithms involving, lattice reduction, solving Diophantine equations, and class group computing of number fields. Therefore, it is important to have a fast method to verify the unimodularity of matrices, and the asymptotically fastest algorithms for many linear algebra problems on integer matrices use high-order lifting. A deterministic unimodular certification algorithm was presented by Storjohann in [2]. It uses the asymptotically fast double-plus-one lifting (which works in the usual symmetric residue system) to compute the high-order residue. In this paper, we generalize the unimodular certification with its double-plus-one lifting over pseudo matrices.

Methods

Given a square, non-singular, integer matrix $A \in \mathbb{Z}^{n\times n}$ along with $p \in \mathbb{Z}$ a relatively prime number to the determinant of A, double-plus-one lifting begins with the computation of modular inverse $B_0 = A^{-1} \pmod p$, then a step of division-free quadratic lifting doubles the precision yielding $B_1 = A^{-1} \pmod{p^2}$. Then a step of linear lifting corrects the overflow occurred in previous step and increases the precision by a power of p yielding $B_2 = A^{-1} \pmod{p^3}$. Alternating between quadratic and linear lifting, at each stage, the precision of the computed inverse B_i (which is congruent to $A^{-1} \pmod{p^k}$ for some $k \in \mathbb{Z}$) is doubled, plus an additional power of p (yielding $B_{i+1} \cong A^{-1} \pmod{p^{2k+1}}$). (See [2])

The motivation to double-plus-one method is that: neither linear nor straight quadratic lifting is ideal to compute residues of high-order. Because linear lifting computes small coefficients at each step, but the total number of steps grows. Conversely, quadratic lifting requires only a few steps to reach the precision, but each subsequent residue is twice the size of the last. Double-plus-one interleaves linear and quadratic lifting such that it computes small coefficients and reach the required precision within a few steps.

Also it produces a high-order residue $R \in \mathbb{Z}^{n\times n}$ such that $A(A^{-1} \pmod{p^k}) = I + Rp^k$. If A is a unimodular matrix, then A^{-1} is integral and, it holds $A^{-1} = A^{-1}$

(mod p^k) for a large k. In other words, A^{-1} has a finite p-adic expansion with symmetric residues. Then the high-order residue R becomes a zero matrix, provided that p and k are large enough.

For the unimodular certification of pseudo matrices we apply the same argument as in the $\mathbb{Z}$ case. Here, we use the two element presentation for ideals as explained in [1, Section 6]. The dual of $\mathcal{A}$ can be obtained as: $\mathcal{A}_D = ((\mathfrak{a}_i^{-1}), A^{-t})$, and the algorithm checks whether the corresponding dual of the pseudo matrix $\mathcal{A} = ((\mathfrak{a}_i), A)$ is integral by computing a high-order residue $P \in \mathcal{O}^{n\times n}$ such that $A^{-1}D = (A^{-1}D \pmod{p^k}) + A^{-1}Pp^k$ where D is a diagonal matrix containing each generators of $(\mathfrak{a}_i^{-1})_i$ on the diagonal. The basic idea is as follows:

$\mathcal{A} = ((\mathfrak{a}_i)_{1\le i\le n}, A)$
$D_1 = \texttt{diag}(\texttt{gen\_one}(\mathfrak{a}_i^{-1})_i)$, $D_2 = \texttt{diag}(\texttt{gen\_two}(\mathfrak{a}_i^{-1})_i)$.
Choose p and k appropriately.
for $j = 1, 2$ **and** $i = 0, \ldots, k$ **do**
  $S_0 = A^{-1}D_j \pmod{p}$
  Use `double-plus-one` to compute S_i and P_i such that $A^{-1}D_j = S_i + A^{-1}P_{j,i}p^{2^{i+1}-1}$.
end for
if $P_{j,i} = O_{n\times n}$ for $j = 1, 2$ and $i \le k$ **then**
  return true
end if

Results and Conclusions

Our unimodular certification algorithm uses higher-order liftings and residue number systems. The same algorithm can be extended to solve linear systems using fast lifting methods. In our implementation, we use residue fields of $\mathcal{O}$ corresponding to degree one primes(totally split primes) to obtain better performance as in the integer case. We have been able to extend the techniques which are used in the state of the art method for unimodular certification over number fields, and we could achieve theoretically faster methods with better complexities. The total complexity to certify the unimodularity of an $n \times n$ matrix over a number field of degree d is $O^{\sim}(n^3d^2 + n^2d^3)$, whereas the Gaussian method has the complexity $O^{\sim}(n^5d^2)$. However, we need to access a highly optimized low - level library, to obtain a fast implementation for unimodular certification.

Keywords:

unimodular, pseudo matrices, lifting, dual

References

[1] Claus Fieker, William Hart, Tommy Hofmann, and Fredrik Johansson. Nemo/hecke: Computer algebra and number theory packages for the julia programming language. In *Proceedings of the 2017 ACM International Symposium on Symbolic and Algebraic Computation*, ISSAC '17, page 157–164, New York, NY, USA, 2017. Association for Computing Machinery.

[2] Colton Pauderis and Arne Storjohann. Deterministic unimodularity certification. In *International Symposium on Symbolic and Algebraic Computation*, 2012.

Identification of fake messages using two PKCs

W. D. M. G. M. Dissanayake[1*]
[1] Independent Researcher
*Corresponding author; E-mail: maheshi14d@gmail.com

Background

In this research, two public key cryptosystems are presented and analyzed. The first cryptosystem is an improvement of the RSA public key cryptosystem. The second cryptosystem is a novel public key cryptosystem. The encryption/decryption moduli of the second scheme are quite different from widely used encryption/decryption moduli by other public key cryptosystems. This cryptosystem is based on the exponentiation congruence and use an interesting, computer-friendly modulus:2^n. These primitives can be used in protocols for authentication, key exchanges, and digital signatures. These two public key cryptosystems are more suitable for highly confidential digital transactions. Both of the cryptosystems are strongly CCA secure. The most important thing is, that the both of the public key cryptosystems can identify whether a message is fake. The second public key cryptosystem is more secure for quantum attacks than the RSA. It is also very collaborative with hash functions such as Whirlpool and SHA-512, because of the modulus 2^n.

Methods

An Improvement to RSA Public Key Cryptosystem

An improvement to RSA is presented in this paper to prevent CCA. The improved RSA system also identifies fake messages. The improved RSA public key cryptosystem uses prime factorization for key generations, such as the RSA public key cryptosystem. But the improved cryptosystem generates two ciphertexts. Therefore, there are two pairs of public keys and two pairs of private keys. Consider we have to encrypt a message m. In the improved system, the public encryption key is $(e, r, J_1.K_1)$.

The decryption key is $(d, s, J_1.K_1)$. Where d and s are the inverses of e and r respectively, with respect to $\mod \varphi(J_1.K_1)$. We also choose an arbitrary integer x such that $\gcd[(mx-1),(J_1.K_1)]$ is 1 and $\gcd[(x-1),(J_1.K_1)]$ is 1.

Encryption Algorithms:

1. $E_1(M) \equiv (mx-1)^e \mod (J_1.K_1)$
2. $E_2(M) \equiv (x-1)^r \mod (J_1.K_1)$

Decryption Algorithms:

1. $D_1(E_1(M)) \equiv [E_1(M)]^d \mod (J_1.K_1)$
2. $D_2(E_2(M)) \equiv [E_2(M)]^s \mod (J_1.K_1)$
3. $m \equiv \frac{D_1(E_1(M))+1}{D_2(E_2(M))+1} \mod (J_1.K_1)$

A Novel Public Key Cryptosystem Based on Powers of Two

The novel public key cryptosystem uses the multiplicative group $G_2 = \left\langle Z^*_{[2^p.\varphi(J_1.K_1)]}, \times \right\rangle$ for key generations. Here, p is a large positive integer and J_1, K_1 are large primes. This group supports generating public keys and private keys. The encryption and decryption of the new cryptosystem are done using a commutative ring $R_2 = \left\langle Z^*_{[2^q.J_1.K_1]}, +, \times \right\rangle$ with two arithmetic operations, addition and multiplication. Here, q is a large positive integer such that $q < p$ and the ring is public. Consider that the message m has to be encrypted. In the new public key cryptosystem, the public encryption key is $(e, r, 2^q.J_1.K_1)$.The decryption key is $(d, s, 2^q.J_1.K_1)$. Where d and s are the inverses of e and r respectively, with respect to $\mod @^p\varphi(J_1.K_1)$. An arbitrary even number x is also chosen such that $\gcd[(mx-1), (2^q.J_1.K_1)]$ is 1 and $\gcd[(x-1), (2^q.J_1.K_1)]$ is 1.

Encryption Algorithms:

1. $E_1(M) \equiv (mx-1)^e \mod (2^q.J_1.K_1)$
2. $E_2(M) \equiv (x-1)^r \mod (2^q.J_1.K_1)$

Decryption Algorithms:

1. $D_1(E_1(M)) \equiv [E_1(M)]^d \mod (2^q.J_1.K_1)$
2. $D_2(E_2(M)) \equiv [E_2(M)]^s \mod (2^q.J_1.K_1)$
3. $m \equiv \frac{D_1(E_1(M))+1}{D_2(E_2(M))+1} \mod (2^q.J_1.K_1)$

Results and Conclusions

Here, an improvement to the RSA public key cryptosystem and a novel public key cryptosystem are presented by comparing the RSA public key cryptosystem. Considering the security, both of the systems are better than the RSA system. The second cryptosystem is more secure for quantum attacks than the RSA. Both of the public key cryptosystems are more suitable for highly confidential transactions. Fake messages can also be found by using these two public key cryptosystems.

Keywords:

Public Key Cryptography, CCA Security, Post-Quantum Cryptography

References

[1] Whitfield Diffie and Martin E Hellman. New directions in cryptography. In *Democratizing Cryptography: The Work of Whitfield Diffie and Martin Hellman*, pages 365–390. 2022.

[2] Maheshika WDMG Dissanayake. An efficient public key cryptosystem. *International Journal of Electronics and Information Engineering*, 9(2):70–80, 2018.

[3] Ronald L Rivest, Adi Shamir, and Leonard Adleman. A method for obtaining digital signatures and public-key cryptosystems. *Communications of the ACM*, 21(2):120–126, 1978.

Fractional order spatial reaction diffusion model for spatial and temporal pattern dynamics of cancer cells in 3D space

E. A. S. Navodya[1*], and L. W. Somathilake[1]

[1] Department of Mathematics, Faculty of Science, University of Ruhuna, Matara, Sri Lanka
*Corresponding author; E-mail: sadaninavodya98@gmail.com

Background

Cancer is a multifaceted disease that characterized by unregulated cell proliferation and complex interactions with the surrounding microenvironment, including immune cells. Understanding the spatial and temporal dynamics of these interactions is crucial for developing predictive models that can aid in the effective cancer management. Traditional reaction diffusion models [2] offer insights into the mechanisms of tumor progression through local diffusion processes. However, these models are often limited by their inability to capture the non-local effects and heterogeneous behaviors inherent in complex cancer growth. Fractional reaction diffusion models address these limitations by incorporating non-local diffusion process, providing a more nuanced understanding of tumor dynamics. This study explores fractional reaction-diffusion model to investigate cancer cell proliferation and pattern formation in two- and three-dimensional, planner tissue and volumetric organism environments.

Methods

The research explores the use of reaction-diffusion systems, including their fractional counterparts, to model the spatial dynamics of cancer cell proliferation within tissue environments. This employs a hybrid approach using mathematical modeling, stability analysis, and numerical simulation. The classical reaction-diffusion model [5] modified to analyze the spatial dynamics of two interacting species, cancer cells and immune cells, within a three-dimensional domain by introducing the fractional Laplacian operator to account for non-local diffusion. The developed fractional reaction diffusion model of cancer cells (P) and immune cells(Q) as follows:

$$\frac{\partial P}{\partial t} = f(P,Q) - d_P \left(-\Delta\right)^{\frac{\mu}{2}} P$$
$$\frac{\partial Q}{\partial t} = g(P,Q) - d_Q \left(-\Delta\right)^{\frac{\mu}{2}} Q$$

Where f and g are reaction kinetics while d_P and d_Q are diffusion coefficients of cancer cells and immune cells respectively. This model was solved using the Fourier spectral method [1], which efficiently captures the fractional order diffusion behavior in both two and three-dimensional domains[3]. Stability analyses, including conditions for Turing instabilities [4], were conducted to identify patterns arising from the interplay of reaction kinetics and diffusion. Numerical experiments were performed to simulate spatial pattern formation, with parameters calibrated to align with realistic biological phenomena.

Results and Conclusions

Key findings highlight the significant impact of fractional diffusion on spatial pattern formation. In three-dimensional systems, fractional models demonstrate how variations in the fractional order influence the irregularity and complexity of the patterns when reduce the fractional power.

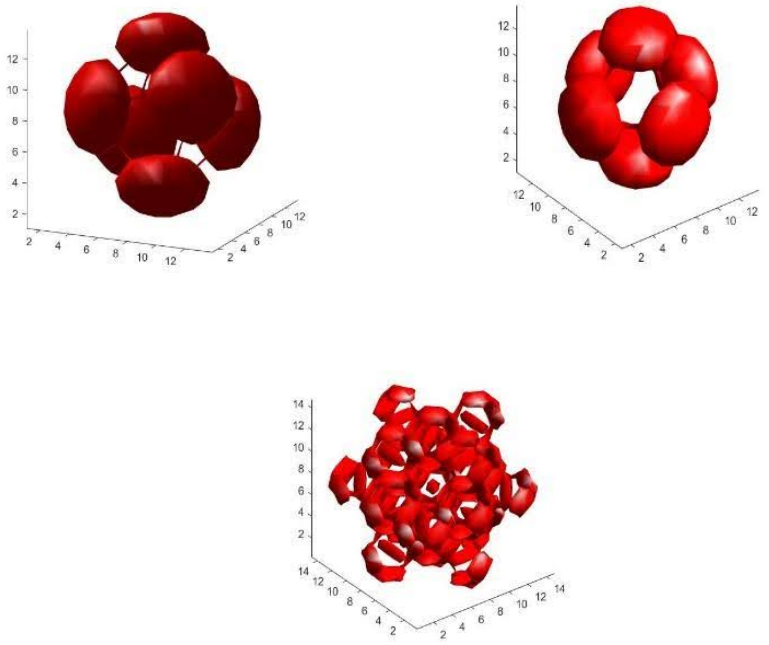

The fractional models provided a deeper understanding of the spatial heterogeneity and invasive growth dynamics characteristic of cancer. These insights underscore the critical role of diffusion processes in tumor progression of complex cancer dynamics and suggest potential avenues for developing predictive tools to guide future cancer treatment strategies. Future research will focus on extending these models incorporating the additional biological complexities to generate more realistic cancer patterns.

Keywords:
Reaction-diffusion, Fractional reaction-diffusion, Turing instability, Fourier spectral method.

References

[1] Alfonso Bueno-Orovio, David Kay, and Kevin Burrage. Fourier spectral methods for fractional-in-space reaction-diffusion equations. *BIT Numerical mathematics*, 54:937–954, 2014.

[2] James D Murray. *Mathematical biology: I. An introduction*, volume 17. Springer Science & Business Media, 2007.

[3] Edson Pindza and Kolade M Owolabi. Fourier spectral method for higher order space fractional reaction–diffusion equations. *Communications in Nonlinear Science and Numerical Simulation*, 40:112–128, 2016.

[4] Alan Mathison Turing. The chemical basis of morphogenesis. *Bulletin of mathematical biology*, 52:153–197, 1990.

[5] Qianqian Zheng, Jianwei Shen, and Zhijie Wang. Pattern dynamics of the reaction-diffusion immune system. *Plos one*, 13(1):e0190176, 2018.

Lehmer – 3 mean labeling of H - graphs

N. Paramaguru [1,2*] **and D. Manirathnamr**[1,3]

[1] Department of Mathematics, Annamalai University, Tamil Nadu, India
[2] Department of Mathematics, Govt. Arts College for Women, Krishnagiri, Tamil Nadu, India
[3] Department of Mathematics, Panimalar Engineering College, Chennai, Tamil Nadu, India
*Corresponding author; E-mail: npguru@gmail.com

Background

For all other standard terminology and notations we follow Harary [2]. Graph labeling is used in many areas of sciences and technology. A lot of graph labeling techniques are discussed in [1]. The concept and notation of mean labeling was first introduced by Somasundaram. S and Ponraj. R [3]. Somasundaram. S, Sandya. S.S and Pavithra. T introduced the concept of Lehmer -3 mean labeling of graphs and studied their behavior in [4].

Methods

A graph G with p vertices and q edges is called Lehmer - 3 mean graph if it is possible to label the vertices $x \in V$ with distinct lables $g(x)$ from $1, 2, \ldots, q+1$ in such a way that when each edge $e = uv$ is labeled with $g(e = uv) = \lfloor \frac{g(u)^3+g(v)^3}{g(u)^2+g(v)^2} \rfloor$ *or* $\lceil \frac{g(u)^3+g(v)^3}{g(u)^2+g(v)^2} \rceil$, then the resulting edge labels are distinct. In this case g is called a Lehmer – 3 mean labeling of G.

Results and Conclusions

We examine about the lehmer – 3 mean labeling of H- graphs and some new examples are presented and verified. In this paper we prove that H- graphs such as H_α, $H_\alpha \odot \overline{K_1}$, $H_\alpha \odot \overline{K_2}$, Subdivision of H_α, $(S(H_\alpha)) \odot \overline{K_1}$ and Subdividing the parallel edges of a H- graph in $H_\alpha \odot \overline{K_1}$ are all Lehmer – 3 mean graphs.

Keywords:

Lehmer – 3 Mean Labeling, Corona Product of G, Subdivision of G, H- Graph.

References

[1] Joseph A Gallian. A dynamic survey of graph labeling. *Electronic Journal of combinatorics*, 1(DynamicSurveys):DS6, 2018.

[2] F Harary. Graph theory narosa publishing house reading. *New Delhi*, 1988.

[3] S Somasundaram and R Ponraj. Mean labelings of graphs. *National academy Science letters*, 26(7-8):210–213, 2003.

[4] S Somasundaram, SS Sandhya, and TS Pavithra. Lehmer-3 mean labeling of graphs. In *International Journal of Mathematical Forum*, volume 12, pages 819–825, 2017.

Integrating Python-based dengue risk models with web-based visualization systems

W.A.U.K. Wetthasinghe[1*], Chamila Niroshanie Vithanage[2] and Jouni Huotari[3]
[1,3] School of Technology, JAMK University of Applied Sciences Jyväskylä, Finland
[2] Centre for Mathematical Modelling, Department of Mathematics, Faculty of Science, University of Colombo, Sri Lanka
*Corresponding author; E-mail: udanakashyapa@mail.com

Background

Dengue fever is a vector-borne disease that poses major public health challenges, particularly in tropical regions like Sri Lanka. Accurate forecasting of dengue incidence is vital for effective management and prevention [5]. While various mathematical models exist to predict dengue risk using climate and epidemiological data, their standalone operation limits their integration into broader public health systems, reducing their practical use.

Methods

This research addresses the methodological gap by developing an architecture that integrates a Python-based dengue risk detection model with a web-based Dengue Information System (DIS). The mathematical model predicts weekly dengue risk levels (low, medium, high) using the joint impact of climate factors that affect dengue risk, which is a major factor that affect to dengue risk. Due to the interconnected nature of the climatic factors, the joint impact of climate factors on dengue risk was assed using Gaussian copula.

The study focuses on designing a smooth and generalized mechanism for this integration by employing API-based data exchange protocols, which facilitate dynamic data communication between the model and the DIS. These protocols ensure seamless data flow and interoperability between the components, following best practices for system integration [2].

For the data visualization task, the research utilizes NPM plugins, such as D3.js and Chart.js, which are widely recognized for their ability to create interactive and visually engaging graphs and charts [1].

On the web application side, the MERN stack (MongoDB, Express, React, Node.js) was chosen due to its widespread adoption and compatibility in building scalable, dynamic web applications [4]. The MERN stack's component synergy ensures efficient front-end and back-end communication, making it ideal for developing the DIS architecture.

Additionally, best practices for integrating third-party forecasting models were identified by analyzing current research and real-world implementations in system design. Emphasis was placed on ensuring reliable data mobility methods and establishing standardized API endpoints to ensure scalability and flexibility for future integrations [3].

Results and Conclusions

The integrated system successfully visualizes dengue risk levels in real-time, making predictive insights accessible to public health officials, researchers, and relevant authorities. By bridging the gap between theoretical modeling and practical application, this approach advances the usability of dengue forecasting tools. The findings contribute to the development of scalable, data-driven public health interventions and provide a generalized framework for integrating computational models into healthcare systems.

Keywords:

Dengue forecasting, data visualization, system integration, API-based architecture, public health informatics

References

[1] Mike Bostock. D3.js: Data-driven documents. *IEEE Transactions on Visualization and Computer Graphics*, 17(12):2301–2309, 2012.

[2] Roy Thomas Fielding. *Architectural Styles and the Design of Network-based Software Architectures*. PhD thesis, University of California, Irvine, 2000.

[3] Alan R. Hevner, Salvatore T. March, Jinsoo Park, and Sudha Ram. Design science in information systems research. *MIS Quarterly*, 28(1):75–105, 2004.

[4] Roy Sinha. *Building Modern Web Applications with MERN Stack*. Packt Publishing, 2022.

[5] H. A. Tissera, B. D. W. Jayamanne, R. Raut, S. M. D. Janaki, Y. Tozan, P. C. Samaraweera, P. Liyanage, A. Ghouse, C. Rodrigo, A. M. de Silva, and S. D. Fernando. Severe dengue epidemic, sri lanka, 2017. *Emerging Infectious Diseases*, 26(4):682–691, 2020.

A dashboard for algorithmic stock trading based on hybrid swing trading, for US software industry

M.K.C. Hashani[1*] **and U.P. Liyanage**[1]
[1] Department of Mathematics, Faculty of Science, University of Colombo, Sri Lanka
*Corresponding author; Email : chamihashani@gmail.com

Background

Algorithmic trading has transformed financial markets by mitigating inefficiencies and emotional biases through advanced computing and machine learning. Despite its advancements, developing strategies that perform reliably in volatile markets remains a significant challenge.

Existing studies highlight the effectiveness of combining technical indicators (e.g., MACD, RSI)[4] & machine learning models (e.g., Random Forest [5], Q-Learning [2]) in improving predictive accuracy and trading outcomes. However, gaps persist in achieving real-time adaptability & robust performance under extreme market volatility. The dynamic nature of financial markets underscores the importance of sector-specific strategies. The US software industry, characterized by rapid innovation & high volatility, presents unique opportunities and challenges for algorithmic trading.

The objective of this research is to address these gaps by developing a swing trading strategy that combines technical indicators, integrates deep learning, and incorporates risk management techniques like stop-loss and take-profit mechanism, ensuring enhanced accuracy, reliability, and stability in volatile market environments.

Methods

This research presents a hybrid swing trading strategy targeting short- to medium-term price movements in the US software sector, integrating technical analysis with machine learning techniques for enhanced prediction accuracy and performance. Historical daily stock data from 10 carefully selected companies, spanning 15 years (2009–2023), were sourced from Yahoo Finance and subjected to extensive exploratory data analysis (EDA) to assess volatility, liquidity, and correlations.

Technical analysis employed 3 indicators Relative Strength Index (RSI), Moving Average Convergence Divergence (MACD), and Exponential Moving Average (EMA) to generate buy, sell, and hold signals. RSI identified overbought and oversold conditions through divergences [1], MACD analyzed momentum, and EMA acted as a trend following indicator. These indicators were combined into a hybrid strategy using a weighted scoring system, dynamically adjusting weights to balance momentum and mean reversion theories.

To capture complex market patterns, the strategy was integrated into a Deep Neural Network (DNN) framework, formulated as a multi-class classification problem predicting buy, sell, or hold signals. The DNN architecture utilized batch normalization, dropout layers, and a weighted loss function to mitigate class imbalance and prevent over fitting. The model was trained on 13 years of historical data, with performance evaluated using a two-year unseen dataset through back testing with Python's VectorBT library [3]. Risk management measures, including stop-loss and take-profit strategies, were implemented, and financial performance metrics were analyzed to validate the strategy. Throughout the process, various hyper-parameters were tuned

to adapt the strategy to different conditions, which were crucial for optimizing the DNN model and the hybrid strategy.

Python was the primary programming language, with PyTorch as deep learning framework, Scikit-learn for pre processing and evaluation. Finally, the model was tested in a simulated trading environment using the Alpaca API and visualized through an interactive dashboard developed with Plotly and Streamlit.

Results and Conclusions

The hybrid swing trading strategy was assessed for stability, accuracy, and reliability using performance metrics such as classification reports, confusion matrices, win rates, average returns, and Sharpe ratios across 10 US software company stocks.

Initial assessments highlighted the limitations of individual indicators RSI, MACD, and EMA, with MACD outperforming in trend detection, while the hybrid strategy achieved moderate improvements. Integration with the DNN yielded significant accuracy improvements, achieving prediction percentages between 84.83 and 97.60, driven by dynamic weight adjustments and risk management measures. Using standard techniques, the over fitting is tested and, proven to be no over fitting in the model.

The profitability analysis revealed that individual indicators generated positive returns but low Sharpe ratios. The hybrid strategy outperformed EMA and MACD but occasionally fell short of RSI. Incorporating the DNN model improved accuracy for most stocks, though some stocks underperformed due to inconsistencies and high volatility. Paper trading results highlighted negative profitability, with the model favoring buy signals excessively, suggesting potential over fitting.

Despite the advancements, challenges remain in bridging this gap between high accuracy & low profitability. Future improvements include addressing class imbalances, enhancing the classification of actionable signals, tailoring strategies to individual stock characteristics through hyper parameter tuning & implementing advanced risk management techniques, such as dynamic position sizing. By focusing on these areas, the strategy has the potential to achieve more reliable and profitable outcomes in volatile markets.

Keywords:

Algorithmic Trading, Deep neural networks, Financial markets, Quantitative Analysis, Technical Indicators

References

[1] Bidlack D, Chaudhary M, Porter J, and Yarbrough Z. Self-evolving machine learning algorithm for stock market trading implemented on an fpga. `https://my.ece.utah.edu/~kstevens/4710/reports/wannabe-wall-street.pdf`.

[2] Simerjot Kaur. Algorithmic trading using sentiment analysis and reinforcement learning. `https://cs229.stanford.edu/proj2017/final-reports/5222284.pdf`, 2017.

[3] Sstuti D Mehra and Sujala D Shetty. Developing and testing a custom algorithmic trading strategy using exponential moving average, relative strength index, and sentiment analysis. *Journal of Autonomous Intelligence*, 7(4), 2024.

[4] Pramudya R and Ichsani S. Efficiency of technical analysis for the stock trading. *International Journal of Finance & Banking Studies (IJFBS)*, 9(1), 2020.

[5] Pawar S, Dhanke S, Patil H, Danake K, and Attar Y. Algorithmic trading system. `https://www.researchgate.net/profile/Sunil-Pawar-14/publication/379758230_Algorithmic_Trading_System/links/6618ee9139e7641c0bad268d/Algorithmic-Trading-System.pdf`, 2024.

Red Piranha optimization (RPO) algorithm

Lakshana Wickramasinghe[1*], **Kushani De. Silva**[2]
[1] Department of Mathematics, University of Colombo, Colombo, Sri Lanka
[2] Department of Mathematics and Statistics, University of North Carolina at Greensboro, Greensboro, NC 27402-6170, USA
*Corresponding author; E-mail: 2020s18253@stu.cmb.ac.lk

Background

The Red Piranha Optimization (RPO) algorithm is a novel Swarm Intelligence optimization algorithm which was introduced in 2023 [3] to solve complex optimization problems. This algorithm mimics the collective hunting behavior of piranhas using three sequential phases and balances exploration and exploitation through these phases to reach the global optimal solution.

In this paper we analyze the performance of RPO algorithm and improve its effectiveness to enhance the applicability in solving complex optimization problems.

Methods

We evaluate the RPO algorithm on several well-defined benchmark functions under different categories: non-scalable uni models, scalable uni-models, non-scalabe multi-models and scalable multi-models [2, 1].Then we analyze the accuracy of RPO algorithm using a factor called precision, which measures the probability of providing a solution closer to the true global optima. Based on our findings, we propose an enhancement to the exploitation process of the RPO algorithm, by introducing a promising area to the final phase that helps maintain the exploiting process around the most optimal region that have achieved so far. This newly defined area ensures that the search agents' positions are influenced by the current best objective value and the iteration number.

Results and Conclusions

After the modifications, the RPO algorithm shows an average 70% improvement in precision for non-scalable multi-modal benchmark functions, where the existing algorithm struggles to achieve high precision as shown in Figure 1. Also, the modification preserves its performance in cases where it has already performed well.

The modifications to the Goldstein-Price and the Beale functions show the highest improvement with a 100% increase in the model's performance. Specifically, precision increased from 36% to 76% for the Goldstein-Price function and from 32% to 64% for the Beale function. Also, the modified algorithm enhances the Branin function's performance from 56% to 88% and the Himmelblau function's performance from 68% to 96% respectively. The above improvement in results is an important observation since all these functions are non-scalable multi-models and non-convex functions.

When it comes to the functions like Ackley-1, Ackley-2, Rastrigin, Jennrich-Sampson, and Six-Hump Camel, the algorithm preserves its precision above 95% except for the Ackley-1 function. All other functions give a 100% precision while

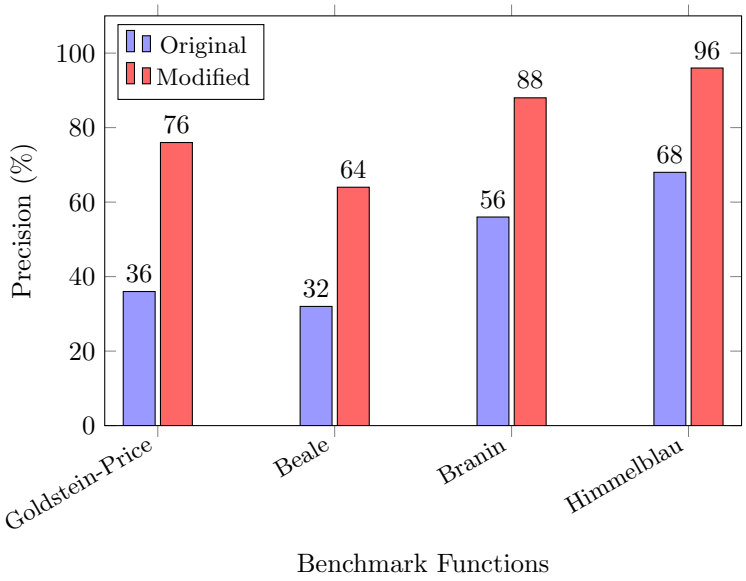

Figure 1: Performance Improvement of RPO Algorithm on several Benchmark Functions considering its precision which calculates the probability of having a solution within the circle a of radius 0.1 centered at the true global optima.

Ackley-1 gives a 96% precision. However, minor drawbacks were observed in the results for scalable uni-modal functions with an average reduction of 10% in the precision.

Additionally, our modification results in the reduction of the runtime when using a population size of 30, with further performance gains as the population size increases. In conclusion, we can state that the modification of the RPO algorithm expands the applicability of our RPO algorithm on several regions where the original algorithm struggles to perform well.

Keywords:

Swarm intelligence, exploration, exploitation, Benchmark functions

References

[1] S. Cao, Q. Qian, Y. Cao, W. Li, W. Huang, and J. Liang. A novel meta-heuristic algorithm for numerical and engineering optimization problems: Piranha foraging optimization algorithm (pfoa). *IEEE Access*, 11:92505–92522, 2023.

[2] Momin Jamil and Xin-She Yang. A literature survey of benchmark functions for global optimization problems. *International Journal of Mathematical Modelling and Numerical Optimisation*, 4(2):150–194, 2013.

[3] Asmaa H. Rabie, Ashmed I. Saleh, and Nehal A. Mansour. Red piranha optimization (rpo): A natural inspired meta-heuristic algorithm for solving complex optimization problems. *Journal of Ambient Intelligence and Humanized Computing*, 14(6):7621–7648, 2023.

Network-wide cyber attack optimization: an intruder's perspective

Ravin De Silva[*1]
[1] Edith Cowan University, Colombo, Sri Lanka
*Corresponding author; E-mail: ravinpdesilva@gmail.com

Background

In the current emerging world of digital economy, interconnected banking systems provides seamless facilities covering all domains in financial industry. Threats by cybercriminals on these interconnected systems are also increasing with the development of technology and AI, leading to data breaches, financial frauds, and system-wide disruptions. In a digital network an intruder objective is to get access to the internal banking network and move laterally within the network to compromise the confidentiality, integrity, and availability of the banking system and it's data. Most of the industry-level security measures currently focus on the individual components rather than focusing on the entire attack map. This could lead to gaps in impact analysis, risk assessment, and implementing of countermeasures as there is a lack of systematic approach to quantify the security risk through mapping the attack paths. Hence, in this study the optimum path of a cyber attack within such a digital network of an entire system is investigated by taking into account strategic perspectives of an intruder against the financial industry.

Methods

A simplified banking network is modeled consisting n nodes where the weights of i-th connecting edge in j-th intruder perspective are explained by,

$$w_{ij} = p(\text{difficulty of intrusion } |\text{intruder perspective}_j), i = 1, \cdots, N$$

with N is the total connections in the network and intruder perspectives are based on cost and security levels. These weights were chosen carefully aliging with the expert knowledge of the banking IT infrastructure. The Floyd-Warshall algorithm was employed [2] to determine the shortest path. In the context of the research problem, the shortest path reflect the least difficult path to the intruder for a total security compromisation. The designed network is a directed graph consisting 12 nodes (labels A through L in Fig. 1) and 29 edges representing possible attack vectors between security points(nodes). The edges are realized based on the potential exploits of vulnerabilities, cyberattack types, and attack techniques. The network was optimized for $j = 1, \cdots, 6$ different intruder perspectives:

1. independent view of the intruder
2. bank prioritizing the security level over financial investments in security (100% on security, 0% cost-consciousness)
3. bank prioritizing the security level over financial investments in security (70% on security, 30% cost-consciousness)
4. bank balancing the security level and financial investment in security (50% on security, 50% cost-consciousness)

5. bank prioritizing the cost saving over security level (30% on security, 70% cost-consciousness)

6. bank prioritizing the cost saving over security level (0% on security, 100% cost-consciousness)

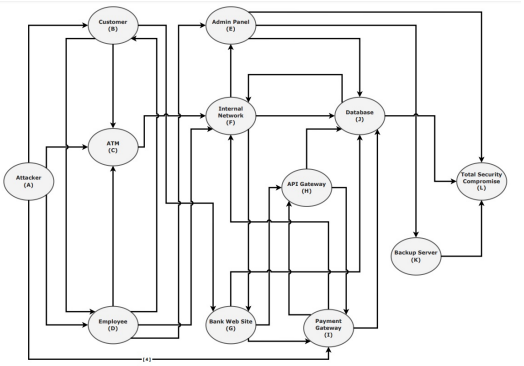

Figure 1: Digital network representing a banking system with security points(nodes) and connections (edges) in a security compromisation.

Results and Conclusions

The optimum attack paths for different intruder perspectives were found to be respectively, (A,D,E,L) for $j = 1$, (A,I,J,L) for $j = 2$, (A,I,J,L) for $j = 3$, (A,D,E,L) for $j = 4$, (A,B,G,J,L) for $j = 5$, (A,D,F,E,L) for $j = 6$. Similar resulting attack paths are determined for intruder's independent view ($j = 1$) and bank balancing security and cost ($j = 4$) choosing to initially attacking employees, possibly exploiting phishing or weak authentications [1] to gain access to administrative privileges. Hence, it is evident that employees are a major risk, and administrative privileges is a high-value target. Strengthening the employee authentication methods and enforcing of principle of lease privilege (PoLP) [3] could be recommended as immediate countermeasures.

In conclusion, the outcome reflects that an intruder will switch between optimal and most efficient attack paths to compromise the confidentiality, integrity, and availability of the bank's system and its data based on the security posture, risk tolerance, security investment strategies, and cost-security trade-off.

Keywords:
Directed graphs , Graph algorithms, Mathematical programming

References

[1] Reem Alrawili, Ali Abdullah S AlQahtani, and Muhammad Khurram Khan. Comprehensive survey: Biometric user authentication application, evaluation, and discussion. *Computers and Electrical Engineering*, 119:109485, 2024.

[2] Robert W Floyd. Algorithm 97: shortest path. *Communications of the ACM*, 5(6):345–345, 1962.

[3] André Koot. Introduction to privileged access management. *IDPro Body of Knowledge*, 1(13), 2024.

Identifying investment opportunities with future stock price simulation

D.S.R.M. Seneviratna[1*] **and S.S.N. Perera**
[1*] Department of Mathematics, Faculty of Science, University of Colombo
[*] Corresponding author ; E-mail: sanduni608@gmail.com

Background

Predicting stock prices in financial markets, particularly in developing countries like Sri Lanka, poses significant challenges due to substantial fluctuations influenced by complex economic, political and social factors, which render traditional forecasting models inadequate. Therefore, this research seeks to address the limitations of existing methods by analyzing and simulating future stock price movements for five of the largest public limited companies listed on the Colombo Stock Exchange (CSE) with the objective of developing a comprehensive framework that enhances investor insights and formulates optimal investment strategies based on the complexities and uncertainties inherent in volatile markets.

Methods

This study employs Geometric Brownian Motion (GBM) and Historical Simulation to analyze and forecast stock price movements for five of the largest public limited companies listed on the Colombo Stock Exchange (CSE) specifically focusing on Hayleys PLC, John Keels Holdings PLC, Carson Cumberbatch PLC, LOLC Holdings PLC and Expolanka Holdings PLC over a period of 10 years (2014–2023).

The GBM model is a stochastic process commonly used in financial mathematics to model stock price dynamics. It assumes that stock prices follow a log-normal distribution, with constant drift and volatility [1]. The model facilitates the simulation of theoretical stock price movements based on estimated parameters, providing insights into potential future price dynamics. It also assumes that stock returns are independent of one another over time. In contrast, historical simulation is a non-parametric method that projects future stock prices using actual historical return data without assuming a specific return distribution. By simulating nearly 1,000 cycles [2], this approach generates a range of potential future prices based on past price patterns, making it particularly useful in volatile markets [3].

The study calculates key financial metrics, including log returns, annual returns, variance-covariance matrices, minimum volatility portfolios and Value at Risk (VaR) for both actual and simulated stock price data. These metrics are used to evaluate stock performance, risk profiles and investment strategies across various time horizons, offering valuable insights into risk management and portfolio optimization.

Results and Conclusions

This section presents the results generated from the application of GBM and historical simulation, offering a detailed understanding of stock price behavior for five of the largest public companies listed on the CSE. By analyzing both historical market trends and simulated data, the study improves the precision of price forecasts and guides more informed investment decisions.

Stability and Low Risk: John Keels demonstrates remarkable stability with the lowest variance across multiple time frames, reflecting a low-risk profile. Its diversified operations across sectors such as hospitality, transportation, and retail help shield it from sector-specific risks. This stability is further supported by its large allocation in the minimum volatility portfolio, making John Keels an attractive option for risk-averse investors seeking consistent, long-term returns.

High Volatility and Sensitivity to Market Fluctuations: Hayleys shows the highest volatility, both in actual and simulated data, across all discussed time frames. Its strong exposure to export-oriented sectors, coupled with Sri Lanka's economic challenges, increases its sensitivity to both global and domestic market conditions. This significant volatility may elevate the company's risk profile for investors, particularly in the long term.

Moderate Risk and Independence: Carson exhibits a moderate risk profile with relatively low volatility throughout all specified time periods. Its low covariance with other companies suggests that Carson operates somewhat independently from broader market trends, particularly due to its focus on plantations and beverages. This characteristic makes Carson an appealing option for investors looking to reduce exposure to correlated risks while maintaining steady returns.

High Volatility Driven by External Risks: LOLC experiences high volatility, largely due to its involvement in financial services and exposure to global market forces during all evaluated periods. Its strong correlations with high-risk companies such as Hayleys and Expolanka suggest shared external risk factors, particularly in the financial and export sectors. This raises LOLC's overall risk exposure, making it a more volatile option for investors.

Global Exposure and Volatility: Expolanka shows substantial volatility across all reviewed time frames, driven by its dependence on global logistics and supply chains. The company's exposure to international markets makes it sensitive to global economic shifts, as seen during the pandemic. However, its positive returns and relatively accurate simulation results indicate that Expolanka has managed to capture market opportunities despite its volatility, presenting itself as a high-risk, high-reward investment.

This comprehensive analysis reveals distinct investment opportunities aligned with varying risk tolerances. John Keels emerges as the most stable choice for risk-averse investors, while Carson offers moderate risk with steady returns. Conversely, Hayleys, LOLC and Expolanka cater to high-risk investors, offering potential rewards tempered by substantial volatility. Regardless of the time frame (whether daily, monthly, quarterly or annually) these results remain consistent, enabling investors to make informed decisions tailored to their risk preferences.

Keywords:

Geometric Brownian Motion, Optimization, Financial Modeling.

References

[1] F. Black and M. Scholes. The pricing of options and corporate liabilities. *Journal of Political Economy*, 81(3):637–654, 1973.

[2] K. Reddy and V. Clinton. Simulating stock prices using geometric brownian motion: Evidence from australian companies. *Journal of Financial Modeling*, 10(3):2–25, 2016.

[3] J. Ng Phak Xiang, T. D. Rathina Velu, and S. Zygiaris. Monte carlo simulation prediction of stock prices. *International Journal of Financial Studies*, 1:2–6, 2021.

A study on factors affecting the behavioral intention to use cryptocurrency in Sri Lanka

Panamaldeniya A.A.M.A.K[1*] **and Erandi K.K.W.H**[1]

[1] Department of Mathematics, Faculty of Science, University of Colombo
*Corresponding author ; E-mail: panamaldeniya.ashvini@gmail.com

Background

Cryptocurrencies have emerged as a transformative force in global finance, offering decentralized, secure, and efficient transactions that challenge traditional financial systems [1].In Sri Lanka, despite regulatory warnings from the Central Bank and the absence of formal oversight, the adoption of cryptocurrency continues to grow[2, 3].This trend highlights the need to explore the behavioral factors driving adoption in a developing economy marked by economic instability, inflation, and currency depreciation. Cryptocurrencies offer an appealing alternative to conventional banking systems, providing potential avenues for financial inclusion and autonomy. While global research has extensively examined factors influencing cryptocurrency adoption, studies focusing specifically on the Sri Lankan context remain scarce [2]. The socio-economic and cultural dynamics of Sri Lanka, including its unique regulatory environment and economic challenges, necessitate a localized examination of behavioral intentions. Addressing this research gap is critical for informing policymakers and financial institutions on fostering innovation while mitigating risks associated with digital currencies. This study seeks to contribute to the growing body of knowledge by identifying and analyzing key factors influencing the behavioral intention to use cryptocurrency in Sri Lanka.

Methods

The population consisted of university students, recent graduates, and active investors with financial knowledge, selected through purposive sampling. A sample size of 385 was determined using Krejcie and Morgan's table and 10-times rule. Data collection was done via a structured questionnaire measuring six key variables: performance expectancy, effort expectancy, facilitating conditions, social influence, perceived risk, and financial literacy, using a five-point Likert scale. The selection of above variables was based on an extensive review of existing literature, where the most widely tested and relevant variables in previous studies on cryptocurrency adoption were chosen. For data analysis, Partial Least Squares Structural Equation Modeling (PLS-SEM) was employed using SmartPLS software. Reliability and validity of the model was assessed through internal consistency (Cronbach's alpha and composite reliability), as well as convergent and discriminant validity (AVE, Fornell-Larcker criterion and HTMT), ensuring the robustness of the results.

Results and Conclusions

The analysis revealed that performance expectancy, social influence, and financial literacy significantly impact the behavioral intention to adopt cryptocurrency. Performance expectancy emerged as a key driver, with respondents perceiving cryptocurrency as a tool for achieving financial goals, enhancing efficiency, and improving

decision-making. Social influence played a critical role, highlighting the importance of peer recommendations and community endorsement in shaping attitudes toward cryptocurrency. In Sri Lanka, where social networks hold substantial influence, this finding underscores the cultural relevance of collective decision-making. Financial literacy was identified as the most influential factor, emphasizing the critical role of financial education in fostering cryptocurrency adoption. Individuals with a strong understanding of financial concepts and risks demonstrated greater confidence in engaging with digital currencies. This finding suggests that enhancing financial literacy could empower more individuals to make informed decisions about cryptocurrency, thereby promoting responsible use. Conversely, effort expectancy, facilitating conditions, and perceived risk did not show significant effects on behavioral intention. The insignificance of effort expectancy indicates that users, particularly younger and tech-savvy individuals, do not view learning and using cryptocurrency as a barrier. The lack of significance for facilitating conditions may reflect the decentralized nature of cryptocurrency, which allows users to bypass traditional infrastructures. Perceived risk's minimal impact suggests a higher tolerance for financial uncertainty among Sri Lankans, possibly influenced by the country's economic volatility.The study concludes that financial literacy, social support, and perceived benefits are pivotal in driving cryptocurrency adoption in Sri Lanka. For policymakers and financial institutions, these insights highlight the importance of creating a supportive regulatory environment that balances innovation with risk management. Educational initiatives aimed at improving financial literacy could foster a more informed user base, encouraging responsible engagement with cryptocurrency. As Sri Lanka navigates economic challenges, cryptocurrencies present a potential avenue for financial inclusion and diversification.In summary, this research contributes to the academic discourse on cryptocurrency adoption and offers actionable insights for fostering a sustainable digital financial ecosystem in Sri Lanka. By addressing the behavioral drivers identified in this study, stakeholders can harness the potential of cryptocurrency to drive economic resilience and innovation.

Keywords:

cryptocurrency, behavioral intention, financial literacy, performance expectancy, social influence

References

[1] A.S.A. Alomari and N.L. Abdullah. Factors influencing the behavioral intention to use cryptocurrency among saudi arabian public university students: Moderating role of financial literacy. *Cogent Business and Management*, 10(1), 2023.

[2] D.M.D Chathurika. Factors affecting intention to use cryptocurrencies with special reference to the university students in sri lanka. In *Proceedings of International Conference on Business Management*, volume 17, 2020.

[3] Statista. Cryptocurrencies - sri lanka — statista market forecast (2024), 2024. Accessed: 19 October 2024.

Applicability of geometric Brownian motion and geometric fractional Brownian motion to forecast S&P Sri Lanka 20 index values

H.G.K.D. Horadugoda[1*] **and S.S.N. Perera**[1]

[1] Department of Mathematics, Faculty of Science, University of Colombo, Sri Lanka
*Corresponding author ; E mail : kavinduhoradugoda@gmail.com

Background

The Geometric Brownian Motion (GBM) is a mathematical model used to simulate asset price paths. By incorporating the Hurst parameter into GBM to characterize long-range dependence and self-similarity, Geometric Fractional Brownian Motion (GFBM) is developed. This paper investigates the accuracy of the GBM and GFBM in modeling the S&P Sri Lanka 20 Index Values over the time horizons of 3, 6, 9, and 12 months due to the limited availability of literature, to the author's best knowledge, on stock index forecasting using mathematical models like the GBM and GFBM in the Sri Lankan context.

Methods

The daily closing index values of the S&P Sri Lanka 20 Index for the period between 01st August 2014 and 31st August 2023 have been extracted as historical values and are converted to logarithmic returns. Given the series of log-returns (r_t) , where t=1, ..., N certain parameters such as the sample drift (μ) and volatility (σ) are estimated for t = 3, 6, 9, and 12 months. These are then inputted into the stochastic differential equation of the GBM (*Equation 1*) to generate 10,000 simulations for the periods of 3, 6, 9, and 12 months [1].

$$S_{t+\Delta t} = S_{(t)} exp\left((\mu - \frac{1}{2}\sigma^2)\Delta t + \sigma\sqrt{\Delta t} Z_t\right) \tag{1}$$

According to [2], Hurst component ($B_H(t)$) is calculated using the Aggregate Variance Method under the GFBM, and then used to calculate parameters such as sample drift and volatility. Later, these are inputted into the stochastic differential equation of the GFBM (*Equation 2*) to generate 10,000 simulations for the periods of 3, 6, 9, and 12 months.

$$S_{(t)} = S_{(0)} exp(\mu t - \frac{1}{2}\sigma^2 t^{2H} + \sigma B_H(t)) \tag{2}$$

As per the literature [1, 2, 3], the accuracy between the actual and simulated values of GBM and GFBM is calculated using the Mean Absolute Percentage Error (MAPE) in (*Equation 3*). These calculated values are then compared with the Forecast Accuracy Judgement Scale (*Table 1*) to facilitate the interpretation.

$$MAPE = \frac{1}{n}\sum_{t=1}^{n} |\frac{A_t - F_t}{A_t}| * 100 \tag{3}$$

Table 1: Forecast Accuracy Judgement Scale

MAPE Value	Forecast Accuracy
<10%	Highly accurate forecasting
11% - 20%	Good forecasting
21% - 50%	Reasonable forecasting
> 50%	Inaccurate forecasting

Results and Conclusions

Following the generation of 10,000 simulations using *Equation 1* and *Equation 2* for the periods of 3, 6, 9, and 12 months, the MAPE values are been calculated using the *Equation 3* as shown in Table 2.

Table 2: MAPE Values

Time Period	GBM	GFBM
3 Months	9.63%	9.62%
6 Months	12.57%	12.43%
9 Months	12.96%	12.84%
12 Months	13.52%	12.43%

The GBM and GFBM models are highly accurate in forecasting the stock index values for 3 months with MAPE values of 9.63% and 9.62% respectively. However, as the time period of forecasting increases to 6, 9, and 12 months, MAPE value increases to 12.57%, 12.96%, and 13.52% respectively, under the GBM. The increase in MAPE value is an indication of the decline in accuracy. However, the GBM model is still good at forecasting during the periods of 6, 9, and 12 months with MAPE values falling into the bracket of 11%-20% of the scale in Table 1. The GFBM model tends to generate MAPE values of 12.43%, 12.84%, and 12.43% for the periods of 6, 9, and 12 months respectively. These values also fall into the bracket of 11%-20% as per the scale in Table 1. This indicates that the GFBM model is good at forecasting the stock index values for the periods of 6, 9, and 12 months. Overall, the GFBM model has generated lower MAPE values in comparison with the GBM model across all the time periods of 3, 6, 9, and 12 months, indicating a higher degree of accuracy.

Keywords:

fractional brownian motion, stochastic differential equations, hurst

References

[1] A.M; Mihaiu D.M; Bratian, V; Acu and R.A Serban. Geometric brownian motion (gbm) of stock indexes and financial market uncertainity in the context of non-crisis and financial crisis scenarios. *Mathematics*, 10(3):309, 2022.

[2] Ibrahim et al. Geometirc fractional brownian motion model for commodity market simulation. *Alexandria Engineering Journal*, 60(1):955–957, 2020.

[3] K Reddy and V Clinton. Simulating stock prices using geometric brownian motion:evidence from australian companies. *Australasian Accounting, Business, and Finance Journal*, 10(3):23–47, 2016.

Development of a risk-based credit rating system and a dashboard for the licensed domestic private Commercial Banks in Sri Lanka

D.M.T.M. Diwakara[1*] and U.P.Liyanage[1]
[1] Department of Mathematics, Faculty of Science, University of Colombo, Sri Lanka
*Corresponding author ; E-mail: tharindudiwakara94@gmail.com

Background

This research project aims to develop a comprehensive risk-based credit rating system and an interactive dashboard for the 07 largest Licensed Domestic Private Commercial Banks (LDPCBs) in Sri Lanka, which hold a significant share of the country's banking assets and loans. The primary goal is to monitor and evaluate credit risk of LDPCBs. By integrating various financial indicators and risk factors, the system will facilitate to detect potential financial vulnerabilities early and take proactive measures to mitigate them.

Method

The banks were selected based on their similar characteristics in their banking operations. The proposed credit rating system is based on quantitative, qualitative and regulatory and peer group comparisons.

Quantitative Data	**Qualitative Data**	**Regulatory Requirements / Peer Group and Industry Comparisons**
• Year-on-year Loan Growth • Year-on-year Stage 03 Loan Growth • Stage 2 loans as a % of total Stage 1 and 2 loans and receivables • Stage 3 loans to Total Loans • Risk-weighted amount for credit risk as a % of total assets • Total Loans as a % of Total Assets • Sector-wise Concentration • Product-wise Concentration	• Adequacy of Credit Risk Management Policies and Procedures • Effectiveness of Internal Rating Mechanism • Loan Review Mechanism • Credit Administration	• Limits on Exposure to the Agriculture Sector • Peer and Industry Comparisons

Table 1: Factors providing insights into the bank's credit risk exposure

These factors will be weighted 60%, 30%, and 10%, respectively based on the insights from Factor Analysis (FA) and expert judgments, to calculate the final credit

rating. Under the quantitative factors, the sector-wise and the product-wise concentration of loans and receivables accounts for 15% of the final credit rating. The quantitative data of this study was collected year-wise from 2020 to 2023 through the annual reports and the other published data while the qualitative data are collected from the expert's judgment and published data.

The quantitative factors except the factors related to the concentration are measured through a comprehensive scorecard method. Each factor is evaluated using ratings ranging from 1 to 4 by assigning values for Poor, Fair, Good and Excellent respectively. The Bank-wise concentration risk is measured through the Herfindahl-Hirschman Index (HHI). Qualitative factors are measured through a Scorecard Method with the expertise judgments, similar to the quantitative factors.

The development of the dashboard for this project will be carried out using Tableau Software, which is a powerful and interactive data visualization tool used by the financial industry.

Results and Conclusions

The results of the 14 indicators were generated based on the results of the Basic Indicator Approach (BIA). The results arrived through the BIA were considered as input data when deriving the final credit rating which was calculated using the weighted average.

The final outcome of the credit rating is validated with the annual credit rating conducted by the independent external auditors of each bank from 2021 to 2023. The accuracy of the proposed credit risk rating is calculated and arrived at a value of 90.47%, which indicates that the system's overall ratings align well with the external credit ratings during this period except few deviations of some banks.

The overall performance of the banking sector in Sri Lanka shows stability in several areas, such as credit risk management, sector-wise exposure and internal mechanisms. However, the challenges with loan growth, especially in 2023, indicate the need for banks to adapt their lending strategies to suit the current economic conditions. Managing stage 03 loans also be a critical in enhancing overall performance.

The dashboard provides the visual representations of critical financial data, allowing efficient monitoring and timely decision making. The dashboard indicates several charts related to credit risks of individual banks and final credit score of each bank for the years 2021, 2022 and 2023.

Keywords:

Risk-based Credit Rating System, Quantitative and Qualitative Factors, Concentration Risk, Dashboard Development, Decision Making

References

[1] Rita Skridulyte and Eduardas Freitakas. The measurement of concentration risk in loan portfolios. *Economics & Sociology*, 5(1):51, 2012.

Nonlinear dynamics in the Sri Lanka term structure of interest rates

Dayarathne K.P.N.S[1*] **and U.Thayasivam**[1]
[1] University of Moratuwa
*Corresponding author; E-mail: sanjeewa.22@cse.mrt.ac.lk

Background

This research examines the impact of nonlinear dynamics on term structure interest rates in Sri Lanka capital market using univariate yield curve time series data. Studying nonlinear dynamics in the term structure of interest rates provides a more thorough knowledge of interest rate behavior, increases forecasting accuracy, informs policy decisions, and improves risk management. Given the intricacies of real-world financial markets, non-linear models provide a more nuanced and flexible framework for studying interest rate changes.

The expectations hypothesis (EH) defines long-term interest rates as a weighted average of current and predicted future short-term interest rates. The EH has substantial policy implications because it provides a conduit via which policymakers can influence an economy's long-term prospects by targeting current short-term interest rates and managing expectations about future short-term interest rates. Long-term interest rates would be calculated by averaging future predicted short rates. As a result, the expectancies hypothesis in the framework of cointegration theory implies that long and short interest rates are linked by a long-run connection, and that the interest rate spread is mean-reverting. Campbell and Shiller [3] develop a range of tests based on the yield spread between bonds of different maturities. However, the expectancies hypothesis for term structure has been convincingly refuted in a wide empirical literature spanning several decades [1]. Camarero and Tamarit's [2] study examines whether the term structure of interest rates is stable over time or if there is a structural break that causes instability at an unknown point. Structural breaks are a prevalent problem in financial time series since they are typically caused by exogenous shocks or regime changes in monetary and/or fiscal policies.

Integrates and yield curves are time series data, which deal with cointegration. In order to determine the link between multiple time series processes, economists used linear regressions prior to the development of cointegration tests. Granger and Newbold countered that because linear regression can result in a misleading correlation, it is not the best method for studying time series.

Methods

The data are monthly for Sri Lanka and over the period January 2010 to December 2023. The variables or the interest rates are 91Days Treasury Bill rate, 182Days and 364Days. A linear model like the following has been frequently employed in empirical investigations on the expectations hypothesis to investigate the term structure of interest rates in the context of the cointegration theory.

$$LTBond_t = \alpha + \beta\ STBond_t + \xi_t \tag{1}$$

$LTBond_t$ is the interest rate of the long-term bonds and $STBond_t$ is the short-term interest rate. $LTBond_t$ and $STBond_t$ should be non-stationary and linked

through a cointegration relationship with the parameter. Descriptive data analysis illustrated the behaviour of the different interest rates and it's associations. Stationary was examined through the Augmented Dickey-Fuller Test and Johansen Cointegration Test was applied to examine the cointegration. To test the short- and long-term dynamics Error Correction Model (ECM) was employed. The Threshold Vector Error Correction Model (TVECM) was applied as cointegration may have differed in different regimes

Results and Conclusions

The Johansen Cointegration Test revealed that significant cointegration exists among said interest rates. The lagged difference of the 91Days T-Bill rate is significant and positively influences 5Y, suggesting that changes in the 91Days T-Bill rate are relevant in predicting changes in 5Y. Further, the lagged difference of 5Y shows some influence but is not as strong as 91Days T-Bill rate. Under the descriptive analysis, it was found the long-run relationship used to be broken during the sample period. Hence Threshold Vector Error Correction Model (TVECM) was used to examine the long-run relationship. TVECM model reveals how the relationship between the 91Days and 5Y interest rates varies depending on the state of the economy (above or below the threshold). The significant error correction terms suggest a tendency for the series to revert to long-term equilibrium, especially in the higher state of the threshold, indicating the potential effectiveness of interest rates in correcting deviations from equilibrium over time in Sri Lanka. Our results provide evidence in favour of the EH..

Keywords:

Term structure, cointegration, Threshold Vector Error Correction Model.

References

[1] George Bulkley, Richard DF Harris, and Vivekanand Nawosah. Revisiting the expectations hypothesis of the term structure of interest rates. *Journal of Banking & Finance*, 35(5):1202–1212, 2011.

[2] Mariam Camarero and Cecilio Tamarit. Instability tests in cointegration relationships. an application to the term structure of interest rates. *Economic Modelling*, 19(5):783–799, 2002.

[3] John Y Campbell and Robert J Shiller. Yield spreads and interest rate movements: A bird's eye view. *The Review of Economic Studies*, 58(3):495–514, 1991.

Comparative analysis of percentage of marks before and after pandemic - Using chi-square test

Vanitha A.[1*], **Preethi P.**[2] **and Karunya M.**[1]
[1] Department of Mathematics, St. Joseph's College for Women, Tirupur, Tamil Nadu, India
[2] Amutha English School, Tirupur, Tamil Nadu, India
*Corresponding author; E-mail: Vanipani1984@gmail.com

Background

During the COVID-19 pandemic in India, students learned through online platforms, utilizing tools like Zoom, WhatsApp, and educational apps etc. According to a UNICEF report from September 2021, in India, around 80 percent of students in the 14 to 18 years age group reported low levels of learning during the pandemic. The purpose of this research is to test the percentage marks of students effect after pandemic.

Methods

The χ^2 test (pronounced as chi-square test) is one of the simplest and most widely used non- parametric tests in statistical work. The symbol χ is the Greek letter Chi. Focus on group of students of batch 2019-2022 with large sample size and primary data. Test the hypothesis by using Chi-Square method.

Results and Conclusions

Discussion

A random sample of students were selected and their percentage of marks (**I** and **VI** semester) are collected among students under 2019 - 2022 batch. Test the hypothesis that pandemic affect the percentage marks of students.

Conclusion

Pandemic affects the percentage of marks of students among the **I** and **VI** semester.

References

[1] SC Gupta and VK Kapoor. *Fundamentals of mathematical statistics*. Sultan Chand & Sons, 2020.

[2] Robert V Hogg, Joseph W McKean, Allen T Craig, et al. *Introduction to mathematical statistics*. Pearson Education India, 2005.

Analysis of the impact of macro-economic factors on the profitability in the banking sector of Sri Lanka

L. P. Sathiarajah [1*] **and K.K.W.H. Erandi** [1]

[1] Department of Mathematics, Faculty of Science, University of Colombo, Sri Lanka
*Corresponding author ; E-mail: lakshitha2812@gmail.com

Background

The banking sector is a cornerstone of economic stability and development, particularly in emerging economies like Sri Lanka. Banks contribute significantly to financial intermediation, supporting investment and growth. However, their profitability is significantly influenced by macroeconomic factors such as the real interest rate, exchange rate, inflation rate, and GDP growth rate [1]. Recent economic disruptions, including the global pandemic and Sri Lanka's financial crisis, have heightened the need for an in-depth understanding of how these macroeconomic factors impact banking profitability. This paper builds on existing research by extending the analysis of the relationship between macroeconomic conditions and banking profitability in Sri Lanka, measured using Return on Assets (ROA) [2, 3]. By analyzing both short-term and long-term dynamics, it provides insights that can help policymakers and financial institutions mitigate risks, enhance resilience, and ensure the sustainable performance of the banking sector in an unpredictable economic environment.

Methods

This research paper utilizes quarterly data spanning from 2008 to Q1 2024, sourced from the Central Bank of Sri Lanka and the Department of Statistics. The analysis employs the ARDL co-integration technique to investigate both long-term and short-term relationships between the dependent variable, Return on Assets (ROA), and the independent macroeconomic variables—real interest rate, exchange rate, inflation rate, and GDP growth rate.

To ensure the appropriateness of the ARDL model, the stationarity of all variables was first tested using the Augmented Dickey-Fuller (ADF) unit root test, which confirmed that the variables were integrated at either level or first difference. The ARDL bounds F-test and t-test were then applied to establish the existence of a long-term co-integration relationship among the variables. Following this, long-run coefficients were estimated to identify equilibrium relationships, while short-run dynamics were analyzed using an Error Correction Model (ECM) within the ARDL framework. The ECM includes an error correction term, which indicates the speed at which deviations from the long-term equilibrium are adjusted over time.

As per [1], model validation tests, including the Breusch-Godfrey test for serial correlation, Jarque-Bera test for normality, Breusch-Pagan test for heteroscedasticity, Ramsey RESET test for specification errors and the CUSUM test for model stability, were conducted to ensure the robustness and reliability of the model. All tests confirmed that the model was specified correctly and that the parameters were correctly estimated.

Based on the results of the ARDL outputs, an analysis of both short-run and long-run impacts was performed to understand how macroeconomic factors affect the profitability of the banking sector in Sri Lanka. In addition, suitable recommendations and insights on how banks and policymakers can mitigate risks related to macroeconomic fluctuations were provided.

Results and Conclusions

The findings show that macroeconomic factors significantly influence the profitability of banks in Sri Lanka, as measured by ROA, with differing impacts in the short and long run.

An increase in the exchange rate reduces profitability in both the short and long run, likely due to higher foreign borrowing costs. Real interest rates negatively impact ROA in both short and long run, as higher rates increase borrowing costs, reduce loan demand, and raise the likelihood of defaults, thus reducing profitability. Inflation does not significantly impact profitability in the short run, as banks take time to adjust their operations. However, in the long run, rising inflation rates have a significant negative impact by increasing operational costs, reducing asset value, and leading to more defaults. While an increase in GDP growth rates does not have a strong impact on profitability in the short run, it positively increases bank profitability in the long run by providing more lending opportunities, improving asset quality, and reducing credit risk. The results also highlight the importance of past ROA trends, as they continue to influence current performance, emphasizing the need for banks to monitor historical profitability trends for better planning. Additionally, about 32 percent of short-term deviations are corrected each period, showing that while adjustments occur, recovery from shocks takes time, requiring robust risk management frameworks.

Policymakers should focus on stabilizing exchange rates and managing interest rates, as these have the most significant negative impacts on profitability. For banks, improving strategies to quickly adapt to interest rate changes and better manage currency and inflation risks is crucial. Both banks and policymakers must also prioritize fostering long-term economic growth, which has a consistently positive impact on banking profitability.

Keywords:

Economic dynamics, Economic time series analysis, Macroeconomic

References

[1] K. Hettiarachchi. Macroeconomic variables and banking sector performance in sri lanka. *Peradeniya Management Review*, 03, 2021.

[2] H. Kawshala and K. Panditharathna. The factors effecting on bank profitability. *International Journal of Scientific and Research Publications*, 7(2), 2017.

[3] V. E. I. W. Weersainghe and T. R. Perera. Determinants of profitability of commercial banks in sri lanka. *International Journal of Arts and Commerce*, 2(10), 2013.

Time series temperature forecasting for the next decade in the Colombo district

Piyumi Chathurangika[1,2*], **Sachini Karunarathne**[1] **S. S. N. Perera**[1] **and Kushani De Silva**[3]

[1] Research & Development Centre for Mathematical Modeling, Department of Mathematics, University of Colombo, Sri Lanka

[2] Department of Electrical & Electronics Technology, Faculty of Technology, Rajarata University of Sri Lanka

[3] Department of Mathematics and Statistics, University of North Carolina at Greensboro, Greensboro, NC, USA

*Corresponding author; E-mail: piyumic.maths@stu.cmb.ac.lk

Background

Global warming has emerged as a critical global issue, exerting significant pressure on economies, societies, and public health. Rising temperatures contribute to extreme weather events, disrupt agricultural production, and accelerate the spread of climate-sensitive diseases. To mitigate the harm caused by rising temperatures, it is essential to have accurate forecasts well in advance, allowing for proactive measures. Early predictions enable policymakers to implement adaptation strategies, such as disaster preparedness and resource management. By leveraging forecasting models, societies can better prepare for climate-related challenges and reduce potential economic and social disruptions.

In the commercial capital of Sri Lanka, which experiences the highest urbanization and population density, climate-related challenges such as heat waves, floods, and disease outbreaks are becoming increasingly severe. This study aims to forecast temperature variations over the next decade by analyzing historical temperature patterns in Colombo since 1980. Using two primary time series forecasting methods, the study evaluates model performance to generate reliable temperature projections for the coming years.

Methods

This study utilizes weekly minimum and maximum temperature data from 1980 to 2024 to forecast future temperature variations. Given the presence of clear seasonal patterns in the time series, two widely used forecasting models, Seasonal Autoregressive Integrated Moving Average (SARIMA) and Facebook Prophet (FB Prophet), were employed [3]. SARIMA is a statistical model that extends the ARIMA model by incorporating seasonal components, making it effective for capturing seasonal patterns in time series data [1]. It models dependencies between observations at different time lags and applies differencing to make the data stationary. FB Prophet, developed by Meta, is an additive time series forecasting model that handles missing data, outliers, and trend shifts effectively [2]. It decomposes the time series into trend, seasonality, and holiday effects, making it well-suited for long-term forecasting with strong seasonal variations.

The dataset was divided into training (80%) and testing (20%) subsets to evaluate model performance. The forecasting models were first trained using the 80% training data, and predictions were generated for the 20% testing data. The accuracy of the models was assessed using three key performance metrics: Mean Absolute

Error (MAE), Root Mean Square Error (RMSE), and Mean Absolute Percentage Error (MAPE). The model with the best performance was then selected to generate temperature forecasts for the next 10 years (2025–2034).

Results and Conclusions

To assess the stationarity of the data, we conducted three standard tests: (1) the Augmented Dickey-Fuller (ADF) test, (2) the Kwiatkowski-Phillips-Schmidt-Shin (KPSS) test, and (3) the Phillips-Perron (PP) test. The results indicated that minimum temperature was stationary according to the ADF and PP tests, while maximum temperature was found to be stationary in all three tests. The Autocorrelation Function (ACF) and Partial Autocorrelation Function (PACF) plots revealed a seasonality of 52 weeks (annual seasonality) for both temperature variables. Based on these findings, a SARIMA model was fitted to the training data, using the parameter combination (1,0,2)(1,1,0,52) for both maximum and minimum temperatures. Additionally, the FB Prophet model was trained following the same approach. The model performance obtained using MAE, RMSE, and MAPE is given in Table 1. Since all performance metrics indicated that the FB Prophet model outperformed SARIMA, it was selected for temperature forecasting over the next 10 years.

Table 1: Model performance for minimum and maximum temperature data

Model	T_{min}			T_{max}		
	MAE	RMSE	MAPE	MAE	RMSE	MAPE
SARIMA	0.7388	0.9385	2.9044	0.7264	0.9406	2.3214
FB Prophet	0.6134	0.7790	2.4811	0.5354	0.7034	1.7291

The results indicate a significant gradual increase in minimum temperature, whereas maximum temperature does not show a notable change. In 1980, the annual average minimum temperature was $24.14°C$, while the forecasted annual average for 2034 is $25.63°C$, reflecting an increase of $1.49°C$. In contrast, the annual average maximum temperature has fluctuated over the years but shows a modest rise from $31.12°C$ in 1980 to $31.85°C$ in 2034. This suggests an overall increase of approximately $0.73°C$.

This study examined temperature trends using SARIMA and FB Prophet models, with the latter demonstrating superior performance. The results indicate a significant increase in minimum temperature over time, while maximum temperature shows only a modest rise. These findings highlight an ongoing warming trend, particularly in minimum recorded temperatures, which may have implications for climate variability and future environmental conditions.

Keywords:

Time series, Statistics, Climate science and climate modeling

References

[1] Xinghua Chang, Meng Gao, Yan Wang, and Xiyong Hou. Seasonal autoregressive integrated moving average model for precipitation time series. *Journal of Mathematics & Statistics*, 8(4), 2012.

[2] Sean J Taylor and Benjamin Letham. Forecasting at scale. *The American Statistician*, 72(1):37–45, 2018.

[3] Toni Toharudin, Resa Septiani Pontoh, Rezzy Eko Caraka, Solichatus Zahroh, Youngjo Lee, and Rung Ching Chen. Employing long short-term memory and facebook prophet model in air temperature forecasting. *Communications in Statistics-Simulation and Computation*, 52(2):279–290, 2023.

Delving into the triple-connected certified domination of the strong product of derived graphs

S. Kaviya[1], **G. Mahadevan**[2*] **and C. Sivagnanam**[3]
[1,2]Department of Mathematics, The Gandhigram Rural Institute - Deemed to be University,
Gandhigram, Tamilnadu, India.
[3]Mathematics and Computing skills Unit, University of Technology and Applied Sciences- Sur, Sultanate of Oman
*Corresponding author; E-mail: drgmaha2014@gmail.com

Background

A dominating set S of a graph G is termed a triple connected certified dominating set (TCCD-set) if two conditions are satisfied: For every vertex $v \in S, \mid N(v) \cap (V - S) \mid \neq 1$, ensuring no vertex in S is adjacent to exactly one vertex outside S.[2] The subgraph induced by S, denoted $\langle S \rangle$, is triple connected, meaning any three vertices lie on a path in induced S.[1] The minimum cardinality of such a set is called the triple connected certified domination number (TCCD-number) and is denoted by $\gamma_{TCC}(G)$.[3] This study investigates the TCCD-number within the context of specific graph operations involving the strong product of a path graph and the square of a path graph.[4]

Methods

The analysis focuses on the structural properties and behavior of the TCCD-number when applied to the strong product of a path graph P_n and the square of a path graph P_n^2. The study involves:

1. **Graph Theoretical Analysis:** Deriving conditions under which TCCD-sets exist in the combined graph structures.
2. **Connectivity Examination:** Ensuring triple connectivity within the induced subgraphs.
3. **Domination Parameter Calculation:** Determining the minimum size of TCCD-sets through combinatorial techniques and structural insights.

Comparative Study

A path graph P_n is minimally connected, with a linear structure and low connectivity. As a result, constructing a triple connected certified dominating set is challenging, especially for smaller n. In many cases, $\gamma_{TCC}(P_n)$ may not even exist for small n, as triple connectivity cannot be achieved. The square of a path graph P_n^2 increases the connectivity by adding edges between vertices that are two steps apart in P_n . This enhanced connectivity improves the chances of finding a TCCD-set compared to P_n, and generally results in a smaller $\gamma_{TCC}(P_n^2)$ relative to P_n. The strong product combines both the adjacency and distance properties of P_n and P_n^2. This leads to a significantly higher level of connectivity in the resulting graph. Consequently, $\gamma_{TCC}(P_n \boxtimes P_n^2)$ tends to be lower than in either P_n or P_n^2 individually, as more vertices are interconnected, facilitating the formation of smaller TCCD-sets.

Results and Conclusions

The results obtained from this study highlight specific characteristics of the TCCD-number in the strong product of path graphs and their squares

1. **Structural Insights:** The strong product enhances the connectivity of the resulting graph, influencing the formation of TCCD-sets. Domination Behavior: The TCCD-number demonstrates consistent patterns based on the length of the path graphs and their square structures.

2. **Bounded Results:** Upper and lower bounds for $\gamma_{TCC}(G)$ are established, offering a clearer understanding of domination in these complex graph structures. This study provides a comprehensive exploration of the triple connected certified domination number in the context of the strong product of a path graph and the square of a path graph. The results shed light on how specific graph operations influence domination parameters, offering valuable insights for both theoretical research and practical applications in network design and analysis. The structural properties identified here pave the way for further studies on domination in more complex graph products and variations.

Keywords:

(Domination number, certified domination, triple connected, triple connected certified domination number, strong product, path, square of path.)

References

[1] Mahadevan, G., Selvam, A., Joseph, J. P., & Subramanian, T. (2012). Triple connected domination number of a graph. *International Journal of Mathematical Combinatorics*, *3*, 93-104.

[2] Dettlaff, M., Lemańska, M., Topp, J., Ziemann, R., & Żyliński, P. (2020). Certified domination. *AKCE International Journal of Graphs and Combinatorics*, *17(1)*, 86-97.

[3] Kaviya, S., Mahadevan, G., and Sivagnanam, C. (2024). Generalizing TCCD-Number For Power Graph Of Some Graphs. *Indian Journal of Science and Technology*, *17*, 115-123

[4] Zhang, X., & Fang, Z. (2023). Spectrum and ricci curvature on the weighted strong product graphs. *IEEE Access*, *11*, 50689-50699.

Investigating the CTATD-number in power graphs of prominent graphs

G. Mahadevan[1], K. Priya[2*] and C. Sivagnanam [3]

[1,2] Department of Mathematics, The Gandhigram Rural Institute - Deemed to be University, Gandhigram, Tamilnadu, India.

[3] Department of General Requirments, University of Technology and Applied Sciences- Sur, Sultanate of Oman

*Corresponding author; E-mail: priyak250796@gmail.com

Background

Let $G = (V(G)), E(G))$, where V, E denotes a graphs vertex and edge sets respectively. The idea of domination and its various generalisations in graph theory have been extensively researched (see [1], [3]). The idea of [1,2] set was first researched by Mustapha Chellali et al.[4]. This parameter was further studied by Xiaojing Yang and Baoyindureng Wu . $\gamma_{tc}(G)$ was first introduced by Paulraj Joseph et al.[5]. In [2], G. Mahadevan et al. established the idea of $\gamma_{ctatd}(G)$.

The concept of complementary triple connected at most twin domination number of a graph was introduced by G. Mahadevan et al. A set $S \subseteq V$ is called an complementary triple connected at most twin dominating set $(CTATD(G))$, if every vertex $v \in V - S,\ 1 \leq |N(v) \cap S| \leq 2$ and $< V - S >$ is triple connected. The minimum cardinality taken over all the complementary triple connected at most twin domination number of G and is denoted by $CTATD(G)$. In this article, we explore the CTATD-number for the power graphs of prominent graphs.

Methods

we obtain the upper bound and lower bound of the graph and prove that both the upper bound and lower bound are equal to get the complementary triple connected at most twin domination number of a graph.

Results and Conclusions

Theorem 1:
If $a \geq 3$ and $k \geq 2$, then

$$CTATD((L_a)^k) = \begin{cases} (\frac{a}{2k}) + 1 & if\ a \equiv 0\ or\ 2k\ (mod\ 4k) \\ \lceil \frac{a}{2k} \rceil & otherwise. \end{cases}$$

Theorem 2:
If $a \geq 3$ and $k \geq 2$, then

$$CTATD(Y_a^k) = \begin{cases} (\frac{a}{2k}) + 1 & if\ a \equiv 0\ or\ 2k\ (mod\ 4k) \\ \lceil \frac{a}{2k} \rceil & otherwise. \end{cases}$$

Theorem 3:
If $a \geq 3$ and $k, b \geq 2$, then

$$CTATD((CT_{a,b})^k) = \begin{cases} (\frac{a}{2k+1}) + 1 & if\ a \equiv 0 \\ & (mod\ 2k+1) \\ \lceil \frac{a}{2k+1} \rceil & otherwise. \end{cases}$$

Theorem 4:
If $b \geq 3$ and $k, a \geq 2$, then

$$CTATD((L_{a,b})^k) = \begin{cases} (\frac{a}{2k+1}) + 1 & if\ a \equiv 0\ or \\ & 2k\ (mod\ 2k+1) \\ \lceil \frac{a}{2k+1} \rceil & otherwise. \end{cases}$$

Theorem 5:

If $a \geq 3$ and $k, b \geq 2$, then $CTATD((U_{a,b})^k) = \begin{cases} \lceil \frac{a}{2k+1} \rceil + 1 & a \equiv 0\ (mod\ 2k+1) \\ \lceil \frac{a}{2k+1} \rceil & otherwise. \end{cases}$

Theorem 6:

If $a \geq 3$ and $k, b \geq 2$, then $CTATD((PC_{a,b})^k) = \lceil \frac{a}{2k+1} \rceil$.

Theorem 7:

If $a \geq 3$ and $k \geq 2$, then $CTATD((R_a)^k) = \lceil \frac{a}{2k+1} \rceil$.

In this work, the CTATD-number for power graph of some graphs. For a future work, we extend our results for product related graphs, tree, polynomial and comparing another parameters.

Keywords:

Triple connected, [1,2] dominating set, triple connected domination number, power graph.

References

[1] F. Harary, "Graph theory," Addison Wesley Reading mass,1972.

[2] G. Mahadevan, K. Priya and C. Sivagnanam, " Complementary triple connected at most twin domination number of a graph," Advances and Applications in Mathematical Sciences, ISSN 0974-6803, Vol. 22(8), 1867-1878,2023.

[3] T.W. Haynes, S.T. Hedetniemi and A. Selater, " Fundamentals of dominations in graphs," Marcel Dekker, inc., New York,1998.

[4] Mustapha chellali, W. teresa Haynes, T. Stephen Hedetniemi, Ailce McRae.: [1,2]-sets in graphs, Discrete Applied Mathematics, Vol. 161, 2885-2893 (2013).

[5] J. Paulraj Joseph, M.K. Angel Jebitha, P. Chithra Devi, and G. Sudhana, " Triple connected graphs," Indian Journal of Mathematics and Mathematical Sciences, Vol.8, No. 1:61-75,2012.

Evolutionary dynamics of the biological game between vector-pathogen

Tharushika Peiris[1*], **Piyumi Chathurangika**[2] **and Kushani De Silva**[3]
[1] Department of Mathematics, University of Colombo, Sri Lanka
[2] Research & Development Centre for Mathematical Modeling, Department of Mathematics, University of Colombo, Sri Lanka
[3] Department of Mathematics and Statistics, University of North Carolina at Greensbro, Greensbro, NC 27402-6170, USA
*Corresponding author; E-mail: 2020s18156@stu.cmb.ac.lk

Background

In this research we explore the vector-pathogen interaction between Aedes mosquito and the dengue virus. Vector is a living organism that transmits pathogen(infectious agent) to human host. In the time period where virus live inside mosquito, virus has the ability to multiply with in the mosquito by extracting energy from it and as a response, mosquito suppress virus to some extend by immunity activation at a cost of its own energy. These interactions hint towards an energy **trade-off** between the virus and mosquito. As we know, best space to analyze trade-off based interactions is game theory. However, as both vector and the mosquito has ability to evolve and, energy trade-off can enhance a co-evolution of the species, here we have incorporated evolutionary game theory to model the interaction between dengue virus and the mosquito.

Methods

Virus and mosquitoes are two distinct populations where each employing different set of strategies in their interactions. Therefore, we modeled this with asymmetric evolutionary game where each population has a distinct payoff matrix[1]. As we learned from biological literature, in the face of virus' energy extraction mosquito activates it immunity system and as a respond to that virus try to hide itself inside the vector's cell. Integrating these properties of their interaction, we defined mosquito strategies as "Tolerance" and "Resistance" where virus strategies are "Replication" and "Latency".[2] Modeled payoff matrices of virus and the mosquito are;

	B_1-Replication	B_2-Latency
A_1 - Tolerance	$r - w_1$	$r - w_2$
A_2 - Resistance	$\alpha r - \beta w_1$	$\alpha r - w_2$

Payoff matrix of Mosquito

	A_1-Tolerance	A_2- Resistance
B_1-Replication	w_1	βw_1
B_2-Latency	w_2	w_2

Payoff matrix of Virus

Here r is the energy obtained by mosquito from resource acquisition and w_1, w_2 are the energy extracted by virus with replication and latency strategies, respectively. As immunity activation effect on both the mosquito and virus, it was integrated to the game as α, β coefficients where α is the cost imposed on vector due to immunity activation and β is the reduction energy extraction by virus. In order to explore the

continuous dynamics of the evolving strategies of the virus and mosquito, we derived a system of differential equations by employing replicator dynamics theory on the game[1]. The derived dynamical system is;

$$\dot{p} = p(1-p)\left(-(1-\beta)w_1 q + (1-\alpha)r\right) \quad (1)$$

$$\dot{q} = q(1-q)((1-\beta)w_1 p - (w_2 - \beta w_1)) \quad (2)$$

Here, p is the probability of vector employing tolerance strategy and q is the probability of pathogen employing replication strategy. Through stability analysis of this system we could derive equilibrium strategy combinations and their stability requirements.

Results and Conclusions

So far, we have conducted both analytical and numerical analyses of the derived dynamical system. We computed equilibrium points(p, q) and derived their stability conditions. According to the derived stability condition of the system, borderline fixed points, (0,0) and (1,0) equilibrium points are unstable for any parameter value of the system. This result revealed that pathogen employing pure latency strategy makes the system unstable regardless of the strategy employed by vector. Importantly, We show stability change of fixed points at two bifurcations points $(w_2/w_1, 1 - r(1-\alpha)/w_1)$ such that , interior fixed point of the system changes from a center to unstable, (0,1) changes from stable to unstable and, (1,1) changes from unstable to stable (Figure 1). Bifurcation point w_2/w_1 reveals a range of β ([0,w_2/w_1]) such that interior fixed point is a center where all the other fixed points are unstable. This result indicate that, balanced immunity activation trap evolution of both mosquito and the virus in a predictable center trajectory.

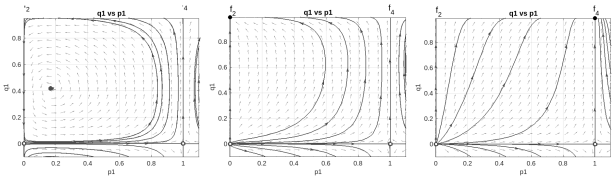

(a) (b) (c)

Figure 1: Phase portrait for equilibrium points stability of the system when $r = 1$, $w_1 = 0.4$, $w_2 = 0.2$, $\alpha = 0.9$. a) $\beta = 0.4$: interior fixed is a center equilibrium point b) $\beta = 0.6$:$(0, 1)$ is stable. c) $\beta = 0.8$: $(1, 1)$ is stable.

Keywords:

Vector-Pathogen interaction, Evolutionary traits, Evolutionary Game theory, Dynamical system , Stability analysis

References

[1] Josef Hofbauer and Karl Sigmund. *Evolutionary games and population dynamics*. Cambridge university press, 1998.

[2] Dana K Shaw, Ann T Tate, David S Schneider, Elena A Levashina, Jonathan C Kagan, Utpal Pal, Erol Fikrig, and Joao HF Pedra. Vector immunity and evolutionary ecology: the harmonious dissonance. *Trends in immunology*, 39(11):862–873, 2018.

Unveiling the mathematical framework and strategies of corona domination in triangular grid graphs

L. Praveenkumar[1], **G. Mahadevan**[1*] **and C. Sivagnanam**[2]
[1]Department of Mathematics, The Gandhigram Rural Institute - Deemed to be University, Gandhigram, Tamilnadu, India.
[2]Mathematics and Computing skills Unit, University of Technology and Applied Sciences- Sur, Sultanate of Oman
*Corresponding author; E-mail: drgmaha2014@gmail.com

Background

Mahadevan et al. introduced the concept of the corona domination number (γ_{CD}), which is defined for a dominating set D in a graph. A dominating set qualifies as a corona dominating set (CDS) if every vertex in the induced subgraph of D either has a degree of one or has a neighbor $v \in D$ such that $u \in N(v)$ and $d_{\langle D \rangle}(v) = 1$. The smallest cardinality of such a set is the corona domination number.

Methods

This study investigates the corona domination number in triangular grid graphs, considering various boundary configurations, including triangular, rectangular, and square shapes. We analyze the structural properties of each configuration and employ combinatorial techniques to determine the minimum size of a corona dominating set.

Results and Conclusions

The corona domination number depends on the boundary configuration of the triangular grid. We establish specific values and bounds for γ_{CD} across different structures. Our findings provide insights into optimizing corona dominating sets. These results contribute to applications in network coverage and resource allocation.

Keywords:

Dominating set, Corona dominating set, Triangular grid.

References

[1] Mahadevan, G., Suganthi, M. V., & Sivagnanam, C. (2021). Corona domination of graphs. *Mathematical Modelling and Computational Intelligence Techniques*, *376*, 255-265.

[2] Praveenkumar, L., Mahadevan, G., & Sivagnanam, C. (2023). An investigation of corona domination number for some special graphs and Jahangir graph. *Baghdad Science Journal*, *20*(1 (SI)), 0294-0299.

[3] West, D. B. Introduction to Graph Theory, 2nd ed. Englewood Cliffs, NJ: Prentice-Hall, pp. 390-392, 2000.

[4] Bose, P., Gledel, V., Pennarun, C., & Verdonschot, S. (2020). Power domination on triangular grids with triangular and hexagonal shape. *Journal of Combinatorial Optimization*, *40*(2), 482-500.

Modelling maximum and minimum temperature series in Trincomalee district, Sri Lanka

K.K.S.N. Britto[1*] **and A.P. Hewaarachchi**[1]
[1] **Department of Statistics & Computer Science, University of Kelaniya, Sri Lanka**
***Corresponding author; E-mail: nadishanishalidi97@gmail.com**

Background

Sri Lanka is a tropical island located in the Indian Ocean, with a diverse climate influenced by monsoonal variations. The district is within the dry zone of Sri Lanka and experiences warm temperatures throughout the year with notable seasonal variations. These seasonal variations significantly impact the region's temperature trends, highlighting the need for accurate forecasting models. The main objective of this research is to compare the effectiveness of Periodic Autoregressive (PAR) and Seasonal Autoregressive Integrated Moving Average (SARIMA) models in forecasting the maximum and minimum temperature series in Trincomalee District. These models are widely used for analyzing climate-related time series due to their ability to capture periodic(Lund et al.[3]) and seasonal fluctuations(Dimri et al.[2]) in temperature data. This study contributes to a deeper understanding of temperature variations by analyzing historical data and assessing the predictive accuracy of both models.

Methods

Data were collected from the records of the Department of Meteorology Sri Lanka. The data set comprises the monthly records of mean minimum and maximum temperature in Trincomalee District, Sri Lanka, from January 2008 to October 2024. The time series model was fitted to both series.

The seasonal ARIMA model incorporates both non-seasonal and seasonal factors in a multiplicative model. The model is denoted by SARIMA $(p,d,q)\times(P,D,Q)_S$. Here, p,q denotes the non-seasonal AR and MA terms, d denotes non-seasonal differencing, P, Q denotes the seasonal AR (SAR) and MA (SMA) terms, D denotes the seasonal differencing, and S denotes time span of repeating seasonal patterns[1].

A Periodic Autoregressive (PAR) model is appropriate for modeling data with periodic correlations, such as climate variables. A periodic autoregressive (PAR) model can be illustrated as below,

$$Y_{nT+v} = \sum_{i=1}^{p} \phi_i(v) v_{nT+v-i} + \epsilon_{nT+v}$$

Here T is the number of periods (for monthly data $T = 12$), v denotes the period (season), ϵ denotes the periodic white noise and n denotes the year, which goes from zero to the total number of full years.

Results and Conclusions

Figure 1(a) presents the time series plot and seasonal boxplots of the monthly mean maximum temperature series, indicating that seasonal components account for most of the variability in the series. A test of periodicity [1] implies that the periodic

autoregressive model does not provide a significantly better fit compared to alternative models (p-value = 0.9321) and the best-fitted model is SARIMA $(1,0,0)(2,1,1)_{[12]}$ based on the accuracy with low RMSE (0.7830), and MAPE (1.7628%).

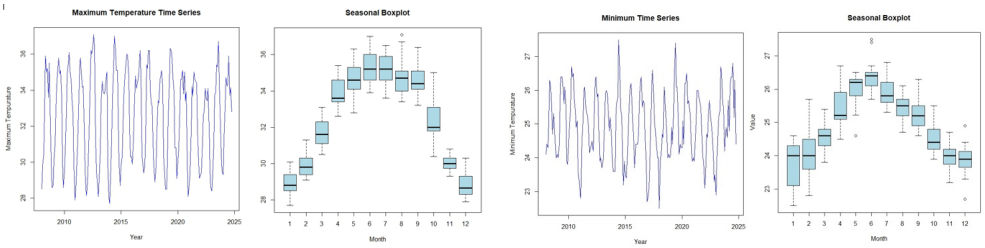

(a) Maximum Temperature Series (b) Minimum Temperature Series

Figure 1: Time Series Plot and Seasonal Boxplots

Figure 1(b) represents the time series plot and seasonal boxplots of the monthly average minimum temperature series, with seasonal boxplots indicating higher variation during peak months (May to July) and lower variation during off-peak months (November and December). The test of periodicity suggests that the monthly mean minimum temperature series consisting of periodic correlations (p-value = 0.0053) and the PAR(1) model with zero mean is the best-fitting periodic autoregressive model. However, SARIMA $(1,0,0)(0,1,1)_{[12]}$ model resulted in the minimum AIC value for this temperature series. In terms of accuracy, the PAR(1) model outperforms the SARIMA $(1,0,0)(0,1,1)_{[12]}$ model, with a slightly lower RMSE (0.4391), and MAPE (1.4071%).

Periodic autoregressive (PAR) models are widely used for analyzing time series data with periodic correlations, providing an effective framework for highlighting seasonality and temporal dependencies. This study analyzes the monthly mean maximum and minimum temperature series to assess their trends and seasonality. The time series plots and seasonal boxplots reveal dominant seasonal patterns with varying trends for both temperature series. For the maximum temperature series, the SARIMA $(1,0,0)(2,1,1)_{[12]}$ model was identified as the best fit with the lowest AIC value. Similarly, periodic correlations were observed for the minimum temperature series. Hence, the PAR(1) model with zero mean was the best-fitted periodic autoregressive model. However, the SARIMA $(1,0,0)(0,1,1)_{[12]}$ model achieved the lowest AIC value and the comparison of these two models revealed that the PAR (1) model has better precision measurements than the SARIMA $(1,0,0)(0,1,1)_{[12]}$ model for monthly mean minimum temperature series in Trincomalee District, Sri Lanka.

Keywords:

PAR, Periodic Correlations, Seasonal ARIMA, Temperature, Trincomalee District

References

[1] Peter J Brockwell. *Time series: Theory and methods*. Springer-Verlag, 1991.

[2] Tripti Dimri, Shamshad Ahmad, and Mohammad Sharif. Time series analysis of climate variables using seasonal arima approach. *Journal of Earth System Science*, 129:1–16, 2020.

[3] Robert Lund, Harry Hurd, Peter Bloomfield, and Richard Smith. Climatological time series with periodic correlation. *Journal of Climate*, 8(11):2787–2809, 1995.

An investigation of usefulness of rapid prototyped components in accelerated life testing

Tennakoon T.A.K.S [1*], **Dissanayaka U.W.M.D.**[1] **and Jayaweera N.D.**[1]
[1] Department of Mechanical Engineering, University of Moratuwa
*Corresponding author; E-mail: kalindusalith115@gmail.com

Background

Rapid prototyping is an evolving technology, with new uses emerging in many industrial sectors. Initially rapid prototyped parts were used for design approval and part verification, but the scope has now spread to vast range of applications.[3],[1],[4] [5].Research carried out in this area has shown that the RP parts can be used to test fit and function. A study discussed the potential to further impact upon the effectiveness and cycle times of the product development process through functional testing performed with RP components, but in the literature as a whole there is no indication of research studies being carried out to infer reliability data through those studies[2].

Conventional Life Data Analysis involves the collection of time-to-failure data, obtained under normal operating conditions, in order to quantify the life characteristics of a component, product or system. The authors have investigated two common rapid prototyping methods to see how the components stand up to repeated use, in comparison with parts made by injection moulding. The experiments involved the Accelerated Life Testing(ALT) of injection-moulded, FDM, surface-treated Fused Deposition Modelling (FDM) and Stereolithography (SLA) parts. Where tests resulted in the destruction of the component, the results were recorded in micrographs, giving a clear indication of the failure modes of the parts.

Methods

At the beginning of this research, it was decided that tests would be centred upon a selection of automotive central locking mechanisms. Computer aided models were created using the Pro/ENGINEER solid modelling software. Reverse engineering techniques were used to duplicate existing components without the aid of the drawings, documentation or computer model data. Through analysis and measurement, sufficient technical data were derived to allow successful reproduction of several key components of a central locking system, initially using FDM. The resulting parts were combined with genuine ones, and were found to fit adequately, permitting operation of the locking mechanism.

The number of cycles achieved, and failure mode for each was recorded. Thereafter, the same components were produced using SLA, and the same destructive testing procedure was employed. Finally, another batch of helical gears, made via FDM, were subjected to same procedure.

Results and Conclusions

The performance of our RP parts can be described as falling into three categories: Functioning perfect, Functioning not perfect and Functioning poor.

Using these criteria, the life of these parts is described as shown in Figure 1 and Figure 2.

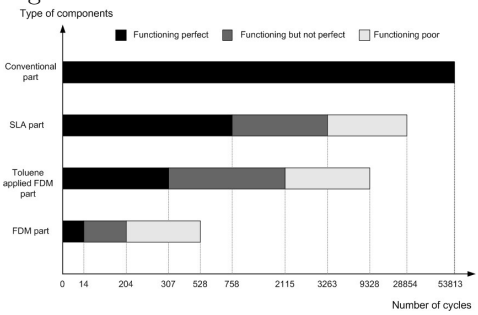

Figure 1: Comparison of large helical gear made by different processes for large helical gear

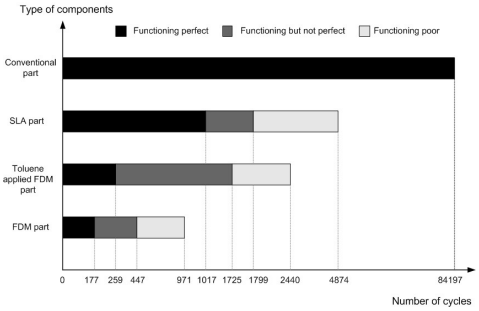

Figure 2: Comparison of small helical gear made by different processes for small helical gear

The modeling and experiments described in this study confirm that both the FDM and SLA processes have the capability to produce complex parts that can be used to test fit and function in the short term. Although the most suitable of the two processes tested (showing the longest useful component life), SLA introduces problems of brittleness in small features. FDM permits part fabrication in a reasonable range of thermoplastics and may match the finish product's material, but material deposited by this process is at reduced density, lacks bonding between the strands and has a poor surface finish that accelerates wear. This paper concludes that some parts can be made via RP processes, and used in ALT, in order to reduce time-to-market, but the components must be selected with care.

Keywords:

Computer-aided design, Mathematical modeling or simulation for problems pertaining to mechanics of deformable solids , 5 Texture in solid mechanics,Experimental work for problems pertaining to mechanics of deformable solids, Experimental studies

References

[1] E. Bassoli and A. Gatto. 3d printing technique applied to rapid casting. *Rapid Prototyping Journal*, 13(3):148–155, 2007.

[2] Un Chong Cho, Kristin L. Wood, and Robert H. Crawford. Online functional testing with rapid prototypes: a novel empirical similarity method. *Rapid Prototyping Journal*, 4(3):128–138, 1998.

[3] Masood S. Morsi Y. El-Katatny, I. Error analysis of fdm fabricated medical replicas. *Rapid Prototyping Journal*, 16(1):36–43, Jan. 2010.

[4] Matthias; Pintat Theo Greulich, Michael; Greul. Fast, functional prototypes via multiphase jet solidification. *Rapid Prototyping Journal*, 1(1):20–25, Feb. 1995.

[5] Ali Mehboob, Muhammad Adeel Abid, Sonia Javed, Tanveer Hussain, Imad Barsoum, and Sharjeel Abid. *Nanotechnology-Derived 3D-Printed Applications: Opportunities and Challenges in Biopolymers*, pages 65–93. Scrivener Publishing LLC, 2025.

Finite element analysis of self-clamping solid tyre manufacturing moulds

S.A. Mawathage[1*], J.A.I. Sanjeewa[1] and N.D. Jayaweera[1]

[1] Department of Mechanical Engineering, University of Moratuwa, Sri Lanka
*Corresponding author; E-mail: mawathagesa.19@uom.lk

Background

The tyre manufacturing industry is a crucial sector within the global economy, enabling mobility and facilitating the transportation of goods and people. Among various tyre categories, solid tyres are widely used in industrial and heavy-duty applications due to their durability and puncture-resistant properties. Sri Lanka is one of the forefront manufacturers of solid tyres, contributing to a substantial portion of the global market. In solid tyre production, the moulding process is a critical stage that determines the final product quality. Among various types of moulds, the self-clamping moulds are preferred in solid tyre manufacturing due to their ability to withstand high cavity pressures, ensure uniform sealing, reduce mould wear, enable faster production cycles, and maintain dimensional stability under high-temperature vulcanization, making them ideal for efficient, large-scale production. During the study, a survey was carried out to collect data on the failures of the clamping tyre moulds as shown in Table 1. Due to the criticality of the failures, understanding the mechanical behaviour of these moulds under operational loads is essential for optimizing mould design and improving manufacturing efficiency. This study presents a finite element analysis (FEA) to investigate the stress distribution and deformation of the solid tyre moulds, with the aim of providing recommendations to enhance their reliability and performance by integrating experimental data. [1]

Table 1: Failure data of self-clamping solid tyre moulds

Failure Type	**Average Number of Failures per 10,000 tyres**	**Standard Deviation**
Clamp Bolt Cracks	42	21.87
Clamping Unit Failure	14	6.92
Tire Mold Housing Permanent Deformation	6	3.11
Mold Internal Components Damage	3	1.63

Methods

The study follows a numerical simulation approach using finite element analysis to evaluate stress and deformation of the self-clamping tyre moulds for four tyre sizes which are, 600-15, 700-15, 800-15 and 900-15 (600-15 notation refers to 6.00 inch tyre width and 15 inch rim diameter). As the initial step, 3D models were developed in SolidWorks based on actual mould dimensions, which were later fetched in to Abaqus FEA software package to analyse the stress and deformation of the mould components. The material was pre-identified as AISI 4340 Steel, where the elastic modulus is 212 GPa, density: 7800 kg/m^3, tensile strength: 1240 N/mm^2 and yield strength is 930 N/mm^2. As the boundary conditions, a rigid virtual wall contact condition

was applied to the tyre mould bottom surface, a uniform distributed pressure load which is normal to surface was applied on the mould cavity surface to incorporate the mould cavity pressure, torque value was applied to nut and bolt connection with the calculated bolt torques and a vertically downward gravitational force was applied to consider the impact of the mould self-weight.

Under the meshing strategy, 10-node tetrahedral element has been employed as the mesh element type. This mesh element type was selected due to the intricacies of the 3D models, necessitating a level of precision beyond what can be achieved with standard 4-node tetrahedral elements. The 10-node tetrahedral element, featuring a higher node count, enhances the overall accuracy, making it a well-suited choice for applications in structural mechanics, particularly when dealing with complex mould designs. Refinements were done to the mesh over 7 iterations, carrying out mesh convergence studies. Later, during the post-processing phase, the stress and deformation contours were analysed to identify the stress concentrated areas and the deformations. [2]

Results and Conclusions

The FEA results provided key insights into the stress distribution and deformation patterns within the solid tyre mould. The study found that the high stress concentrations are occurred at the bolt clamping regions and near the mould cavity edges, where pressure-induced expansion was most pronounced. Similarly the mould exhibited elastic deformation under typical operating conditions, with maximum deformations occurring at the inner circumference of mould. Numerical values of the maximum stress and deformation is shown in Table 2.

Table 2: FEA results of maximum stress and deformation

Mould	**Max. stress (MPa)**	**Max. deformation (mm)**
600-15	914.7	1.72
700-15	903.7	1.53
800-15	713.5	1.60
900-15	780.0	1.95

Based on the results, the study provides impactful recommendations for implementing design alterations to avoid excessive stress concentrations at the mould edges. Further, it is recommended to introduce clamping bolts to inner edges of mould to reduce the deformations. These modifications directly improve not only the dimensional accuracy and the quality of the final tyre product, but also the mould parts life due to enhanced fatigue performance.

Keywords:

Finite Element Analysis, Stress Distribution, Deformation, Computational Modeling

References

[1] Vidyaratne K. *Review on National Competitive Advantage for Marketing Potentials for Off-The Road (OTR) Tyre Industry in Sri Lanka.* Sri Lanka Journal of Marketing, 2022.

[2] Zhang Yang Wen Runsheng. *Simulation of Stress Distribution and Deformation Analysis for Cantilever I-beams Using ABAQUS Software.* IOP Conference Series: Materials Science and Engineering, 2 edition, 2019.

A retrit–based superdense coding protocol

Anuradha Mahasinghe[1*], Nisal Bimsara[1] and Kaushika De Silva[2]
[1] Department of Mathematics
University of Colombo, Colombo 03, Sri Lanka
[2] Department of Mathematics
University of Sri Jayewardenapura, Nugegoda, Sri Lanka
*Corresponding author; E-mail: anuradhamahasinghe@maths.cmb.ac.lk

Background

The simplest quantum systems exhibiting quantum properties are called *qubits* and they are the quantum counterpart of classical bits. Some recent works proposed using three–level quantum systems called *qutrits* (states in a superposition of three basis states $|0\rangle$, $|1\rangle$ and $|2\rangle$) instead of qubits for quantum information transfr, due to robust decoherence[2].

Very recently, the possibility of using qutrits with real amplitudes was investigated. The pioneering work appeared in 2020, proving efficient quantum compiling with real quitrits is possible [3]. Later, real qutrits were named *retrits* and several interesting results were obtained[1].

However, the question whether it is possible to achieve quantum advantage for information transfer on a retrit–based computing platform remained unanswered. We answered this positively, by devising a retrit–based quantum protocol for superdense coding (SDC).

Methods

When devising our method we got several insights from [4] in which SDC was done with non–maximally entangled states. We designed the circuit in Figure 1 with $\hat{H} = \begin{pmatrix} \sqrt{\frac{2}{3}} & \frac{1}{\sqrt{3}} & 0 \\ \frac{1}{\sqrt{3}} & -\sqrt{\frac{2}{3}} & 0 \\ 0 & 0 & 1 \end{pmatrix}$ and the orthogonal matrices applied by sender (Alice) who wishes to send information to receiver (Bob), according to Table 1.

Alice wishes to send	by applying	generating the state
00	$U_1 = \begin{pmatrix} 1 & 0 & 0 \\ 0 & 1 & 0 \\ 0 & 0 & 1 \end{pmatrix}$	$\|\varphi_1\rangle = \sqrt{\frac{2}{3}}\|00\rangle + \frac{1}{\sqrt{3}}\|11\rangle$
01	$U_2 = \begin{pmatrix} 0 & 0 & 1 \\ 1 & 0 & 0 \\ 0 & 1 & 0 \end{pmatrix}$	$\|\varphi_2\rangle = \sqrt{\frac{2}{3}}\|10\rangle + \frac{1}{\sqrt{3}}\|21\rangle$
10	$U_3 = \begin{pmatrix} -\frac{1}{2} & 0 & -\frac{\sqrt{3}}{2} \\ 0 & 1 & 0 \\ \frac{\sqrt{3}}{2} & 0 & -\frac{1}{2} \end{pmatrix}$	$\|\varphi_3\rangle = -\frac{1}{\sqrt{6}}\|00\rangle + \frac{1}{\sqrt{3}}\|11\rangle + \frac{1}{\sqrt{2}}\|20\rangle$

11	$U_4 = \begin{pmatrix} -\frac{1}{2} & 0 & \frac{\sqrt{3}}{2} \\ 0 & 1 & 0 \\ -\frac{\sqrt{3}}{2} & 0 & -\frac{1}{2} \end{pmatrix}$	$\|\varphi_4\rangle = -\frac{1}{\sqrt{6}}\|00\rangle + \frac{1}{\sqrt{3}}\|11\rangle - \frac{1}{\sqrt{2}}\|20\rangle$

Table 1: Summary of Alice's encoding process in RSCP

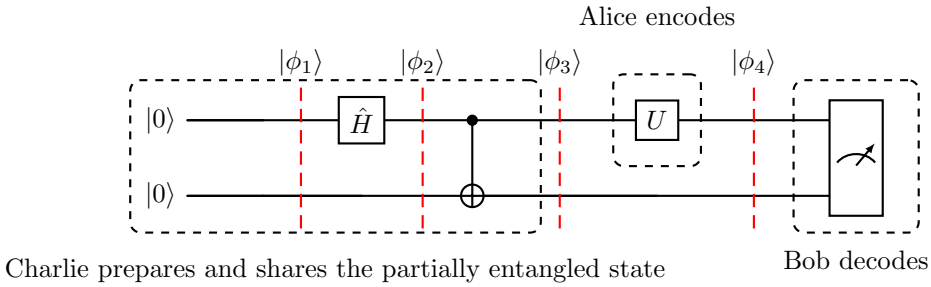

Figure 1: Circuit diagram for RSCP

Results

The set $\{|\varphi_1\rangle, |\varphi_2\rangle, |\varphi_3\rangle, |\varphi_4\rangle\}$ is contained in an orthonormal basis of partially entangled states. Once Alice shares her retrit with Bob, he performs a quantum measurement on the composite system with respect to the orthonormal basis to determine what message Alice has encoded. By doing this, he can distinguish each of the states from the four partially entangled states that Alice generated using the orthogonal gate at the encoded step. Thus, Bob can determine which one out of the four different messages Alice has sent him.

References

[1] Sabino Di Trani, Willem A de Graaf, and Alessio Marrani. Classification of real and complex three-qutrit states. *Journal of Mathematical Physics*, 64(9), 2023.

[2] Pranav Gokhale, Jonathan M Baker, Casey Duckering, Frederic T Chong, Natalie C Brown, and Kenneth R Brown. Extending the frontier of quantum computers with qutrits. *IEEE Micro*, 40(3):64–72, 2020.

[3] Anuradha Mahasinghe, Sachiththa Bandaranayake, and Kaushika De Silva. Solovay–kitaev approximations of special orthogonal matrices. *Advances in Mathematical Physics*, 2020(1):2530609, 2020.

[4] Shay Mozes, Jonathan Oppenheim, and Benni Reznik. Deterministic dense coding with partially entangled states. *Physical Review A—Atomic, Molecular, and Optical Physics*, 71(1):012311, 2005.

Developing dengue risk index for selected districts in Sri Lanka

Chamila Niroshanie[1*], **Hasitha Erandi**[1], **Sanjeewa Perera**[1] **and Yashika Jayathunga**[1]

[1] Centre for Mathematical Modelling, Department of Mathematics, Faculty of Science, University of Colombo, Sri Lanka

*Corresponding author; E-mail: chamila1vithanage@gmail.com

Background

Dengue is a mosquito-borne viral disease that can be fatal in severe cases and poses a significant health and economic burden. Early identification of the risk of dengue is crucial to mitigate the burden [1]. This study aimed to develop a risk index based on the combined impacts of the most affected climate elements on dengue transmission in selected districts of Sri Lanka considering climate variability, high incidence of dengue, and dense population of districts.

Due to the inter-correlation between climate factors, a copula was used to model their joint impact on dengue for each district. The Gaussian copula was used to effectively represent the joint distribution of normally distributed variables [2, 3].

Methods

The periodicity of dengue cases in each district was determined using the Fast Fourier Transform method before applying the copula [4]. In order to capture the relationship between climate factors when their favorable ranges fall within the middle of their usual ranges, the Gaussian copula was used. The Gaussian copula uses a multivariate normal distribution, transforming marginals into uniform distributions. Samples from the copula can be generated by using the uniform marginals. This process allows the Gaussian copula to model the dependency structure while permitting different marginal distributions for the individual variables. Firstly, two major climate factors that affect the risk of dengue were selected by computing the correlation between each climate factor and dengue cases in each district. In order to obtain the marginal distributions, the influence of climatic variables on the risk of dengue was considered. Marginal distributions were derived using a Gaussian membership function, then converted to normal distributions. Then the joint impact of climate factors on the risk of dengue was calculated using the Gaussian copula [2]. Based on the joint impact, three dengue risk levels were identified. The medium risk level was defined by the lowest joint impact when one climate factor is within a favourable range while the other is in an unfavourable range for the risk of dengue. Joint impact values lower than this threshold were classified as low risk. The medium risk range was established between the lower risk threshold and a value calculated by averaging the joint impact when one climate factor is favourable and the other is unfavourable for dengue risk. Values exceeding this range were classified as high risk.

Results and Conclusions

Taking into account the different possible ways from geographical and climate factors that can affect dengue transmission, the Colombo, Kandy, Galle and Jaffna districts

of Sri Lanka were selected for our study. Rainfall and humidity were identified as key climatic factors in the Jaffna district. Rainfall and temperature were identified as key climatic factors in the other selected districts. The risk level for each week was calculated from the joint impact of the key climate factors. The reported weekly dengue cases from 2013 to 2020 in the districts Colombo, Galle, Jaffna and Kandy are illustrated in Figure 1. The findings suggest that the risk of dengue for certain weeks was not adequately captured by the combined effects of key climatic factors. This might be due to the exclusion of effect of other factors on dengue risk. This indicates the need for future studies to improve the risk index by taking into account other factors that contribute to dengue outbreaks.

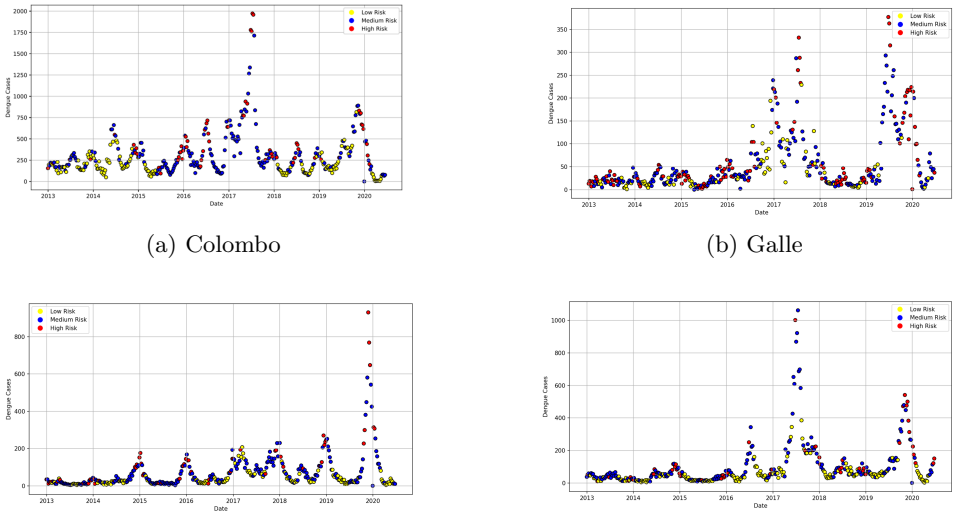

(a) Colombo

(b) Galle

(c) Jaffna

(d) Kandy

Figure 1: Reported dengue cases and risk from the joint impact of climate factors in each district.

Keywords:

Dengue, Climate factors, Correlation, Gaussian Copula

References

[1] M Derouich, A Boutayeb, and EH Twizell. A model of dengue fever. *Biomedical engineering online*, 2:1–10, 2003.

[2] Guido Masarotto and Cristiano Varin. Gaussian copula regression in r. *Journal of Statistical Software*, 77:1–26, 2017.

[3] Roger B Nelsen. *An Introduction to Copulas*. Springer, New York, NY, USA, second edition, 2006.

[4] Wickramaarachchillage Pieris Tharindu Mihiruwan Wickramaarachchi, Kaluhath Karunathilaka Withanage Hasitha Erandi, and Shyam Sanjeewa Nishantha Perera. 9 - mathematical tools and their applications in dengue epidemic data analytics. In Hemen Dutta and Khalid Hattaf, editors, *Advances in Epidemiological Modeling and Control of Viruses*, pages 253–283. Academic Press, 2023.

Implementation of RNN-LSTM with L1 regularization for predicting labels from chimpanzee DNA sequences using pseudo-labeling

Sugiyarto Surono[1*], Goh Khang Wen[2] , Rohmatul Fajriyah[1], Arief Rahman[2], Lalu M. Irham[1] and Sintia Afriyani[1]
[1] Universitas Ahmad Dahlan Yogyakarta,Indonesia
[2] INTI International University, Nilai, Malaysia
*Corresponding author; E-mail: sugiyarto@math.uad.ac.id

Background

Chimpanzee genome research plays a crucial role in understanding evolution, biological functions, and health-related genetics. However, a significant challenge in genomic studies is the presence of incomplete or unlabelled DNA sequence data, which hinders accurate classification and functional analysis. Conventional deep learning models, such as Convolutional Neural Networks (CNNs) and Long Short-Term Memory (LSTM) networks, have been widely employed in genomic analysis but struggle with limited labelled data. To address this challenge, this study integrates **pseudo-labelling**, a semi-supervised learning approach, with an **RNN-LSTM model enhanced by L1 regularization** to improve DNA sequence classification. By leveraging both labelled and pseudo-labelled data, this method enhances model generalization and classification accuracy, particularly for imbalanced datasets. The study aligns with **Goal 3: Good Health and Well-being** of the Sustainable Development Goals (SDGs) by advancing genetic research methods that support early disease detection and precision medicine.

Methods

This research employs a **pseudo-labelling strategy combined with an RNN-LSTM architecture and L1 regularization** to classify chimpanzee DNA sequences. The workflow includes:

1. **Data Preprocessing**: One-Hot Encoding, K-mer Embedding (k=3), and Padding are applied to convert DNA sequences into numerical formats suitable for deep learning models.
2. **Feature Selection**: L1 Regularization (Lasso) is used to **remove irrelevant genetic features**, reducing dimensionality and improving model interpretability.
3. **RNN-LSTM Model Training**: An LSTM-based recurrent neural network is trained using labelled DNA sequences.
4. **Pseudo-Labeling**: The trained model predicts labels for previously unlabelled sequences, incorporating them into the training dataset.
5. **Retraining with Augmented Data**: The updated dataset (labelled + pseudo-labelled) is used for further training to improve generalization.
6. **Evaluation Metrics**: The model is assessed using **accuracy, cross-entropy loss, ROC-AUC score, and precision-recall curve** to evaluate classification performance.

Results and Conclusions

The experimental results demonstrate that **pseudo-labelling significantly improves DNA sequence classification accuracy**, particularly for sequences with missing annotations. Key findings include:

- The **RNN-LSTM model with L1 regularization** effectively selects significant genetic features, reducing feature dimensionality from **1,775 to 62**, while maintaining prediction accuracy.
- **Model Performance**: After integrating pseudo-labelling, the model achieved an **AUC ranging from 0.94 to 0.99**, indicating excellent classification capability.
- **Training Accuracy**: The accuracy increased from **20.27% (epoch 1) to 85.41% (epoch 50)**, while validation accuracy reached **80.67%**, demonstrating stable learning trends.
- Loss Curve Analysis: The **best validation loss was recorded at 0.5550**, ensuring a well-optimized model without overfitting.
- **Precision-Recall Curve**: The **Average Precision (AP) ranged from 0.58 to 0.80**, reflecting improved handling of imbalanced genomic data.

These findings validate the effectiveness of **semi-supervised learning (pseudo-labelling) in genomic classification tasks**, allowing deep learning models to **leverage unlabelled data to enhance performance**. This approach provides a scalable solution for handling large-scale genomic datasets, contributing to improved **genetic research methodologies and biomedical applications**. Future work may explore the integration of **Transformer-based architectures** and **graph neural networks (GNNs)** for more complex genomic sequence analysis.

Keywords:

Genomic Data Classification, Semi-Supervised Learning, RNN-LSTM for DNA Sequences, Pseudo-Labelling in Genomics, Feature Selection in Bioinformatics.

References

[1] Zeeshan Ahmed, Saman Zeeshan, Dinesh Mendhe, and XinQi Dong. Human gene and disease associations for clinical-genomics and precision medicine research. *Clinical and translational medicine*, 10(1):297–318, 2020.

[2] Adnan Khan, Mai A Shaaban, and Muhammad Haris Khan. Improving pseudo-labelling and enhancing robustness for semi-supervised domain generalization. *arXiv preprint arXiv:2401.13965*, 2024.

[3] Lefteris Koumakis. Deep learning models in genomics; are we there yet? *Computational and Structural Biotechnology Journal*, 18:1466–1473, 2020.

[4] Maria V Suntsova and Anton A Buzdin. Differences between human and chimpanzee genomes and their implications in gene expression, protein functions and biochemical properties of the two species. *BMC genomics*, 21(Suppl 7):535, 2020.

[5] Aimin Yang, Wei Zhang, Jiahao Wang, Ke Yang, Yang Han, and Limin Zhang. Review on the application of machine learning algorithms in the sequence data mining of dna. *Frontiers in Bioengineering and Biotechnology*, 8:1032, 2020.

Real-time 3D load planning: enhancing logistics with dynamic optimization models

Deshinta Arrova Dewi[1*], Tri Basuki Kurniawan[2],Misinem[3] and Hafiz Muhammad Kurniawan [4]

[1] Faculty of Data Science and Information Technology, INTI International University, Nilai, Malaysia

[2] Universitas Bina Darma, Palembang, Indonesia

[3] Faculty of Vocational, Universitas Bina Darma, Palembang, Indonesia

[4] Faculty of Computer Science, Universitas Sriwijaya, Palembang, Indonesia

*Corresponding author; E-mail: deshinta.ad@newinti.edu.my

Background

Efficient 3D load planning is crucial in logistics to maximize space utilization, reduce costs, and improve operational efficiency. Traditional methods rely on static algorithms or human expertise, leading to suboptimal packing, poor weight distribution, and increased fuel consumption [1]. Real-world logistics involve dynamic constraints such as varying cargo dimensions, weight balancing, and priority-based deliveries, making static models inadequate for real-time decision-making [2][2]. AI-based approaches and intense reinforcement learning (DRL) methods such as Deep Q-Networks (DQN) and Proximal Policy Optimization (PPO) dynamically adjust cargo placement but require extensive offline training and significant computational resources. Other AI models, including Convolutional Neural Networks (CNNs) and Graph Neural Networks (GNNs), enhance packing predictions but lack real-time adaptability. Hybrid approaches combining AI and heuristic methods aim to balance efficiency and adaptability but introduce computational overhead [3]. This research proposes a dynamic optimization model for real-time 3D load planning by integrating reinforcement learning with heuristic algorithms.

Methods

To develop and evaluate the proposed real-time 3D load planning model, we utilize real-world logistics datasets from industries such as e-commerce, freight transportation, and warehouse logistics. These datasets include detailed cargo attributes, enhancing the model's adaptability across various logistical challenges. The preprocessing stage ensures data consistency, quality, and usability for real-time 3D load planning. It includes data cleaning (removing duplicates, handling missing values, and standardizing units) and feature engineering (deriving Volume-to-Weight Ratio, Aspect Ratio, and Stacking Compatibility Score) [4]. Real-time constraints, such as priority-based loading and dynamic slot allocation, enhance adaptability. These steps optimize space utilization, cargo stability, and compliance with weight regulations. The processed dataset is then fed into the optimization model, ensuring efficient and accurate load placement in dynamic logistics environments.

Results and Conclusions

The real-time 3D load planning model was tested in various simulation environments to evaluate its efficiency in space utilization, stability, and adaptability. Figure 1 a)

and b) show the results for real-world and synthetic datasets.

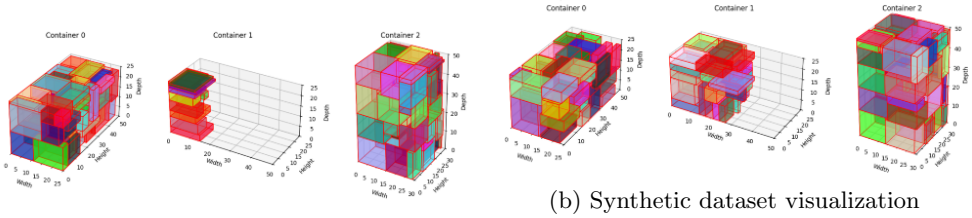

(a) Real-world dataset visualization

(b) Synthetic dataset visualization

.

Figure 1: placement results

Key findings are summarised as follows:

- **Space Utilization Efficiency:**
  The model achieved an 87% space utilization rate, significantly improving over traditional static load planning methods (75%). Dynamic slot allocation allowed continuous optimization, reducing container space by 10%.
- **Load Stability and Weight Distribution:**
  The computed center of mass remained within an acceptable range in 96% of simulated scenarios, ensuring stable and balanced cargo loads. The stacking compatibility algorithm prevented cargo damage, with no improper stacking reported in over 1,000 simulation runs.
- **Real-Time Adaptability:**
  When new cargo was introduced mid-loading, the model successfully adjusted placement strategies without disrupting pre-loaded items in 93% of cases. The system dynamically reprioritized high-urgency shipments, reducing retrieval time by an average of 20% compared to baseline models.

The results demonstrate that the proposed real-time 3D load planning model significantly enhances space utilization, cargo stability, and adaptability compared to traditional static models.

Keywords:

Real-time 3D Load Planning, Dynamic Optimization, Logistics Efficiency, Reinforcement Learning, Process Innovation

References

[1] Ali Akbar Firoozi, Magdeline Tshambane, Ali Asghar Firoozi, and Sajid Mubashir Sheikh. Strategic load management: Enhancing eco-efficiency in mining operations through automated technologies. *Results in Engineering*, page 102890, 2024.

[2] Bernard Atta Adjei, Charles Sebil, Dominic Otoo, and Joseph Ackora-Prah. A quadratically constrained mixed-integer non-linear programming model for multiple sink distributions. *Heliyon*, 10(19), 2024.

[3] Martín Bueno and Frédéric Bosché. Pre-processing and analysis of building information models for automated geometric quality control. *Automation in Construction*, 165:105557, 2024.

[4] Samiayya Duraimurugan, P Jesu Jayarin, Suleiman Ibrahim Mohammad, N Hariprasad, Asokan Vasudevan, Eddie Eu Hui Soon, Abdelrahman H Hussein, and Muhammad Turki Alshurideh. Enhanced server-client framework for optimizing qos in video streaming over diverse networks. *Appl. Math*, 19(1):61–73, 2025.

Resource-efficient waste collection: A computational approach for load and route optimization

Tri Basuki Kurniawan[1*], Deshinta Arrova Dewi[2] and Hafiz Muhammad Kurniawan[3]
[1] Universitas Bina Darma, Palembang, Indonesia
[2] Faculty of Data Science and Information Technology, INTI International University, Nilai, Malaysia
[3] Faculty of Computer Science, Universitas Sriwijaya, Palembang, Indonesia
*Corresponding author; E-mail: tribasukikurniawan@binadarma.ac.id

Background

Rapid urbanization has intensified waste management challenges, particularly in metropolitan areas where inefficient garbage collection increases costs, pollution, and flooding risks [1]. Traditional static waste collection schedules fail to adapt to fluctuating waste generation patterns, leading to routing, truckload distribution inefficiencies, and environmental impact [2]. This study proposes an advanced computational framework integrating machine learning-based waste prediction with multi-objective optimization for load balancing and route planning. The framework consists of three key components: (1) a Waste Prediction Model utilizing historical waste data, rainfall intensity, and population density for accurate forecasting; (2) Clustered Load Optimization, which employs constrained k-means clustering to balance truckloads efficiently; and (3) Route Optimization, which minimizes travel distance and fuel consumption using Google OR-Tools. Key performance indicators (KPIs) include transportation distance, vehicle utilization rate, operational cost reduction, and environmental impact [3].

Methods

This study integrates predictive analytics, constrained clustering, and route optimization to enhance waste collection efficiency, reduce costs, and improve sustainability [4]. The methodology comprises waste forecasting, load balancing, and optimized routing for collection trucks.

Machine learning models use historical data, population density, and weather conditions to predict waste accumulation. A Multiple Linear Regression (MLR) model estimates daily waste at Gross Pollutant Traps (GPTs), while an LSTM Neural Network is used for non-linear patterns, improving scheduling efficiency.

A constrained k-means clustering method assigns GPTs to collection trucks while balancing loads and minimizing required vehicles. The model ensures that truck capacities are not exceeded while optimizing resource allocation.

A Travelling Salesman Problem (TSP) solution using Google OR-Tools minimizes travel distance and fuel consumption by determining the shortest collection truck route. This reduces operational costs and environmental impact.

Evaluation Metrics and Mathematical Models

1. Total Transportation Distance – Measures the cumulative distance travelled by collection trucks, influencing fuel consumption and costs.

2. Vehicle Utilization Rate – Assesses truck capacity efficiency, ensuring optimal space utilization per trip.

3. Operational Cost Reduction – Evaluate cost efficiency by incorporating fuel expenses, route distances, and unused truck capacity.

Results and Conclusions

The dataset comprises waste collection records from 23 Gross Pollutant Traps (GPTs) over seven days, including waste accumulation, geolocation, vehicle capacities, and route information. Pre-processing steps include data cleaning, transformation, normalization, and feature engineering to prepare the data for predictive modeling and optimization. A multiple linear regression (MLR) model predicts daily waste accumulation based on historical data, rainfall levels, and population density. The model achieves an $\mathbf{R^2}$ score of 0.87, demonstrating substantial predictive accuracy. Integrating this model into waste collection scheduling helps reduce operational inefficiencies. Figure 1 shows the Comparison of Actual vs. Predicted Waste Accumulation from GPT 1.

The trained model is applied to the test set, yielding the following results:

- **MAE**: 12.45 kg (indicating an average deviation of ±12.45 kg in predictions)
- **RMSE**: 15.78 kg (highlighting slightly larger errors in some cases)
- R^2 **Score**: 0.87 (indicating that the model explains 87% of the variance in waste accumulation)

Clustered Load and Route Optimization

K-means clustering with capacity constraints is used to group GPTs efficiently, followed by OR tools to optimize vehicle routes using the Vehicle Routing Problem (VRP). Optimization reduces total transportation distance by 31.3%, increases vehicle utilization from 62.5% to 91.2%, and cuts operational costs by 31.2%, as shown In Table 1.

Table 1: Table 1. The results summarise

Scenario	**Total Distance (km)**	**Vehicle (%) Utilization (%)**	**Cost Reduction (%)**
Before Optimization	240 km	62.5%	-
After k-Means + OR-Tools Optimization	**165 km**	**91.2%**	**31.2%**

Keywords:

Waste Collection Optimization, Vehicle Routing Problem (VRP), k-means Clustering, AI-driven Logistics, Process Innovation

References

[1] Gopal Kumar, Supriya Vyas, Shashikant Nishant Sharma, and Kavita Dehalwar. Challenges of environmental health in waste management for peri-urban areas. In *Solid Waste Management: Advances and Trends to Tackle the SDGs*, pages 149–168. Springer, 2024.

[2] Vikram Pasupuleti, Bharadwaj Thuraka, Chandra Shikhi Kodete, and Saiteja Malisetty. Enhancing supply chain agility and sustainability through machine learning: Optimization techniques for logistics and inventory management. *Logistics*, 8(3):73, 2024.

[3] Subramanian Petchimuthu, Hüseyin Kamacı, Tapan Senapati, et al. Evaluation of artificial intelligence-based solid waste segregation technologies through multi-criteria decision-making and complex q-rung picture fuzzy frank aggregation operators. *Engineering Applications of Artificial Intelligence*, 133:108154, 2024.

[4] Wenwen Chen, Yangchongyi Men, Noelia Fuster, Celia Osorio, and Angel A Juan. Artificial intelligence in logistics optimization with sustainable criteria: A review. *Sustainability*, 16(21):9145, 2024.

Robust fuzzy regression analysis using method of moments estimation for air quality index data

Sugiyarto Surono[1*], **Ummu F.Nursholihah1**[1] **and Goh Khang Wen**[2]
[1] Universitas Ahmad Dahlan Yogyakarta,Indonesia
[2] INTI International University, Nilai, Malaysia
*Corresponding author; E-mail: sugiyarto@math.uad.ac.id

Background

Outliers are data points that significantly deviate from the overall pattern in a dataset, often leading to biased statistical estimation. The Least Squares Method (LSM) is widely used for parameter estimation but is highly sensitive to outliers, which can affect its accuracy and reliability. To address this issue, robust regression techniques have been developed to improve estimation stability. This study extends the Method of Moments (MM) estimation to fuzzy regression analysis, creating a model that is more resistant to the presence of outliers. By integrating fuzzy regression with robust statistical techniques, we propose an approach that effectively models fuzzy data contaminated with outliers.

Air pollution is a critical environmental issue, and accurate air quality monitoring is essential for effective policy-making and public health management. Traditional regression models often struggle with the uncertainty and variability inherent in environmental data. Fuzzy regression, enhanced with robust estimation techniques, provides a powerful tool for analyzing air quality data and improving predictive accuracy.

Methods

In this study, air quality index data from Yogyakarta was analyzed using fuzzy regression integrated with robust estimation techniques. The independent variables included temperature (x_1), wind speed (x_2), and humidity (x_3), while the air quality index (y) served as the dependent variable. The study applied three robust weighting functions:

- Huber function
- Tukey Bisquare function
- Welsch function

The triangular fuzzy number approach was used to construct fuzzy representations of the variables. A random sampling technique was applied to select 100 observations from the dataset. The MM estimation method was then utilized to develop robust fuzzy regression models, and their accuracy was evaluated using Mean Squared Error (MSE).

Results and Conclusions

The study findings indicate that the MM estimation model incorporating the Huber weighting function outperforms other approaches, as reflected in its lowest MSE

value of 8.948057. This suggests that the Huber function effectively mitigates the influence of outliers while maintaining estimation accuracy. Comparatively, the models employing Tukey Bisquare and Welsch weighting functions exhibited higher MSE values, indicating reduced robustness in handling extreme values.

The results demonstrate that integrating robust statistical techniques with fuzzy regression enhances the predictive performance of air quality models. This approach effectively captures the uncertainty and variability in environmental data, making it well-suited for applications in environmental monitoring and predictive analytics. Furthermore, the findings align with previous research supporting MM estimation's effectiveness in robust regression modeling.

Keywords:

Linear regression, Robust estimation, Fuzzy logic and applications, Fuzzy and stochastic programming, Environmental applications of mathematics

References

[1] Özlem Gürünlü Alma. Comparison of robust regression methods in linear regression. *Int. J. Contemp. Math. Sciences*, 6(9):409–421, 2011.

[2] Samprit Chatterjee and Jeffrey S Simonoff. *Handbook of regression analysis*. John Wiley & Sons, 2013.

[3] Richard B Darlington and Andrew F Hayes. *Regression analysis and linear models: Concepts, applications, and implementation*. Guilford Publications, 2016.

[4] Qiang Song and Brad S Chissom. Fuzzy time series and its models. *Fuzzy sets and systems*, 54(3):269–277, 1993.

[5] Rami Zwick. Fuzzy set theory and its applications, 1993.

Mathematical expression recognition: statistical analysis of expression types and dataset complexity

Khang Wen Goh[1*], Zhanjiang Wei[1] and Zupeng Chang[2]

[1] Faculty of Data Science and Information Technology, INTI International University, Nilai, Malaysia

[2] School of Mathematics and Computer Science, Yunnan University of nationalities, 650000 Kunming, China

*Corresponding author; E-mail: khangwen.goh@newinti.edu.my

Background

Mathematical expression recognition (MER) [1] is one of the key research directions in the fields of computer vision [3] and artificial intelligence. With the advancement of digital education [5], automated scientific research and big data analysis, its application in academia, finance, engineering, physics and other fields has become particularly important, especially in the fields of automated indexing of the scientific literature, educational tutoring software, conversion of handwritten formulas and automatic reasoning, which has significantly improved processing efficiency and accuracy. Although modern algorithms based on deep learning have made significant progress in MER technology, most research still focuses on algorithm optimization and symbol recognition, lacking statistical analysis of data set types and complexity, leading to instability of the effectiveness of existing methods in different data sets. Therefore, based on the idea of data-centric AI, mathematical expression recognition should focus on accurate recognition of expression types. This paper summarises the types of mathematical expressions and conducts statistical analysis of commonly used datasets, hoping to promote the development of MER technology and provide data support for future research [4].

Methods

Summary of expression types. In this work, we classified mathematical expressions in detail according to the development history of mathematics and summarized 18 detailed expression types in 6 categories.

Multidimensional Classification System of Expressions. In order to comprehensively analyze mathematical expressions, this paper proposes an analysis method based on a multidimensional classification system. The system classifies mathematical expressions from the following dimensions. Symbol classification: including symbols such as variables, constants, operators, and functions. Structural classification: evaluating complexity based on nesting depth and expression hierarchy. Type classification: counting the number and proportion of expressions of different types. Complexity analysis: analyzing the complexity of expressions by calculating indicators such as the number of symbols and nesting depth.

Multidimensional Classification System of Expressions. In order to comprehensively analyze mathematical expressions, this paper proposes an analysis method based on a multidimensional classification system. The system classifies mathematical expressions from the following dimensions. Symbol classification: including symbols such as variables, constants, operators, and functions. Structural classification: evaluating complexity based on nesting depth and expression hierarchy. Type classification:

counting the number and proportion of expressions of different types. Complexity analysis: analyzing the complexity of expressions by calculating indicators such as the number of symbols and nesting depth.

Results and Conclusions

The statistical analysis of the three datasets reveals significant differences in their expression types and complexities. The im2latex-100k dataset stands out for its high type entropy, indicating diverse expression types. On the other hand, the real formula dataset shows higher average depth, reflecting its more complex structure. Coverage, measured by the proportion of expression types covered, is highest in im2latex-100k, which supports a broad range of expression types. These findings suggest that while the im2latex-100k dataset excels in diversity, the complex structure of real formulas offers a deeper understanding of mathematical expressions. The results highlight the importance of balancing diversity and complexity for more effective training in the MER model.

The main goal of this study is to summarize various mathematical expressions and classify and count representative mathematical data sets. In the future, it will be used to explore solutions to the problems existing in the current mathematical expression recognition, such as complex nested structures, multi-line expressions, special expression symbol recognition (superscripts, subscripts, fractions, square roots, etc.), multimodal expression input, and similar expression retrieval, so as to improve the MER recognition and retrieval capabilities. This research aims to be applied in practical scenarios, such as guiding the creation of high school mathematics datasets covering e-books, test papers, and exercise books. Teachers can quickly search for key expressions (e.g., pictures, LaTeX, or text input), find relevant results, and automatically assemble questions using preset templates. These contents can then be pushed to students through third-party platforms (e.g., Yuketang). Ultimately, teachers can keep track of students' learning progress and adjust teaching strategies in a timely manner.

Keywords:

Mathematical Expressions, Expression Recognition, Mathematical Expression Complexity, Statistical Analysis, Datasets

References

[1] Dorothea Blostein and Ann Grbavec. Recognition of mathematical notation. In *Handbook of character recognition and document image analysis*, pages 557–582. World Scientific, 1997.

[2] Thomas M Cover. *Elements of information theory*. John Wiley & Sons, 1999.

[3] Alex Graves, Marcus Liwicki, Santiago Fernández, Roman Bertolami, Horst Bunke, and Jürgen Schmidhuber. A novel connectionist system for unconstrained handwriting recognition. *IEEE transactions on pattern analysis and machine intelligence*, 31(5):855–868, 2008.

[4] Kai Hu, Zhuoyao Zhong, Lei Sun, and Qiang Huo. Mathematical formula detection in document images: A new dataset and a new approach. *Pattern Recognition*, 148:110212, 2024.

[5] Paul-Philipp Luley, Jan M Deriu, Peng Yan, Gerrit A Schatte, and Thilo Stadelmann. From concept to implementation: The data-centric development process for ai in industry. In *2023 10th IEEE Swiss Conference on Data Science (SDS)*, pages 73–76. IEEE, 2023.

Research & Development
Centre for
MATHEMATICAL MODELLING

CM^2

ISBN 978-624-5518-29-6